3-22-2018

Discovery and Targeted Monitoring of Biomarkers Using Liquid Chromatography, Ion Mobility Spectrometry , and Mass Spectrometry

Kendra J. Adams
Florida International University, kadam034@fiu.edu

DOI: 10.25148/etd.FIDC006592

FLORIDA INTERNATIONAL UNIVERSITY

Miami, Florida

DISCOVERY AND TARGETED MONITORING OF BIOMARKERS USING LIQUID CHROMATOGRAPHY, ION MOBILITY SPECTROMETRY, AND MASS SPECTROMETRY

A dissertation submitted in partial fulfillment of

the requirements for the degree of

DOCTOR OF PHILOSOPHY

in

CHEMISTRY

by

Kendra J. Adams

2018

To: Dean Michael R. Heithaus
College of Arts, Sciences and Education

This dissertation, written by Kendra J. Adams, and entitled Discovery and Targeted Monitoring of Biomarkers Using Liquid Chromatography, Ion Mobility Spectrometry, and Mass Spectrometry, having been approved in respect to style and intellectual content, is referred to you for judgment.

We have read this dissertation and recommend that it be approved.

_____
David Chatfield

_____
Anthony DeCaprio

_____
Piero Gardinali

_____
Fernando Noriega

_____
Francisco Fernandez-Lima, Major Professor

Date of Defense: March 22, 2018

The dissertation of Kendra J. Adams is approved.

_____
Dean Michael R. Heithaus
College of Arts, Sciences and Education

_____
Andrés G. Gil
Vice President for Research and Economic Development
and Dean of the University Graduate School

Florida International University, 2018

DEDICATION

This work is dedicated to all those who have lifted me up in life, to make me the strong, independent and confident woman I am today.

You know who you are.

Thank you.

ACKNOWLEDGMENTS

First and foremost, I would like to thank Dr. Fernandez-Lima, thank you for all your knowledge, assistance, patience and support. When things got tough, you were always there to push me along to the next level and proudly accomplish this goal.

To my Lima Lab family, Alyssa, Alan, Anthony, Camilo, Jacob and Paolo, we've been through it all together. I know things would not have been the same without the support, love and camaraderie we've shared with one another. Thank you all for having my back. See you on the other side!

To the rest of the Lima Lab, old and new, thank you for your help and advice throughout the years, I will always remember the time we have shared together in this lab. And to my undergrads, Dennise and Natalie, thank you for all your assistance with science and life in general; you two really helped to keep me sane throughout this journey!

To Dr. Cesar Ramirez, I will never be able to thank you enough for what you have taught me. You have helped me to become a better scientist and person. I have learned and immeasurable amount from you. Thanks for helping me develop my Teflon coating. Another thanks to Dr. Mario Gomez for your advice and for always being a ray of sunshine and an optimistic presence, even when things seemed at their worst.

Thank you to my committee: Dr. Anthony DeCaprio, Dr. Piero Gardinali, Dr. Fernando Noriega and Dr. David Chatfield for the time and effort you have dedicated to my path to Doctorate. I would also like to thank other FIU faculty members for their dedication to my success, namely, Dr. Jeremy Chambers, for always having something nice to say and Dr. Lidia Kos for her encouragement and support.

Thank you to the Department of Chemistry for their assistance in getting to this point, special thanks to Maggie, for always ensuring my various forms were filled out in a proper and timely fashion, and Jackie, for working her magic getting our entire group to conferences on a grad student budget, you guys rock! Additional thanks to the Biomolecular Sciences Institute for their support, especially to Stephanie who is always there to answer any question, big or small.

Thank you to the Florida International University Graduate School for their support in the form of a Dissertation Year Fellowship. This award has given me the opportunity to dedicate all my time towards finishing this dissertation and I greatly appreciate the luxury it has given me. Thanks to the GPSC and the Deans Office for the travel funding which has allowed me to present my research all over the country.

Finally, giant thanks to my family near and far. My parents, Kevin and Julie, who were always a phone call or quick plane ride away. Always there to lend an ear and some parental advice to keep me moving in the direction of my dreams. My sisters, Brooke and Madison, for keeping things light and fun and allowing me to vent when needed, even if you weren't completely sure what I was talking about. Grandma Adams, for believing in me and keeping the cookies coming. And lastly, to my rock and My Thunder, Ethan. Thank you for never leaving my side, through all the ups-and-downs, you were always there for a shoulder to cry on. You are my best friend and my biggest fan.

Thank you.

I hope I have made every one of you proud.

ABSTRACT OF THE DISSERTATION

DISCOVERY AND TARGETED MONITORING OF BIOMARKERS USING LIQUID CHROMATOGRAPHY, ION MOBILITY SPECTROMETRY, AND MASS SPECTROMETRY

by

Kendra J. Adams

Florida International University, 2018

Miami, Florida

Professor Francisco Fernandez-Lima, Major Professor

The complexity of biological matrices makes the detection and quantification of compounds of interest challenging. For successful targeted or untargeted identification of compounds within a biological environment, the use of complementary separation techniques is routinely required; in many situations, a single analytical technique is not sufficient. In the present dissertation, a multidimensional analytical technique was developed and evaluated, a combination of new sample preparation/extraction protocols, liquid chromatography, trapped ion mobility and mass spectrometry (e.g., LC-TIMS-MS and LC-TIMS-MS/MS). The performance of these techniques was evaluated for the detection of polybrominated diphenyl ethers metabolites, polychlorinated biphenyls metabolites in human plasma, opioid metabolites in human urine, and lipids in *Dictyostelium discoideum* cells. The new workflows and methods described in the body of this dissertation allows for rapid, selective, sensitive and high-resolution detection of biomarkers in biological matrices with increased confidence, sensitivity and shorter sample preparation and analysis time.

TABLE OF CONTENTS

CHAPTER PAGE

CHAPTER ONE: Introduction 1
1.1 Biomarker Monitoring 2
1.2 Analytical Techniques for Biomarker Monitoring 2
1.2.1 Mass Spectrometry 2
1.2.2 Chromatographic Separations 3
1.2.3 Ion Mobility Spectrometry 4
1.3 Types of Biomarkers 5
1.3.1 Exogenous Biomarkers 6
1.3.2 Endogenous Biomarkers 8
1.4 Objectives of the Dissertation 9
1.5 References 10

CHAPTER TWO: Isomer Separation of Polybrominated Diphenyl Ether Metabolites Using NanoESI-TIMS-MS 16
Abstract 17
2.2 Introduction 17
2.3 Experimental Methods 20
2.3.1 Material and reagents 20
2.3.2 TIMS-MS Analysis 21
2.3.3 Theoretical Calculations 23
2.4 Results and Discussion 23
2.5 Conclusions 28
2.6 Acknowledgements 29
2.7 References 29

CHAPTER THREE: Discovery and Targeted Monitoring of Polychlorinated Biphenyl Metabolites in Blood Plasma using LC-TIMS-TOF MS 37
3.1 Abstract 38
3.2 Introduction 38
3.3 Experimental Methods 41
3.3.1 Materials and Reagents 41
3.3.2 OH-PCB Human Blood Plasma Samples 42
3.3.3 LC-ESI- TIMS-MS Analysis 42
3.3.4 Theoretical calculations 44
3.4 Results and Discussion 45
3.5 Conclusions 54
3.6 Acknowledgements 54
3.7 References 55

CHAPTER FOUR: Analysis of Isomeric Opioids in Urine using LC-TIMS-TOF MS ... 64
4.1 Abstract 65

4.2 Introduction 65
4.3 Experimental Methods 68
4.3.1 Materials and Reagents 68
4.3.2 Human Urine “dilute-and-shoot” Sample Preparation 68
4.3.3 LC- TIMS-MS Analysis 69
Theoretical calculations 71
4.4 Results and Discussion 71
4.5 Conclusions 84
4.6 Acknowledgements 84
4.7 References 85

CHAPTER FIVE: Lipid Specific Molecular Ion Emission as a Function of the Primary Ion Characteristics in TOF-SIMS 91
5.1 Abstract 92
5.2 Introduction 92
5.3 Experimental 95
5.3.1 Sample Preparation 95
5.3.2 SIMS Analysis 96
5.4 Results and Discussion 97
5.4.1 Lipid Characterization by Class 97
5.4.2 SI Yield as a Function of the Projectile Size 103
5.4.3 SI Yield as a Function of the Projectile Energy 105
5.4.4 SI Yield as a Function of Chemical Environment 109
5.5 Summary and Conclusions 112
5.6 Acknowledgments 113
5.7 References 113

CHAPTER SIX: Discovery and Targeted Monitoring of *Dictyostelium. discoideum* Lipids Using Multidimensional LC-TIMS-MS/MS Separations 121
6.1 Abstract 122
6.2 Introduction 122
6.3 Experimental Parameters 125
6.3.1 Standards and Chemicals 125
6.3.2 Calibration Standard Preparation. 126
6.3.3 Dictyostelium discoideum Cell Preparation. 126
6.3.4 Lipid Extraction 127
6.3.5 LC-TIMS-MS/MS Separation 127
6.3.6 Data Processing and Analysis 129
6.4 Results and Discussion 130
6.5 Conclusions 144
6.6 References 144

APPENDICES 151

VITA 184

LIST OF TABLES

TABLE PAGE

Table 2.1: Experimental and theoretical CCSs for 2'-OH-BDE-68, 6-OH-BDE-47, 3-OH-BDE-47, 5-OH-BDE-47 and 4'-OH-BDE-49 isomers. 24

Table 3.1. List of experimental and theoretical m/z and CCS values for the penta-, hexa-, and hepta-CB considered in this study. 47

Table 4.1: Experimental and theoretical m/z and CCS values for the opioid analytes considered. Note: values in parentheses refer to previously reported data from DT-IMS$_{Air}$ [18, 24, 26, 44-46] 74

Table 4.2: Calibration results for analytes with (Matrix) and without urine (No Matrix) for LC-TIMS-qTOF MS and LC-qTOF MS 81

Table 4.3: Intraday Variability of CCS and RT with and without urine represented by percent relative standard deviation (%RSD) 82

Table 6.1: *sn*-positional isomer CCS and %RSD over 5 days 132

Table 6.2: Limits of detection using timsTOF with and without TIMS for lipids preferentially ionized in negative mode Note: *= visually estimated LOD 138

Table 6.3: Limits of detection using timsTOF with and without TIMS for lipids preferentially ionized in positive mode $^{+}[M+Na]^{+}$, $^{+\ +}[M-H_2O+H]^{+}$, $^{+++}[M+NH_4]^{+}$, *=visually estimated 139

LIST OF FIGURES

FIGURE PAGE

Figure 2.1. Typical mass spectra (left), IMS projections (middle) and candidate structures (right) of 2'-OH-BDE-68, 6-OH-BDE-47, 3-OH-BDE-47, 5-OH-BDE-47 and 4'-OH-BDE-49 25

Figure 2.2: Typical 2D-IMS-MS contour and IMS projection plots for the binary mixture of 3-OH-BDE-47 and 2'-OH-BDE-68 (a) and b)) and the mixture of 6-OH-BDE-47 and 4'-OH-BDE-47 (c) and d)). 27

Figure 2.3: Typical IMS projection plots from the ternary mixture of 3-OH-BDE-47, 5-OH-BDE-47 and 2'-OH-BDE-68 (a) and the mixture of 4'-OH-BDE-49, 5-OH-BDE-47 and 6-OH-BDE-47 (b). 28

Figure 3.1. Typical mobility profiles of single standards of penta-, hexa- and hepta-CBs 46

Figure 3.2. Typical mobility profiles of the single standards and binary mixtures for the hepta-CBs. 48

Figure 3.3. Typical 2D-IMS-MS contour maps of the penta-, hexa-, and hepta-CBs in water (a) and in human blood plasma (b). Note the separation of the PCB signals from potential interferences in the IMS-MS domain. 49

Figure 3.4. Typical MS projection, LC projection and extracted ion mobility profiles for a mixture of hepta-CBs, (OH-PCB 187, OH-PCB 180 and OH-PCB 172), from the LC-TOF-MS analysis of the CBs in human blood plasma. 51

Figure 3.5. Typical response curves for LC-TIMS-TOF MS as a function of a) penta- b) hexa- and c) hepta-CBs concentration in human blood plasma. Note the linear response for the penta-, hexa- and hepta- CBs from 0-5000 pg/mL in both the LC-TOF MS and LC-TIMS-TOFMS analysis 53

Figure 4.1: Typical mobility profiles of analytes and their corresponding internal standards 73

Figure 4.2: Candidate structures optimized at the DFT/B3LYP/6-311G(d,p) of the opioids considered 75

Figure 4.3: Typical IMS separations of binary mixtures: top) 6-acetylmorphine and naloxone; middle) hydromorphone and norhydrocodone; bottom) morphine and norcodeine 76

Figure 4.4: Typical LC-TIMS-TOF MS analysis of isomeric opioids. 2D-IMS-MS contour plots are shown for the highlighted LC bands 78

Figure 4.5: Relative percent deviation of RT, CCS compared to non-matrix sample and δ m/z across calibration levels (*= no change) 83

Figure 5.1. Fragmentation schemes of lipid standards of a) sphingomyelin b) phosphatidylcholine c) phosphatidylethanolamine and d) phosphatidylglycerol for positive (red) and negative (blue) mode TOF-SIMS analysis..... 100

Figure 5.2. Typical TOF-SIMS mass spectra of familiar lipids in positive and negative mode. Characteristic fragment ions (*), fatty acid fragments and intact molecular ions are denoted in the spectra. 101

Figure 5.3. intact molecular ion si yield emission using small polyatomic bi3+ and nanoparticle ar1000+ primary ion projectiles for familiar lipid standards using tof-sims in a) negative and b) positive mode. 104

Figure 5.4. Secondary ion yields as a function of the nanoparticle Au_{400}^{+4} projectile energy or Ar_n^+ cluster size for a lipid model target of phosphatidylglycerol (18:0-18:1 PG) a) Au_{400}^+ and b) Ar_n^+ negative and c) Au_{400}^+ positive mode. Notice the break in vertical axis in b)..... 108

Figure 5.5. Secondary ion yields of intact molecular ions from a single lipid standard sample and a mixture of lipid standards sample in a) positive mode Ar_{1000}^+, b) negative mode Ar_{1000}^+ c) positive mode Bi_3^+ d) negative mode Bi_3^+. 110

Figure 6.1: Interday analysis of PC lipids (n=5)..... 133

Figure 6.2: Ion mobility profiles for *sn*-isomeric phosphatidylcholine lipids using high resolution TIMS-MS. Note the shift in CCS between $[M+H]^+$ and $[M+Na]^+$ adducts 134

Figure 6.3: Signal changes in response to changes in duty cycle of the TIMS-MS 135

Figure 6.4: LOD comparison between LC-TIMS MS and LC-MS for neat lipid standards (top). Reproducibility and accuracy parameters for lipid standards spiked in blood plasma at two different spiked levels (1x and 20x) with respect to a control mix 137

Figure 6.5: Lipids from *D. discoideum* cells depicted by subclass, m/z, CCS, and RT 142

Figure 6.6: Quantitation results of select lipid subclasses PGs and PEs 143

ABBREVIATIONS AND ACRONYMS

ACN	Acetonitrile
CCS	Collisional Cross Section
DMS	Differential Mobility Spectrometry
DTIMS	Drift Time Ion Mobility Spectrometry
EDC	Endocrine Disrupting Compound/Chemical
FA	Fatty Acyls
FAIMS	high Field Asymmetric Ion Mobility Spectrometry
GC	Gas Chromatography
GL	Glycerolipids
GP	Glycerophospholipids
IMS	Ion Mobility Spectrometry
IPA	Isopropylalcohol
K_0	Mobility
LC	Liquid Chromatography
LOD	Limit of Detection
LOQ	Limit of Quantitation
MS	Mass Spectrometry
ms	Millisecond
MS/MS	Tandem Mass Spectrometry
MRM	Multiple Reaction Monitoring
m/z	mass-to-charge ratio
OH-PBDEs	Hydroxylated Polybrominated Diphenyl Ethers

OH-PCBs	Hydroxylated Polychlorinated Biphenyls
PBDEs	Polybrominated Diphenyl Ethers
PC	Glycerophosphocholine
PCBs	Polychlorinated Biphenyls
PE	Glycerophosphoethanolamine
PG	Glycerophosphoglyerol
PI	Glycerophosphoinositol
PK	Polyketides
PR	Prenol Lipids
PS	Glycerophosphoserine
RT	Retention Time
SL	Saccharolipids
SP	Sphingolipids
ST	Sterol Lipids
TIMS	Trapped Ion Mobility Spectrometry
TLC	Thin Layer Chromatography
TWIMS	Travelling Wave Ion Mobility Spectrometry
US	United States

CHAPTER ONE:
Introduction

1.1 Biomarker Monitoring

The monitoring of biomarkers has become a necessary practice in several areas of human health research over the past decade, including: drug development[1], cancer therapeutics[2-3], disease monitoring[4-5], and exposure assessment.[6-7] Biomarkers are broadly defined as.[8] Major health and research organizations such as the FDA allow for the qualification of biomarkers for drug development, basic research and clinical practices.[9] A wide variety of biomarkers exist, for example, there are genomic biomarkers, proteomic biomarkers or metabolomic biomarkers which originate from various biological processes and have the ability to reveal information based on a biological question or challenge. The chemical diversity of biomarkers makes their simultaneous detection, identification and measurement difficult within a single analytical acquisition. My dissertation focuses on the development of novel multidimensional analytical techniques for biomarkers in biological matrices.

1.2 Analytical Techniques for Biomarker Monitoring

Various analytical techniques can be utilized for biomarkers detection; they are constantly changing and developing as the advancement of technology continues. The combination of detection and separation techniques allows for a more comprehensive analytical approach for biomarker monitoring within complex matrices.

1.2.1 Mass Spectrometry

A relatively new technique for biomarker analysis includes the use of mass spectrometry (MS).[10-11] Depending on the analytical need, a MS technique can exist to provide both qualitative and quantitative results including identification of targeted or untargeted compounds using the mass-to-charge (m/z) ratio of the ions analyzed.[12-13] Mass

spectrometry is primarily used in proteomic research relating to the discovery and validation of biomarkers for cancer and other diseases.[10] A targeted multiple reaction monitoring (MRM) approach has been defined as the standard of analysis for validation of biomarkers in complex matrices.[14] Imaging mass spectrometry has been used for the identification, validation and spatial mapping of biomarkers within biological tissues for cancer diagnostics; imaging mass spectrometry allows for untargeted examination of a sample with the possibility of back-extraction of the data following initial analyses.[15-16]

The ability to discover and validate biomarkers is afforded by mass spectrometry as the primary analytical technique. Although MS provides a large share of the data in typical biomarker analysis, working with biological matrices creates complications for the technique by itself. To optimize mass spectrometry methods for compounds in biological matrices, other analytical techniques, specifically separations, are used prior to, or in tandem with, MS. Separations using chromatography are widely popular for biomarker analysis, especially those involving proteomics.

1.2.2 Chromatographic Separations

Gas chromatography (GC) and liquid chromatography (LC) are separation techniques that depend on the retention of an analyte to a certain phase of media. Gas chromatography and LC have been coupled to MS for several years and have assisted in answering major biological questions.

With the use of liquid chromatography, time is needed to flow solvents through a stationary phase and separate the compounds on the basis of a physical or chemical property such as size, polarity or hydrophobicity. Separation times needed in chromatographic procedures can vary depending on the application; from minutes (~5 min) for high throughput

methods[17-18] to hours for certain lipid or protein applications.[19] In addition to the time needed for these separations, there are other necessary items such as the proper column, (e.g., C18, monolithic, silica, C8, etc.) and the appropriate mobile phases for the separation and elution of, not only the compounds of interest, but also matrix interferences. Amounts and types of solvent also depend on the application LC is utilized for. Flow rates, temperatures and maximum pressures vary depending on the system being utilized. While liquid chromatography has provided baseline separations for compounds of similar mass and size; not all compounds can be separated by LC within the constraints of time and other resources needed.

1.2.3 Ion Mobility Spectrometry

In addition to chromatographic separations, ion mobility spectrometry (IMS) separations can be included for biomarker characterization and analysis. Ion mobility spectrometry allows for post-ionization separations in the gas phase and provides differentiation of molecules using their size and shape, or collisional cross section (CCS). Ion mobility spectrometry operates on a millisecond (ms) time scale and pairs well with chromatographic and mass spectrometric platforms. By combining IMS and chromatography, multiple dimensions of separation are achieved with the ability to couple with a variety of MS separation and detection techniques. A multi-dimensional separation allows multiple routes, not only for separations but also for identification of unknown and untargeted compounds. In contrast to LC, ion mobility separations occur in the gas phase and do not require the use of solvents. The CCS of a molecule is a physiochemical property which does not change with instrumental parameters unlike the retention time of a molecule in chromatography; an experimentally calculated CCS can be used as an identification

parameter, much like its m/z. A variety of IMS platforms have been developed to separate ions on the basis of different principles. Commercial ion mobility analyzers include platforms that operate using drift time (DTIMS), those that operate using ions travelling through a wave of changing voltages (TWIMS), ions separated on the basis of the differences in mobilities in high versus low-electric fields (FAIMS) or those based on the mobility of an ion moving through a ramp of electric field voltages and a flow of gas (TIMS).[20-21] Each IMS instrument has advantages and disadvantages, including the ability to report accurate CCS values, the ability of simultaneous dual polarity analyses, its sensitivity, and the maximum resolving power achieved by the technique. The TIMS was pioneered in our research group in collaboration with Dr. Melvin A. Park and Dr. Mark E Ridgeway from Bruker Daltonics Inc. and its advantages will be demonstrated herein. The TIMS platform displays unrivaled sensitivity and resolving power and the ability to report CCS using first principles. Noteworthy is that the highest reported liner IMS resolving power is included as part of this dissertation (R ~ 400).

1.3 Types of Biomarkers

Compounds such as proteins, lipids and metabolites have proven helpful in following changes in a system after it has been subjected to an external disease or other stimulation. We know that biomolecules in a system change according to the health of that system but we are still working on what those changes mean and what types of changes are associated with which diseases and how biomarker monitoring can be used to diagnose and treat diseases rapidly and accurately. For the research included, the biomarkers analyzed will be broken down into two subclasses: exogenous and endogenous.

1.3.1 Exogenous Biomarkers

There are thousands of compounds that can be considered exogenous biomarkers, or compounds that exist in an organism that are not naturally occurring, have entered the organism from the environment and can be related to a change in an organism. Exogenous biomarkers are typically analyzed in the field of exposomics, which refers to the study of the entirety of chemicals an individual has encountered throughout their lifetime. These compounds come from the external environment and the effects those compounds have on the individuals' health are studied. A human's exposome will fluctuate throughout their lifetime as a function of their location, diet and lifestyle choices. The study of exposomics is an "up-and-coming" –omics comparable to genomics, proteomics, metabolomics and lipidomics.[22]

One major class of compounds that has been involved in the human exposome includes endocrine disrupting chemicals (EDCs), which are compounds that negatively impact the endocrine system. Polybrominated diphenyl ethers (PBDEs) and polychlorinated biphenyls (PCBs) are two groups of EDCs that are discussed and analyzed in the subsequent research. Polychlorinated biphenyls and PBDEs are man-made compounds that were developed and used for consumer purposes such as flame-retardants for textiles and furniture, insulators in electric equipment, caulk, plasticizers in paints, and other plastic and rubber products.[23] Polybrominated diphenyl ethers were developed and used in the United States beginning in the 1970s and have been slowly and voluntarily phased out of production by their manufacturers beginning in the early 2000s.[24] Polybrominated diphenyl ethers consist of groups of compounds with differing amounts of bromine atoms on diphenyl ether rings called congeners. Homologous, or isomeric compounds exist within each of the congener

groups and have the same chemical formula and mass spectrometric profile. In the US, there are three classes of PBDE congeners that have been commercially produced: pentabromodiphenyl ethers, octabromodiphenyl ethers and decabromodiphenyl ethers.[23] The PBDEs are not easily decomposed and, lower brominated congeners typically bioaccumulate in the environment and have been detected in water[25-26], soil[27-29] and aquatic species.[30] In humans, PBDEs have been found in breast milk, blood and tissue Polybrominated diphenyl ethers are converted to hydroxylated-PBDEs (OH-PBDEs) through metabolism via oxidative pathways in human liver cells.[31-34]

Polychlorinated biphenyls were produced and used in the US from 1929 until 1979 when they were banned from production due to the major negative health effects they have on humans.[35-38] Like PBDEs, they exist as groups of congeners with a varying number of chlorine atoms attached to a biphenyl group. Polychlorinated biphenyls can be found across the world due to their robust nature and their ability to be streamlined into the water cycle and carried across oceans in both air and water medium. Polychlorinated biphenyls have been extensively studied for several decades and researchers have concluded that they are likely human carcinogens on the basis of animal and human exposure research.[39-40] Metabolism of PCBs to hydroxylated-PCBs (OH-PCBs) occurs via Cytochrome P-450 with the location of the chlorines and the OH group posing a significant impact on the toxicity of the compound.[36, 41-43]

Another example of exogenous compounds includes intentionally administered substances such as drugs. Although drugs are not technically considered biomarkers, for this research, they are used as a tool for the development of analytical methods for the detection and identification of compounds in human urine, which can be applied to

traditional biomarker analysis. A major concern across the US is the rising use and abuse of opioids.[44-45] In this research, opioids are used as biomarkers for illicit and prescription pain management drug use. Drugs are considered part of the human exposome and reveal key facts about the human such as certain habits or locations they have been in.

1.3.2 Endogenous Biomarkers

Many naturally occurring compounds are considered useful biomarkers for detection and determination of causation of diseases. Compounds such as lipids, peptides, proteins, and DNA have been used as monitoring tools for various types of disease in humans and model organisms. In this work, lipids are the endogenous biomarker of choice for analysis. Lipids are fats involved in cell signaling, neurotransmissions and energy storage, and play an integral part of bilipid layered cell membranes. Lipids are a diverse class of molecules containing several categories including: fatty acyls (FA), glycerolipids (GL), glycerophospholipids (GP), sphingolipids (SP), sterol lipids (ST), prenol lipids (PR), saccharolipids, (SL) and polyketides (PK). Each lipid category differs on the basis of its "building-block"; whether it is derived from a ketoacyl or an isoprene group as well as its general structure and make-up.[46-47] Lipid categories can be further broken-down into lipid subclasses, for example GPs are broken down into several subclasses, including: glycerophosphocholine (PC), glycerophosphoethanolamines (PE), glycerophosphoserine (PS), glycerophosphoglycerol (PG) and glycerophosphoinositol (PI). Lipids have served as biomarkers for various disease pathways or exposures such as, markers for air pollution[6], Alzheimer's Disease[48-49], multiple sclerosis[50], and many others.[51] With such diversity in structure and size, method development for lipidomics analysis has become a popular topic for publications in recent years.[52-54] Although much as been discovered regarding lipids in

biological structures, the research has been accomplished using several analytical methods to target different lipid classes and groups.[51, 55] The future of lipidomic research lies in the development of an singular analytical method for complete lipid discovery, monitoring and quantitation.[55-56]

1.4 Objectives of the Dissertation

This dissertation is built on the development of new analytical workflows for the analysis of biomarkers in biological matrices. Six chapters are included beginning with the Introduction. Chapter Two, published in the International Journal for Ion Mobility Spectrometry 2016, Vol. 19 Issue 2-3, focuses on the analytical power of TIMS-MS for the separation of isomeric metabolites of endocrine disruptors. Chapter Three combines LC, TIMS and MS for separation and analysis of OH-PCBs in human blood plasma. Chapter Three was published in The International Journal of Mass Spectrometry and is currently available online. Chapter Four, currently accepted with minor revisions in Talanta, proposes a multidimensional LC-TIMS-MS approach for untargeted screening and quantitation of opioids in human urine. Chapter Five entails the surface analysis of lipids using TOF-SIMS with minimal sample volume and little preparation prior to analysis. Chapter Five was published in The Journal of Vacuum Science and Technology B, 2016 Volume 34, Issue 5. The final chapter included in this dissertation combines LC-TIMS-MS/MS for lipidomic discovery and monitoring for the case of *Dictyostelium discoideum* cells at different biological stages. Chapter Six will be submitted to *Analytical Chemistry* for publication before the dissertation defense.

1.5 References

1. Hurko, O., The uses of biomarkers in drug development. *Annals of the New York Academy of Sciences* **2009,** *1180* (1), 1-10.

2. Topalian, S. L.; Taube, J. M.; Anders, R. A.; Pardoll, D. M., Mechanism-driven biomarkers to guide immune checkpoint blockade in cancer therapy. *Nature Reviews. Cancer* **2016,** *16* (5), 275-287.

3. Khleif, S. N.; Doroshow, J. H.; Hait, W. N., AACR-FDA-NCI Cancer Biomarkers Collaborative consensus report: advancing the use of biomarkers in cancer drug development. *Clinical Cancer Research* **2010,** *16* (13), 3299-3318.

4. Benitez, J.-M.; Meuwis, M.-A.; Reenaers, C.; Van Kemseke, C.; Meunier, P.; Louis, E., Role of endoscopy, cross-sectional imaging and biomarkers in Crohn's disease monitoring. *Gut* **2013,** *62* (12), 1806-1816.

5. Mangialasche, F.; Solomon, A.; Winblad, B.; Mecocci, P.; Kivipelto, M., Alzheimer's disease: clinical trials and drug development. *The Lancet Neurology* **2010,** *9* (7), 702-716.

6. Møller, P.; Loft, S., Oxidative damage to DNA and lipids as biomarkers of exposure to air pollution. *Environmental Health Perspectives* **2010,** *118* (8), 1126.

7. Haug, L. S.; Huber, S.; Becher, G.; Thomsen, C., Characterisation of human exposure pathways to perfluorinated compounds — Comparing exposure estimates with biomarkers of exposure. *Environment International* **2011,** *37* (4), 687-693.

8. Strimbu, K.; Tavel, J. A., What are Biomarkers? *Current Opinion in HIV and AIDS* **2010,** *5* (6), 463-466.

9. Biomarker Qualification Program. www.fda.gov/Drugs/DevelopmentApprovalProcess/DrugDevelopmentToolsQualificationProgram/BiomarkerQualificationProgram/default (accessed 12/30/2017).

10. Smith, R. D., Mass spectrometry in biomarker applications: from untargeted discovery to targeted verification, and implications for platform convergence and clinical application. *Clinical Chemistry* **2012,** *58* (3), 528-530.

11. Hawkridge, A. M.; Muddiman, D. C., Mass spectrometry–based biomarker discovery: toward a global proteome index of individuality. *Annual Review of Analytical Chemistry* **2009,** *2*, 265-277.

12. Khamis, M. M.; Adamko, D. J.; El-Aneed, A., Mass spectrometric based approaches in urine metabolomics and biomarker discovery. *Mass Spectrometry Reviews* **2017,** *36* (2), 115-134.

13. Diamandis, E. P., Mass spectrometry as a diagnostic and a cancer biomarker discovery tool opportunities and potential limitations. *Molecular & Cellular Proteomics* **2004,** *3* (4), 367-378.

14. Gillette, M. A.; Carr, S. A., Quantitative analysis of peptides and proteins in biomedicine by targeted mass spectrometry. *Nature Methods* **2013,** *10* (1), 28-34.

15. Schwamborn, K., Imaging mass spectrometry in biomarker discovery and validation. *Journal of Proteomics* **2012,** *75* (16), 4990-4998.

16. Cazares, L. H.; Troyer, D. A.; Wang, B.; Drake, R. R.; Semmes, O. J., MALDI tissue imaging: from biomarker discovery to clinical applications. *Analytical and Bioanalytical Chemistry* **2011,** *401* (1), 17-27.

17. House, C.; Lyttle, C.; Blanchard, C., An ultra-high-pressure liquid chromatography tandem mass spectrometry (UPLC-MS/MS) method for the detection of cannabinoids in whole blood using solid phase extraction. *Canadian Society of Forensic Science Journal* **2017**, 1-11.

18. Muñoz-Muñoz, A. C.; Pekol, T.; Schubring, D.; Johnson, C.; Andrade, L., Identification of Novel Opioid Interferences using High-Resolution Mass Spectrometry. *Journal of Analytical Toxicology* **2017**, 1-11.

19. Baglai, A.; Gargano, A. F. G.; Jordens, J.; Mengerink, Y.; Honing, M.; van der Wal, S.; Schoenmakers, P. J., Comprehensive lipidomic analysis of human plasma using multidimensional liquid- and gas-phase separations: Two-dimensional liquid chromatography–mass spectrometry vs. liquid chromatography–trapped-ion-mobility–mass spectrometry. *Journal of Chromatography A* **2017,** *1530* (Supplement C), 90-103.

20. Kanu, A. B.; Dwivedi, P.; Tam, M.; Matz, L.; Hill, H. H., Ion mobility–mass spectrometry. *Journal of Mass Spectrometry* **2008,** *43* (1), 1-22.

21. Cumeras, R.; Figueras, E.; Davis, C.; Baumbach, J. I.; Gracia, I., Review on ion mobility spectrometry. Part 1: current instrumentation. *Analyst* **2015,** *140* (5), 1376-1390.

22. Exposome and Exposomics. www.cdc.gov/niosh/topics/exposome/default.html (accessed January 2, 2018).

23. Agency, U. S. E. P. Technical Fact Sheet- Polybrominated Diphenyl Ethers (PBDEs). https://www.epa.gov/sites/production/files/2014-03/documents/ffrrofactsheet_contaminant_perchlorate_january2014_final_0.pdf (accessed November 11, 2017).

24. Darnerud, P. O.; Eriksen, G. S.; Jóhannesson, T.; Larsen, P. B.; Viluksela, M., Polybrominated diphenyl ethers: occurrence, dietary exposure, and toxicology. *Environmental Health Perspectives* **2001,** *109* (Suppl 1), 49.

25. Moon, H.-B.; Choi, M.; Yu, J.; Jung, R.-H.; Choi, H.-G., Contamination and potential sources of polybrominated diphenyl ethers (PBDEs) in water and sediment from the artificial Lake Shihwa, Korea. *Chemosphere* **2012,** *88* (7), 837-843.

26. Ueno, D.; Darling, C.; Alaee, M.; Pacepavicius, G.; Teixeira, C.; Campbell, L.; Letcher, R. J.; Bergman, Å.; Marsh, G.; Muir, D., Hydroxylated polybrominated diphenyl ethers (OH-PBDEs) in the abiotic environment: surface water and precipitation from Ontario, Canada. *Environmental Science & Technology* **2008,** *42* (5), 1657-1664.

27. Wang, J.; Lin, Z.; Lin, K.; Wang, C.; Zhang, W.; Cui, C.; Lin, J.; Dong, Q.; Huang, C., Polybrominated diphenyl ethers in water, sediment, soil, and biological samples from different industrial areas in Zhejiang, China. *Journal of Hazardous Materials* **2011,** *197*, 211-219.

28. Hites, R. A., Polybrominated diphenyl ethers in the environment and in people: a meta-analysis of concentrations. *Environmental Science & Technology* **2004,** *38* (4), 945-956.

29. Huang, H.; Zhang, S.; Christie, P., Plant uptake and dissipation of PBDEs in the soils of electronic waste recycling sites. *Environmental Pollution* **2011,** *159* (1), 238-243.

30. Szlinder-Richert, J.; Barska, I.; Usydus, Z.; Grabic, R., Polybrominated diphenyl ethers (PBDEs) in selected fish species from the southern Baltic Sea. *Chemosphere* **2010,** *78* (6), 695-700.

31. Stapleton, H. M.; Kelly, S. M.; Pei, R.; Letcher, R. J.; Gunsch, C., Metabolism of polybrominated diphenyl ethers (PBDEs) by human hepatocytes in vitro. *Environmental Health Perspectives* **2009,** *117* (2), 197.

32. Covaci, A.; Voorspoels, S.; de Boer, J., Determination of brominated flame retardants, with emphasis on polybrominated diphenyl ethers (PBDEs) in environmental and human samples—a review. *Environment International* **2003,** *29* (6), 735-756.

33. Athanasiadou, M.; Cuadra, S. N.; Bergman, A.; Jakobsson, K., Polybrominated Diphenyl Ethers (PBDEs) and Bioaccumulative Hydroxylated PBDE MEtabolites in Young Humans from Managua, Nicaragua. *Environmental Health Perspectives* **2008,** *116* (2), 400-408.

34. Lupton, S. J.; McGarrigle, B. P.; Olson, J. R.; Wood, T. D.; Aga, D. S., Analysis of hydroxylated polybrominated diphenyl ether metabolites by liquid chromatography/atmospheric pressure chemical ionization tandem mass spectrometry. *Rapid Communications in Mass Spectrometry* **2010,** *24* (15), 2227-2235.

35. Diamond, M. L.; Melymuk, L.; Csiszar, S. A.; Robson, M., Estimation of PCB stocks, emissions, and urban fate: will our policies reduce concentrations and exposure? ACS Publications: 2010.

36. Kania-Korwel, I.; Lehmler, H.-J., Chiral polychlorinated biphenyls: absorption, metabolism and excretion—a review. *Environmental Science and Pollution Research* **2016,** *23* (3), 2042-2057.

37. Quinete, N.; Schettgen, T.; Bertram, J.; Kraus, T., Occurrence and distribution of PCB metabolites in blood and their potential health effects in humans: a review. *Environmental Science and Pollution Research* **2014,** *21* (20), 11951-11972.

38. Ross, G., The public health implications of polychlorinated biphenyls (PCBs) in the environment. *Ecotoxicology and Environmental Safety* **2004,** *59* (3), 275-291.

39. Agency, U. S. E. P. Learn About Polychlorinated Biphenyls (PCBs). https://www.epa.gov/pcbs/learn-about-polychlorinated-biphenyls-pcbs#healtheffects (accessed November 11, 2017).

40. Lauby-Secretan, B.; Loomis, D.; Grosse, Y.; El Ghissassi, F.; Bouvard, V.; Benbrahim-Tallaa, L.; Guha, N.; Baan, R.; Mattock, H.; Straif, K., Carcinogenicity of

polychlorinated biphenyls and polybrominated biphenyls. *The Lancet. Oncology* **2013,** *14* (4), 287.

41. Bergman, A.; Klasson-Wehler, E.; Kuroki, H., Selective retention of hydroxylated PCB metabolites in blood. *Environmental Health Perspectives* **1994,** *102* (5), 464.

42. Letcher, R. J.; Klasson-Wehler, E.; Bergman, A., Methyl sulfone and hydroxylated metabolites of polychlorinated biphenyls. In *Volume 3 Anthropogenic Compounds Part K*, Springer: 2000; pp 315-359.

43. Purkey, H. E.; Palaninathan, S. K.; Kent, K. C.; Smith, C.; Safe, S. H.; Sacchettini, J. C.; Kelly, J. W., Hydroxylated polychlorinated biphenyls selectively bind transthyretin in blood and inhibit amyloidogenesis: rationalizing rodent PCB toxicity. *Chemistry & Biology* **2004,** *11* (12), 1719-1728.

44. Okie, S., A flood of opioids, a rising tide of deaths. *New England Journal of Medicine* **2010,** *363* (21), 1981-1985.

45. Rudd, R. A., Increases in drug and opioid-involved overdose deaths—United States, 2010–2015. *Morbidity and Mortality Weekly Report* **2016,** *65*, 1445-1452.

46. Fahy, E.; Subramaniam, S.; Brown, H. A.; Glass, C. K.; Merrill, A. H.; Murphy, R. C.; Raetz, C. R.; Russell, D. W.; Seyama, Y.; Shaw, W., A comprehensive classification system for lipids. *Journal of Lipid Research* **2005,** *46* (5), 839-862.

47. Fahy, E.; Subramaniam, S.; Murphy, R. C.; Nishijima, M.; Raetz, C. R.; Shimizu, T.; Spener, F.; van Meer, G.; Wakelam, M. J.; Dennis, E. A., Update of the LIPID MAPS comprehensive classification system for lipids. *Journal of Lipid Research* **2009,** *50* (Supplement), S9-S14.

48. Kosicek, M.; Hecimovic, S., Phospholipids and Alzheimer's disease: alterations, mechanisms and potential biomarkers. *International Journal of Molecular Sciences* **2013,** *14* (1), 1310-1322.

49. González-Domínguez, R.; García-Barrera, T.; Gómez-Ariza, J. L., Metabolomic study of lipids in serum for biomarker discovery in Alzheimer's disease using direct infusion mass spectrometry. *Journal of Pharmaceutical and Biomedical Analysis* **2014,** *98* (Supplement C), 321-326.

50. Quintana, F. J.; Yeste, A.; Weiner, H. L.; Covacu, R., Lipids and lipid-reactive antibodies as biomarkers for multiple sclerosis. *Journal of Neuroimmunology* **2012,** *248* (1), 53-57.

51. Zhao, Y.-Y.; Cheng, X.; Lin, R.-C., Lipidomics applications for discovering biomarkers of diseases in clinical chemistry. *International Review of Cell and Molecular Biology* **2014,** *313* (7), 1.

52. Lam, S. M.; Shui, G., Lipidomics as a Principal Tool for Advancing Biomedical Research. *Journal of Genetics and Genomics* **2013,** *40* (8), 375-390.

53. Stock, J., The emerging role of lipidomics. *Atherosclerosis* **2012,** *221* (1), 38-40.

54. Sandra, K.; Sandra, P., Lipidomics from an analytical perspective. *Current Opinion in Chemical Biology* **2013,** *17* (5), 847-853.

55. Brügger, B., Lipidomics: analysis of the lipid composition of cells and subcellular organelles by electrospray ionization mass spectrometry. *Annual Review of Biochemistry* **2014,** *83*, 79-98.

56. Southam, A. D.; Weber, R. J.; Engel, J.; Jones, M. R.; Viant, M. R., A complete workflow for high-resolution spectral-stitching nanoelectrospray direct-infusion mass-spectrometry-based metabolomics and lipidomics. *Nature protocols* **2017,** *12* (2), 310.

CHAPTER TWO:
Isomer Separation of Polybrominated Diphenyl Ether Metabolites Using NanoESI-TIMS-MS

This chapter was published in the International Journal for Ion Mobility Spectrometry

and adapted with permission from all authors.

Kendra J. Adams., Dennise Montero, Diana Aga, Francisco Fernandez-Lima (2016).

International Journal for Ion Mobility Spectrometry, *19*(2-3), 69-76

Abstract

In this paper, high-resolution nano-electrospray ionization-trapped ion mobility spectrometry coupled to mass spectrometry (nESI-TIMS-MS) is used for the study of hydroxylated polybrominated diphenyl ether (OH-PBDE) metabolites. In particular, experimental ion-neutral collision cross sections (CCS) were measured for five structural OH-PBDE isomers using TIMS-MS. Candidate structures were proposed for each IMS band observed in good agreement with the experimental CCS measurements (5% error). The analytical power of TIMS-MS to baseline and partially separate structural isomers of OH-BDE in binary and ternary mixtures is shown for single charge species with a mobility resolving power of $R_{IMS} \sim 400$. This work provides the proof of concept for the analysis of low concentration OH-PBDE in environmental samples based on accurate collision cross section and mass measurements without the need for derivatization and pre-fractionation protocols, thus significantly reducing the cost and analysis time.

2.2 Introduction

Polybrominated diphenyl ethers (PBDEs) are members of the brominated flame retardant family (BFR), which have been frequently added since the 1970s to commercial products (e.g., plastics and textiles).[1] PBDEs are not chemically bound to the products and are easily released and accumulated in the environment, wildlife and humans.[1-3] There are three major classes of PBDEs; PBDEs, methoxylated PBDEs (MeO-PBDEs) and hydroxylated PBDEs (OH-PBDEs). The former class is anthropogenically created and released into the environment from commercial production. Previous research has shown that both MeO- and OH-PBDEs are formed from two sources:they are naturally occurring and produced by alga or they are metabolites from commercially produced PBDEs that

have been released into the environment.[4-6] Studies have shown that PBDE metabolites such as OH-PBDEs are more toxic than their PBDE counterparts.[7-10] Differences in toxicity/activity of PBDEs and their metabolites have been noted based on the location of hydroxyl group and bromine atoms on the diphenyl rings.[9-14] The variation in toxicity makes separation and identification of isomeric OH-PBDEs important for exposome profiling in the environment, humans and wildlife.

Traditional methods such as gas chromatography-mass spectrometry (GC-MS) and liquid chromatography-mass spectrometry (LC-MS) have allowed for separation and identification of PBDEs and their metabolites. For example, previous studies have utilized GC-MS for profiling of PBDEs, OH-PBDEs and MeO-PBDEs in human breast milk and serum.[15-17] In addition, GC-MS has been utilized for PBDE analysis in wildlife and environmental samples (e.g., different species of fish and various river sediment samples).[17-18] The use of GC-MS for analysis of OH-PBDEs requires derivatiziation of the molecules to more volatile metabolites such as MeO-.[15, 17, 19] Previously, Simpson *et al.* analyzed hydroxylated PBDE metabolites via GC-MS and COSMO-RS to determine experimental retention times and theoretical boiling points of the compounds. The COnductor-like Screening MOdel for Realistic Solvents (COSMO-RS) is a method that is used to calculate chemical potentials in liquids using the screening charge density.[20-22] Thermodynamic properties of molecules, such as boiling points, were predicted using COSMO-RS, converted to relative retention times and compared to experimental retention time values from GC-MS studies.[19, 21-22] This research proved that OH-PBDE isomers could be separated via retention on a GC-MS column and unknown metabolites could be identified by the combination of theoretically calculated boiling points and experimentally

determined retention times after derivatization of the hydroxylated compounds.[19] In addition, four out of the five OH-PBDE metabolites analyzed in this research have previously been extracted and identified from human serum based on GC-MS analysis.[15]

Liquid chromatography-mass spectrometry (LC-MS) has also been used for both identification and quantification of PBDE metabolites within various matrices. Lacorte *et al.* developed an LC-ISP-MS/MS methodology in which eight different OH-PBDEs were identified and quantified from soil, fish and sludge.[23] In these analyses, no sample derivatization was required, saving time and resources as well as allowing for the simultaneous analysis of both OH-PBDEs and MeO-PBDEs metabolites.[23-25] LC-MS techniques have also been used to successfully analyze for similar metabolites, such as the chromatographic separation of 3-OH-BDE-47, 5-OH-BDE-47, and 6-OH-BDE-47 and the subsequent identification and confirmation via tandem mass spectrometry.[24] Although both GC-MS and LC-MS have proven valid methods for analysis and quantification of OH-PBDEs as standards and within biological matrices, the analyses still require a significant amount of time (i.e., chromatographic separations typically lasting 40 minutes) and derivatizing agents for GC-MS.

Recent progress in gas-phase, post-ionization separations has been focused on the development of hyphenated techniques in order to achieve higher sensitivity, better separation and reduction of the chemical noise. Different variants of ion mobility spectrometry have been successfully coupled to mass spectrometry (e.g., periodic focusing DC ion guide,[26-28] segmented quadrupole drift cell,[29] multistage IMS,[30-32] field asymmetric waveform IMS,[33-34] travelling wave IMS,[35] trapped ion mobility spectrometry,[36-38] and cyclic drift tube mobility spectrometry.[39-40] In particular, TIMS-MS has proved to provide

high mobility resolution separations (R~150-300)[37, 41] and the measurement of accurate mobility values using first principles.[37] TIMS-MS provides complementary information separating samples in two dimensions: size-to-charge and mass-to-charge separation on a very short time scale of analysis (hundreds of milliseconds).[36-37] We have previously used TIMS-MS for detection of small molecules within complex matrices,[42] the separation of polyaromatic hydrocarbons,[43-44] targeted analysis of endocrine disruptors,[45] and the analysis of the conformational dynamics of small molecules and biomolecules.[41, 46-52]

In this paper, we explore the potential of TIMS-MS for the analysis of isomeric metabolites of PBDEs. Five OH-tetra-brominated diphenyl ethers are studied: 3-OH-BDE-47, 5-OH-BDE-47, 6-OH-BDE-47, 4'-OH-BDE-49 and 2'-OH-BDE-68. Accurate mobility and ion-neutral CCSs were measured using nESI-TIMS-MS. Candidate structures were proposed for each IMS band observed of the individual OH-BDE. The capability of TIMS to separate structural isomers was evaluated for binary and ternary mixtures of OH-BDE. This is the first time resolving powers of ~350-400 are reported for single charge species using TIMS-MS.

2.3 Experimental Methods

2.3.1 Material and reagents

Hydroxylated tetra-brominated diphenyl ether standards were purchased from Accustandard Inc. (New Haven, CT, USA) and used as received. Five OH-PBDEs were analyzed in this study: 3-OH-BDE-47, 5-OH-BDE-47, 6-OH-BDE-47, 4'-OH-BDE-49 and 2'-OH-BDE-68. Binary and ternary mixtures were created by mixing equal volumes of individual standards and diluted to a final concentration of 200 nM. An aliquot (15μL) of each sample was deposited into a pulled glass capillary tip for nESI-TIMS-MS analysis.

All solvents used in these studies were analytical grade or better and purchased from Fisher Scientific (Pittsburg, PA).

2.3.2 TIMS-MS Analysis

TIMS-MS is a technique that combines size separation using ion mobility techniques and mass-to-charge separation via mass spectrometry allowing for ion identification.[36-38] This separation technique is built on the utilization of an electric field to hold ions against a flow of gas which pushes ions toward the exit of the cell. The difference in pressure across the cell ($P_1>P_2$; where P_1 is measured at the entrance and P_2 is measured at the exit) dictates the velocity of the gas (N_2) and subsequently ensures the ions consistently move toward the exit of the mobility region. A variation in voltage across the mobility region (low potential at the entrance and high potential at the exit) of the cell allows for the ions to be held in a place against the bath gas flow based on their size-to-charge ratio.[36-38] The mobility separation in a TIMS cell depends on the velocity of the bath gas, radial ion confinement (applied by an RF potential (measured as Vpp)) and ion elution parameters (ramp).[36-38] The ions are successively eluted from the tunnel by decreasing the electric field in stepwise increments (referred as the "ramp"). The eluted ions are further separated by mass in a time-of-flight (TOF) mass spectrometer. The results provide both a mass spectrum of the sample and mobility values which are correlated to collisional cross sections to determine the size of the molecules.[36-38, 53-57] The mobility in a TIMS analyzer can be described as:

$$K_i = \upsilon_g / E_x(i) \cong A(1/(V_{out} - V_{elu}(i)) \quad (1)$$

where υ_g is the velocity of the bath gas in the mobility cell and $E_x(i)$ is the electric field at which the specific packet of ions elute. These parameters can be related to the voltage the

ions elute at (V_{elu}(i)) and the voltage of the mobility region exit. The A value is a calibration constant that is experimentally determined using a standard of known mobility. From the K or mobility value, the collisional cross section (CCS) can be related by the following equation:

$$CCS = \frac{(18\pi)^{\frac{1}{2}}}{16}\frac{z}{(k_b T)^{\frac{1}{2}}}\left[\frac{1}{m_1}+\frac{1}{m_b}\right]^{\frac{1}{2}}\frac{1}{K}\frac{760}{P}\frac{T}{273.15}\frac{1}{N^*} \quad (2)$$

The charge of the ion is represented by *z*, k_b represents the Boltzman constant, m_1 and m_b are the masses of molecular ion and the bath gas and N^* is the number density.

The mobility resolving power for the analysis considered was calculated as

$$R = CCS/\Delta CCS \quad (3)$$

Collisional cross sections were calculated using Tunemix as a calibration standard. Details on the Tunemix structures (e.g., *m/z* = 322 K_0 = 1.376 $cm^2\ V^{-1}\ s^{-1}$ and *m/z* = 622 K_0 = 1.013 $cm^2\ V^{-1}\ s^{-1}$) can be found elsewhere.[37, 58] The instrument was operated in wide and narrow mobility selection modes, depending on the analytical challenge. For wide range mobility analysis, the gas velocity was defined by the entrance and exit TIMS roughing impedance (P_1 = 1.6 and P_2 = 0.62 mbar) and a voltage ramp of 200 V with V_{out} = 60 V were used. For narrow mobility selection experiments (higher resolving power), the velocity of the gas was increased (P_1= 3.2 and P_2=1.4 mbar) and a voltages 10 V and 60 V were used for the ramp and V_{out}, respectively. A Vpp = 300 V and 880 kHz radiofrequency was kept constant for all the experiments and allowed for radial confinement of the ions within the TIMS analyzer. For the nESI source, quartz glass capillaries (O.D.: 1.0 mm and I.D.: 0.70 mm) were pulled utilizing a P-2000 micropipette laser puller (Sutter Instruments,

Novato, CA) and loaded with 15 µL aliquot of each sample solution. A typical nESI source voltage of - 600-1200 V was applied.

2.3.3 Theoretical Calculations

A pool of candidate structures was proposed for each OH-BDE standard analyzed in the TIMS- MS experiments. Final structures were optimized at the DFT/B3LYP/6-311G(d,p) level using Gaussian software.[59] Vibrational frequencies were calculated to guarantee that the optimized structures correspond to actual minima in the energy space and zero-point energy corrections were applied to calculate the relative stability between the structures. Theoretical ion-neutral collision cross sections were calculated using MOBCAL [60-61] software for nitrogen as a bath gas at ca. 300K. Partial atomic charges were calculated using the Merz-Singh-Kollman scheme constrained to the molecular dipole moment.[62-63]

2.4 Results and Discussion

TIMS-MS analyses of individual OH-BDE standards including 3-OH-BDE-47, 5-OH-BDE-47, 6-OH-BDE-47, 4'-OH-BDE-49 and 2'-OH-BDE-68 resulted in a single IMS band for each structural isomer. Analysis of the mass spectra revealed the expected isotopic pattern of a tetra-brominated compound for the deprotonated molecular ion $[M-H]^-$ (Figure 2.2.1). Analysis of the IMS projections showed that all individual compounds have very similar experimental CCS values, ranging from 194.5-197.3 $Å^2$ (Figure 2.1 and Table 4.2.1). In particular, 2'-OH-BDE-68 has the smallest CCS (194.5 $Å^2$) while 4'-OH-BDE-49 has the largest CCS (197.3 $Å^2$). The 6'-OH-BDE-47 and 2'-OH-BDE-68 have very similar CCSs (194.7 $Å^2$ and 194.5 $Å^2$, respectively). In addition, 3-OH-BDE-47 and 5-OH-BDE-47 also have very similar experimental CCS (196.0 and 196.6 $Å^2$, respectively).

Candidate structures were proposed for each IMS band observed (see Figure 2.2.1). Inspection of the optimized structures at the DFT/B3LYP/6-311G(d,p) shows that OH-BDE are near planar conformations, with a slight twist around the central oxygen atom, depending on the position of the Br atoms (ortho *vs* para positions) (Figure 2.2.1). A small error was observed between the theoretical and experimental CCS values (less than ±5%). This small error can be attributed to the fact that the MOBCAL program does not properly describe bromine atoms for the CCS calculations.[60-61]

	$[M-H]^-$ **m/z**	**Experimental**	**Theoretical**
		TIMS ($Å^2$)	TM ($Å^2$)
2'-OH-BDE-68	500.7834	194.5	192
6-OH-BDE-47	500.7834	194.7	186
3-OH-BDE-47	500.7834	196.0	188
5-OH-BDE-47	500.7834	196.6	190
4'-OH-BDE-49	500.7834	197.3	193

Table 2.1: Experimental and theoretical CCSs for 2'-OH-BDE-68, 6-OH-BDE-47, 3-OH-BDE-47, 5-OH-BDE-47 and 4'-OH-BDE-49 isomers.

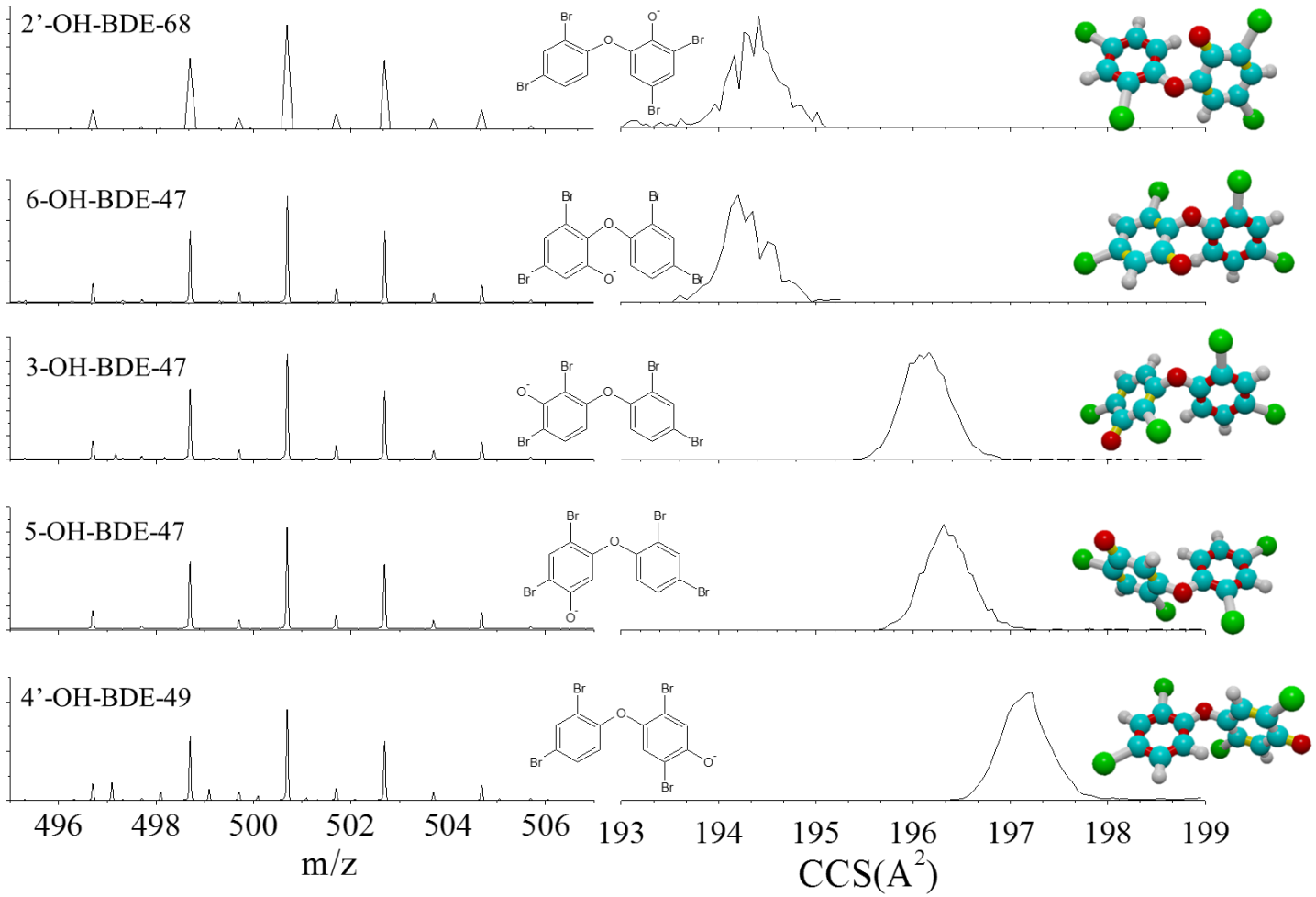

Figure 2.1. Typical mass spectra (left), IMS projections (middle) and candidate structures (right) of 2'-OH-BDE-68, 6-OH-BDE-47, 3-OH-BDE-47, 5-OH-BDE-47 and 4'-OH-BDE-49

Following analysis of individual OH-PBDE compounds, binary and ternary mixtures of OH-PBDE standards were analyzed in order to evaluate the potential of nESI-TIMS-MS for the separation of isomeric mixtures of these compounds. The analysis of a binary mixture containing 2'-OH-BDE-68 and 3-OH-BDE-47 shows that these two isomers can be baseline resolved with a mobility resolving power of ~350 (Figure 2.2). Closer inspection shows that 3-OH-BDE-47 elutes from the mobility cell at a voltage of 143 V and 2'-OH-BDE-68 elutes at a voltage of 141 V while the same isotopic pattern was observed in the *m/z* domain (Figure 2.2a). Conversion of the trapping voltage to CCS shows that the 3-OH-BDE-47 peak is centered at 196.0 $Å^2$ while 2'-OH-BDE-68 is centered at 194.7 $Å^2$ (Figure 2.2b), which are in good agreement with the analysis of individual compounds (Figure 2.2.1). A binary mixture of 4'-OH-BDE-49 and 6-OH-BDE-47 was analyzed using the same instrumental conditions. The 2D-IMS-MS contour plot shows two mobility bands eluting from the cell at trapping voltages of 144 V and 142 V respectively with the same *m/z* profile corresponding to the isotopic distribution of tetra-brominated OH-BDEs (Figure 2.2c). Conversion of the trapping voltage to the CCS shows baseline separation of 4'-OH-BDE-49 centered at 197.3 $Å^2$ and 6-OH-BDE-47 centered at 194.7 $Å^2$ with a resolving power of ~ 320-350 (Figure 2.2d). It should be noted that in both analyses the narrow range of the ramp voltage (10 V), the higher gas flow velocity and the slow ramp speed permitted the achievement of high resolving power. In addition, the rigidity of the OH-PBDE molecules in contrast with previously studied systems (e.g., peptides and proteins) utilizing TIMS allows for the observation of narrower IMS bands.

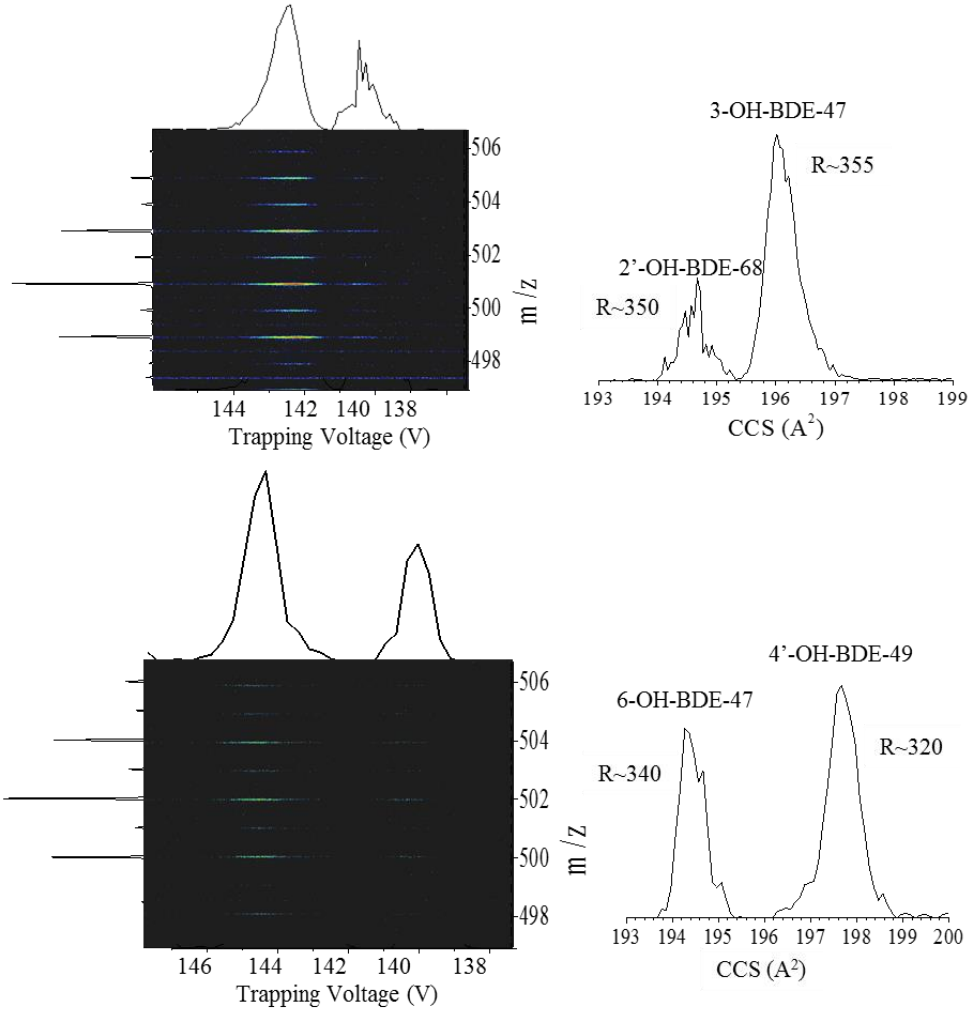

Figure 2.2: Typical 2D-IMS-MS contour and IMS projection plots for the binary mixture of 3-OH-BDE-47 and 2'-OH-BDE-68 (a) and b)) and the mixture of 6-OH-BDE-47 and 4'-OH-BDE-47 (c) and d)).

Ternary mixtures of OH-BDE compounds were also created and subsequently analyzed via nESI-TIMS-MS. A mixture of 3-OH-BDE-47, 5-OH-BDE-47 and 2'-OH-BDE-68 showed baseline separation between 2'-OH-BDE-68 and 3-OH-BDE-47 (CCS=194.5 $Å^2$ and 196.0 $Å^2$) with a resolving power of 320-400. The two BDE-47 compounds in the mixture (3-OH-BDE-47 and 5-OH-BDE47) were only partially resolved; however, the IMS peak clearly shows a bimodal peak with two well defined centers that correlate to the CCS of the single standards (Figure 2.3a). A second ternary mixture containing 6-OH-BDE-47, 5-OH-BDE-47 and 4'-OH-BDE-49 was analyzed to further

evaluate TIMS-MS as a method to separate isomeric mixtures (Figure 2.3b). In this mixture the two metabolites from BDE-47 were baseline separated with a resolving power in the order of 350-400; however, the 4'-OH-BDE-49 and 5-OH-BDE-47 were only partially resolved with centers that correlate to the CCS of the single standards (197.4 $Å^2$ and 196.6 $Å^2$, respectively).

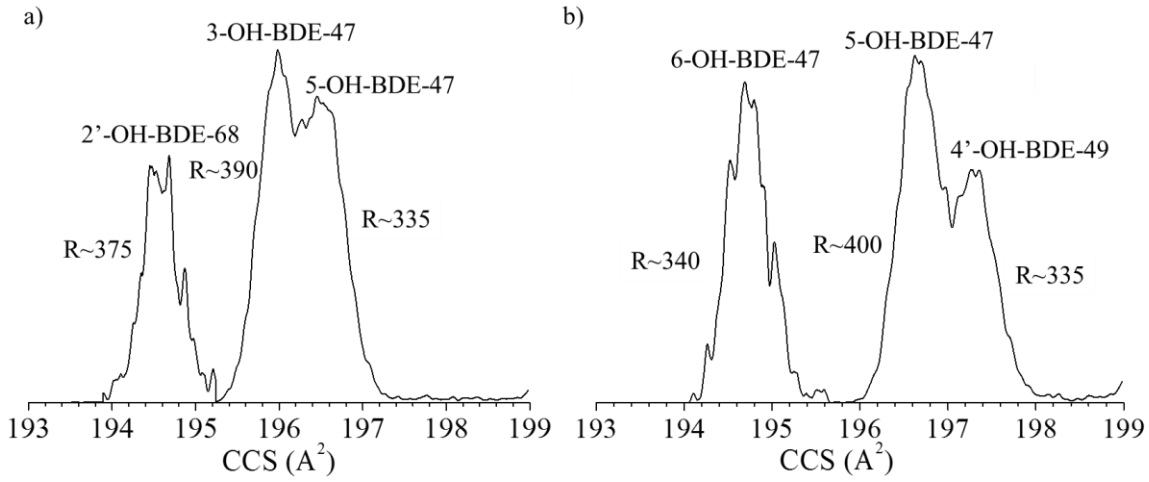

Figure 2.3: Typical IMS projection plots from the ternary mixture of 3-OH-BDE-47, 5-OH-BDE-47 and 2'-OH-BDE-68 (a) and the mixture of 4'-OH-BDE-49, 5-OH-BDE-47 and 6-OH-BDE-47 (b).

2.5 Conclusions

In this work we provide the framework for rapid isomer separation of hydroxylated polybrominated diphenyl ethers using nESI-TIMS-MS. During the analysis of five OH-BDE standards, experimental CCS values were calculated using TuneMix as a mobility standard. Candidate structures were proposed for all the IMS bands observed in good agreement with the experimental CCS (within ±5%). Analysis of binary mixtures showed that baseline separation is possible between 2'-OH-BDE-68 and 3-OH-BDE-47, 6-OH-BDE-47 and 4'-OH-BDE-49, and 6- OH-BDE-47 and 5-OH-BDE-47 with a resolving

power of 350-400. Moreover, 3-OH-BDE-47 and 5-OH-BDE-47, and 5-OH-BDE-47 and 4'-OH-BDE-49 isomers were only partially resolved. This work provides the foundation for the analysis of OH-BDE from complex mixtures utilizing small volumes (15 μL), significantly decreasing the amount of material necessary for the analysis without the need for derivatization or chromatographic separation. In addition, separation in the TIMS cell occurred on the millisecond range and experiments typically take less than 5 minutes per sample significantly decreasing the amount of analysis time when compared to GC-MS and LC-MS analyses. It should be noted that the TIMS-MS operation (as low as 50ms analysis time[37]) can be easily coupled to GC and LC pre-separation as a way to diminish the matrix effects during nESI for the analysis of complex mixtures.

2.6 Acknowledgements

This work was supported by the National Institute of Health (Grant No. R00GM106414). The authors wish to acknowledge Paolo Benigni for helpful discussions during the theoretical calculations. The authors also acknowledge computing resources provided by the Instructional & Research Computing Center (IRCC) at Florida International University.

2.7 References

1. Darnerud, P. O.; Eriksen, G. S.; Jóhannesson, T.; Larsen, P. B.; Viluksela, M., Polybrominated diphenyl ethers: occurrence, dietary exposure, and toxicology. *Environmental Health Perspectives* **2001,** *109* (Suppl 1), 49.

2. Eriksson, P.; Jakobsson, E.; Fredriksson, A., Brominated flame retardants: a novel class of developmental neurotoxicants in our environment? *Environmental Health Perspectives* **2001,** *109* (9), 903.

3. Siddiqi, M. A.; Laessig, R. H.; Reed, K. D., Polybrominated diphenyl ethers (PBDEs): new pollutants–old diseases. *Clinical Medicine & Research* **2003,** *1* (4), 281-290.

4. Malmvärn, A.; Marsh, G.; Kautsky, L.; Athanasiadou, M.; Bergman, Å.; Asplund, L., Hydroxylated and methoxylated brominated diphenyl ethers in the red algae Ceramium tenuicorne and blue mussels from the Baltic Sea. *Environmental Science & Technology* **2005,** *39* (9), 2990-2997.

5. Malmvärn, A.; Zebühr, Y.; Kautsky, L.; Bergman, Å.; Asplund, L., Hydroxylated and methoxylated polybrominated diphenyl ethers and polybrominated dibenzo-p-dioxins in red alga and cyanobacteria living in the Baltic Sea. *Chemosphere* **2008,** *72* (6), 910-916.

6. Marsh, G.; Athanasiadou, M.; Bergman, Å.; Asplund, L., Identification of hydroxylated and methoxylated polybrominated diphenyl ethers in Baltic Sea salmon (Salmo salar) blood. *Environmental Science & Technology* **2004,** *38* (1), 10-18.

7. Feo, M. L.; Gross, M. S.; McGarrigle, B. P.; Eljarrat, E.; Barceló, D.; Aga, D. S.; Olson, J. R., Biotransformation of BDE-47 to potentially toxic metabolites is predominantly mediated by human CYP2B6. *Environmental Health Perspectives (Online)* **2013,** *121* (4), 440.

8. Feo, M. L.; Barón, E.; Aga, D. S.; Eljarrat, E.; Barceló, D., Development of a liquid chromatography–electrospray chemical ionization tandem mass spectrometry analytical method for analysis of eleven hydroxylated polybrominated diphenyl ethers. *Journal of Chromatography A* **2013,** *1301*, 80-87.

9. Zhao, J.; Zhu, X.; Xu, T.; Yin, D., Structure-dependent activities of polybrominated diphenyl ethers and hydroxylated metabolites on zebrafish retinoic acid receptor. *Environmental Science and Pollution Research* **2015,** *22* (3), 1723-1730.

10. Wiseman, S. B.; Wan, Y.; Chang, H.; Zhang, X.; Hecker, M.; Jones, P. D.; Giesy, J. P., Polybrominated diphenyl ethers and their hydroxylated/methoxylated analogs: environmental sources, metabolic relationships, and relative toxicities. *Marine Pollution Bulletin* **2011,** *63* (5), 179-188.

11. Kim, K. H.; Bose, D. D.; Ghogha, A.; Riehl, J.; Zhang, R.; Barnhart, C. D.; Lein, P. J.; Pessah, I. N., Para- and Ortho-Substitutions Are Key Determinants of Polybrominated Diphenyl Ether Activity toward Ryanodine Receptors and Neurotoxicity. *Environmental Health Perspectives* **2010,** *119* (4), 519-526.

12. Su, G.; Yu, H.; Lam, M. H. W.; Giesy, J. P.; Zhang, X., Mechanisms of toxicity of hydroxylated polybrominated diphenyl ethers (HO-PBDEs) determined by toxicogenomic

analysis with a live cell array coupled with mutagenesis in Escherichia coli. *Environmental Science & Technology* **2014,** *48* (10), 5929-5937.

13. Mercado-Feliciano, M.; Bigsby, R. M., Hydroxylated Metabolites of the Polybrominated Diphenyl Ether Mixture DE-71 Are Weak Estrogen Receptor-[alpha] Ligands. *Environmental Health Perspectives* **2008,** *116* (10), 1315.

14. Qiu, X.; Mercado-Feliciano, M.; Bigsby, R. M.; Hites, R. A., Measurement of polybrominated diphenyl ethers and metabolites in mouse plasma after exposure to a commercial pentabromodiphenyl ether mixture. *Environmental Health Perspectives* **2007**, 1052-1058.

15. Butryn, D. M.; Gross, M. S.; Chi, L.-H.; Schecter, A.; Olson, J. R.; Aga, D. S., "One-shot" analysis of polybrominated diphenyl ethers and their hydroxylated and methoxylated analogs in human breast milk and serum using gas chromatography-tandem mass spectrometry. *Analytica Chimica Acta* **2015**.

16. Qiu, X.; Bigsby, R. M.; Hites, R. A., Hydroxylated metabolites of polybrominated diphenyl ethers in human blood samples from the United States. *Environmental Health Perspectives* **2009,** *117* (1), 93-98.

17. Lacorte, S.; Ikonomou, M. G.; Fischer, M., A comprehensive gas chromatography coupled to high resolution mass spectrometry based method for the determination of polybrominated diphenyl ethers and their hydroxylated and methoxylated metabolites in environmental samples. *Journal of Chromatography A* **2010,** *1217* (3), 337-347.

18. Mackintosh, S. A.; Pérez-Fuentetaja, A.; Zimmerman, L. R.; Pacepavicius, G.; Clapsadl, M.; Alaee, M.; Aga, D. S., Analytical performance of a triple quadrupole mass spectrometer compared to a high resolution mass spectrometer for the analysis of polybrominated diphenyl ethers in fish. *Analytica Chimica Acta* **2012,** *747*, 67-75.

19. Simpson, S.; Gross, M. S.; Olson, J. R.; Zurek, E.; Aga, D. S., Identification of polybrominated diphenyl ether metabolites based on calculated boiling points from COSMO-RS, experimental retention times, and mass spectral fragmentation patterns. *Analytical Chemistry* **2015,** *87* (4), 2299-2305.

20. Klamt, A., Conductor-like screening model for real solvents: a new approach to the quantitative calculation of solvation phenomena. *The Journal of Physical Chemistry* **1995,** *99* (7), 2224-2235.

21. Klamt, A.; Eckert, F.; Arlt, W., COSMO-RS: an alternative to simulation for calculating thermodynamic properties of liquid mixtures. *Annual Review of Chemical and Biomolecular Engineering* **2010,** *1*, 101-122.

22. Lei, Z.; Chen, B.; Li, C.; Liu, H., Predictive molecular thermodynamic models for liquid solvents, solid salts, polymers, and ionic liquids. *Chemical Reviews* **2008,** *108* (4), 1419-1455.

23. Mas, S.; Jáuregui, O.; Rubio, F.; de Juan, A.; Tauler, R.; Lacorte, S., Comprehensive liquid chromatography–ion-spray tandem mass spectrometry method for the identification and quantification of eight hydroxylated brominated diphenyl ethers in environmental matrices. *Journal of Mass Spectrometry* **2007,** *42* (7), 890-899.

24. Lupton, S. J.; McGarrigle, B. P.; Olson, J. R.; Wood, T. D.; Aga, D. S., Analysis of hydroxylated polybrominated diphenyl ether metabolites by liquid chromatography/atmospheric pressure chemical ionization tandem mass spectrometry. *Rapid Communications in Mass Spectrometry* **2010,** *24* (15), 2227-2235.

25. Kato, Y.; Okada, S.; Atobe, K.; Endo, T.; Matsubara, F.; Oguma, T.; Haraguchi, K., Simultaneous determination by APCI-LC/MS/MS of hydroxylated and methoxylated polybrominated diphenyl ethers found in marine biota. *Analytical Chemistry* **2009,** *81* (14), 5942-5948.

26. Gillig, K. J.; Russell, D. H. A periodic field focusing ion mobility spectrometer. 2001-US6398
2001065589, 20010228., 2001.

27. Gillig, K. J.; Ruotolo, B. T.; Stone, E. G.; Russell, D. H., An electrostatic focusing ion guide for ion mobility-mass spectrometry. *Int. J. Mass Spectrom.* **2004,** *239* (1), 43-49.

28. Silveira, J. A.; Gamage, C. M.; Blase, R. C.; Russell, D. H., Gas-phase ion dynamics in a periodic-focusing DC ion guide. *International Journal of Mass Spectrometry* **2010,** *296* (1-3), 36-42.

29. Guo, Y.; Wang, J.; Javahery, G.; Thomson, B. A.; Siu, K. W. M., Ion Mobility Spectrometer with Radial Collisional Focusing. *Analytical Chemistry* **2004,** *77* (1), 266-275.

30. Koeniger, S. L.; Merenbloom, S. I.; Valentine, S. J.; Jarrold, M. F.; Udseth, H. R.; Smith, R. D.; Clemmer, D. E., An IMS-IMS Analogue of MS-MS. *Analytical Chemistry* **2006,** *78* (12), 4161-4174.

31. Kurulugama, R. T.; Nachtigall, F. M.; Lee, S.; Valentine, S. J.; Clemmer, D. E., Overtone mobility spectrometry: Part 1. Experimental observations. *Journal of the American Society for Mass Spectrometry* **2009,** *20* (5), 729-737.

32. Glaskin, R. S.; Valentine, S. J.; Clemmer, D. E., A Scanning Frequency Mode for Ion Cyclotron Mobility Spectrometry. *Analytical Chemistry* **2010,** *82* (19), 8266-8271.

33. Kolakowski, B. M.; Mester, Z., Review of applications of high-field asymmetric waveform ion mobility spectrometry (FAIMS) and differential mobility spectrometry (DMS). *Analyst* **2007,** *132* (9), 842-864.

34. Purves, R. W.; Guevremont, R., Electrospray ionization high-field asymmetric waveform ion mobility spectrometry-mass spectrometry. *Analytical Chemistry* **1999,** *71* (13), 2346-2357.

35. Shvartsburg, A. A.; Smith, R. D., Fundamentals of traveling wave ion mobility spectrometry. *Analytical Chemistry* **2008,** *80* (24), 9689-9699.

36. Fernandez-Lima, F.; Kaplan, D. A.; Suetering, J.; Park, M. A., Gas-phase separation using a trapped ion mobility spectrometer. *International Journal for Ion Mobility Spectrometry* **2011,** *14* (2-3), 93-98.

37. Hernandez, D. R.; DeBord, J. D.; Ridgeway, M. E.; Kaplan, D. A.; Park, M. A.; Fernandez-Lima, F., Ion dynamics in a trapped ion mobility spectrometer. *Analyst* **2014,** *139* (8), 1913-1921.

38. Fernandez-Lima, F. A.; Kaplan, D. A.; Park, M. A., Note: Integration of trapped ion mobility spectrometry with mass spectrometry. *Review of Scientific Instruments* **2011,** *82* (12), 126106.

39. Merenbloom, S. I.; Glaskin, R. S.; Henson, Z. B.; Clemmer, D. E., High-resolution ion cyclotron mobility spectrometry. *Analytical Chemistry* **2009,** *81* (4), 1482-1487.

40. Glaskin, R. S.; Ewing, M. A.; Clemmer, D. E., Ion trapping for ion mobility spectrometry measurements in a cyclical drift tube. *Analytical Chemistry* **2013,** *85* (15), 7003-7008.

41. Silveira, J. A.; Ridgeway, M. E.; Park, M. A., High resolution trapped ion mobility spectrometery of peptides. *Analytical Chemistry* **2014,** *86* (12), 5624-5627.

42. McKenzie-Coe, A.; DeBord, J. D.; Ridgeway, M.; Park, M.; Eiceman, G.; Fernandez-Lima, F., Lifetimes and stabilities of familiar explosive molecular adduct complexes during ion mobility measurements. *Analyst* **2015,** *140* (16), 5692-5699.

43. Castellanos, A.; Benigni, P.; Hernandez, D. R.; DeBord, J. D.; Ridgeway, M. E.; Park, M. A.; Fernandez-Lima, F., Fast screening of polycyclic aromatic hydrocarbons using trapped ion mobility spectrometry–mass spectrometry. *Analytical Methods* **2014,** *6* (23), 9328-9332.

44. Benigni, P.; Marin, R.; Fernandez-Lima, F., Towards unsupervised polyaromatic hydrocarbons structural assignment from SA-TIMS –FTMS data. *International Journal for Ion Mobility Spectrometry* **2015**, 1-7.

45. Benigni, P.; Thompson, C. J.; Ridgeway, M. E.; Park, M. A.; Fernandez-Lima, F., Targeted high-resolution ion mobility separation coupled to ultrahigh-resolution mass spectrometry of endocrine disruptors in complex mixtures. *Analytical Chemistry* **2015,** *87* (8), 4321-4325.

46. Schenk, E. R.; Ridgeway, M. E.; Park, M. A.; Leng, F.; Fernandez-Lima, F., Isomerization kinetics of AT hook decapeptide solution structures. *Analytical Chemistry* **2014,** *86* (2), 1210-1214.

47. Molano-Arevalo, J. C.; Hernandez, D. R.; Gonzalez, W. G.; Miksovska, J.; Ridgeway, M. E.; Park, M. A.; Fernandez-Lima, F., Flavin adenine dinucleotide structural motifs: from solution to gas phase. *Analytical Chemistry* **2014,** *86* (20), 10223-10230.

48. Schenk, E. R.; Mendez, V.; Landrum, J. T.; Ridgeway, M. E.; Park, M. A.; Fernandez-Lima, F., Direct Observation of Differences of Carotenoid Polyene Chain cis/trans Isomers Resulting from Structural Topology. *Analytical Chemistry* **2014,** *86* (4), 2019-2024.

49. Schenk, E. R.; Nau, F.; Fernandez-Lima, F., Theoretical predictor for candidate structure assignment from IMS data of biomolecule-related conformational space. *International Journal of Ion Mobility Spectrometry* **2015,** *18* (1-2), 23-29.

50. Schenk, E. R.; Almeida, R.; Miksovska, J.; Ridgeway, M. E.; Park, M. A.; Fernandez-Lima, F., Kinetic Intermediates of Holo- and Apo-Myoglobin Studied Using HDX-TIMS-MS and Molecular Dynamic Simulations. *Journal of the American Society for Mass Spectrometry* **2015,** *26* (4), 555-563.

51. Frost, L.; Baez, M. A. M.; Harrilal, C.; Garabedian, A.; Fernandez-Lima, F.; Leng, F., The Dimerization State of the Mammalian High Mobility Group Protein AT-Hook 2 (HMGA2). *Plos One* **2015,** *10* (6), e0130478.

52. Gonzalez, W. G.; Ramos, V.; Diaz, M.; Garabedian, A.; Molano-Arevalo, J. C.; Fernandez-Lima, F.; Miksovska, J., Characterization of the Photophysical, Thermodynamic, and Structural Properties of the Terbium(III)–DREAM Complex. *Biochemistry* **2016,** *55* (12), 1873-1886.

53. Fernandez-Lima, F. A.; Blase, R. C.; Russell, D. H., A study of ion-neutral collision cross-section values for low charge states of peptides, proteins, and peptide/protein complexes. *International Journal of Mass Spectrometry* **2010,** *298* (1-3), 111-118.

54. Fernandez-Lima, F. A.; Wei, H.; Gao, Y. Q.; Russell, D. H., On the structure elucidation using IMS and Molecular Dynamics. *J. Phys. Chem. A* **2009,** *113* (29), 8221-8234.

55. Fernandez-Lima, F. A.; Becker, C.; McKenna, A. M.; Rodgers, R. P.; Marshall, A. G.; Russell, D. H., Petroleum Crude Oil Characterization by IMS-MS and FTICR MS. *Analytical Chemistry* **2009,** *81* (24), 9941-9947.

56. May, J. C.; Goodwin, C. R.; Lareau, N. M.; Leaptrot, K. L.; Morris, C. B.; Kurulugama, R. T.; Mordehai, A.; Klein, C.; Barry, W.; Darland, E.; Overney, G.; Imatani, K.; Stafford, G. C.; Fjeldsted, J. C.; McLean, J. A., Conformational Ordering of Biomolecules in the Gas Phase: Nitrogen Collision Cross Sections Measured on a Prototype High Resolution Drift Tube Ion Mobility-Mass Spectrometer. *Analytical Chemistry* **2014,** *86* (4), 2107-2116.

57. Bush, M. F.; Hall, Z.; Giles, K.; Hoyes, J.; Robinson, C. V.; Ruotolo, B. T., Collision Cross Sections of Proteins and Their Complexes: A Calibration Framework and

Database for Gas-Phase Structural Biology. *Analytical Chemistry* **2010,** *82* (22), 9557-9565.

58. Flanagan, L. A. Mass Spectrometry Calibration Using Homogeneously substituted fluorinated triazatriphosphorines. 1999.

59. Frisch, M. J.; Trucks, G. W.; Schlegel, H. B.; Scuseria, G. E.; Robb, M. A.; Cheeseman, J. R.; Montgomery, J., J. A.; Vreven, T.; Kudin, K. N.; Burant, J. C.; Millam, J. M.; Iyengar, S. S.; Tomasi, J.; Barone, V.; Mennucci, B.; Cossi, M.; Scalmani, G.; Rega, N.; Petersson, G. A.; Nakatsuji, H.; Hada, M.; Ehara, M.; Toyota, K.; Fukuda, R.; Hasegawa, J.; Ishida, M.; Nakajima, T.; Honda, Y.; Kitao, O.; Nakai, H.; Klene, M.; Li, X.; Knox, J. E.; Hratchian, H. P.; Cross, J. B.; Bakken, V.; Adamo, C.; Jaramillo, J.; Gomperts, R.; Stratmann, R. E.; Yazyev, O.; Austin, A. J.; Cammi, R.; Pomelli, C.; Ochterski, J. W.; Ayala, P. Y.; Morokuma, K.; Voth, G. A.; Salvador, P.; Dannenberg, J. J.; Zakrzewski, V. G.; Dapprich, S.; Daniels, A. D.; Strain, M. C.; Farkas, O.; Malick, D. K.; Rabuck, A. D.; Raghavachari, K.; Foresman, J. B.; Ortiz, J. V.; Cui, Q.; Baboul, A. G.; Clifford, S.; Cioslowski, J.; Stefanov, B. B.; Liu, G.; Liashenko, A.; Piskorz, P.; Komaromi, I.; Martin, R. L.; Fox, D. J.; Keith, T.; Al-Laham, M. A.; Peng, C. Y.; Nanayakkara, A.; Challacombe, M.; Gill, P. M. W.; Johnson, B.; Chen, W.; Wong, M. W.; Gonzalez, C.; Pople, J. A. *Gaussian 03, Revision C.02*, Wallingford CT, 2004.

60. Campuzano, I.; Bush, M. F.; Robinson, C. V.; Beaumont, C.; Richardson, K.; Kim, H.; Kim, H. I., Structural characterization of drug-like compounds by ion mobility mass spectrometry: comparison of theoretical and experimentally derived nitrogen collision cross sections. *Analytical Chemistry* **2011,** *84* (2), 1026-1033.

61. Kim, H. I.; Kim, H.; Pang, E. S.; Ryu, E. K.; Beegle, L. W.; Loo, J. A.; Goddard, W. A.; Kanik, I., Structural characterization of unsaturated phosphatidylcholines using traveling wave ion mobility spectrometry. *Analytical Chemistry* **2009,** *81* (20), 8289-8297.

62. Singh, U. C.; Kollman, P. A., An approach to computing electrostatic charges for molecules. *Journal of Computational Chemistry* **1984,** *5* (2), 129-145.

63. Besler, B. H.; Merz, K. M.; Kollman, P. A., Atomic charges derived from semiempirical methods. *Journal of Computational Chemistry* **1990,** *11* (4), 431-439.

CHAPTER THREE:
Discovery and Targeted Monitoring of Polychlorinated Biphenyl Metabolites in Blood Plasma using LC-TIMS-TOF MS

This chapter was published in the International Journal of Mass Spectrometry and adapted with permission.

Kendra J. Adams, Natalie F. Smith; Cesar E. Ramirez; Francisco Fernandez-Lima (2017). *International Journal of Mass Spectrometry*. 427, 133-140.

3.1 Abstract

In the present work, the potential for rapid, targeted analysis of hydroxylated metabolites of polychlorinated biphenyls (OH-PCBs) in diluted human blood plasma using liquid chromatography coupled with trapped ion mobility spectrometry and time-of-flight high resolution mass spectrometry (LC-TIMS-TOF MS) was evaluated. Experimental OH-PCB collisional cross section (CCS_{N2}) and gas-phase candidate structures (<3% error) are reported for the first time and used, in addition to the LC retention time and accurate m/z, as OH-PCB identification features to increase the detection selectivity. The proposed LC-TIMS-TOF MS workflow combines a "dilute-and-shoot" sample preparation strategy, a robust liquid chromatography step, a high-resolving power mobility separation (R~150) and high-resolution mass spectrometry (R~30-40k) for the separation, identification and quantification of common OH-PCB isomers with limits of detection comparable to traditional workflows (e.g., LOD and LOQ of ~10 pg/mL and ~50 pg/mL, respectively). The high selectivity and low detection limits provide multiple advantages compared to current methodologies that typically require long, labor-intensive preparation and/or derivatization steps prior to gas or liquid chromatography-mass spectrometry.

3.2 Introduction

Polychlorinated biphenyls (PCBs) are endocrine disruptors that have antagonistic effects on reproductive, neurological, and immune systems in humans and wildlife.[1] Production of PCBs was banned in the United States during the 1970's; however, these compounds are still found in the environment and considered persistent organic pollutants.[2-4] PCBs are metabolized to hydroxylated PCBs (OH-PCBs) and/or methyl sulfone PCBs (MeSO-PCBs) via cytochrome P-450.[3] Hydroxylation occurs through

epoxidation, which forms an arene oxide intermediate followed by the formation of a hydroxyl-PCB.[3, 5-9] The location of the hydroxyl group on the biphenyl rings is directly correlated to the toxicity of analyte.[1, 10] When the hydroxylation occurs at *para*- or *meta*-positions in combination with an adjacent chlorine atom, the compound bears significant resemblance to the thyroid hormones triiodothyronine (T3) and thyroxine (T4).[11-12] The OH-PCBs competitively bind to the thyroid hormone receptors and can have up to 10-times higher binding affinity to transthyretin than the hormones themselves.[5, 11-12] This competitive binding causes a high retention of OH-PCBs in blood plasma, resulting in various toxicological effects such as neurodevelopmental, reproductive impairment and carcinogenicity.[5, 9, 13]

The most common experimental methods for the separation and detection of PCB metabolites are gas chromatography and liquid chromatography coupled to mass spectrometry (GC-MS and LC-MS). Traditionally, GC-MS analysis has been utilized for PCB metabolites, although, to analyze phenolic compounds, derivatization is required.[7, 14-16] Other studies have proposed the use of LC-MS/MS strategies for separation, detection, and quantification of OH-PCBs in humans and wildlife.[7-8, 15, 17-18] Typically, before introducing the sample to a LC-MS system, an analyte extraction and sample cleanup protocol is required. Several methods of extraction have been utilized for various biological matrices such as whole blood, serum and plasma, most of which include liquid-liquid extraction followed by partitioning.[18] Cleanup procedures have also been implemented using silica columns.[18] After the lengthy extraction and cleanup steps for biological samples, a secondary cleanup is typically performed using solid phase extraction immediately prior to separation in the analytical column.[8] The addition of these extraction

and cleanup procedures significantly increases the analysis time and typically require the use of added resources throughout the analytical procedure. Despite the progress made over the years, there is a clear need for simplified analytical workflows with enhanced selectivity and increased sensitivity.

An alternative approach includes the use of gas-phase, post-ionization separations such as ion mobility spectrometry coupled to mass spectrometry (IMS-MS), which promises further gains in the speed, sensitivity and selectivity for the analysis of complex biological mixtures.[19-20] Specifically, the added mobility dimension of separation yields an increase in peak coverage,[21-24] a factor that has often inhibited the analysis of complex mixtures with MS-only detection. The ion's mobility gives information on its size and shape via the momentum transfer ion-neutral collision cross section (CCS).[25] While this description holds true for most contemporary IMS analyzers (e.g., periodic focusing DC ion guide,[26-28] segmented quadrupole drift cell,[29] multistage IMS,[30-32] transient wave ion guide,[33-34] and SLIM devices[35]), a common pursuit has been to increase IMS resolving power and ion transmission. [36-44] Since the introduction of TIMS-MS in 2011,[45-46] our group,[47-60] and others,[61-70] have shown the potential of TIMS-MS for gas-phase separation and for molecular structural elucidation. In particular, we have demonstrated the advantages of TIMS for screening[47] and targeted[48] analysis of molecular ions from complex chemical mixtures; the study of isomerization kinetics of small molecules,[49, 51-52] peptides,[50] DNA,[59] proteins,[54-55] DNA-protein complexes and protein-protein complexes in their native and denatured states.[58] In a more recent report, we showed the isomer separation of polybrominated diphenyl ether metabolites using nanoESI-TIMS-TOF MS

with mobility resolving powers of up to 400 (the highest reported mobility resolving power for singly charged species).[56]

In the present work, the potential for rapid, targeted analysis of hydroxylated metabolites of polychlorinated biphenyls (OH-PCB) using online liquid chromatography in tandem with trapped ion mobility spectrometry and TOF mass spectrometry (LC-TIMS-TOF MS) was studied for the first time. Several OH-PCB congeners, ranging from penta-chlorinated to hepta-chlorinated biphenyls, were studied as single standards, as mixtures and in the presence of a complex matrix-human blood plasma. The advantages of LC-TIMS-TOF MS over traditional GC-MS and LC-MS/MS analysis are discussed based on analysis time, selectivity and sensitivity.

3.3 Experimental Methods

3.3.1 Materials and Reagents

All solvents were purchased from Fisher Scientific (Pittsburg, PA) and were of LC-MS quality or better. Hydroxylated polychlorinated biphenyl standards were purchased from Wellington Laboratories (ON, Canada) and Accustandard, Inc. (New Haven, CT, USA). Pooled human plasma was purchased from Innovative Research (Novi, MI, USA). Nine OH-PCBs were used in this study: 2,3,3’,4’,5-Pentachloro-4-biphenylol (4-OH CB 107), 2’,3,3’,4’,5-Pentachloro-4-biphenylol (4-OH CB 108), and 2,3’,4,4’,5-Pentachloro-3-biphenylol (3-OH CB 118), 2,2’,3,3’,4’,5-Hexachloro-4-biphenylol (4-OH CB 130), 2,2’,3’,4,4’,5-Hexachloro-3-biphenylol (3-OH CB 138), and 2,2’,3,4’,5,5’-Hexachloro-4-biphenylol (4-OH CB 146), 2,2’,3,3’,4’,5,5’-Heptachloro-4-biphenylol (4-OH-PCB 172), 2,2’,3’,4,4’,5,5’-Heptachloro-3-biphenylol (3-OH CB 180), and 2,2’,3,4’,5,5’,6-

Heptachloro-4-biphenylol (4-OH CB 187). Binary isomer mixtures were created by mixing equal volumes of the individual standards.

3.3.2 OH-PCB Human Blood Plasma Samples

Pooled human plasma was removed from storage at -20° C and thawed to room temperature. A 150 μL aliquot of plasma was mixed with an equal amount of acetonitrile and spiked with a mixture of OH-PCBs for final concentrations of 0, 10, 25, 50, 100, 500, 1000, 5000, and 10000 pg/mL. It has been reported that acetonitrile would break the cell membranes, as well as precipitate the large proteins as a way to increase extraction of the intracellular components.[71-72] Three OH-PCB standards were used for the spike mixture: 4-Hydroxy-2',3,3',4',5'-pentachlorobiphenyl, 5-Hydroxy-2,2',3,4,4',5'-hexachlorobiphenyl and 4'-Hydroxy-2,2',3,3',4,5,5'-heptachlorobiphenyl. Samples were vortex mixed for 1 minute and centrifuged at 4 ^{o}C for 10 minutes at 4500 rpm to remove the proteins from the aqueous layer. Following centrifugation, the supernatant was transferred, without any further clean-up, to LC vials with borosilicate glass inserts for analysis.

3.3.3 LC-ESI- TIMS-MS Analysis

The LC-ESI-TIMS-TOF MS analysis was performed using a custom-built TIMS-TOF MS based on the maXis impact Q-ToF MS (Bruker Daltonics Inc, Billerica, MA). Sample injection (40 μL) and LC separation was performed on a Shimadzu Prominence HPLC system consisting of two 20AD pumps, a SIL-20AC auto-sampler and a CTO 20-A column oven held at 40° C (Kyoto, Japan). An Onyx Monolithic C18 HPLC column (100 x 4.6 mm) was used protected by an Onyx guard column (5 x 4.6 mm), both from Phenomenex (Torrance, CA, USA). A 15-minute gradient separation was performed at a

variable flow rate (2 mL/min for two minutes and then decreased to 1 mL/min for the remaining 13 minutes of the program) using water and acetonitrile. Mobile phase composition was changed as follows: hold 10% B for two minutes; increase to 97% B in three minutes and hold for 6.75 minutes; return to 10% B in 0.5 min and hold for 2.75 min for re-equilibration. Samples were ionized and introduced into the TIMS-TOF-MS using an ionBooster ESI source in negative ion mode (Bruker Daltonics Inc, Billerica, MA). Typical ionBooster operating conditions were 1000 V capillary voltage, 400 V end plate offset, 300 V charging voltage, 4.1 bar nebulizer pressure, 3.0 l/min dry gas, 270 ^{o}C dry heater, and 400 ^{o}C APCI heater.

A detailed overview of the TIMS analyzer and its operation can be found elsewhere. [45-46, 53] The nitrogen bath gas flow is defined by the pressure difference between entrance funnel P_1 = 2.7 mbar and the exit funnel P_2 = 1.1 mbar at *ca.* 300 K. The TIMS analyzer is comprised of three regions: an entrance funnel, analyzer tunnel (46 mm axial length), and exit funnel. A 2040 kHz and 250 Vpp RF potential was applied to each section creating a dipolar field in the funnel regions and a quadrupolar field inside the tunnel. During TIMS operation, multiple ion species are trapped simultaneously at different E values resulting from a voltage gradient applied across the TIMS tunnel. After thermalization, species are eluted from the TIMS cell by decreasing the electric field in stepwise decrements (referred to as the "ramp"). The TIMS cell was operated using a fill/ramp sequence of 10/100ms or 100/100ms for a 10% and 50% duty cycle for better chromatography and higher sensitivity, respectively. The TOF analyzer was operated at 10 kHz (*m/z* 100-1500). The data was segmented in LC frames over 10 analysis cycles yielding an LC-TIMS-TOF MS step size of ~2 s. Mobility calibration was performed using the Tuning Mix calibration standard

(G24221A, Agilent Technologies, Santa Clara, CA) in positive ion mode (e.g., *m/z* 322, K_0 = 1.376 cm^2 V^{-1} s^{-1} and *m/z* 622, K_0 = 1.013 cm^2 V^{-1} s^{-1}) resulting in *A* = 231.064 for the instrumental and method conditions employed.[53] The TIMS operation was controlled using in-house software, written in National Instruments Lab VIEW, and synchronized with the maXis Impact Q-ToF acquisition program.[45]

Reduced mobility values (K_0) were correlated with collisional cross section (Ω) using the equation:

$$\Omega = \frac{(18\pi)^{1/2}}{16}\frac{z}{(k_B T)^{1/2}}\left[\frac{1}{m_I}+\frac{1}{m_b}\right]^{1/2}\frac{1}{K_0}\frac{1}{N^*} \quad (1)$$

where z is the charge of the ion, k_B is the Boltzmann constant, N^* is the number density of the bath gas, and m_I and m_b refer to the masses of the ion and bath gas, respectively.[25] All resolving power ($R=\Omega/\Delta\Omega$) values were determined from Gaussian peak fits after smoothing of peaks (Savitzky-Golay with 30-80 points of window) using OriginPro (version 8.0). LC-TIMS-TOF MS data were processed using Data Analysis software v. 5.0 (Bruker Daltonics Inc, Billerica, MA) and the calibration plots utilized mobility selected data in the *m/z* domain.

3.3.4 Theoretical calculations

A pool of candidate structures were proposed for each OH-PCB analyzed using TIMS-TOF MS. Final structures were optimized at the DFT/B3LYP/6-311G(d,p) level using Gaussian software.[73] Vibrational frequencies were calculated to guarantee that the optimized structures correspond to actual minima in the energy space, and zero-point energy corrections were applied to calculate the relative stability between the structures. Theoretical ion-neutral collision cross sections were calculated using iMOS[74-75] software

for nitrogen as a bath gas at ca. 300K. Partial atomic charges were calculated using the Merz-Singh-Kollman scheme constrained to the molecular dipole moment.[76-77]

3.4 Results and Discussion

The TIMS-TOF MS analysis of the penta-chlorinated (4-OH CB 107, 4-OH CB 108, and 3-OH CB 118), hexa-chlorinated (4-OH CB 130, 3-OH CB 138, and 4-OH CB 146), and hepta-chlorinated (4-OH CB 172, 3-OH CB 180, and 4-OH CB 187) biphenyls is summarized in Figure 3.1 and Table 3.1. Inspection of the TIMS-TOF MS spectra showed the presence of deprotonated molecular ions $[M-H]^-$ with isotope patterns characteristics of compounds with five, six and seven chlorine atoms. Inspection of the corresponding mobility profiles for the single standards showed the presence of a single mobility band, with resolving powers of R~150. Experimental CCS are reported for all the analyzed single standards (Table 3.1). Inspection of Table 3.1 shows that there are very small CCS differences between the penta- (<0.4%), hexa- (<0.1%) and hepta- (<1.1%) chlorinated biphenyls. For example, the penta-CBs have an experimental CCS of 165.0 $Å^2$, 165.2 $Å^2$ and 165.6 $Å^2$ for the 4-OH CB 107, 4-OH CB 108 and 4-OH CB 118, respectively. Calculated CCS for the penta-CB proposed candidate structures show good agreement with the experimental CCS values (< 3% difference). The hexa-CBs have an experimental CCS of 170.0 $Å^2$, 170.1 $Å^2$ and 170.2 $Å^2$ for the 4-OH CB 130, 3-OH CB 138 and 4-OH CB 146, respectively. Calculated CCS for the hexa-CB proposed candidate structures show good agreement with the experimental CCS values (< 3% difference). The hepta-CBs have an experimental CCS of 172.6 $Å^2$, 173.4 $Å^2$ and 171.4 $Å^2$ for the 4- OH CB 172, 3-OH CB 180 and 4-OH CB 187, respectively. Calculated CCS values for the hepta-CB proposed candidate structures show good agreement with the experimental CCS (<2% difference).

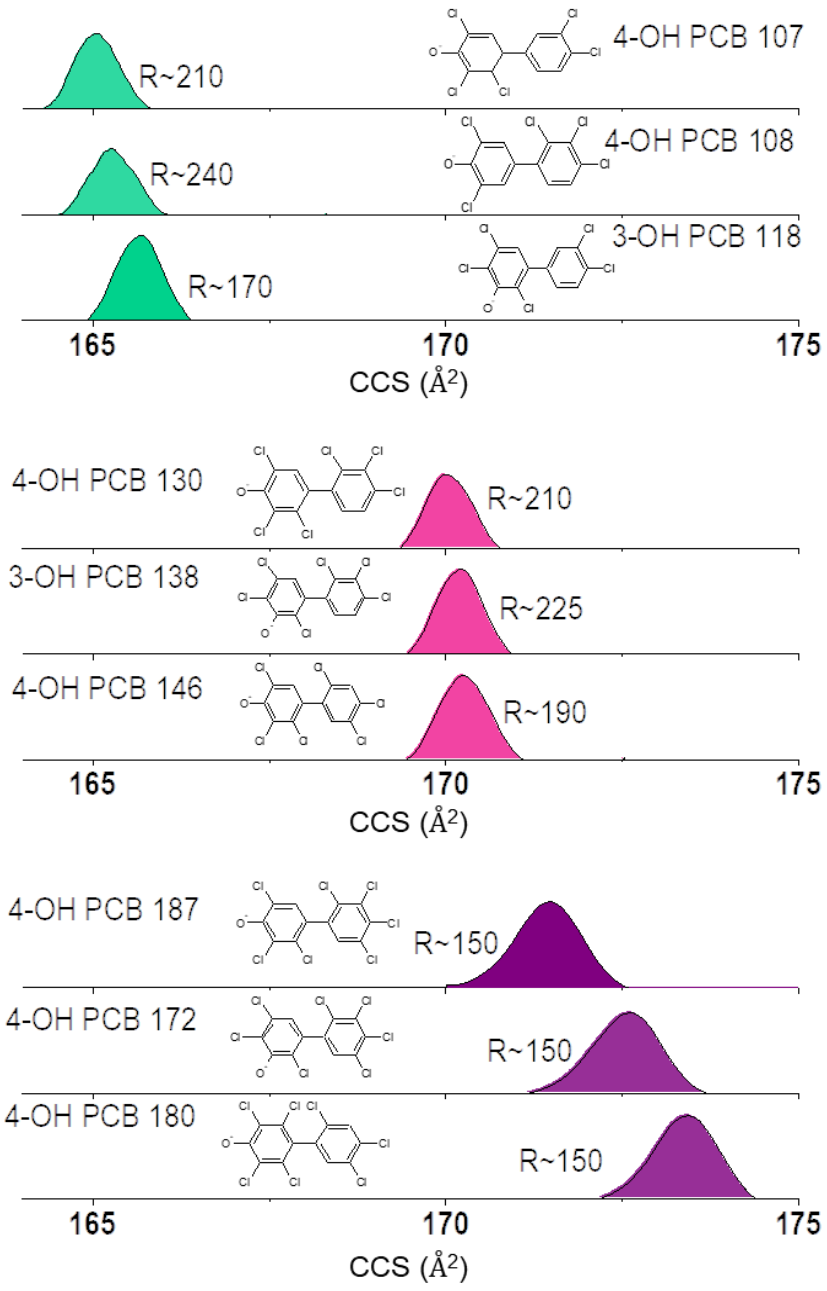

Figure 3.1. Typical mobility profiles of single standards of penta-, hexa- and hepta-CBs

Name	Chemical Formula	Theoretical m/z $[M-H]^-$	Experimental m/z $[M-H]^-$	Error (ppm)	Theoretical CCS (A^2)	Experimental CCS (A^2)
4 OH 107	$C_{12}H_5Cl_5O$				161.3	165.0
4 OH 108	$C_{12}H_5Cl_5O$	340.8681	340.8682	0.293	161.2	165.2
3 OH 118	$C_{12}H_5Cl_5O$				161.1	165.6
4 OH 130	$C_{12}H_4Cl_6O$				164.1	170.0
3 OH 138	$C_{12}H_4Cl_6O$	374.8291	374.8291	0.000	165.0	170.1
4 OH 146	$C_{12}H_4Cl_6O$				166.0	170.2
4 OH 172	$C_{12}H_3Cl_7O$				171.0	172.6
3 OH 180	$C_{12}H_3Cl_7O$	408.7901	408.7905	0.975	171.0	173.4
4 OH 187	$C_{12}H_3Cl_7O$				171.3	171.4

Table 3.1. List of experimental and theoretical m/z and CCS values for the penta-, hexa-, and hepta-CB considered in this study.

When analyzed as binary mixtures, mobility separation was not observed between the penta-CBs (4-OH CB 107, 4-OH CB 108 and 3-OH CB 118) and hexa-CBs (4-OH CB 130, 3-OH CB 138, and 4-OH CB146). We attribute these results to the similarity in CCS between the isomers (Table 3.1). The separation of these compounds is analytically challenging, and only attempts using SPE-LC-MS/MS has been shown to separate the penta-CBs 3-OH CB 118 to the 4-OH CB107/108[8, 17] and the hexa-CBs 4-OH CB 130 to the 4-OH CB146/138.[8, 17, 78] Moreover, baseline mobility separation was achieved for the case of the binary mixtures of the hepta-CBs with a mobility resolving power of R~150 for the case of 4-OH CB 187 and 4-OH-CB172/180; however, mobility separation was not observed for the case of 4-OH CB 172/180 (Figure 3.2). This mobility separation trend shows similarities with results observed using SPE-LC-MS/MS, where baseline separation is only observed between 4-OH CB 187 and 4-OH CB 172/180.[8]

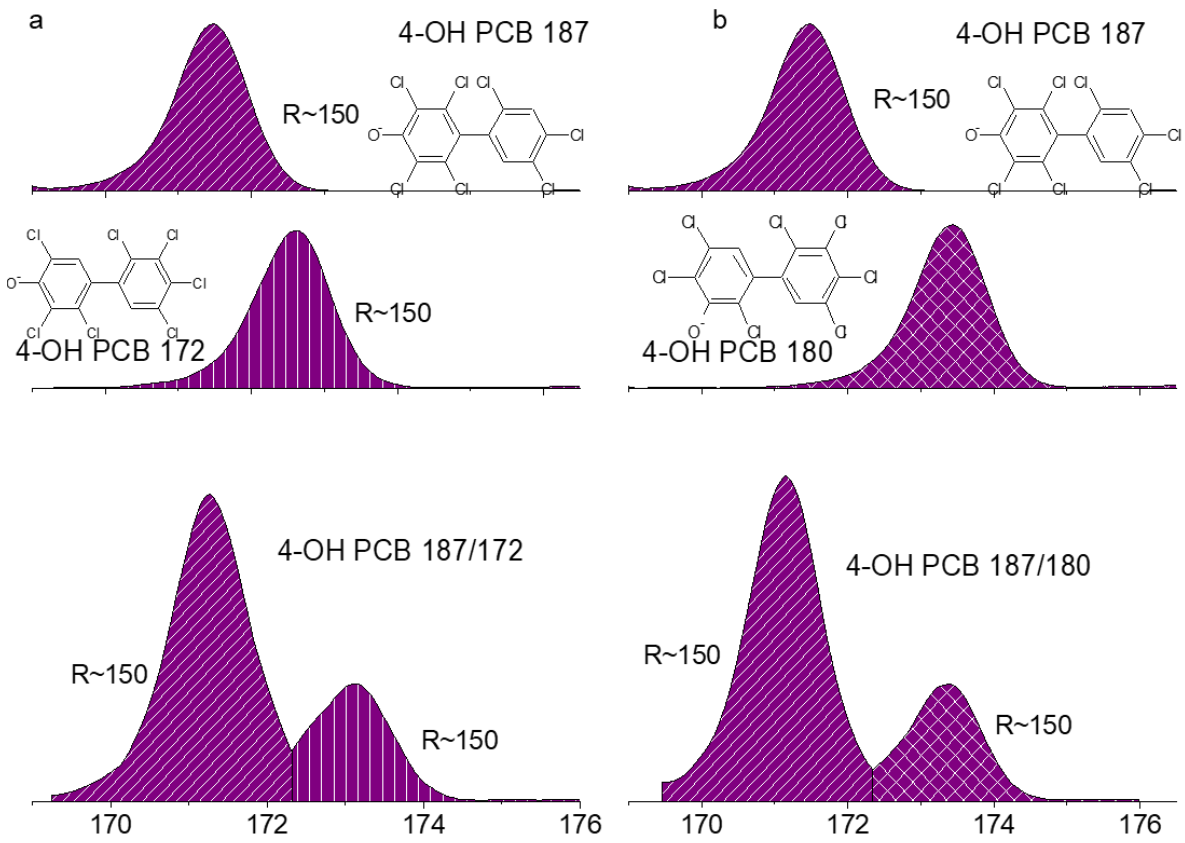

Figure 3.2. Typical mobility profiles of the single standards and binary mixtures for the hepta-CBs.

To reduce sample preparation steps and maximize throughput a "dilute-and-shoot" strategy was adopted. Previous studies for extraction of OH-PCBs from plasma involve the use of preliminary extraction and cleanup steps followed by lengthy chromatographic analyses.[7-8, 15, 17, 79] The proposed method uses a quick clean-up step using acetonitrile to precipitate the proteins, followed by centrifugation. The supernatant is injected into the LC system, without further preparation, for three-dimensional separation in chromatographic, ion mobility and mass spectrometric domains. The short LC method was developed using an Onyx Monolithic C18 column, which has been used previously, for direct plasma injections and thus was selected to account for minimal sample preparation and clean-up

prior to LC-TIMS-TOF MS analysis. The column output was combined with the ionBooster source, to allow high eluent flow-rates (~1 ml/min). In Figure 3.3, a two-dimensional IMS-MS plot is shown for samples containing 2 ppb of a 9-component mixture of OH-PCBs in water (3a) and plasma (3b). The marked regions pertain to the penta-, hexa- and hepta-CBs (Figure 3.3). Inspection of the 2D-IMS-MS of the water sample shows clear mobility and mass separation of the penta-, hexa-, and hepta-CBs (Figure 3.3a).

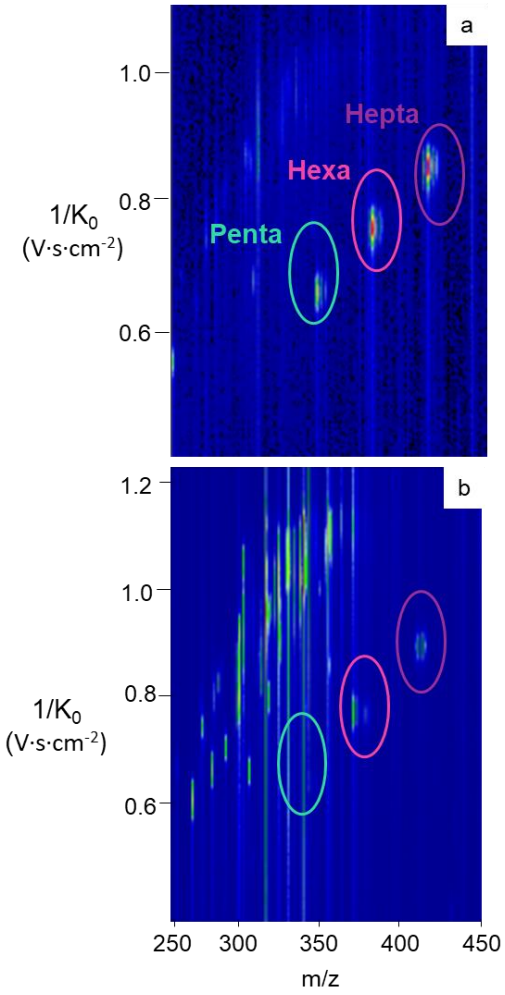

Figure 3.3. Typical 2D-IMS-MS contour maps of the penta-, hexa-, and hepta-CBs in water (a) and in human blood plasma (b). Note the separation of the PCB signals from potential interferences in the IMS-MS domain.

Inspection of the LC-TIMS-TOF MS data showed a two band chromatographic separation for the hexa- and hepta-CBs, and a single chromatographic band (RT=7.18 minutes) for the penta-CBs. For example, the extracted ion chromatogram (EIC) for the hexa-CBs (*m/z* 374.8291) and the hepta-CBs (*m/z* 408.7905) showed the separation of 4-OH CB 130 (RT=7.22 minutes) to the 4-OH CB 146/138 (RT=7.31 minutes) and 4-OH CB 187 (RT=7.26 minutes) to the 4-OH CB 172/180, respectively (RT=7.58 minutes). In the case of the plasma sample (Figure 3.3b), multiple peaks are observed in the 2D-IMS MS domain; moreover, a clear separation of the targeted CBs from the plasma signal is observed in the IMS-MS domain. That is, high selectivity can be achieved during CBs detection on the proposed LC-TIMS-TOF MS workflow. For example, the advantages for higher selectivity of the LC-TIMS-TOF MS workflow are shown for the case of the hepta-CBs (Figure 3.4) combining LC separation with accurate CCS and m/z measurements. It should be noted, that the CBs CCS values can be used as universal parameters for routine identifications, specially, in the cases where single standards of CBs are not accessible.

A comparative study of limit of detection (LOD) was conducted using traditional LC-ESI-TOF MS and the here proposed LC-ESI-TIMS-TOF MS for quantitative detection of OH-PCBs. The main purpose of the study was to assess the effect of the TIMS separation, while all other experimental parameters are kept constant (Figure 3.5). A nine-point matrix-matched calibration curve was built with peak intensity as a function of analyte concentration. A linear response for the penta-, hexa- and hepta- CBs from 0-5000 pg/mL was observed in both the LC-TOF MS and LC-TIMS-TOFMS analysis (R^2>0.99). Differences in the response curve are related to the duty cycle during

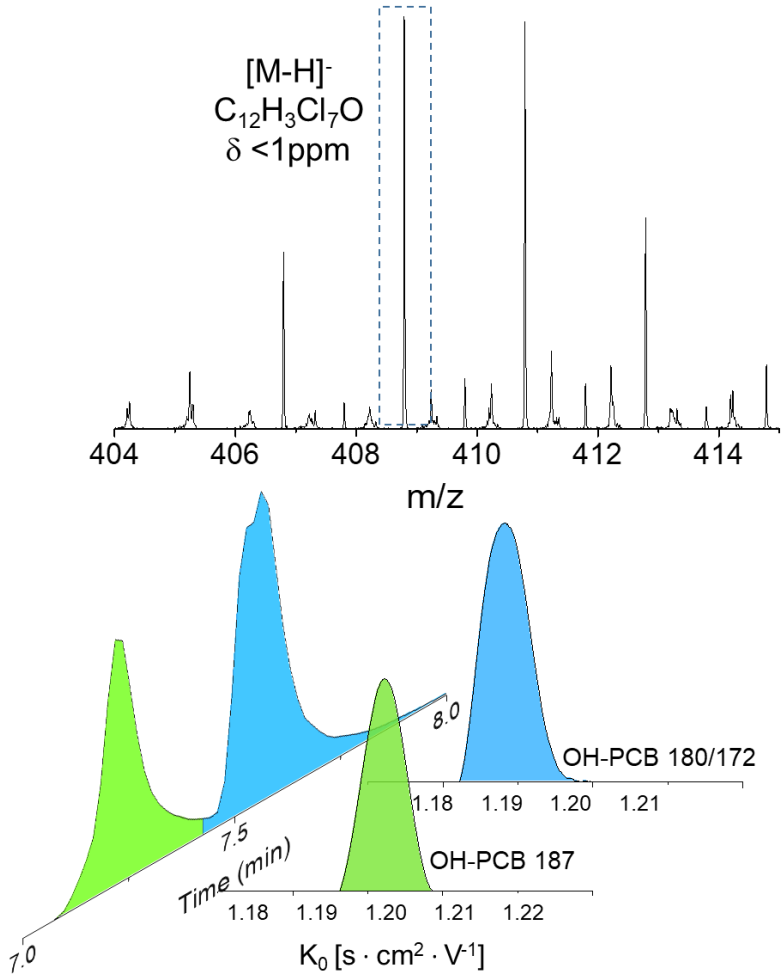

Figure 3.4. Typical MS projection, LC projection and extracted ion mobility profiles for a mixture of hepta-CBs, (OH-PCB 187, OH-PCB 180 and OH-PCB 172), from the LC-TOF-MS analysis of the CBs in human blood plasma.

the LC-TIMS-TOF MS measurements. That is, the use of single stage TIMS analyzer requires initial trapping followed by an elution step; during the elution step new ions are not introduced in the analyzer, which reduces the overall duty cycle. More recent version of the TIMS-TOF MS operate using a dual TIMS analyzer which allows for almost 100%

duty cycle.[19] The limit of detection (LOD, defined as the concentration that produces a signal three times higher than the background noise) for LC-TIMS-TOF MS was established at ~10 pg/mL for penta-CBs, hexa-CBs and hepta-CBs (Figure 3.5). In contrast, the LOD for LC-TOF MS was obtained from the calibration plot at ~25 pg/mL, 2.5-times higher than the proposed technique (See Appendix 2). This highlights the ability of the LC-TIMS-TOF MS to reduce the background interferences, cleaning up the detection of the targeted analytes during full scan detection (see Figure 3.3). The limit of quantification (LOQ, defined as the concentration 10-times higher than the background noise of the un-spiked plasma) was established at 35 pg/mL for each analyte in spiked in plasma (Figure 3.5), which is comparable to previous studies that employed GC and LC-MS/MS and reported LOQs between 1 and 100 pg/mL.[8, 18, 78] In particular, Quinete et al.[8] reported LOQs in the range of 20-50 pg/mL for the same analytes using a triple-quadrupole instrument to perform LC-MS/MS operating under multiple-reaction-monitoring (MRM) mode. The latter technique is considered the current standard for analytical quantitation but has the inherent disadvantage of focusing only on pre-programmed transitions that leave out any untargeted species. Therefore, our presented LC-TIMS-TOF MS technique offers similar sensitivity to triple-quadrupole instruments with the added benefit of detection of untargeted species, enhancing the value of the obtained data by enabling back-interrogation of analytes of interest that may arise in the future. This high sensitivity using a full-scan detection could be attributed to the very high selectivity of the LC-TIMS-MS approach, which provides with very low background levels thanks to the separation of the analytes from isobaric interferences contained in plasma (see Figure 3.3).

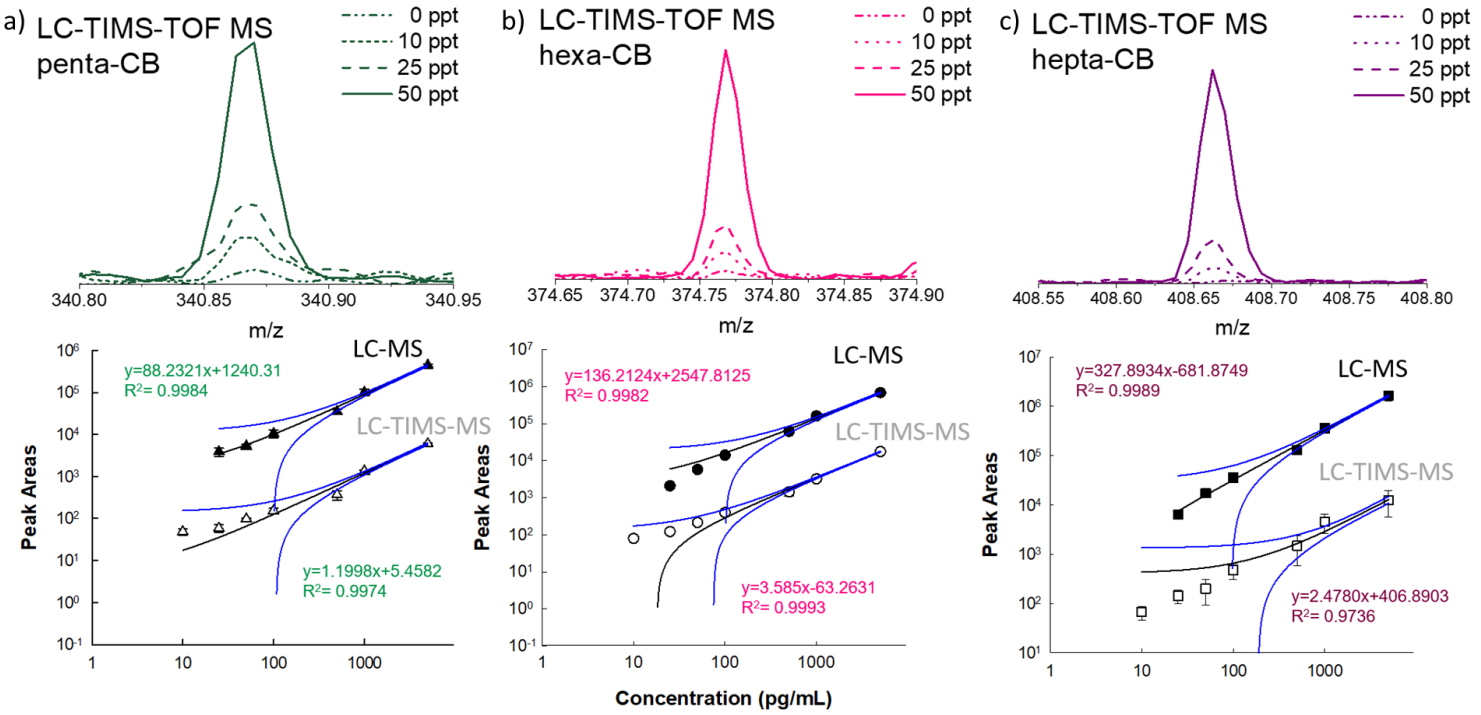

Figure 3.5. Typical response curves for LC-TIMS-TOF MS as a function of a) penta- b) hexa- and c) hepta-CBs concentration in human blood plasma. Note the linear response for the penta-, hexa- and hepta- CBs from 0-5000 pg/mL in both the LC-TOF MS and LC-TIMS-TOFMS analysis.

3.5 Conclusions

This work demonstrated a rapid screening of OH-PCBs in diluted human plasma using LC coupled with tandem trapped ion mobility spectrometry and TOF mass spectrometry (LC-TIMS-TOF MS) detection. Experimental collisional cross sections and gas-phase candidate structures were reported for the first time for nine OH-PCB standards. The high mobility resolving power (R~150) of the TIMS analyzer permitted baseline separation of the hepta-CB 4-OH CB 187 and 4-OH-CB172/180, with differences in CCS of less 1%. Despite the high chemical complexity of human blood plasma samples (multiple peaks observed in the 2D-IMS MS domain during the analysis), a clear separation of the targeted CBs from other potential interferences is observed in the IMS-MS domain and used as quantitative signal with very high signal-to-noise ratios (LOD and LOQ of ~10 pg/mL and ~35 pg/mL, respectively). The LC-TIMS-TOF MS performance is comparable to established techniques such as LC-MS/MS which, unlike this work, do not allow for untargeted analysis and back-interrogation of data. High throughput was achieved by limiting sample clean-up steps to protein precipitation followed by direct supernatant injection on a monolithic column for HPLC separation and tandem ion mobility/mass spectrometric detection. The superior performance of this simplified LC-TIMS-TOF MS analytical workflow removes the need for labor-intensive preparation steps to minimize chemical noise and represents a viable alternative to currently available methodologies.

3.6 Acknowledgements

This work was supported by the National Institutes of Health (R00GM106414), a Bruker Daltonics Inc. fellowship, and a National Science Foundation Division of Chemistry, under CAREER award CHE-1654274, with co-funding from the Division of Molecular and

Cellular Biosciences to F.F.-L.. The authors will also like to acknowledge the helpful discussions and technical support from Dr. Mark E. Ridgeway and Dr. Melvin A. Park from Bruker Daltonics Inc. during the development and installation of the custom-built TIMS-TOF MS instrument.

3.7 References

1. Quinete, N.; Schettgen, T.; Bertram, J.; Kraus, T., Occurrence and distribution of PCB metabolites in blood and their potential health effects in humans: a review. *Environmental Science and Pollution Research* **2014,** *21* (20), 11951-11972.

2. Ross, G., The public health implications of polychlorinated biphenyls (PCBs) in the environment. *Ecotoxicology and Environmental Safety* **2004,** *59* (3), 275-291.

3. Kania-Korwel, I.; Lehmler, H.-J., Chiral polychlorinated biphenyls: absorption, metabolism and excretion—a review. *Environmental Science and Pollution Research* **2016,** *23* (3), 2042-2057.

4. Diamond, M. L.; Melymuk, L.; Csiszar, S. A.; Robson, M., Estimation of PCB Stocks, Emissions, and Urban Fate: Will our Policies Reduce Concentrations and Exposure? *Environmental Science & Technology* **2010,** *44* (8), 2777-2783.

5. Bergman, A.; Klasson-Wehler, E.; Kuroki, H., Selective retention of hydroxylated PCB metabolites in blood. *Environmental Health Perspectives* **1994,** *102* (5), 464.

6. Matthews, H.; Anderson, M., Effect of chlorination on the distribution and excretion of polychlorinated biphenyls. *Drug Metabolism and Disposition* **1975,** *3* (5), 371-380.

7. Letcher, R. J.; Li, H. X.; Chu, S. G., Determination of hydroxylated polychlorinated biphenyls (HO-PCBs) in blood plasma by high-performance liquid chromatography-electrospray ionization-tandem quadrupole mass spectrometry. *Journal of Analytical Toxicology* **2005,** *29* (4), 209-216.

8. Quinete, N.; Kraus, T.; Belov, V. N.; Aretz, C.; Esser, A.; Schettgen, T., Fast determination of hydroxylated polychlorinated biphenyls in human plasma by online solid

phase extraction coupled to liquid chromatography-tandem mass spectrometry. *Analytica Chimica Acta* **2015,** *888*, 94-102.

9. Letcher, R. J.; Klasson-Wehler, E.; Bergman, A., Methyl sulfone and hydroxylated metabolites of polychlorinated biphenyls. In *Volume 3 Anthropogenic Compounds Part K*, Springer: 2000; pp 315-359.

10. Kinch, L. N.; Grishin, N. V., Evolution of protein structures and functions. *Current Opinion in Structural Biology* **2002,** *12* (3), 400-408.

11. Brouwer, A.; Morse, D. C.; Lans, M. C.; Gerlienke Schuur, A.; Murk, A. J.; Klasson-Wehler, E.; Bergman, Å.; Visser, T. J., Interactions of persistent environmental organohalogens with the thyroid hormone system: mechanisms and possible consequences for animal and human health. *Toxicology and Industrial Health* **1998,** *14* (1-2), 59-84.

12. Lans, M. C.; Klasson-Wehler, E.; Willemsen, M.; Meussen, E.; Safe, S.; Brouwer, A., Structure-dependent, competitive interaction of hydroxy-polychlorobiphenyls,-dibenzo-p-dioxins and-dibenzofurans with human transthyretin. *Chemico-Biological Interactions* **1993,** *88* (1), 7-21.

13. Purkey, H. E.; Palaninathan, S. K.; Kent, K. C.; Smith, C.; Safe, S. H.; Sacchettini, J. C.; Kelly, J. W., Hydroxylated polychlorinated biphenyls selectively bind transthyretin in blood and inhibit amyloidogenesis: rationalizing rodent PCB toxicity. *Chemistry & Biology* **2004,** *11* (12), 1719-1728.

14. Berger, U.; Herzke, D.; Sandanger, T. M., Two trace analytical methods for determination of hydroxylated PCBs and other halogenated phenolic compounds in eggs from Norwegian birds of prey. *Analytical Chemistry* **2004,** *76* (2), 441-452.

15. Liang, R.; Zhao, Y.; Su, Y.; Qin, W., Determination of hydroxylated polychlorinated biphenyls by offline solid-phase extraction-liquid chromatography–tandem mass spectrometry using a molecularly imprinted polymer as a sorbent for sample preconcentration. *Talanta* **2015,** *144*, 115-121.

16. Hovander, L.; Malmberg, T.; Athanasiadou, M.; Athanassiadis, I.; Rahm, S.; Bergman; Wehler, E. K., Identification of Hydroxylated PCB Metabolites and Other Phenolic Halogenated Pollutants in Human Blood Plasma. *Arch. Environ. Contam. Toxicol.* **2002,** *42* (1), 105-117.

17. Quinete, N.; Esser, A.; Kraus, T.; Schettgen, T., Determination of hydroxylated polychlorinated biphenyls (OH-PCBs) in human urine in a highly occupationally exposed German cohort: New prospects for urinary biomarkers of PCB exposure. *Environment International* **2016,** *97*, 171-179.

18. Quinete, N.; Schettgen, T.; Bertram, J.; Kraus, T., Analytical approaches for the determination of PCB metabolites in blood: a review. *Analytical and Bioanalytical Chemistry* **2014,** *406* (25), 6151-6164.

19. Meier, F.; Beck, S.; Grassl, N.; Lubeck, M.; Park, M. A.; Raether, O.; Mann, M., Parallel Accumulation-Serial Fragmentation (PASEF): Multiplying Sequencing Speed and Sensitivity by Synchronized Scans in a Trapped Ion Mobility Device. *Journal of proteome research* **2015,** *14* (12), 5378-87.

20. Lanucara, F.; Holman, S. W.; Gray, C. J.; Eyers, C. E., The power of ion mobility-mass spectrometry for structural characterization and the study of conformational dynamics. *Nature Chemistry* **2014,** *6* (4), 281-294.

21. Benigni, P.; Thompson, C. J.; Ridgeway, M. E.; Park, M. A.; Fernandez-Lima, F. A., Targeted High-Resolution Ion Mobility Separation Coupled to Ultrahigh-Resolution Mass Spectrometry of Endocrine Disruptors in Complex Mixtures. *Analytical Chemistry* **2015,** *87* (8), 4321-4325.

22. Valentine, S. J.; Plasencia, M. D.; Liu, X.; Krishnan, M.; Naylor, S.; Udseth, H. R.; Smith, R. D.; Clemmer, D. E., Toward Plasma Proteome Profiling with Ion Mobility-Mass Spectrometry. *Journal of proteome research* **2006,** *5* (11), 2977-2984.

23. Valentine, S. J.; Counterman, A. E.; Hoaglund, C. S.; Reilly, J. P.; Clemmer, D. E., Gas-phase separations of protease digests. *Journal of the American Society for Mass Spectrometry* **1998,** *9* (11), 1213-6.

24. Venne, K.; Bonneil, E.; Eng, K.; Thibault, P., Improvement in Peptide Detection for Proteomics Analyses Using NanoLC−MS and High-Field Asymmetry Waveform Ion Mobility Mass Spectrometry. *Analytical Chemistry* **2005,** *77* (7), 2176-2186.

25. McDaniel, E. W.; Mason, E. A., *Mobility and diffusion of ions in gases*. John Wiley and Sons, Inc., New York: New York, 1973; p 381.

26. Gillig, K. J.; Russell, D. H. A periodic field focusing ion mobility spectrometer. 2001-US6398
2001065589, 20010228., 2001.

27. Gillig, K. J.; Ruotolo, B. T.; Stone, E. G.; Russell, D. H., An electrostatic focusing ion guide for ion mobility-mass spectrometry. *Int. J. Mass Spectrom.* **2004,** *239* (1), 43-49.

28. Silveira, J. A.; Gamage, C. M.; Blase, R. C.; Russell, D. H., Gas-phase ion dynamics in a periodic-focusing DC ion guide. *International Journal of Mass Spectrometry* **2010,** *296* (1-3), 36-42.

29. Guo, Y.; Wang, J.; Javahery, G.; Thomson, B. A.; Siu, K. W. M., Ion Mobility Spectrometer with Radial Collisional Focusing. *Analytical Chemistry* **2004,** *77* (1), 266-275.

30. Koeniger, S. L.; Merenbloom, S. I.; Valentine, S. J.; Jarrold, M. F.; Udseth, H. R.; Smith, R. D.; Clemmer, D. E., An IMS-IMS Analogue of MS-MS. *Analytical Chemistry* **2006,** *78* (12), 4161-4174.

31. Kurulugama, R. T.; Nachtigall, F. M.; Lee, S.; Valentine, S. J.; Clemmer, D. E., Overtone mobility spectrometry: Part 1. Experimental observations. *Journal of the American Society for Mass Spectrometry* **2009,** *20* (5), 729-737.

32. Glaskin, R. S.; Valentine, S. J.; Clemmer, D. E., A Scanning Frequency Mode for Ion Cyclotron Mobility Spectrometry. *Analytical Chemistry* **2010,** *82* (19), 8266-8271.

33. Pringle, S. D.; Giles, K.; Wildgoose, J. L.; Williams, J. P.; Slade, S. E.; Thalassinos, K.; Bateman, R. H.; Bowers, M. T.; Scrivens, J. H., An investigation of the mobility separation of some peptide and protein ions using a new hybrid quadrupole/travelling wave IMS/oa-ToF instrument. *Int. J. Mass Spectrom.* **2007,** *261* (1), 1-12.

34. Bush, M. F.; Hall, Z.; Giles, K.; Hoyes, J.; Robinson, C. V.; Ruotolo, B. T., Collision Cross Sections of Proteins and Their Complexes: A Calibration Framework and Database for Gas-Phase Structural Biology. *Analytical Chemistry* **2010,** *82* (22), 9557-9565.

35. Webb, I. K.; Garimella, S. V. B.; Tolmachev, A. V.; Chen, T.-C.; Zhang, X.; Norheim, R. V.; Prost, S. A.; LaMarche, B.; Anderson, G. A.; Ibrahim, Y. M.; Smith, R. D., Experimental Evaluation and Optimization of Structures for Lossless Ion

Manipulations for Ion Mobility Spectrometry with Time-of-Flight Mass Spectrometry. *Analytical Chemistry* **2014,** *86* (18), 9169-9176.

36. Dugourd, P.; Hudgins, R. R.; Clemmer, D. E.; Jarrold, M. F., High-resolution ion mobility measurements. *Review of Scientific Instruments* **1997,** *68* (2), 1122-1129.

37. Merenbloom, S. I.; Glaskin, R. S.; Henson, Z. B.; Clemmer, D. E., High-resolution ion cyclotron mobility spectrometry. *Analytical Chemistry* **2009,** *81* (4), 1482-1487.

38. Kemper, P. R.; Dupuis, N. F.; Bowers, M. T., A new, higher resolution, ion mobility mass spectrometer. *International Journal of Mass Spectrometry* **2009,** *287* (1-3), 46-57.

39. Blase, R. C.; Silveira, J. A.; Gillig, K. J.; Gamage, C. M.; Russell, D. H., Increased ion transmission in IMS: A high resolution, periodic-focusing DC ion guide ion mobility spectrometer. *International Journal of Mass Spectrometry* **2011,** *301* (1-3), 166-173.

40. May, J.; Russell, D., A Mass-Selective Variable-Temperature Drift Tube Ion Mobility-Mass Spectrometer for Temperature Dependent Ion Mobility Studies. *Journal of the American Society for Mass Spectrometry* **2011,** *22* (7), 1134-1145.

41. Kemper, P. R.; Bowers, M. T., A hybrid double-focusing mass spectrometer--high-pressure drift reaction cell to study thermal energy reactions of mass-selected ions. *Journal of the American Society for Mass Spectrometry* **1990,** *1* (3), 197-207.

42. Wu, C.; Siems, W. F.; Asbury, G. R.; Hill, H. H., Electrospray Ionization High-Resolution Ion Mobility Spectrometry−Mass Spectrometry. *Analytical Chemistry* **1998,** *70* (23), 4929-4938.

43. Liu, Y.; Clemmer, D. E., Characterizing Oligosaccharides Using Injected-Ion Mobility/Mass Spectrometry. *Analytical Chemistry* **1997,** *69* (13), 2504-2509.

44. Jarrold, M. F.; Constant, V. A., Silicon cluster ions: Evidence for a structural transition. *Physical Review Letters* **1991,** *67* (21), 2994.

45. Fernandez-Lima, F. A.; Kaplan, D. A.; Suetering, J.; Park, M. A., Gas-phase separation using a Trapped Ion Mobility Spectrometer. *International Journal for Ion Mobility Spectrometry* **2011,** *14* (2-3), 93-98.

46. Fernandez-Lima, F. A.; Kaplan, D. A.; Park, M. A., Note: Integration of trapped ion mobility spectrometry with mass spectrometry. *Review of Scientific Instruments* **2011,** *82* (12), 126106.

47. Castellanos, A.; Benigni, P.; Hernandez, D. R.; DeBord, J. D.; Ridgeway, M. E.; Park, M. A.; Fernandez-Lima, F. A., Fast Screening of Polycyclic Aromatic Hydrocarbons using Trapped Ion Mobility Spectrometry – Mass Spectrometry. *Analytical Methods* **2014,** *6*, 9328-9332.

48. Benigni, P.; Thompson, C. J.; Ridgeway, M. E.; Park, M. A.; Fernandez-Lima, F., Targeted High-Resolution Ion Mobility Separation Coupled to Ultrahigh-Resolution Mass Spectrometry of Endocrine Disruptors in Complex Mixtures. *Anal. Chem.* **2015,** *87* (8), 4321-4325.

49. Schenk, E. R.; Mendez, V.; Landrum, J. T.; Ridgeway, M. E.; Park, M. A.; Fernandez-Lima, F., Direct Observation of Differences of Carotenoid Polyene Chain cis/trans Isomers Resulting from Structural Topology. *Analytical Chemistry* **2014,** *86* (4), 2019-2024.

50. Schenk, E. R.; Ridgeway, M. E.; Park, M. A.; Leng, F.; Fernandez-Lima, F., Isomerization Kinetics of AT Hook Decapeptide Solution Structures. *Anal. Chem.* **2014,** *86* (2), 1210-1214.

51. Molano-Arevalo, J. C.; Hernandez, D. R.; Gonzalez, W. G.; Miksovska, J.; Ridgeway, M. E.; Park, M. A.; Fernandez-Lima, F., Flavin Adenine Dinucleotide structural motifs: from solution to gas-phase. *Anal. Chem.* **2014,** *86* (20), 10223-30.

52. McKenzie, A.; DeBord, J. D.; Ridgeway, M. E.; Park, M. A.; Eiceman, G. A.; Fernandez-Lima, F., Lifetimes and Stabilities of familiar explosives molecular adduct complexes during ion mobility measurements. *Analyst* **2015**.

53. Hernandez, D. R.; DeBord, J. D.; Ridgeway, M. E.; Kaplan, D. A.; Park, M. A.; Fernandez-Lima, F. A., Ion dynamics in a trapped ion mobility spectrometer. *Analyst* **2014,** *139* (8), 1913-1921.

54. Schenk, E. R.; Nau, F.; Fernandez-Lima, F., Theoretical predictor for candidate structure assignment from IMS data of biomolecule-related conformational space. *International Journal of Ion Mobility Spectrometry* **2015,** *18* (1-2), 23-29.

55. Schenk, E. R.; Almeida, R.; Miksovska, J.; Ridgeway, M. E.; Park, M. A.; Fernandez-Lima, F., Kinetic Intermediates of Holo- and Apo-Myoglobin Studied Using HDX-TIMS-MS and Molecular Dynamic Simulations. *Journal of the American Society for Mass Spectrometry* **2015,** *26* (4), 555-563.

56. Adams, K. J.; Montero, D.; Aga, D.; Fernandez-Lima, F., Isomer separation of polybrominated diphenyl ether metabolites using nanoESI-TIMS-MS. *International Journal for Ion Mobility Spectrometry* **2016**, 1-8.

57. Benigni, P.; Fernandez-Lima, F., Oversampling Selective Accumulation Trapped Ion Mobility Spectrometry Coupled to FT-ICR MS: Fundamentals and Applications. *Analytical Chemistry* **2016**.

58. Benigni, P.; Marin, R.; Molano-Arevalo, J. C.; Garabedian, A.; Wolff, J. J.; Ridgeway, M. E.; Park, M. A.; Fernandez-Lima, F., Towards the analysis of high molecular weight proteins and protein complexes using TIMS-MS. *International Journal for Ion Mobility Spectrometry* **2016**, 1-10.

59. Garabedian, A.; Butcher, D.; Lippens, J. L.; Miksovska, J.; Chapagain, P. P.; Fabris, D.; Ridgeway, M. E.; Park, M. A.; Fernandez-Lima, F., Structures of the kinetically trapped i-motif DNA intermediates. *Physical Chemistry Chemical Physics* **2016,** *18* (38), 26691-26702.

60. Benigni, P.; Sandoval, K.; Thompson, C. J.; Ridgeway, M. E.; Park, M. A.; Gardinali, P.; Fernandez-Lima, F., Analysis of Photoirradiated Water Accommodated Fractions of Crude Oils Using Tandem TIMS and FT-ICR MS. *Environmental Science & Technology* **2017**.

61. Silveira, J. A.; Ridgeway, M. E.; Laukien, F. H.; Mann, M.; Park, M. A., Parallel accumulation for 100% duty cycle trapped ion mobility-mass spectrometry. *International Journal of Mass Spectrometry*.

62. Michelmann, K.; Silveira, J. A.; Ridgeway, M. E.; Park, M. A., Fundamentals of Trapped Ion Mobility Spectrometry. *Journal of The American Society for Mass Spectrometry* **2015,** *26* (1), 14-24.

63. Silveira, J. A.; Michelmann, K.; Ridgeway, M. E.; Park, M. A., Fundamentals of Trapped Ion Mobility Spectrometry Part II: Fluid Dynamics. *Journal of The American Society for Mass Spectrometry* **2016,** *27* (4), 585-595.

64. Silveira, J. A.; Danielson, W.; Ridgeway, M. E.; Park, M. A., Altering the mobility-time continuum: nonlinear scan functions for targeted high resolution trapped ion mobility-mass spectrometry. *International Journal for Ion Mobility Spectrometry* **2016**, 1-8.

65. Ridgeway, M. E.; Silveira, J. A.; Meier, J. E.; Park, M. A., Microheterogeneity within conformational states of ubiquitin revealed by high resolution trapped ion mobility spectrometry. *Analyst* **2015,** *140* (20), 6964-6972.

66. Meier, F.; Beck, S.; Grassl, N.; Lubeck, M.; Park, M. A.; Raether, O.; Mann, M., Parallel Accumulation–Serial Fragmentation (PASEF): Multiplying Sequencing Speed and Sensitivity by Synchronized Scans in a Trapped Ion Mobility Device. *Journal of proteome research* **2015,** *14* (12), 5378-5387.

67. Silveira, J. A.; Ridgeway, M. E.; Park, M. A., High resolution trapped ion mobility spectrometery of peptides. *Analytical Chemistry* **2014,** *86* (12), 5624-5627.

68. Ridgeway, M. E.; Wolff, J. J.; Silveira, J. A.; Lin, C.; Costello, C. E.; Park, M. A., Gated trapped ion mobility spectrometry coupled to fourier transform ion cyclotron resonance mass spectrometry. *International Journal for Ion Mobility Spectrometry* **2016**, 1-9.

69. Pu, Y.; Ridgeway, M. E.; Glaskin, R. S.; Park, M. A.; Costello, C. E.; Lin, C., Separation and Identification of Isomeric Glycans by Selected Accumulation-Trapped Ion Mobility Spectrometry-Electron Activated Dissociation Tandem Mass Spectrometry. *Analytical Chemistry* **2016,** *88* (7), 3440-3443.

70. Liu, F. C.; Kirk, S. R.; Bleiholder, C., On the structural denaturation of biological analytes in trapped ion mobility spectrometry–mass spectrometry. *Analyst* **2016,** *141* (12), 3722-3730.

71. Au, J.; Su, M.-H.; Wientjes, M., Extraction of intracellular nucleosides and nucleotides with acetonitrile. *Clinical Chemistry* **1989,** *35* (1), 48-51.

72. Bi, H.; Krausz, K. W.; Manna, S. K.; Li, F.; Johnson, C. H.; Gonzalez, F. J., Optimization of harvesting, extraction, and analytical protocols for UPLC-ESI-MS-based metabolomic analysis of adherent mammalian cancer cells. *Analytical and Bioanalytical Chemistry* **2013,** *405* (15), 5279-5289.

73. Frisch, M. J.; Trucks, G. W.; Schlegel, H. B.; Scuseria, G. E.; Robb, M. A.; Cheeseman, J. R.; Montgomery, J., J. A.; Vreven, T.; Kudin, K. N.; Burant, J. C.; Millam, J. M.; Iyengar, S. S.; Tomasi, J.; Barone, V.; Mennucci, B.; Cossi, M.; Scalmani, G.; Rega, N.; Petersson, G. A.; Nakatsuji, H.; Hada, M.; Ehara, M.; Toyota, K.; Fukuda, R.; Hasegawa, J.; Ishida, M.; Nakajima, T.; Honda, Y.; Kitao, O.; Nakai, H.; Klene, M.; Li, X.; Knox, J. E.; Hratchian, H. P.; Cross, J. B.; Bakken, V.; Adamo, C.; Jaramillo, J.; Gomperts, R.; Stratmann, R. E.; Yazyev, O.; Austin, A. J.; Cammi, R.; Pomelli, C.; Ochterski, J. W.; Ayala, P. Y.; Morokuma, K.; Voth, G. A.; Salvador, P.; Dannenberg, J. J.; Zakrzewski, V. G.; Dapprich, S.; Daniels, A. D.; Strain, M. C.; Farkas, O.; Malick, D. K.; Rabuck, A. D.; Raghavachari, K.; Foresman, J. B.; Ortiz, J. V.; Cui, Q.; Baboul, A. G.; Clifford, S.; Cioslowski, J.; Stefanov, B. B.; Liu, G.; Liashenko, A.; Piskorz, P.; Komaromi, I.; Martin, R. L.; Fox, D. J.; Keith, T.; Al-Laham, M. A.; Peng, C. Y.; Nanayakkara, A.; Challacombe, M.; Gill, P. M. W.; Johnson, B.; Chen, W.; Wong, M. W.; Gonzalez, C.; Pople, J. A. *Gaussian 03, Revision C.02*, Wallingford CT, 2004.

74. Campuzano, I.; Bush, M. F.; Robinson, C. V.; Beaumont, C.; Richardson, K.; Kim, H.; Kim, H. I., Structural characterization of drug-like compounds by ion mobility mass spectrometry: comparison of theoretical and experimentally derived nitrogen collision cross sections. *Analytical Chemistry* **2011,** *84* (2), 1026-1033.

75. Kim, H. I.; Kim, H.; Pang, E. S.; Ryu, E. K.; Beegle, L. W.; Loo, J. A.; Goddard, W. A.; Kanik, I., Structural characterization of unsaturated phosphatidylcholines using traveling wave ion mobility spectrometry. *Analytical Chemistry* **2009,** *81* (20), 8289-8297.

76. Singh, U. C.; Kollman, P. A., An approach to computing electrostatic charges for molecules. *Journal of Computational Chemistry* **1984,** *5* (2), 129-145.

77. Besler, B. H.; Merz, K. M.; Kollman, P. A., Atomic charges derived from semiempirical methods. *Journal of Computational Chemistry* **1990,** *11* (4), 431-439.

78. Letcher, R.; Li, H.; Chu, S., Determination of hydroxylated polychlorinated biphenyls (HO-PCBs) in blood plasma by high-performance liquid chromatography-electrospray ionization-tandem quadrupole mass spectrometry. *Journal of Analytical Toxicology* **2005,** *29* (4), 209-216.

79. Hovander, L.; Malmberg, T.; Athanasiadou, M.; Athanassiadis, I.; Rahm, S.; Wehler, E. K., Identification of hydroxylated PCB metabolites and other phenolic halogenated pollutants in human blood plasma. *Arch. Environ. Contam. Toxicol.* **2002,** *42* (1), 105-117.

CHAPTER FOUR:
Analysis of Isomeric Opioids in Urine using LC-TIMS-TOF MS

This chapter was published in Talanta and adapted with permission from all authors.

Kendra J. Adams, Cesar E. Ramirez, Natalie F. Smith, Ana Celia Muñoz-Muñoz,

Lawrence Andrade, Francisco Fernandez-Lima. (2018). *Talanta*. 183, 177-183.

4.1 Abstract

In the present work, a fast separation, identification and quantification workflow based on liquid chromatography coupled to trapped ion mobility in tandem with mass spectrometry (LC-TIMS-MS) is described for the analysis of common isomeric drugs of abuse and their metabolites in human urine. In particular, the analytical performance of LC-TIMS-MS is shown for identification based on retention time, collision cross section and accurate mass for three sets of common isomeric opioids and their deuterated analogs in urine. The LC-TIMS-MS analysis provided limits of detection of 1.4 - 35.2 ng/mL with demonstrated linearity up to 500 ng/mL, enabling discovery and targeted monitoring (DTM) of opioids in urine, with high precision in retention times (RT) (<0.3%), collision cross sections (CCS) (<0.6%) and mass accuracy (<1 ppm) across multiple measurements using external calibration. A good agreement was observed between theoretical and experimental CCS from candidate structures optimized at the DFT/B3LYP level. The need for complementary liquid and mobility separations prior to mass analysis is shown for the analysis of complex mixtures, with mobility resolving power of 80-130. The reproducibility and high speed of LC-TIMS-MS analysis provides a powerful platform for drug and metabolite screening in biological matrices with higher precision and confidence than traditional LC-multiple reaction monitoring (MRM) approaches.

4.2 Introduction

An opioid epidemic has existed in the United States for almost twenty years; however, the rate of ongoing drug abuse continues to increase. Since 2000, deaths from drug overdose have virtually tripled and deaths involving opioids (including opioid painkillers and heroin) have increased nearly 200% [1]. In 2015 ~62% of the ca. 50000 deaths

related to drug overdose are associated to opioid use, involving both illicit and legally prescribed drugs.[2-5] This ever-increasing incidence of drug-related mortalities translates into a clear and present need for more sensitive techniques for drug detection and identification.[6-7] Low therapeutic and abuse concentrations pose a challenge for screening and quantification of illicit drugs, analytical methods with high selectivity and sensitivity are need as monitoring tools for opioids to aid health care providers in their assessment for addiction treatment compliance and misuse. [8-9]

Urine testing is a common first step when caring for opioid addicts or individuals using drugs for pain management purposes.[10-13] Preliminary drug testing in urine typically includes the use of immunoassays, which provide qualitative results allowing the analyst to confirm the presence of broad drug classes.[14-17] Although immunoassays provide rapid results, they typically fail to identify specific drugs types and lack sensitivity (cut-off concentrations ~300 ng/mL) and are also prone to cross-reactivity, increasing the possibility of false results.[14-17] In comparison, liquid chromatography coupled to tandem mass spectrometry (LC-MS/MS) provides specific drug identifications based on retention time, intact mass and fragmentation patterns, and is becoming the gold standard for the detection of drugs of abuse and their metabolites in human fluids.[14, 18-21] The use of LC-MS/MS significantly decreases the rate of false results and is traditionally employed following a positive immunoassay test as a confirmatory tool.[14, 16, 22-23] Identification, confirmation, and quantification of opioids in biological fluids, including urine and plasma, have been accomplished with LC-MS/MS, typically using triple-quadrupole instruments operating under multiple reaction monitoring (MRM) scan mode.[9, 14-16] Chromatography methods range from 6-35 minutes in length and report cut-off concentrations, or limits of

detection (LODs) significantly lower than those of immunoassays ranging from 0.1 to 126 ng/mL in urine. [14]

Ion mobility spectrometry coupled to mass spectrometry (IMS-MS) has been used for detection and separation of opioid compounds.[18, 24-32] Previous studies have reported mobility values for codeine, morphine, normorphine, norcodeine, acetylcodeine, O^6-monoacetylmorphine, heroin and several other drugs using drift tube ion mobility spectrometers (DT-IMS).[18, 25, 30, 32] In a more recent opioid analysis using high-field asymmetric wave-form ion mobility spectrometry (FAIMS), the separation of various isomeric opioids was shown with limits of detection (LODs) in urine for morphine and codeine of 60 ng/mL and 20 ng/mL, respectively.[26, 28-29, 31] With the recent advent of higher resolving powers (R up to 400 [33]) and more sensitive ion mobility analyzers (e.g., Trapped Ion Mobility Spectrometers [34-36]) there is a need to further develop complementary separations based on mass spectrometry for the study and characterization of complex biological samples. [37-39] In particular, liquid chromatography and trapped ion mobility separation techniques have proven useful for the analysis of single components in biological matrices.[37]

In the present study, for the first time, LC is coupled to TIMS in tandem with high resolution MS to provide a cohesive, multidimensional method to achieve high throughput analysis of isomeric opioids in urine. As a proof of concept, three sets of common isomeric opioids and their corresponding deuterated analogs are detected at trace levels in human urine after a "dilute-and-shoot" strategy. The compounds are identified based on their retention time, collisional cross section (CCS) and accurate mass, providing detection levels similar to those obtained with LC-MS/MS applications. With the additional

selectivity provided by the TIMS separation much higher selectivity is afforded (decreased false positives). In this method, because detection is not limited to a few MRM transitions the discovery of new targets or metabolites and/or data back-interrogation is enabled.

4.3 Experimental Methods

4.3.1 Materials and Reagents

All solvents were purchased from Fisher Scientific (Pittsburg, PA) and were of LC-MS quality or better. Opioid compounds and deuterated standards were purchased from Cerilliant (Round Rock, TX). Eight opioid compounds and their deuterated analogs were analyzed: 6-acetylmorphine (A-009), 6-acetylmorphine-D3 (A-006), naloxone (N-004), naloxone-D5 (N-063), codeine (C-006), codeine-D6 (C-040), hydrocodone (H-003), hydrocodone-D3 (H-005), morphine (M-005), morphine-D3 (M-003), hydromorphone (H-004), hydromorphone-D3 (H-006), norcodeine (N-005), norcodeine-D3 (N-082), norhydrocodone (N-053) and norhydrocodone-D3 (N-054). Human urine was purchased from Innovative Research (Novi, MI, USA) and supplied by opioid-free volunteers.

4.3.2 Human Urine “dilute-and-shoot” Sample Preparation

Calibration curves were prepared by adding a known amount of a mixture of the Cerilliant standards in human urine or water and spiking with 50 uL of deuterated internal standard (IS) mix. The curves consisted of seven calibration points ranging from 0.1 - 500 ng/mL with a constant 50 ng/mL of deuterated IS mix. The spiked samples were diluted with water with 10% methanol for a final sample volume of 300 uL. No further extraction or preparation procedures were performed prior to analysis. Limits of detection (LODs) were determined using the linear regression method, where the lowest detectable signal is calculated from the intercept and standard error of the regression line calculated;

limits of quantification (LOQs) are reported as 5-times the LOD. Matrix effect experiments were performed using ten opioid-free urine samples spiked at low (75 ng/mL) and high (400 ng/mL) concentrations with 50 ng/mL of IS. Matrix effects were calculated by comparing the ratios of the spiked matrix samples to the average of six matrix -free water samples to obtain a matrix factor (MF).

4.3.3 LC- TIMS-MS Analysis

The LC-TIMS-TOF MS analysis was performed using a custom-built TIMS-TOF MS based on the maXis impact Q-ToF MS (Bruker Daltonics Inc, Billerica, MA). Sample injection (50 μL) and LC separation was performed on a Shimadzu Prominence HPLC system consisting of two 20AD pumps, a SIL-20AC auto-sampler and a CTO 20-A column oven held at 40° C (Kyoto, Japan). An Onyx Monolithic C18 HPLC column (100 x 4.6 mm) was used protected by an Onyx guard column (5 x 4.6 mm), both from Phenomenex (Torrance, CA, USA). The mobile phase A composition consisted of 50 mM ammonium acetate in water and the mobile phase B consisted of 50 mM ammonium acetate in 96:4 methanol:water v:v. Mobile phase composition was changed as follows: sample injection at 0% B and hold for 1.5 minutes. From 1.5 to 2.5 minutes increase to 99% B and hold until 4.25 minutes. Decrease to 0% B at 4.5 minutes and hold until 6 minutes for column re-equilibration at a flow rate of 2 mL/min.

Samples were ionized using an ionBooster ESI source (Bruker Daltonics Inc, Billerica, MA) in positive ion mode. Typical ionBooster operating conditions were 1000 V capillary voltage, 400 V end plate offset, 300 V charging voltage, 4.1 bar nebulizer pressure, 3.0 L/min dry gas, 250 ^{o}C dry heater, and 375 ^{o}C vaporizer.

A detailed overview of the TIMS analyzer and its operation can be found elsewhere [34-36]. The nitrogen bath gas flow is defined by the pressure difference between entrance funnel P_1 = 3.0 mbar and the exit funnel P_2 = 0.9 mbar at *ca.* 300 K (see Figure S1). The TIMS separation depends on the gas flow velocity (v_g), ramp voltage (V_{ramp}), base voltage (V_{out}) and ramp time (t_{ramp}= number of steps x TOF time). The scan rate ($Sr = \Delta V_{ramp}/t_{ramp}$) is directly related to the resolving power of the TIMS analyzer.

Each isomer emerges at a characteristic voltage ($V_{elution}$):

$$K_0 = v_g/E \approx A/(V_{elution} - V_{out}) \qquad (1)$$

where A is a calibration constant that can be determined using standards of known mobilities (*i.e.,* Tuning Mix calibration standard *m/z* 322, K_0 = 1.376 $cm^2\ V^{-1}\ s^{-1}$ and *m/z* 622, K_0 = 1.013 $cm^2\ V^{-1}\ s^{-1}$) [36]. The TIMS cell was operated using a fill/ramp sequence of 10ms/100ms for ~10% duty cycle and the TOF analyzer was operated at 10 kHz (*m/z* 100-2500). Typical values were $V_{deflector}$ = 180, $V_{capillary}$ = 150, $V_{funnel\ 1\ in}$ = 90V, V_{ramp} = -175 - 20, V_{out} = 60V, and a 250 Vpp at 880 kHz rf. A typical scan rate of S_r = 1.95 V/ms was used, or lower as needed to increase the mobility resolution. All voltages were controlled using custom software in LabView (National Instruments) synchronized with the MS platform controls. The data was segmented in LC frames over 10 analysis cycles yielding an LC-TIMS-TOF MS step size of ~2 s. The TIMS operation was controlled using in-house software, written in National Instruments Lab VIEW, and synchronized with the maXis Impact Q-ToF acquisition program [34].

Reduced mobility values (K_0) were correlated with collisional cross section (Ω) using the equation:

$$\Omega = \frac{(18\pi)^{1/2}}{16}\frac{z}{(k_B T)^{1/2}}\left[\frac{1}{m_I}+\frac{1}{m_b}\right]^{1/2}\frac{1}{K_0}\frac{1}{N^*} \quad (2)$$

where z is the charge of the ion, k_B is the Boltzmann constant, N^* is the number density of the bath gas, and m_I and m_b refer to the masses of the ion and bath gas, respectively [40]. LC-TIMS-TOF MS data were processed using Data Analysis software v. 5.0 (Bruker Daltonics Inc, Billerica, MA).

Theoretical calculations

A pool of candidate structures was proposed for all molecules of interest. Final structures were optimized at the DFT/B3LYP/6-311G(d,p) level using Gaussian software.[41] Vibrational frequencies were calculated to guarantee that the optimized structures correspond to actual minima in the energy space, and zero-point energy corrections were applied to calculate the relative stability between the structures. Theoretical ion-neutral collision cross sections were calculated using MOBCAL[42-43] software for nitrogen as a bath gas at ca. 300K. Partial atomic charges were calculated using the Merz-Singh-Kollman scheme constrained to the molecular dipole moment [44-45]

4.4 Results and Discussion

Ion mobility profiles of isomeric opioid compounds (6-acetylmorphine (6-AM) and naloxone; codeine and hydrocodone; morphine, hydromorphone, norcodeine and norhydrocodone; and their respective deuterated analogs) show a single band for each of

the protonated molecules $[M+H]^+$ (Figure 4.1) with small differences in ion-neutral collision cross section values in nitrogen ($^{TIMS}CCS_{N2}$): 6-AM and naloxone (176.7 and 171.1 $Å^2$, ~3%), codeine and hydrocodone (168.2 and 167.8 $Å^2$, <1%) and morphine, hydromorphone, norcodeine, and norhydrocodone (162.9, 163.2, 167.9 and 167.4 $Å^2$, <1-3%) (see Table 4.1). These CCS values agree (Table 4.1) with theoretically calculated CCS (<5%) and previous studies that measured reduced mobilities using drift tube ion mobility spectrometry (DT-IMS).[18, 24-25, 27, 32, 46] Upon review of the proposed candidate structures, visual similarities and differences in the size and shape, and, therefore, the theoretical CCS, are observed between opioid isomers (Figure 4.2). For example, major differences in the orientation of the nitrogen group as well as the methyl group on the oxygen atom are observed between 6-AM and naloxone (as highlighted in Figure 4.2). These differences are also observed in the measured experimental and theoretical CCS, which allow isomer separation, even at fast scanning rates (Table 4.1 and Figure 4.1). The candidate structures of codeine and hydrocodone, vary by the presence or absence of a carbonyl group on a six-membered ring. This difference results in minimal changes in size; that is, the CCS values only slightly differ from each other (Figure 4.2). Morphine, hydromorphone, norcodeine and norhydrocodone differ in structure at the nitrogen, depending on whether a secondary (norcodeine and norhydrocodone) or tertiary amine (morphine and hydromorphone) is present in the compound. The difference in orientation of the amine group alters the theoretically calculated and experimentally measured CCS (Figure 4.2). Specifically, the similar amine group orientations of morphine and hydromorphone mean that the compounds cannot be separated based on CCS. Conversely, morphine/norcodeine and

hydromorphone/norhydrocodone have different amine orientations can be baseline separated in their mobility profiles (see Figures 4.2 and 4.3).

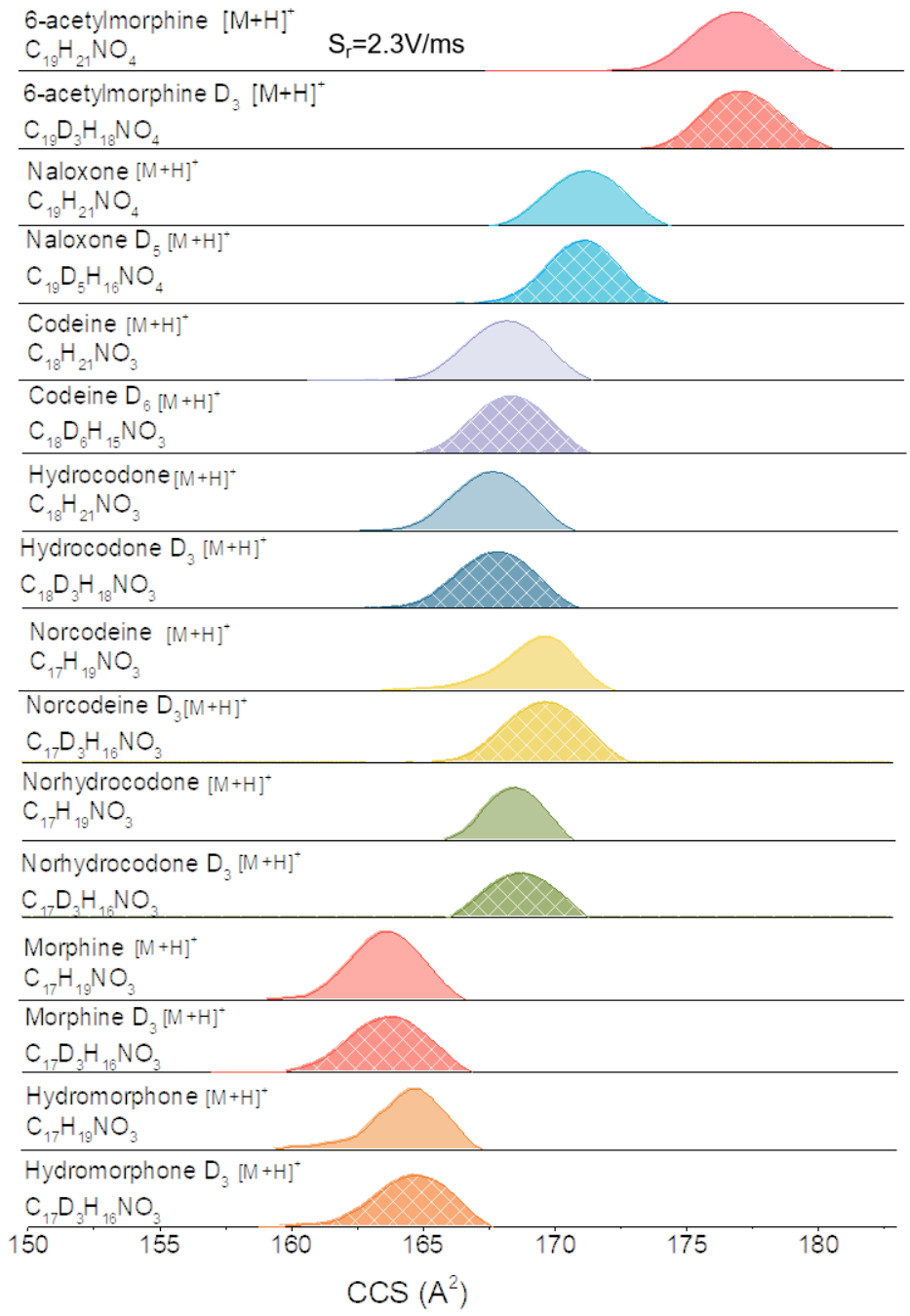

Figure 4.1: Typical mobility profiles of analytes and their corresponding internal standards

Name	Chemical Formula	Theoretical m/z $[M+H]^+$	Experimental m/z $[M+H]^+$	Error (ppm)	Theoretical CCS ($Å^2$)	Experimental $^{TIMS}CCS_{N2}$ ($Å^2$)	Experimental K_0 ($cm^2V^{-1}s^{-1}$)
6-Acetylmorphine	$C_{19}H_{21}NO_4$	328.1543	328.1545	0.609	166.2	176.7 (167-171.1)	1.182
6-Acetylmorphine-D3	$C_{19}H_{18}D_3NO_4$	331.1732	331.1733	0.302	166.3	176.9	1.189
Naloxone	$C_{19}H_{21}NO_4$	328.1543	328.1542	0.305	166.7	171.1	1.221
Naloxone-D5	$C_{19}H_{16}D_5NO_4$	333.1857	333.1855	0.600	166.6	171.0	1.229
Codeine	$C_{18}H_{21}NO_3$	300.1594	300.1596	0.600	171.6	168.2 (168.9-178.9)	1.268
Codeine-D6	$C_{18}H_{18}D_6NO_3$	306.1971	306.1969	0.653	171.7	168.0	1.256
Hydrocodone	$C_{18}H_{21}NO_3$	300.1594	300.1592	0.666	171.8	167.8	1.271
Hydrocodone-D3	$C_{18}H_{18}D_3NO_3$	303.1782	303.1783	0.330	171.7	167.9	1.257
Morphine	$C_{17}H_{19}NO_3$	286.1438	286.1437	0.349	162.6	162.9 (172.8-189.0)	1.290
Morphine-D3	$C_{17}H_{16}D_3NO_3$	289.1626	289.1625	0.346	162.4	164.0	1.289
Hydromorphone	$C_{17}H_{19}NO_3$	286.1438	286.1437	0.349	161.6	163.2 (160.3)	1.287
Hydromorphone-D3	$C_{17}H_{16}D_3NO_3$	289.1626	289.1625	0.692	161.5	164.4	1.286
Norcodeine	$C_{17}H_{19}NO_3$	286.1438	286.1440	0.699	168.8	167.9 (196.1)	1.252
Norcodeine-D3	$C_{17}H_{16}D_3NO_3$	289.1626	289.1625	0.346	168.9	167.9	1.259
Norhydrocodone	$C_{17}H_{19}NO_3$	286.1438	286.1438	0.000	168.9	167.4	1.256
Norhydrocodone-D3	$C_{17}H_{16}D_3NO_3$	289.1626	289.1625	0.692	168.9	168.0	1.259

Table 4.1: Experimental and theoretical m/z and CCS values for the opioid analytes considered. Note: values in parentheses refer to previously reported data from DT-IMS_{Air} [18, 24, 26, 44-46]

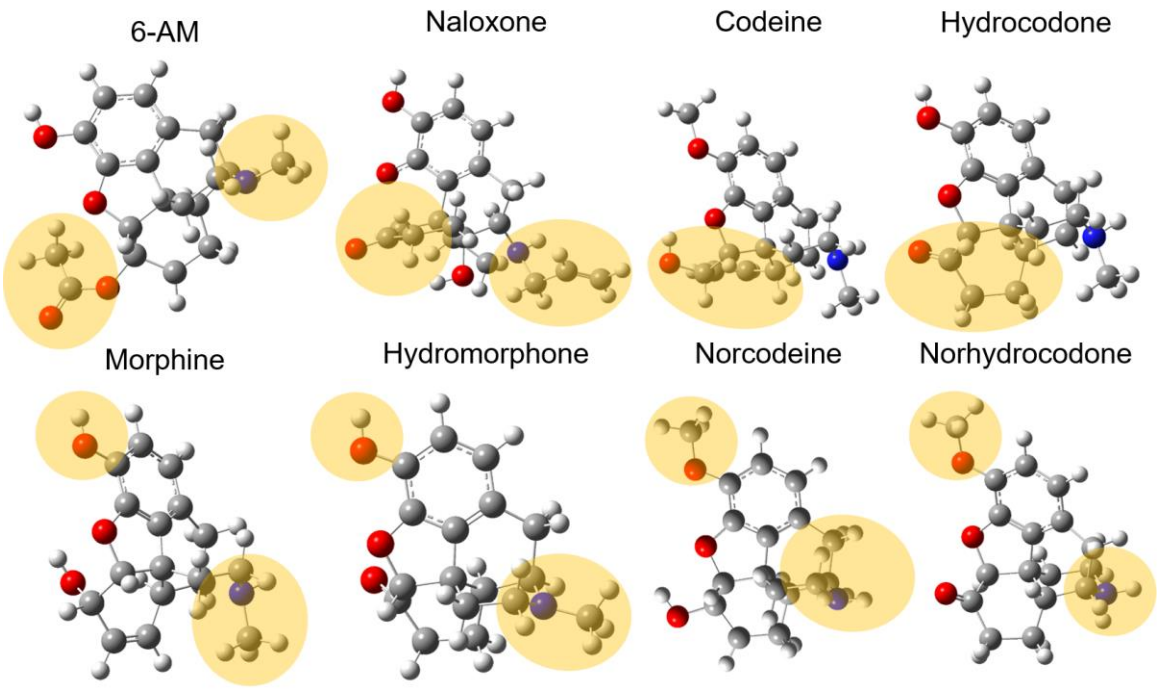

Figure 4.2: Candidate structures optimized at the DFT/B3LYP/6-311G(d,p) of the opioids considered

While mobility separation was observed using fast scan rates (Sr = 0.5-1.5 V/ms); it is noteworthy that baseline mobility separations are observed between 6-AM and naloxone, hydromorphone and norhydrocodone and morphine and norcodeine using slower scan rates (Sr = 0.2 V/ms) with resolving power in excess of 100 (see Figure 4.3). The ability to obtain baseline separation between these isomeric opioids can be attributed to the size and shape of the individual compounds, based the reported candidate structures (Figure 4.2). Previous mobility analyses using drift tube IMS report resolving powers of about 70 for codeine and morphine, which are not isomers.[30] Despite the high resolving power of the TIMS analyzer, complete separation for all the isomers considered was not obtained (e.g., codeine and hydrocodone, morphine and hydromorphone, nor norcodeine and norhydrocodone), due to the marginal structural differences leading to minimal variations in CCS between these isomers (<1 $Å^2$). Isomeric opioids that have previously separated

include: hydromorphone, morphine and norhydrocodone, via field asymmetric ion mobility spectrometry (FAIMS) MRM-MS[28] and codeine and hydrocodone using a modified differential mobility spectrometry (DMS) cell.[47]

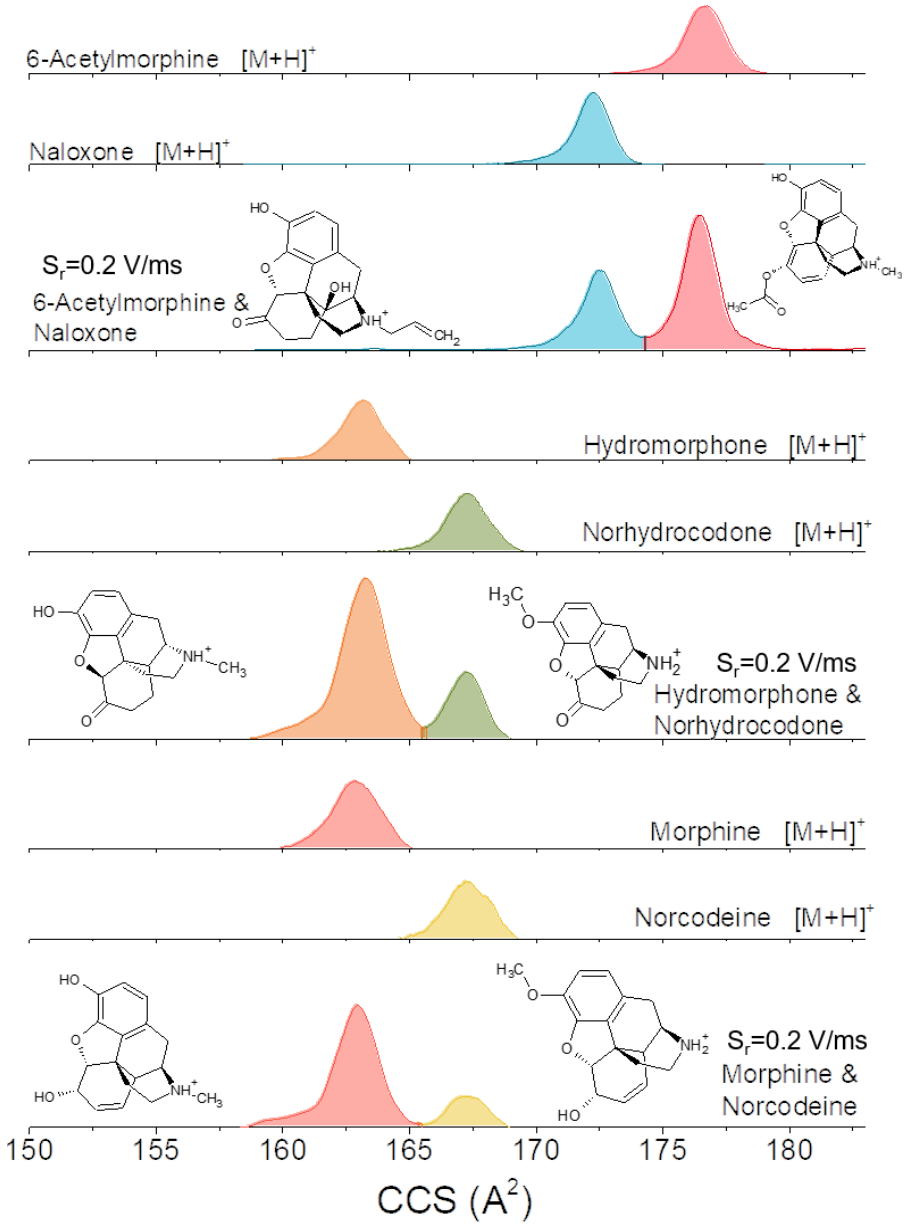

Figure 4.3: Typical IMS separations of binary mixtures: top) 6-acetylmorphine and naloxone; middle) hydromorphone and norhydrocodone; bottom) morphine and norcodeine

The influence of matrix effects on the "dilute and shoot" LC-TIMS-MS workflow was studied by comparing the separation of opioid standards in water and in human urine. Inspection of the 2D-IMS-MS plots show a single trendline, containing the opioids as well as other potential interferences from the urine sample. Closer inspection of the opioid region reveals the separation of the opioid signals; however, potential molecular interferences from the urine may lead to higher limits of detection when compared to other IMS-MS-based DTM methods where the compounds of interest fall in a different trendline (data not shown).[37] Moreover, the added advantage of liquid chromatography as a third dimension of separation allows for a clear separation of the potential matrix interferants as well as the separation of isomeric analytes that were not possible by TIMS-MS alone (Figure 4.4). The chromatographic program in this research had a final separation time of 6 min which is comparable to the reported LC-MRM times (e.g., 6-35 min) for opioid analysis.[14] Notice that the IS can be easily identified since they share the same retention time and CCS as their corresponding analyte. For example, naloxone and 6-AM can be separated by TIMS and by LC (retention times of 2.90 and 2.94 min, respectively). For quantification purposes, while the potential targets for naloxone and 6-AM isomers will have the same mass value, the IS of choice have different levels of deuteration so that they can be easily separated in the MS domain. That is, naloxone shows peaks at *m/z* 328.1542 and 333.1857 corresponding to the $[M+H]^+$ of the analyte and the IS $[M(D_5)+H]^+$ containing five deuterium atoms. The mass spectrum for 6-AM contains two main peaks at m/z 328.1542 and 331.1730, corresponding to the analyte $[M+H]^+$ and the IS $[M(D_3)+H]^+$ with three deuterium atoms (Figure 4.4a). Codeine and hydrocodone are not separated in the mobility domain, yet there is near-baseline separation in the LC (2.92 and

2.97 minutes, respectively) (Figure 4.4b). Analogous to the naloxone and 6-AM quantification, the IS for codeine and hydrocodone are chosen with different amounts of deuterium so that they can be easily separated in the MS domain. Norcodeine and norhydrocodone are not separated in the mobility domain, yet there is near-baseline separation in the LC (2.91 and 2.97 min, respectively) (Figure 4.4c).

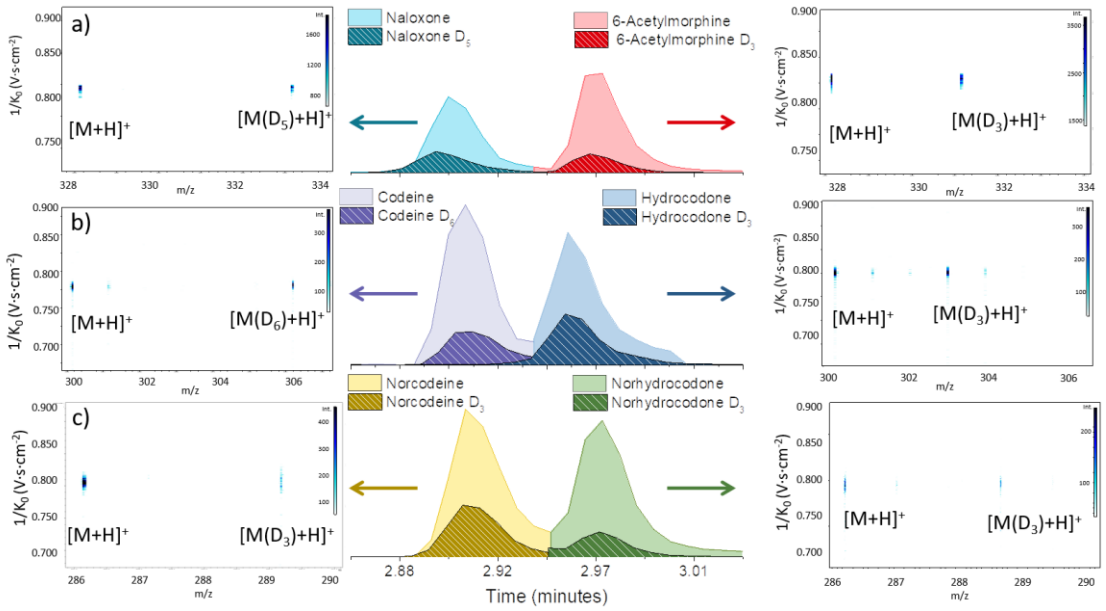

Figure 4.4: Typical LC-TIMS-TOF MS analysis of isomeric opioids. 2D-IMS-MS contour plots are shown for the highlighted LC bands

Limits of detection (LODs) were compared between traditional two-dimensional separation (e.g., LC-TOF MS) and the currently proposed three-dimensional separation (e.g., LC-TIMS-TOF MS) for rapid and robust analysis of drugs of abuse and their metabolites. The LC-TOF MS and LC-TIMS-TOF MS results are summarized in Table 4.2; noteworthy are the LC-TIMS-TOF MS LODs for the common opioids in human urine:

1.4-31.2 ng/mL using a DTM method. These results compare to reported LODs of 0.6-2.5 ng/mL with 4-160 ng/mL linearity range using various extraction methods with MRM.[14, 48-50] An increase in the LODs was generally observed in the presence of human urine which is consistent with increased background levels and/or decreased ionization yields associated with matrix effects. The limits of quantitation (LOQs) range from 30.2-156 ng/mL which are in agreement with reported LOQs of 0.1-126 ng/mL from single reaction monitoring (SRM) and MRM approaches.[14, 48-50]

Evaluation of reproducibility and effect of chemical environment for three identification parameters (CCS, RT and m/z) is illustrated across the calibration levels analyzed (Figure 4.5). In the CCS domain, marginal deviations were observed between samples with and without urine (relative percent deviation, RPD, <0.5%). Additionally, CCS values did not change across calibration levels, suggesting that CCS is a valid parameter for analyte identification in the tested range and that this parameter could be a valuable addition to the traditionally used for qualitative analysis such as retention time (RT) and, when possible, accurate mass. In this case, RTs were minimally affected in the presence of urine (RPD of samples analyzed in urine compared to water were below 0.5%) and a high mass accuracy (<1 ppm) was observed for all analytes across calibration levels in the presence of urine. In addition, intra-day reproducibility is shown by small (<0.25%) percent relative standard (%RSD) for individual analytes in water and human urine across the seven calibration points (Table 4.3). These results demonstrate the reliability of this methodology for identifications in multiple dimensions using LC-TIMS-MS for quantitative analyses at the low ng/mL levels. During the performance of the matrix effect

experiments, no significant differences in the matrix factor (MF) of ten individual urine samples were observed for morphine, norhydromorphone, norcodeine, norhydrocodone, codeine and hydrocodone spiked at high (400 ng/mL) and low (75 ng/mL) concentrations (coefficient of variance, CV>15%) (See Figure S2).

.

Analyte	LC-TIMS-qTOF MS						LC-qTOF MS					
	Water			Urine			Water			Urine		
	LOD (ng/mL)	LOQ (ng/mL)	R^2	LOD (ng/mL)	LOQ (ng/mL)	R^2	LOD (ng/mL)	LOQ (ng/mL)	R^2	LOD (ng/mL)	LOQ (ng/mL)	R^2
Codeine	2.0	10.4	0.994	9.9	49.6	0.996	1.4	6.9	0.997	3.0	15.0	0.994
Hydrocodone	3.0	15.1	0.994	6.0	30.2	0.996	1.8	9.1	0.997	7.6	38.2	0.995
Morphine	7.9	39.5	0.996	27.9	138.6	0.993	7.9	39.5	0.996	31.9	159.4	0.999
Norcodeine	8.3	41.6	0.997	31.2	156.0	0.999	7.4	37.3	0.997	35.2	176.0	0.999
Norhydrocodone	8.1	40.4	0.995	29.1	145.8	0.996	8.1	40.7	0.996	20.7	103.5	0.996

Table 4.2: Calibration results for analytes with (Matrix) and without urine (No Matrix) for LC-TIMS-qTOF MS and LC-qTOF MS

Intraday Variability	RT (% RSD)		CCS (% RSD)	
Compound	**Water**	**Urine**	**Water**	**Urine**
6-Acetylmorphine	0.07	0.04	0.18	0.22
Naloxone	0.12	0.12	0.19	0.23
Codeine	0.08	0.10	0.19	0.18
Hydrocodone	0.08	0.10	0.22	0.27
Norcodeine	0.09	0.07	0.22	0.21
Norhydrocodone	0.05	0.07	0.20	0.22

Table 4.3: Intraday Variability of CCS and RT with and without urine represented by percent relative standard deviation (%RSD)

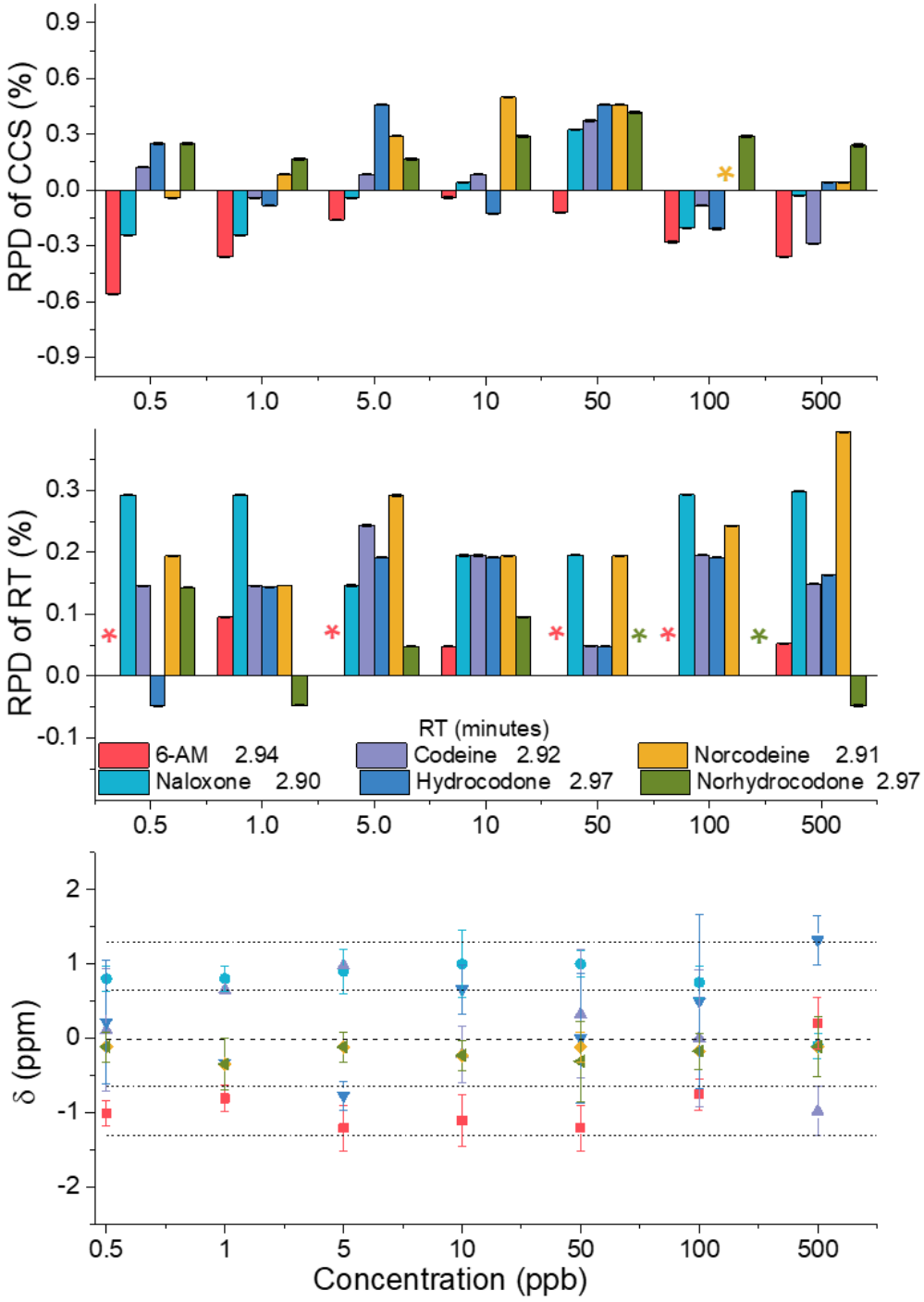

Figure 4.5: Relative percent deviation of RT, CCS compared to non-matrix sample and δ m/z across calibration levels (*= no change)

4.5 Conclusions

For the first time, liquid chromatography, trapped ion mobility spectrometry and mass spectrometry were combined for fast separation, identification and quantitation of opioids and their metabolites in human urine using a "dilute and shoot" approach. The proposed workflow provides analytical separation in the mobility and chromatographic domains within a 6 min analysis time, with LODs of 1.4 - 35.2 ng/mL with 0.5-500 ng/mL linearity range using DTM of opioids in urine. A good agreement was observed between the previously reported ^{DTIMS}CCS, measured ^{TIMS}CCS, and the theoretical CCS of the candidate structures for the familiar opioids optimized at the DFT/B3LYP level. Beside the higher confidence during LC-TIMS-TOF MS analyses, similar LODs and LOQs are reported to those obtained using traditional LC-MRM measurements, with small relative percent deviations in retention times (<0.3%), and collision cross sections (<0.6%) and high mass accuracy (<1ppm). The need for complementary liquid and mobility separations prior to mass analysis is shown for the analysis of complex mixtures, with a two-fold increase in mobility resolving power (R~ 80-130) compared to previous reports using DT-IMS (R~50-70).

4.6 Acknowledgements

This work was supported by a National Science Foundation Division of Chemistry, under CAREER award CHE-1654274, with co-funding from the Division of Molecular and Cellular Biosciences to F.F.-L. The authors would also like to acknowledge the helpful discussions and technical support from Dr. Mark E. Ridgeway and Dr. Melvin A. Park from Bruker Daltonics Inc. during the development and installation of the custom-built

TIMS-TOF MS instrument. KJA would like to thank the financial support from an FIU Dissertation Year Fellowship.

4.7 References

1. Rudd, R. A.; Aleshire, N.; Zibbell, J. E.; Matthew Gladden, R., Increases in drug and opioid overdose deaths—United States, 2000–2014. *American Journal of Transplantation* **2016,** *16* (4), 1323-1327.

2. Rudd, R. A., Increases in drug and opioid-involved overdose deaths—United States, 2010–2015. *Morbidity and Mortality Weekly Report* **2016,** *65*, 1445-1452.

3. Volkow, N. D.; McLellan, A. T., Opioid abuse in chronic pain—misconceptions and mitigation strategies. *New England Journal of Medicine* **2016,** *374* (13), 1253-1263.

4. Gladden, R. M., Fentanyl law enforcement submissions and increases in synthetic opioid–involved overdose deaths—27 states, 2013–2014. *MMWR. Morbidity and mortality weekly report* **2016,** *65*.

5. Chen, L. H.; Hedegaard, H.; Warner, M., Drug-poisoning deaths involving opioid analgesics: United States, 1999-2011. *NCHS data brief* **2014,** (166), 1-8.

6. Wong, S. H. Y.; Sunshine, I., *Handbook of Analytical Therapeutic Drug Monitoring and Toxicology*. CRC Press: 1996.

7. Okie, S., A flood of opioids, a rising tide of deaths. *New England Journal of Medicine* **2010,** *363* (21), 1981-1985.

8. Smith, M. L.; Hughes, R. O.; Levine, B.; Dickerson, S.; Darwin, W. D.; Cone, E. J., Forensic drug testing for opiates. VI. Urine testing for hydromorphone, hydrocodone, oxymorphone, and oxycodone with commercial opiate immunoassays and gas chromatography-mass spectrometry. *Journal of Analytical Toxicology* **1995,** *19* (1), 18-26.

9. Gergov, M.; Nokua, P.; Vuori, E.; Ojanperä, I., Simultaneous screening and quantification of 25 opioid drugs in post-mortem blood and urine by liquid chromatography–tandem mass spectrometry. *Forensic Science International* **2009,** *186* (1), 36-43.

10. Yang, A.; Arfken, C. L.; Johanson, C. E., Steps physicians report taking to reduce diversion of buprenorphine. *The American Journal on Addictions* **2013,** *22* (3), 184-187.

11. Marsch, L. A.; Stephens, M. A. C.; Mudric, T.; Strain, E. C.; Bigelow, G. E.; Johnson, R. E., Predictors of outcome in LAAM, buprenorphine, and methadone treatment for opioid dependence. *Experimental and Clinical Psychopharmacology* **2005,** *13* (4), 293.

12. Manchikanti, L.; Manchukonda, R.; Pampati, V.; Damron, K. S.; Brandon, D.; Cash, K.; McManus, C., Does random urine drug testing reduce illicit drug use in chronic pain patients receiving opioids? *Pain Physician* **2006,** *9* (2), 123.

13. Katz, N.; Fanciullo, G. J., Role of urine toxicology testing in the management of chronic opioid therapy. *The Clinical journal of pain* **2002,** *18* (4), S76-S82.

14. French, D., The challenges of LC–MS/MS analysis of opiates and opioids in urine. *Bioanalysis* **2013,** *5* (22), 2803-2820.

15. Manchikanti, L.; Malla, Y.; Wargo, B. W.; Fellows, B., Comparative evaluation of the accuracy of immunoassay with liquid chromatography tandem mass spectrometry (LC/MS/MS) of urine drug testing (UDT) opioids and illicit drugs in chronic pain patients. *Pain Physician* **2011,** *14* (2), 175-187.

16. Pesce, A.; Rosenthal, M.; West, R.; West, C.; BCrews, B.; Mikel, C.; Almazan, P.; Latyshev, S., An evaluation of the diagnostic accuracy of liquid chromatography-tandem mass spectrometry versus immunoassay drug testing in pain patients. *Pain Physician* **2010,** *13*, 273-281.

17. Wu, A. H.; McKay, C.; Broussard, L. A.; Hoffman, R. S.; Kwong, T. C.; Moyer, T. P.; Otten, E. M.; Welch, S. L.; Wax, P., National academy of clinical biochemistry laboratory medicine practice guidelines: recommendations for the use of laboratory tests to support poisoned patients who present to the emergency department. *Clinical Chemistry* **2003,** *49* (3), 357-379.

18. Matz, L. M.; Hill, H. H., Evaluation of opiate separation by high-resolution electrospray ionization-ion mobility spectrometry/mass spectrometry. *Analytical Chemistry* **2001,** *73* (8), 1664-1669.

19. Dienes-Nagy, A.; Rivier, L.; Giroud, C.; Augsburger, M.; Mangin, P., Method for quantification of morphine and its 3-and 6-glucuronides, codeine, codeine glucuronide and

6-monoacetylmorphine in human blood by liquid chromatography–electrospray mass spectrometry for routine analysis in forensic toxicology. *Journal of Chromatography A* **1999,** *854* (1), 109-118.

20. Blanchet, M.; Bru, G.; Guerret, M.; Bromet-Petit, M.; Bromet, N., Routine determination of morphine, morphine 3-β-d-glucuronide and morphine 6-β-d-glucuronide in human serum by liquid chromatography coupled to electrospray mass spectrometry. *Journal of Chromatography A* **1999,** *854* (1), 93-108.

21. Muñoz-Muñoz, A. C.; Pekol, T.; Schubring, D.; Johnson, C.; Andrade, L., Identification of Novel Opioid Interferences using High-Resolution Mass Spectrometry. *Journal of Analytical Toxicology* **2017**, 1-11.

22. Langman, L. J.; Korman, E.; Stauble, M. E.; Boswell, M. V.; Baumgartner, R. N.; Jortani, S. A., Therapeutic monitoring of opioids: a sensitive LC–MS/MS method for quantitation of several opioids including hydrocodone and its metabolites. *Therapeutic Drug Monitoring* **2013,** *35* (3), 352-359.

23. Yang, H. S.; Wu, A. H.; Lynch, K. L., Development and validation of a novel LC-MS/MS opioid confirmation assay: Evaluation of β-glucuronidase enzymes and sample cleanup methods. *Journal of Analytical Toxicology* **2016,** *40* (5), 323-329.

24. Eatherton, R.; Morrissey, M.; Hill, H. H., Comparison of ion mobility constants of selected drugs after capillary gas chromatography and capillary supercritical fluid chromatography. *Analytical Chemistry* **1988,** *60* (20), 2240-2243.

25. Lawrence, A., Ion mobility spectrometry/mass spectrometry of some prescription and illicit drugs. *Analytical Chemistry* **1986,** *58* (6), 1269-1272.

26. Liu, C.; Gómez-Ríos, G. A.; Schneider, B. B.; Le Blanc, J. Y.; Reyes-Garcés, N.; Arnold, D. W.; Covey, T. R.; Pawliszyn, J., Fast quantitation of opioid isomers in human plasma by differential mobility spectrometry/mass spectrometry via SPME/open-port probe sampling interface. *Analytica Chimica Acta* **2017,** *991*, 89.

27. Liuni, P.; Romanov, V.; Binette, M.-J. e.; Zaknoun, H.; Tam, M.; Pilon, P.; Hendrikse, J.; Wilson, D. J., Unambiguous Characterization of Analytical Markers in Complex, Seized Opiate Samples Using an Enhanced Ion Mobility Trace Detector-Mass Spectrometer. *Analytical Chemistry* **2014,** *86* (21), 10772-10779.

28. Manicke, N. E.; Belford, M., Separation of opiate isomers using electrospray ionization and paper spray coupled to high-field asymmetric waveform ion mobility spectrometry. *Journal of the American Society for Mass Spectrometry* **2015,** *26* (5), 701-705.

29. McCooeye, M. A.; Ells, B.; Barnett, D. A.; Purves, R. W.; Guevremont, R., Quantitation of morphine and codeine in human urine using high-field asymmetric waveform ion mobility spectrometry (FAIMS) with mass spectrometric detection. *Journal of Analytical Toxicology* **2001,** *25* (2), 81-87.

30. Midey, A. J.; Patel, A.; Moraff, C.; Krueger, C. A.; Wu, C., Improved detection of drugs of abuse using high-performance ion mobility spectrometry with electrospray ionization (ESI-HPIMS) for urine matrices. *Talanta* **2013,** *116*, 77-83.

31. O'Donnell, R. M.; Sun, X.; Harrington, P. d. B., Pharmaceutical applications of ion mobility spectrometry. *Trends in Analytical Chemistry* **2008,** *27* (1), 44-53.

32. Wu, C.; Siems, W. F.; Hill, H. H., Secondary electrospray ionization ion mobility spectrometry/mass spectrometry of illicit drugs. *Analytical Chemistry* **2000,** *72* (2), 396-403.

33. Adams, K. J.; Montero, D.; Aga, D.; Fernandez-Lima, F., Isomer separation of polybrominated diphenyl ether metabolites using nanoESI-TIMS-MS. *International Journal for Ion Mobility Spectrometry* **2016,** *19* (2), 69-76.

34. Fernandez-Lima, F. A.; Kaplan, D. A.; Suetering, J.; Park, M. A., Gas-phase separation using a Trapped Ion Mobility Spectrometer. *International Journal for Ion Mobility Spectrometry* **2011,** *14* (2-3), 93-98.

35. Fernandez-Lima, F. A.; Kaplan, D. A.; Park, M. A., Note: Integration of trapped ion mobility spectrometry with mass spectrometry. *Review of Scientific Instruments* **2011,** *82* (12), 126106.

36. Hernandez, D. R.; DeBord, J. D.; Ridgeway, M. E.; Kaplan, D. A.; Park, M. A.; Fernandez-Lima, F. A., Ion dynamics in a trapped ion mobility spectrometer. *Analyst* **2014,** *139* (8), 1913-1921.

37. Adams, K. J.; Smith, N. F.; Ramirez, C. E.; Fernandez-Lima, F., Discovery and targeted monitoring of polychlorinated biphenyl metabolites in blood plasma using LC-TIMS-TOF MS. *International Journal of Mass Spectrometry* **2017**.

38. Benigni, P.; Thompson, C. J.; Ridgeway, M. E.; Park, M. A.; Fernandez-Lima, F. A., Targeted High-Resolution Ion Mobility Separation Coupled to Ultrahigh-Resolution Mass Spectrometry of Endocrine Disruptors in Complex Mixtures. *Analytical Chemistry* **2015,** *87* (8), 4321-4325.

39. Castellanos, A.; Benigni, P.; Hernandez, D. R.; DeBord, J. D.; Ridgeway, M. E.; Park, M. A.; Fernandez-Lima, F. A., Fast Screening of Polycyclic Aromatic Hydrocarbons using Trapped Ion Mobility Spectrometry – Mass Spectrometry. *Analytical Methods* **2014,** *6*, 9328-9332.

40. McDaniel, E. W.; Mason, E. A., *Mobility and diffusion of ions in gases*. John Wiley and Sons, Inc., New York: New York, 1973; p 381.

41. Frisch, M. J.; Trucks, G. W.; Schlegel, H. B.; Scuseria, G. E.; Robb, M. A.; Cheeseman, J. R.; Montgomery, J., J. A.; Vreven, T.; Kudin, K. N.; Burant, J. C.; Millam, J. M.; Iyengar, S. S.; Tomasi, J.; Barone, V.; Mennucci, B.; Cossi, M.; Scalmani, G.; Rega, N.; Petersson, G. A.; Nakatsuji, H.; Hada, M.; Ehara, M.; Toyota, K.; Fukuda, R.; Hasegawa, J.; Ishida, M.; Nakajima, T.; Honda, Y.; Kitao, O.; Nakai, H.; Klene, M.; Li, X.; Knox, J. E.; Hratchian, H. P.; Cross, J. B.; Bakken, V.; Adamo, C.; Jaramillo, J.; Gomperts, R.; Stratmann, R. E.; Yazyev, O.; Austin, A. J.; Cammi, R.; Pomelli, C.; Ochterski, J. W.; Ayala, P. Y.; Morokuma, K.; Voth, G. A.; Salvador, P.; Dannenberg, J. J.; Zakrzewski, V. G.; Dapprich, S.; Daniels, A. D.; Strain, M. C.; Farkas, O.; Malick, D. K.; Rabuck, A. D.; Raghavachari, K.; Foresman, J. B.; Ortiz, J. V.; Cui, Q.; Baboul, A. G.; Clifford, S.; Cioslowski, J.; Stefanov, B. B.; Liu, G.; Liashenko, A.; Piskorz, P.; Komaromi, I.; Martin, R. L.; Fox, D. J.; Keith, T.; Al-Laham, M. A.; Peng, C. Y.; Nanayakkara, A.; Challacombe, M.; Gill, P. M. W.; Johnson, B.; Chen, W.; Wong, M. W.; Gonzalez, C.; Pople, J. A. *Gaussian 03, Revision C.02*, Wallingford CT, 2004.

42. Campuzano, I.; Bush, M. F.; Robinson, C. V.; Beaumont, C.; Richardson, K.; Kim, H.; Kim, H. I., Structural characterization of drug-like compounds by ion mobility mass spectrometry: comparison of theoretical and experimentally derived nitrogen collision cross sections. *Analytical Chemistry* **2011,** *84* (2), 1026-1033.

43. Kim, H. I.; Kim, H.; Pang, E. S.; Ryu, E. K.; Beegle, L. W.; Loo, J. A.; Goddard, W. A.; Kanik, I., Structural characterization of unsaturated phosphatidylcholines using traveling wave ion mobility spectrometry. *Analytical Chemistry* **2009,** *81* (20), 8289-8297.

44. Singh, U. C.; Kollman, P. A., An approach to computing electrostatic charges for molecules. *Journal of Computational Chemistry* **1984,** *5* (2), 129-145.

45. Besler, B. H.; Merz, K. M.; Kollman, P. A., Atomic charges derived from semiempirical methods. *Journal of Computational Chemistry* **1990,** *11* (4), 431-439.

46. Kanu, A. B.; Leal, A., Identity Efficiency for High-Performance Ambient Pressure Ion Mobility Spectrometry. *Analytical Chemistry* **2016,** *88* (6), 3058-3066.

47. Liu, C.; Gómez-Ríos, G. A.; Schneider, B. B.; Le Blanc, J. Y.; Reyes-Garcés, N.; Arnold, D. W.; Covey, T. R.; Pawliszyn, J., Fast quantitation of opioid isomers in human plasma by differential mobility spectrometry/mass spectrometry via SPME/open-port probe sampling interface. *Analytica Chimica Acta* **2017,** *991*, 89-94.

48. Edinboro, L. E.; Backer, R. C.; Poklis, A., Direct analysis of opiates in urine by liquid chromatography-tandem mass spectrometry. *Journal of Analytical Toxicology* **2005,** *29* (7), 704-710.

49. Cao, Z.; Kaleta, E.; Wang, P., Simultaneous quantitation of 78 drugs and metabolites in urine with a dilute-and-shoot LC–MS-MS assay. *Journal of Analytical Toxicology* **2015,** *39* (5), 335-346.

50. Schaefer, N.; Peters, B.; Schmidt, P.; Ewald, A. H., Development and validation of two LC-MS/MS methods for the detection and quantification of amphetamines, designer amphetamines, benzoylecgonine, benzodiazepines, opiates, and opioids in urine using turbulent flow chromatography. *Analytical and Bioanalytical Chemistry* **2013,** *405* (1), 247-258.

CHAPTER FIVE:
Lipid Specific Molecular Ion Emission as a Function of the Primary Ion Characteristics in TOF-SIMS

This chapter was published in the Journal of Vacuum Science and Technology B and adapted with permission.

Kendra J. Adams, John Daniel DeBord, Francisco Fernandez-Lima (2016) *Journal of Vacuum Science & Technology B, Nanotechnology and Microelectronics: Materials, Processing, Measurement, and Phenomena*, 34(5), 051804.

5.1 Abstract

In the present work, the emission characteristics of lipids as a function of the primary ion cluster size and energy were studied using time-of-flight secondary ion mass spectrometry (TOF-SIMS). Characteristic fragmentation patterns for common lipids are described and changes in secondary ion (SI) yields using various primary ion beams are reported. In particular, emission characteristics were studied for pairs of small polyatomic and nanoparticle primary ion beams (*e.g.*, Bi_3^+ *vs* Ar_{1000}^+ and Au_3^+ *vs* Au_{400}^{+4}) based on the secondary ion yield of characteristic fragment and intact molecular ions as a function of the lipid class. Detailed descriptions of the fragmentation patterns is shown for positive and negative mode TOF-SIMS. Results demonstrate that the lipid structure largely dictates the spectral presence of molecular and/or fragment ions in each ionization mode due to the localization of the charge carrier (head group or fatty acid chain). Our results suggest that the larger the energy per atom for small polyatomic projectiles (Bi_3^+ and Au_3^+), the larger the SI yield; in the case of nanoparticle projectiles, the SI increase with primary ion energy (200-500 keV range) for Au_{400}^{+4} and with the decrease of the energy per atom (10-40 eV/atom range) for $Ar_{n=500-2000}^+$ clusters. Ion suppression due to matrix effects showed no correlation with the type of primary ion was observed.

5.2 Introduction

Secondary ion mass spectrometry (SIMS) is the gold standard for surface analysis of biological samples with submicron spatial resolution.[1-6] Over the years, the primary ion beam of choice has changed as new ion sources have been developed and capabilities by application (*e.g.*, organic *vs* inorganic surfaces) have been documented.[7-9] For example, atomic and small polyatomic projectiles have shown distinct advantages for high spatial

resolution, while larger clusters and nanoparticle projectiles have shown enhanced molecular ion emission.[7-8, 10-12] In addition, for the analysis of biological surfaces, the reduced damaged cross section of some nanoparticle projectiles (e.g., C_{60}, argon and water clusters) has triggered recent developments for tridimensional biological imaging and profiling.[7, 13-17] For example, a continuous Ar_{1000}^{+} beam provides a somewhat 'softer' desorption process which reduces the internal energy imparted to desorbed molecules, resulting in significant improvements of molecular ion or pseudo-molecular ion yields. These types of molecular ions tend to be more diagnostic for structural characterization and identification of the biological systems from which they are generated.[18] It has been reported that for an argon cluster beam, ideal ion yields are achieved when $E_{atom} \geq 10$ eV and ion yields will quickly decline as the E_{atom} decreases.[15] It was also observed that when water molecules are used as primary ion beams, the optimal energy was about 3 eV/atom, which leads authors to believe further exploration into larger cluster projectiles is possible.[15] During the study of peptides using various primary ion energies of an argon cluster it has been shown that larger peptide fragments were observed with lower energy beams as long as they were above 10 eV/atom; in addition, fragment intensity tends to decrease with increasing mass at 20 or 40 eV/atom.[18]

Lipid profiling of biological samples is traditionally based on liquid extraction followed by liquid chromatography coupled to mass spectrometry (LC-MS/MS), with the collision induced dissociation spectra providing the necessary structural identification of the lipid class.[19-21] Alternatively, we have recently shown that lipid identification can be performed using direct surface probe analysis (matrix-assisted laser desorption/ionization, MALDI), coupled to ultrahigh resolution mass spectrometry (Fourier transform ion

cyclotron resonance mass spectrometry, FT-ICR MS) followed by statistical analysis of variability and reproducibility across batches using internal standards.[22] Lipid assignment from MS data can be performed utilizing the LIPIDMAPS database, where lipids are divided into eight major classes; fatty acyls (FA), glycerolipids (GL), glycerophospholipids (GP), sphingolipids (SP), sterol lipids (ST), prenol lipids (PR), saccharolipids (SL) and polyketides (PK).[23-25] Analogous to MALDI probes, SIMS allows for *in situ* analysis of native biological surfaces, with higher spatial resolution. Due to the nature of molecular ion emission during SIMS analysis (not as soft as MALDI), fragmentation and intact molecular ion emission can be observed, with relative intensities varying with projectile size and energy. That is, the selection of the primary ion and energy determines the energy deposited per surface layer and the desorption volume, which corresponds to the observation of specific secondary ions.[26-27] For example, during the analysis of lipid components from a biological surface, analyte specific fragment ions (lipid head groups and fatty acid fragments) are mainly observed under monoatomic and small polyatomic bombardment (*e.g.*, In, Ga, Cs, Au_3^+, Bi_3^+, sources)[28] while lipid molecular ions are increased under larger projectile bombardment (*e.g.*, C_{60} and Au_{400}^{+4}). In a comparison of 40 keV C_{60}^+ to 40 keV Ar_{4000}^+ by Angerer and coworkers, it was observed that a majority of intact lipids from mouse brain were seen at higher secondary ion yields with the Ar_{4000}^+ primary ion, that is the primary ion beam that provided the larger cluster size but lower E_{atom}.[29] This study also analyzed the signal of the pseudo-molecular ion of cholesterol $[M+H-H_2O]^+$ using the aforementioned primary ion species and observed that similar secondary ion yields were detected for both of the projectiles, however, using Ar_{4000}^+ a lower yield in the smaller lipid fragments was observed.[29]

In the present paper, we study the lipid specific molecular ion emission as a function of the primary ion characteristics utilizing time-of-flight, secondary ion mass spectrometry (TOF-SIMS). In particular, we revisit the molecular ion emission characteristics for two pairs of small polyatomic and nanoparticle primary ion beams (*e.g.*, Bi_3^+ *vs* Ar_{1000}^+ and Au_3^+ *vs* Au_{400}^{+4}) using the secondary ion yield of fragment and intact molecular ions for familiar lipids. Emphasis is made on the relative distribution of lipid-specific fragment ions and molecular ions as a function of the projectile size and energy as well as the matrix effects on the ionization efficiency and secondary ion yields.

5.3 Experimental

5.3.1 Sample Preparation

Lipid standards of sulfatides [131305, Brain, Porcine, (major component 18:1/24:1 ST)], sphingomyelin [860061, Egg, Chicken (major component 18:1/16:0 SM)], 1,2-dipalmitoyl-sn-glycero-3-phosphocholine [850355, (16:0 PC DPPC)], 1-stearoyl-2-oleoyl-sn-glycero-3-phospho-(1'-rac-glycerol) (sodium salt) [840503, (18:0-18:1 PG)] and 1,2-dimyristoyl-sn-glycero-3-phosphoethanolamine [850745, (14:0 PE)] were purchased from Avanti Lipids Inc. (Alabaster, AL) and used as received. Each standard was dissolved in a dichloromethane: methanol (60:40) solution for a final concentration of 1 mg/mL each. Each standard was deposited onto an ITO slide (Sigma Aldrich, St. Louis, MO) by aerosol spray of 1 mL to guarantee surface homogeneity. The aerosol sprayer was washed with the same solvent solution in between spraying of individual standards. The samples were allowed to dry in a chemical hood prior to SIMS analysis. The same procedure was followed for the preparation of a mixture of lipid standards consisting of sulfatides, SM, DPPC, PE, and PG all equivolume with concentrations of 0.167 mg/mL.

5.3.2 SIMS Analysis

Standards were analyzed using Bi_3^+, Ar_{1000}^+, Au_3^+ and Au_{400}^{+4} primary ions in positive and negative ionization modes. A commercial IonTOF[5] instrument (Chestnut Ridge, NY) containing a hybrid detector with a single microchannel plate, scintillator and photomultiplier was used for the 25 keV Bi_3^+ and 20 keV $Ar_{500\text{-}2000}^+$ analysis. The 25 keV Bi_3^+ (0.12 pA) and 20 keV Ar_{1000}^+ (0.04 pA) primary ion beams were rastered in sawtooth mode over a 250x250 μm^2 field of view and mass spectra were collected for a total dose density of 2×10^{11} ions/cm^2. Measurements were obtained in pulsed mode static SIMS at a frequency of 7.7 kHz. The opening time of the second plate of the dual blanking plate has been reduced to obtain a lower beam current for Bi_3^+ and subsequently avoid saturation of the detector. Secondary ion yields were normalized to the number of primary ions used to generate the mass spectral peak or total ion dose. A low energy flood gun is also utilized between pulses to ensure the sample surface remains neutral throughout the analysis. An internal calibration was performed using low mass ions and lipid head groups typically present in the sample: $C_2H_3^+$, $C_2H_5^+$, $C_3H_7^+$, $C_5H_{12}N^+$ and $C_5H_{14}NO^+$ in positive mode and CH^-, CH_2-, OH^-, CN^- Cl^-, CNO^-, PO_2^-, PO_3^-, H_2PO_4, $C_4H_{10}PO_4^-$ in negative ion mode. For comparison of primary ion beam (Results and Discussion Section B), SI yield as a function of primary ion energy (Results and Discussion Section C) and SI yield as a function of chemical environment (Results and Discussion Section D), triplicate analyses were performed; error bars are calculated by the standard deviation between the SI yields of each replicate. The mass resolution of each primary ion beam was on average 1500 for Ar_{1000}^+ and 4500 for Bi_3^+ at *m/z* 400. For Au_3^+ and Au_{400}^{+4} analysis, the primary ions were obtained from a 120 kV Pegase Platform,[30-32] equipped with a gold liquid metal ion source capable

of producing a variety of projectiles (*e.g.*, 150 nA for Au_1^+, 15 nA for Au_3^+ and 1 nA for Au_{400}^{+4} without beam collimation/pulsing at the target[33]). The primary ion projectiles were mass-selected using a Wien filter and focused into the TOF-SIMS analysis chambers. Negative mode TOF-SIMS was performed in the analysis chamber 1, where the target voltage is held at -10 kV (total acceleration voltage of up to 130 kV), whereas positive mode TOF-SIMS was performed in analysis chamber 2, where the target voltage is held at +10 kV (total acceleration voltage of up to 110 kV).[33] Further information about the instrumental setup can be found in references.[30-33] The average mass resolution for Au_3^+ and Au_{400}^{+4} analysis at *m/z* 400 is 2000 and 450 in chamber 1 (equipped with a reflectron TOF) and in chamber 2 (equipped with a linear TOF), respectively.

5.4 Results and Discussion

5.4.1 Lipid Characterization by Class

TOF-SIMS analysis can provide sufficient information to identify a lipid of a specific class based on the simultaneous detection of analyte specific fragment and intact molecular and/or pseudo-molecular ions (*e.g.* $[M]^+$, $[M+H]^+$, $[M+Na]^+$, $[M]^-$ and $[M-H]^-$). For example, phospholipids are a class of lipids that are predominantly abundant in biological membranes and consist of two fatty acids, glycerol, phosphate and an alcohol group. There are several subclasses of phospholipids which differ based on the alcohol moiety present in the molecule (*i.e.* serine, ethanolamine, choline, glycerol or inositol). In previous reports, various lipid species including intact lipids, head group fragments and fatty acyls have been identified in cell lines using several mass spectrometry techniques (e.g., ESI-MS/MS, DESI-MS/MS, MALDI-MS/MS and SIMS). DESI-MS/MS, MALDI-MS/MS and SIMS have the advantage over traditional ESI-MS/MS in that lipid

identification may not require sample extraction protocols and direct analysis can be performed from the biological tissue of interest; while there are major differences between the ionization mechanism of DESI-MS/MS, MALDI-MS/MS and SIMS, all three techniques can provide spatial information with SIMS providing the highest spatial resolution. A tradeoff is that in the case of TOF-SIMS, the ratio of molecular to fragment ion and the spatial resolution significantly depends on the projectile size and energy as well as on the lipid species of interest and TOF-SIMS analysis mode (positive *versus* negative). For example, in positive mode TOF-SIMS head group fragments corresponding to the sphingomyelin and phosphatidylcholine are identified at *m/z:* 206 $C_5H_{14}NPO_4Na^+$, 184 $C_5H_{15}NPO_4^+$, 104 $C_5H_{14}NO^+$ and 86 $C_5H_{12}N^+$ via TOF-SIMS, ESI-MS/MS (Figure 5.1a and 5.1b).[1, 4, 34-41] Both of these lipid classes yield an internal fragment at *m/z* 125 in positive ionization mode arising from fragmentation of the head group to yield a cyclic $C_2H_6PO_4^+$ fragment. [40, 42] Negative mode TOF-SIMS of sphingomyelin and phosphatidylcholine reveals two head group fragments at *m/z* 123 $C_2H_4PO_4^-$ and *m/z* 168 $C_4H_{11}NPO_4^-$.[43] Three larger fragments of higher mass are detected in sphingomyelin analysis related to the loss of methyl $[M\text{-}CH_3]^-$, trimethylamine $[M\text{-}C_3H_9N]^-$ and ethyltrimethylammonium $[M\text{-}C_5H_{13}N]^-$ groups from the head group of the lipid (Figure 5.1a and Appendix 4).[4, 42] In addition, fragment ions corresponding to the carboxylic acid chain are typically detected from phosphatidylcholine only (see example in Figure 5.1b). Lipids in the sphingomyelin and phosphatidylcholine classes have the same head group and therefore cannot be differentiated from each other exclusively based on the head group fragment detection. There are few differences between the ionization of sphingomyelin and phosphatidylcholine by TOF-SIMS; the major difference is attributed to the head group

fragment at *m/z* 224 which is not observed in sphingomyelin.[44-47] A second difference in the TOF-SIMS of PC *versus* SM is the presence of fatty acid fragments in the phosphatidylcholine lipid profile in negative mode, which are not observed in sphingomyelin (Figure 5.1a, 5.1b, and 5.2f).

In addition to phosphatidylcholine and sphingomyelin, phosphatidylethanolamine and phosphatidylglycerol fragmentation patterns by TOF-SIMS analysis are described herein. Fragments observed in the phosphatidylethanolamine lipid class include, the internal fragments of *m/z* 125 $C_2H_6PO_4^+$ and *m/*z 123 $C_2H_4PO_4^-$ in positive and negative mode, respectively. [40] A tail group fragment after the loss of the head group $[M - C_2H_7NPO_4]^-$ and the loss of a fatty acid chain [M-FA Chain]$^-$ were detected (Figure 5.1c and 5.2b). Two major characteristic fragments of phosphatidylethanolamine were detected at *m/z* 141 $C_2H_8NPO_4^+$, and *m/z* 140 $C_2H_7NPO_4^-$ and *m/z* 196 $C_5H_{11}NPO_5^-$[43] in positive and negative TOF-SIMS modes, respectively, allowing for identification of the phosphatidylethanolamine class *versus* all other lipids considered in this study.

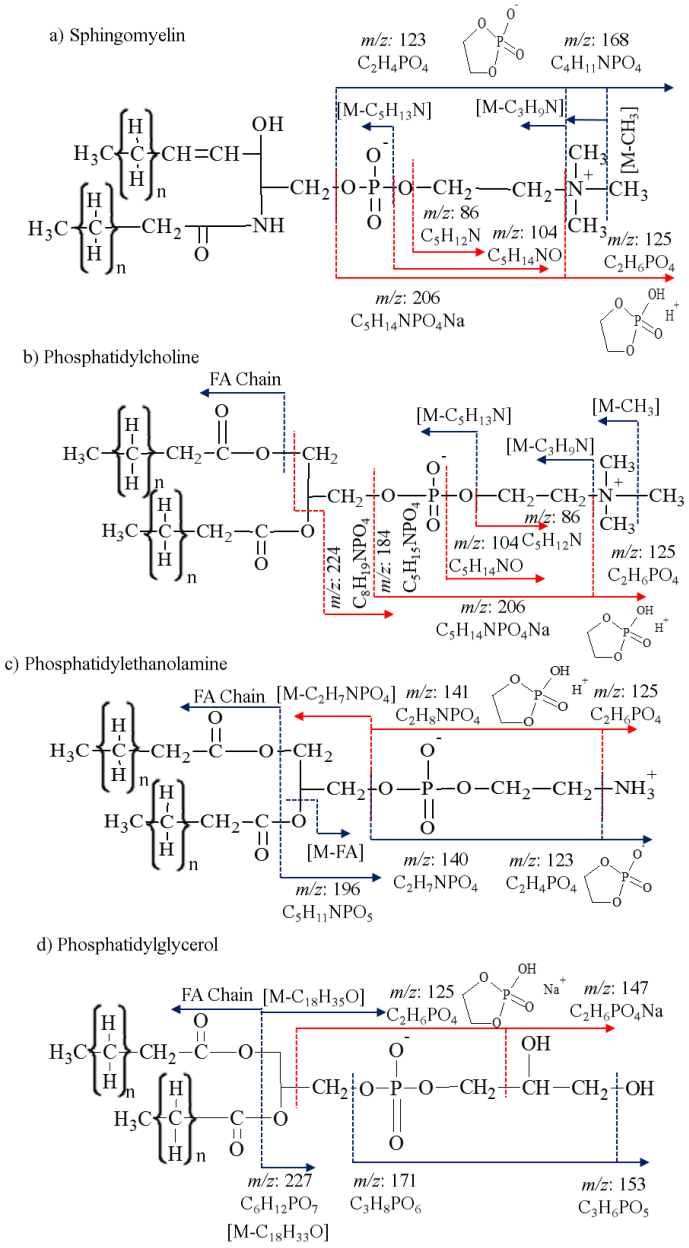

Figure 5.1. Fragmentation schemes of lipid standards of a) sphingomyelin b) phosphatidylcholine c) phosphatidylethanolamine and d) phosphatidylglycerol for positive (red) and negative (blue) mode TOF-SIMS analysis.

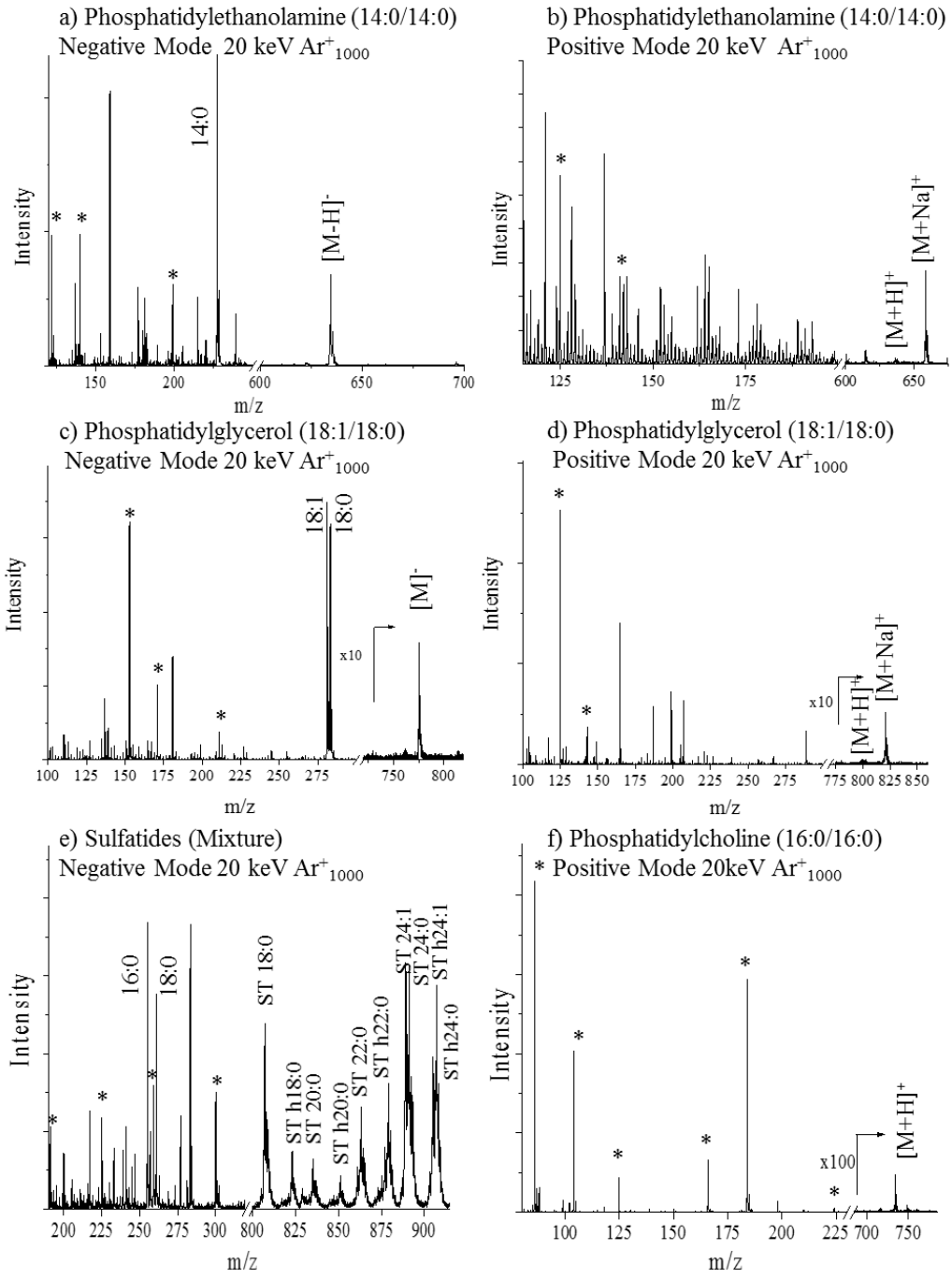

Figure 5.2. Typical TOF-SIMS mass spectra of familiar lipids in positive and negative mode. Characteristic fragment ions (*), fatty acid fragments and intact molecular ions are denoted in the spectra.

Analysis of phosphatidylglycerol in positive mode TOF-SIMS yields the cyclic head group fragment at *m/z* 125 $C_2H_6PO_4^+$ as well as the sodiated form of that fragment ion at *m/z* 147 $C_2H_6PO_4Na^+$.[48] Fragments at *m/z* 171 $C_6H_8PO_6^-$ and *m/z* 152 $C_3H_6PO_5^-$ are characteristic fragments significant to the phosphatidylglycerol class in negative mode TOF-SIMS. A *m/z* 227 $C_6H_{12}PO_7^-$ is also observed corresponding to the loss of both fatty acid chains from the phosphatidylglycerol lipid in negative mode TOF SIMS (Figure 5.1d and 5.2c).[49] The sulfatide class is typically analyzed in negative mode TOF-SIMS. Characteristic fragments are detected for the head group at *m/z*: 97 HSO_4^-, 199 $C_4H_7O_7S^-$, 225 $C_6H_9O_7S^-$, 257 $C_6H_9O_9S^-$, 259 $C_6H_{11}O_9S^-$ and 300 $C_8H_{14}NO_9^-$. All head group fragments are specific to the sulfatides due to the presence of a sulfur atom. A mixture of sulfatides with varying fatty acid composition results in the observation of a variety of intact molecular ions (Figure 5.2e and Appendix 6).

Fatty acid chains are typically observed in negative mode TOF-SIMS in phosphatidylethanolamine, phosphatidylglycerol, phosphatidylcholine and sulfatides. For example, phosphatidylethanolamine and phosphatidylglycerol analysis show peaks at *m/z* 227 $C_{14}H_{29}O_2^-$ and *m/z* 283 $C_{18}H_{35}O^-$ corresponding to the 14:0 and 18:0 fatty acid chain fragments (Figure 5.1c and 5.2a). The sulfatide standard contains a mixture of lipids and fatty acids fragment peaks are observed in the mixture at *m/z* 255 (16:0), *m/z* 283 (18:0) and *m/z* 311 (20:0) (Figure 5.2e and Appendix 6). By combining the information obtained from the head group fragments, fragment fatty acid chains, tail group fragment, loss of a fatty acid chain, and the pseudo-molecular ions, it may be possible to directly correlate the TOF-SIMS spectral features to the lipid structure in complex biological matrices. The later

analysis can be simplified further when using coincidence TOF-SIMS techniques during single ion bombardment.[50]

5.4.2 SI Yield as a Function of the Projectile Size

Lipid standards were analyzed as a function of the projectile size (Bi_3^+ and Au_3^+, Ar_{1000}^+ and Au_{400}^{+4}) and energy. An increase in secondary ion yield (SI yield) was observed between small polyatomic and nanoparticle projectiles throughout all lipid classes in positive and negative ionization mode (see example for Bi_3^+ and Ar_{1000}^+ in Figure 5.3). In the sulfatide class, over ten-fold increase is observed for 20 keV Ar_{1000}^+ when compared to 25 keV Bi_3^+ in negative mode TOF-SIMS. The $[M-H]^-$ SI yields of the other lipids showed an increase when going from Bi_3^+ to Ar_{1000}^+ primary ions, but most of the changes were not as large as that seen in the ST class (Figure 5.3a). In the cases of sphingomyelin and phosphatidylethanolamine the SI yield of the $[M-H]^-$ molecular ion had less than an order of magnitude of change in abundance, whereas phosphatidylglycerol and phosphatidylcholine had a more significant abundance increase. Phosphatidylcholine had the second largest increase in SI yield when changing from Bi_3^+ to Ar_{1000}^+ primary ions. SI signal enhancements were previously reported for argon clusters relative to bismuth clusters for the analysis of biological molecules (diadenosine triphosphate and diadenosine tetraphosphate).[51] In positive mode TOF-SIMS a different trend is observed for SI yield variation with the primary ion projectile size (see Figure 5.3b). The only protonated molecular ion showing significant differences in the SI yield corresponds to the sphingomyelin class. The remaining $[M+H]^+$ molecular ions of the lipids do not show significant changes in SI yield using the two different primary ion beams. A variation between the SI yields of the intact lipid molecular ion ($[M-H]^-/[M+H]^+$) of each lipid class

is observed for both positive and negative mode TOF-SIMS; however, negative mode TOF-SIMS shows greater variation in the SI yields (Figure 5.3). The increase in SI yield with the Ar_{1000}^+ beam can be attributed to the "softer" desorption regime compared to that of Bi_3^+. The E_{atom} for each beam is discussed in detail later; however, in the examples shown the Ar_{1000}^+ beam has an energy per atom closest to that deemed the ideal (E_{atom} = 10 eV/atom).[15]

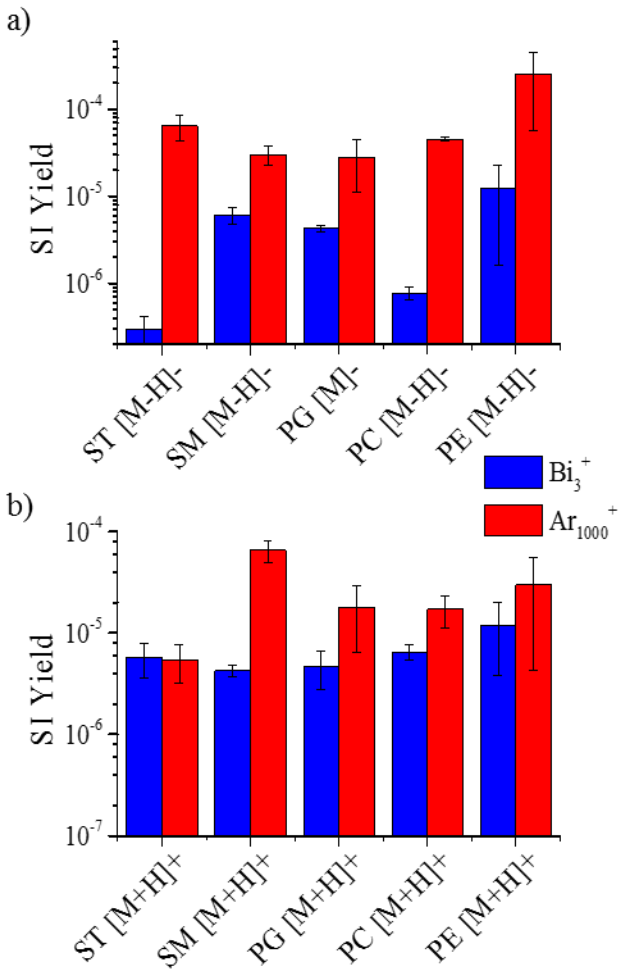

Figure 5.3. intact molecular ion si yield emission using small polyatomic bi3+ and nanoparticle ar1000+ primary ion projectiles for familiar lipid standards using tof-sims in a) negative and b) positive mode.

The comparison of SI yields of lipids using gold projectiles showed that the nanoparticle projectile Au_{400}^{+4} may provide over tenfold increase in the SI yield when compared to the small polyatomic projectile Au_3^+ (Appendix 7). For example, during sulfatide analysis the intact molecular ion (ST 40:1) showed a 100-fold increase in the secondary ion yield from 50 keV Au_3^+ to 440 keV Au_{400}^{+4} and a 10-fold increase for the smaller gold beam when compared to 25 keV Bi_3^+ (Appendix 7). There is a 2-3 order of magnitude increase in the SI yield when using 440 keV Au_{400}^{+4} versus 20 keV Ar_{1000}^+ that can be primarily attributed to the incident energy of the projectile (Appendix 7). Overall, the analysis of lipids using Au_{400}^{+4} followed the same trend with a two order of magnitude increase in SI yield compared to Au_3^+ (Appendices 7 and 8). SI yields of 440 keV Au_{400}^{+4} were 2-3 orders of magnitude higher than those obtained using the Ar_{1000}^+ primary ion beam for most lipid classes (e.g., sphingomyelin, phosphatidylglycerol, phosphatidylcholine and phosphatidylethanolamine, see Appendix 7). It has been previously noted that the estimated Au_3^+ SI yields would be equal to Bi_3^+ yields because they are of similar nature and size.[52] For a more detailed analysis, the E_{atom} needs to be considered due to the large differences in energies used for each primary ion beam. For the small polyatomic projectiles, the E_{atom} are calculated at approximately 8000 eV and 16000 eV for Bi_3^+ and Au_3^+, respectively. Our results suggest that the larger the E_{atom} for small polyatomic projectiles, the larger the SI yield. A discussion of the SI yield as a function of the energy and cluster size is provided for the $Ar_{n=500\text{-}2000}^+$ and Au_{400}^{+4} nanoparticle projectiles.

5.4.3 SI Yield as a Function of the Projectile Energy

Previous work has shown that high energy, massive gold projectiles are advantageous for biological sample analysis and that the higher the cluster size the higher

the SI yield.[32] This correlates to data obtained by Vickerman *et al.* and by Yokoyama *et al.* where SI yields of both metals and organic substances increases with the primary ion impact energy (up to 120 keV for C_{60} projectiles), being most notable for higher mass fragments.[53-54] Here, we further investigate the effect of the primary ion energy and size on the SI yield for the case of the phosphatidylglycerol (18:0-18:1 PG) lipid standard (see Figure 5.4). Two studies are carried out: i) the influence of the projectile energy on the SI yield for nanoparticle Au_{400}^{+4} projectiles, and ii) the influence of the projectile size on the SI yield for 20 keV Ar_n^+ (n = 500-2000 atoms) projectiles.

In positive and negative mode TOF-SIMS, as the primary Au_{400}^{4+} ion energy increases, there is a net SI yield increase of molecular and fragment ions (Figure 5.4a and 4c). For example, in negative mode TOF-SIMS closer inspection shows that small (*m/z*: 153, 281 and 283) and larger (*m/z* 509 and 511) mass fragments show a slightly different increasing slope, being a steeper positive slope for the smaller fragments (see Appendix 9a and Appendix 8). Notice that analyte-specific fragment ions corresponds to the head group (*m/z* 153), fatty acid groups (*m/z* 281 and 283 for 18:1 and 18:0, respectively) and the loss of one fatty acid group (*m/z* 509 and 511). For the low mass fragments, results show that as the Au_{400}^{4+} ion energy increases the ratio of molecular to fragment ion also increases in a non-linear fashion. That is, the SI yield of $[M]^-$ increases more than the SI yield of the low mass fragments. For the higher mass fragments (*m/z* 509 and 511), the opposite trend is observed where the ratio of $[M]^-$ to larger fragment ions decreases. In positive mode TOF-SIMS, the molecular ion emission also increases with the Au_{400}^{+4} projectile energies. Closer inspection shows that as the Au_{400}^{4+} ion energy increases a proportional increase in M^+, $[M+Na]^+$ and $[2M+Na]^+$ emission is observed (Figure 5.4c and Appendix 12). These

positive and negative mode TOF-SIMS results suggest that as the Au_{400}^{+4} ion energy increases the nanoparticle penetration into the sample also increases thus creating a larger emission volume in a way that scales the emission of intact molecular and fragment ions.

In a different scenario, an increase of the 20 keV Ar_n^+ cluster size from 500 to 2000 atoms (or decrease in the E_{atom}) results in an increase in SI yield of M^-, head group fragments and fatty acid fragments (Figure 5.4b). The SI yield of the molecular ion is rising at a faster rate than all of the fragment ions as the cluster size ranges from 500 to 2000 argon atoms, being the most significant between Ar_{1500} and Ar_{2000} (Figure 5.4b, Appendix 11 and Appendix 8b). This SI yield dependence on the Ar_n^+ cluster size is in good agreement with recent observations by Yokoyama *et al.* using 20 keV $Ar_{n=2000-5000}$ cluster impacts.[54] Previous report of Ar_n cluster impacts at 10-40 eV/atom have also shown that larger fragments are more favorable with the Ar_n projectile size increase.[18] These results suggest that as the size of the Ar_n^+ projectile increases a larger impact cross section is achieved that enhances the emission volume; the weak forces that hold the Ar_n cluster together do not lead to penetration/implantation into the surface. Notice that this mechanism is very different from that of the nanoparticle Au_{400}^{+4} projectiles.

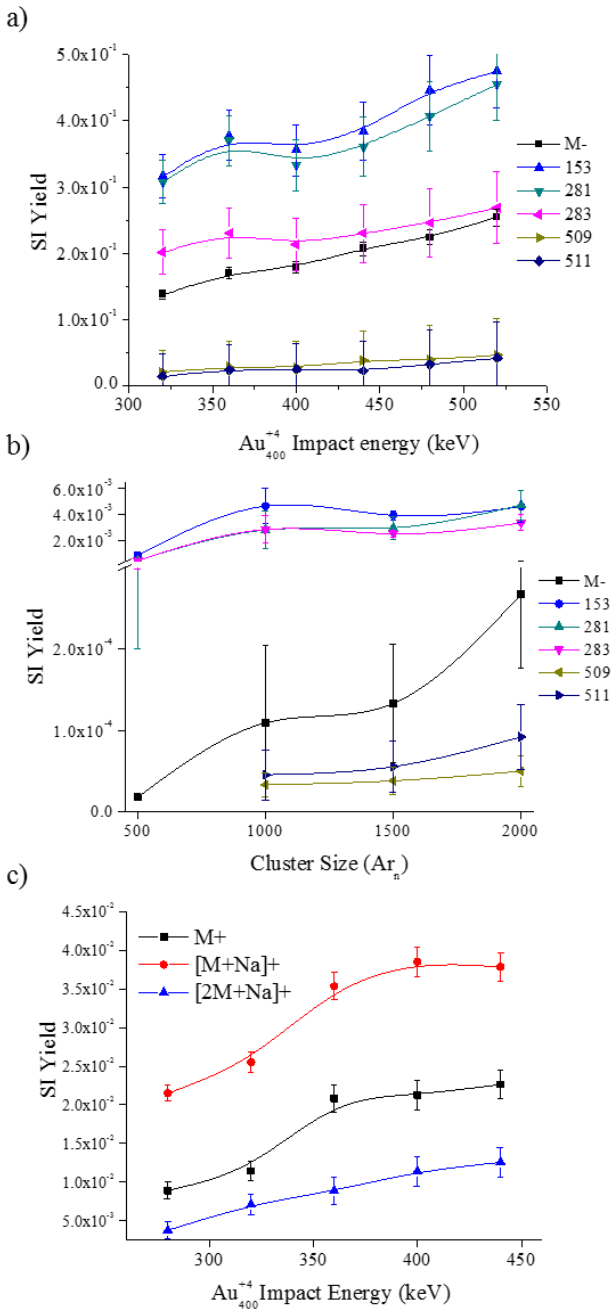

Figure 5.4. Secondary ion yields as a function of the nanoparticle Au_{400}^{+4} projectile energy or Ar_n^+ cluster size for a lipid model target of phosphatidylglycerol (18:0-18:1 PG) a) Au_{400}^+ and b) Ar_n^+ negative and c) Au_{400}^+ positive mode. Notice the break in vertical axis in b).

5.4.4 SI Yield as a Function of Chemical Environment

SIMS is a very useful mass spectrometry tool for the analysis of biological matrices as previously described.[2, 16, 18, 32, 43, 55-56] The chemical environment (matrix) of compounds of interest has a significant impact on the limit of detection, ionization efficiency and ion suppression for TOF-SIMS and for other ionization sources.[57] To evaluate the influence a matrix has on the SI yield, we compared the emission from the single lipid component sample to the emission from a sample containing a mixture of all five-lipid classes at equal concentrations. The protonated and deprotonated molecular ion of each lipid was utilized for comparison in positive and negative mode TOF-SIMS, respectively. The analysis of the sulfatides mixture in negative and positive mode TOF-SIMS using Ar_{1000}^+ showed no suppression or enhancement for the deprotonated/protonated molecular ion (Figure 5.5a and Figure 5.5b). For Bi_3^+ analysis, in negative mode TOF-SIMS ion enhancement is observed for the sulfatides and in positive TOF-SIMS no change is observed from the single standard to the mixture (Figure 5.5d and Figure 5.5c). Typically, sulfatides are preferentially ionized in negative ionization mode and this could contribute to the fact that opposite trends are observed between the two ionization modes for Bi_3 analysis. For a characteristic ion of the sulfatide lipid class (HSO_4^-) the SI yields of the fragments are on the same order of magnitude in both alone and as a mixture using Ar_{1000}^+ and Bi_3^+projectiles (data not shown). For the sphingomyelin class of lipids, positive mode TOF-SIMS shows no suppression in the SI yield of the $[M+H]^+$, however in negative mode TOF-SIMS, an order of magnitude decrease is observed between the SI yield of the single lipid and the SI yield of the lipid mixture (Figure 5.5a and Figure 5.5b). Using the Bi_3^+ projectiles, no significant changes are observed between single lipid and lipid mixture analysis of

sphingomyelin in positive ionization mode TOF-SIMS and a slight decrease in SI yield is observed in negative mode TOF-SIMS (Figure 5.5c and Figure 5.5d).

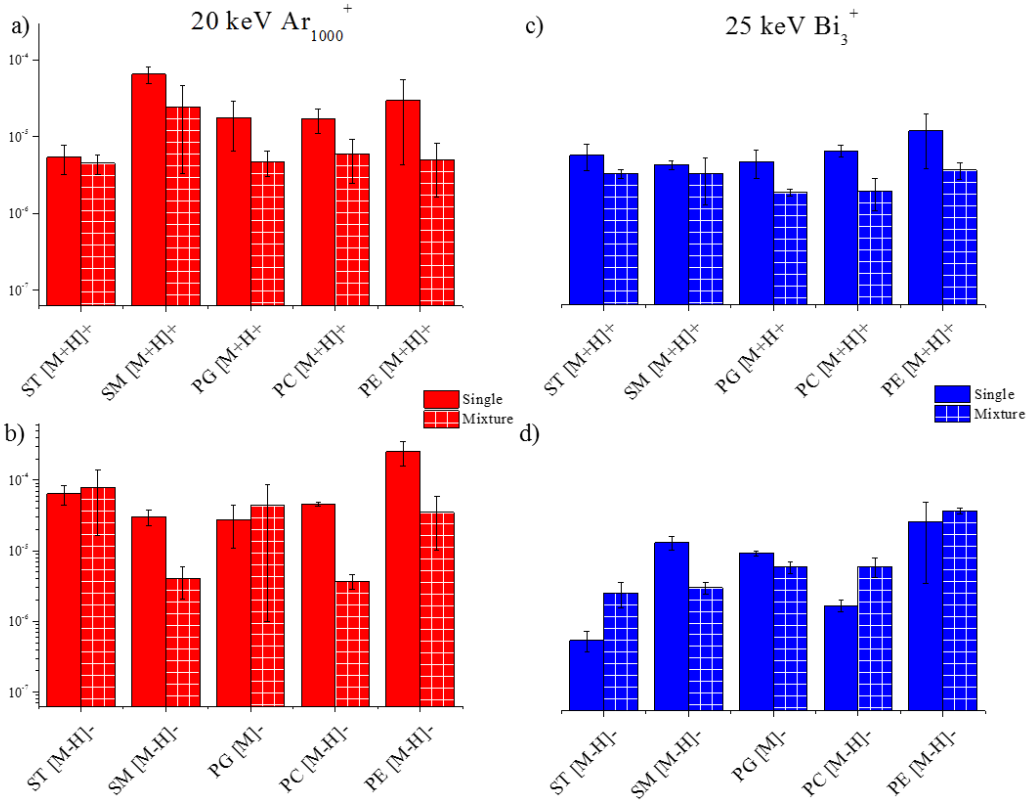

Figure 5.5. Secondary ion yields of intact molecular ions from a single lipid standard sample and a mixture of lipid standards sample in a) positive mode Ar_{1000}^+, b) negative mode Ar_{1000}^+ c) positive mode Bi_3^+ d) negative mode Bi_3^+.

Analysis of phosphatidylglycerol in positive mode TOF-SIMS demonstrates no significant changes with the Ar_{1000}^+ projectiles and a small decrease in SI yield using the Bi_3^+ projectiles (Figure 5.5a and Figure 5.5c). For the analysis of phosphatidylglycerol in negative mode TOF-SIMS, no ionization suppression or enhancement is observed for either of the primary ion projectiles (Figure 5.5b and Figure 5.5d). SI yields of characteristic fragment peaks for phosphatidylglycerol (*i.e.*, *m/z* 153 and 171) also showed no change between single and mixture conditions (data not shown). As previously

mentioned, phosphatidylcholine is a lipid typically analyzed in positive mode TOF-SIMS; in positive mode TOF-SIMS, the SI yield of the $[M+H]^+$ ion does not show a major matrix effect and no large changes in ion abundance are observed for Ar_{1000}^+ or Bi_3^+ (Figure 5.5a and Figure 5.5c). In negative mode TOF-SIMS, a different trend is seen for phosphatidylcholine, with suppression in the mixture signal observed using Ar_{1000}^+ and an enhancement in SI yield observed for Bi_3^+ projectiles (Figure 5.5b and Figure 5.5d); this difference in trend between positive and negative mode TOF-SIMS could be attributed to the fact that phosphatidylcholine is preferentially ionized in positive mode TOF-SIMS. A previous study by Jones *et. al*. of matrix effects in TOF-SIMS used phosphatidylcholine as a complex matrix while looking for targeted drug analytes.[57] It was determined that the lipid had a very strong suppression effect on the abundance of the molecular ion of the drug due to its proton affinity.[57] In our study we observed a similar suppression effect on the pseudo-molecular ions of the lipids in the mixture, potentially from the presence of phosphatidylcholine (Figure 5.5a and Figure 5.5b). For the analysis of phosphatidylethanolamine by Ar_{1000}^+ there is less than 10-fold suppression of ion signal going from the single lipid to the mixture of lipids (Figure 5.5a and Figure 5.5b). No major changes are observed using Bi_3^+ for the $[M-H]^-$ or $[M+H]^+$ from phosphatidylethanolamine (Figure 5.5c and Figure 5.5d). No major changes in SI yield are seen for the characteristic peaks (*m/z* 141 and 196) of the phosphatidylethanolamine lipid class. In general, these matrix studies have shown that matrix effects are minimal on the SI yield of lipid standards when the lipid is analyzed in either ionization polarity. According to previous studies, chemical environment of a sample has a large impact on the SI yield of targeted molecules as shown with the large suppressive effects phosphatidylcholine has on the M and the

enhancement effects cholesterol induced when used as a comparative matrix.[57-58] More recently, matrix enhanced TOF-SIMS has been developed in order to more easily and efficiently ionize samples within complex biological matrices via TOF-SIMS. [57, 59-61] Our studies suggest that whether compounds of interest exist as a single standard or co-exist as a mixture of lipids does not significantly change the secondary ion yield of the molecular ion of the selected lipids regardless of primary ion identity or ionization mode.

5.5 Summary and Conclusions

In this paper, we provide detailed information on the TOF-SIMS fragmentation pattern for sphingomyelins, phosphatidylcholine, phosphatidylglycerol, sulfatides and phosphatidylethanolamine lipid classes. Typical mass spectra for common lipids are shown and discussed based on their fragmentation patterns. Changes in secondary ion yields were analyzed as a function of the primary ion (Bi_3^+ *vs* Ar_{1000}^+ and Au_3^+ *vs* Au_{400}^{+4}) using TOF-SIMS. For the case of lipid analysis, the results suggest that for polyatomic projectiles (Bi_3^+ and Au_3^+), the increase in the primary ion energy leads to an increase in the SI yield. However, larger SI yields are obtained for molecular ions using nanoparticle projectiles. Two different trends were observed in the case of the nanoparticle projectiles (Ar_n^+ and Au_{400}^{+4}) that may be related to their intramolecular forces. For example, in the case of Au_{400}^{+4} projectiles, as the projectile energy increases a larger SI yield is observed for fragment and molecular ions, with small variation on their relative ratio. That is, the larger the E_{atom} for Au_{400}^{+4} projectiles the larger the SI yield. In the case of the Ar_n^+ projectiles, the lower the E_{atom} the larger the SI yield. We interpret these effects as consequence of two ways to increase the desorption volume: i) the larger the incident energy in the case of the Au_{400}^{+4} projectiles the larger the penetration depth and emission volume, and ii) the higher

the number of atoms in the Ar_n^+ projectiles the larger the impact cross section and emission volume. The matrix studies showed that the sample composition has a minimal effect on the desorption yields of intact molecular ions of familiar lipids and no correlation with the type of primary ion was observed. This work further provides more information on the main factors that affect the SI yield as well as characteristic patterns that allow lipid analysis in biological environments using TOF-SIMS.

5.6 Acknowledgments

This work was supported by NIGMS grant GM106414 to FF-L. We acknowledge the support of Dr. Emile Schweikert and Dr. Serge Della-Negra during the acquisition of the Au_3^+/Au_{400}^{+4} data in the 120 kV Pegasus platform at Texas A&M University and for helpful discussions.

5.7 References

1. Passarelli, M. K.; Winograd, N., Lipid imaging with time-of-flight secondary ion mass spectrometry (ToF-SIMS). *Biochimica et Biophysica Acta (BBA)-Molecular and Cell Biology of Lipids* **2011,** *1811* (11), 976-990.

2. DeBord, J. D.; Smith, D. F.; Anderton, C. R.; Heeren, R. M.; Pasa-Tolic, L.; Gomer, R. H.; Fernandez-Lima, F. A., Secondary ion mass spectrometry imaging of Dictyostelium discoideum aggregation streams. *PLoS One* **2014,** *9* (6), e99319.

3. Nie, H.-Y.; Francis, J.; Taylor, A.; Walzak, M.; Chang, W.; MacFabe, D.; Lau, W., Imaging subcellular features of a sectioned rat brain using time-of-flight secondary ion mass spectrometry and scanning probe microscopy. *Applied Surface Science* **2008,** *255* (4), 1079-1083.

4. Saleem, M.; Galla, H.-J., Surface view of the lateral organization of lipids and proteins in lung surfactant model systems—A ToF-SIMS approach. *Biochimica et Biophysica Acta (BBA)-Biomembranes* **2010,** *1798* (4), 730-740.

5. Touboul, D.; Brunelle, A.; Halgand, F.; De La Porte, S.; Laprévote, O., Lipid imaging by gold cluster time-of-flight secondary ion mass spectrometry: application to Duchenne muscular dystrophy. *Journal of Lipid Research* **2005,** *46* (7), 1388-1395.

6. Touboul, D.; Halgand, F.; Brunelle, A.; Kersting, R.; Tallarek, E.; Hagenhoff, B.; Laprévote, O., Tissue molecular ion imaging by gold cluster ion bombardment. *Analytical Chemistry* **2004,** *76* (6), 1550-1559.

7. Rabbani, S.; Barber, A. M.; Fletcher, J. S.; Lockyer, N. P.; Vickerman, J. C., TOF-SIMS with argon gas cluster ion beams: a comparison with C60+. *Analytical Chemistry* **2011,** *83* (10), 3793-3800.

8. Ninomiya, S.; Ichiki, K.; Yamada, H.; Nakata, Y.; Seki, T.; Aoki, T.; Matsuo, J., Precise and fast secondary ion mass spectrometry depth profiling of polymer materials with large Ar cluster ion beams. *Rapid Communications in Mass Spectrometry* **2009,** *23* (11), 1601-1606.

9. Yamada, I.; Matsuo, J.; Toyoda, N.; Kirkpatrick, A., Materials processing by gas cluster ion beams. *Materials Science and Engineering: R: Reports* **2001,** *34* (6), 231-295.

10. Lechene, C.; Hillion, F.; McMahon, G.; Benson, D.; Kleinfold, A. M.; Kampf, J. P.; Distel, D.; Luyten, Y.; Bonventre, J.; Hentschel, D.; Park, K. M.; Ito, S.; Schwartz, M.; Benichou, G.; Slodzian, G., High Resolution Quantitative Imaging of Mammalian and Bacterial Cells Using Stable Isotope Mass Spectrometry. *Journal of biology* **2006,** *5*, 20.1-20.3.

11. Braun, R. M.; Beyder, A.; Xu, J.; Wood, M. C.; Ewing, A. G.; Winograd, N., Spatially Resolved Detection of Attomole Quantities of Organic Molecules Localized in Picoliter Vials Using Time-of-Flight Secondary Ion Mass Spectrometry. *Analytical Chemistry* **1999,** *71* (16), 3318-3324.

12. Boxer, S. G.; Kraft, M. L.; Weber, P. K., Advances in Imaging Secondary Ion Mass Spectrometry for Biological Samples. *Annual Reviews of Biophysics* **2009,** *38*, 53-74.

13. Schweikert, E.; van Stipdonk, M. J.; Harris, R. D., A comparison of desorption yields from C+ 60 to atomic and polyatomic projectiles at keV energies. *Rapid Communications in Mass Spectrometry* **1996,** *10* (15), 1987-1991.

14. Sheraz née Rabbani, S.; Barber, A.; Fletcher, J. S.; Lockyer, N. P.; Vickerman, J. C., Enhancing secondary ion yields in time of flight-secondary ion mass spectrometry using water cluster primary beams. *Analytical Chemistry* **2013,** *85* (12), 5654-5658.

15. Sheraz née Rabbani, S.; Razo, I. B.; Kohn, T.; Lockyer, N. P.; Vickerman, J. C., Enhancing Ion Yields in Time-of-Flight-Secondary Ion Mass Spectrometry: A Comparative Study of Argon and Water Cluster Primary Beams. *Analytical Chemistry* **2015,** *87* (4), 2367-2374.

16. Fletcher, J. S.; Lockyer, N. P.; Vickerman, J. C., Developments in molecular SIMS depth profiling and 3D imaging of biological systems using polyatomic primary ions. *Mass Spectrometry Reviews* **2011,** *30* (1), 142-174.

17. Gode, D.; Volmer, D. A., Lipid imaging by mass spectrometry–a review. *Analyst* **2013,** *138* (5), 1289-1315.

18. Aoyagi, S.; Fletcher, J. S.; Sheraz, S.; Kawashima, T.; Razo, I. B.; Henderson, A.; Lockyer, N. P.; Vickerman, J. C., Peptide structural analysis using continuous Ar cluster and C60 ion beams. *Analytical and Bioanalytical Chemistry* **2013,** *405* (21), 6621-6628.

19. Wolf, C.; Quinn, P. J., Lipidomics: Practical aspects and applications. *Progress in Lipid Research* **2008,** *47* (1), 15-36.

20. Wenk, M. R., Lipidomics: new tools and applications. *Cell* **2010,** *143* (6), 888-895.

21. Layre, E.; Moody, D. B., Lipidomic profiling of model organisms and the world's major pathogens. *Biochimie* **2013,** *95* (1), 109-115.

22. Schenk, E. R.; Nau, F.; Thompson, C. J.; Tse-Dinh, Y.-C.; Fernandez-Lima, F., Changes in lipid distribution in E. coli strains in response to norfloxacin. *Journal of Mass Spectrometry* **2015,** *50*, 88-94.

23. Fahy, E.; Subramaniam, S.; Brown, H. A.; Glass, C. K.; Merrill, A. H.; Murphy, R. C.; Raetz, C. R.; Russell, D. W.; Seyama, Y.; Shaw, W., A comprehensive classification system for lipids. *Journal of Lipid Research* **2005,** *46* (5), 839-862.

24. Fahy, E.; Subramaniam, S.; Murphy, R. C.; Nishijima, M.; Raetz, C. R.; Shimizu, T.; Spener, F.; van Meer, G.; Wakelam, M. J.; Dennis, E. A., Update of the LIPID MAPS

comprehensive classification system for lipids. *Journal of Lipid Research* **2009,** *50* (Supplement), S9-S14.

25. Schmelzer, K.; Fahy, E.; Subramaniam, S.; Dennis, E. A., The lipid maps initiative in lipidomics. *Methods in Enzymology* **2007,** *432*, 171-183.

26. Wucher, A., Molecular secondary ion formation under cluster bombardment: A fundamental review. *Applied Surface Science* **2006,** *252* (19), 6482-6489.

27. Wehbe, N.; Fallavier, M.; Della-Negra, S.; Depauw, J.; Brunelle, A.; Andersen, H. H., Cluster size and velocity dependences of sputtering and secondary ion emission under gold cluster impact. *Nuclear Instruments and Methods in Physics Research Section B: Beam Interactions with Materials and Atoms* **2010,** *268* (17–18), 2596-2602.

28. Pacholski, M. L.; Cannon, D. M.; Ewing, A. G.; Winograd, N., Static time-of-flight secondary ion mass spectrometry imaging of freeze-fractured, frozen-hydrated biological membranes. *Rapid Communications in Mass Spectrometry* **1998,** *12* (18), 1232-1235.

29. Angerer, T. B.; Blenkinsopp, P.; Fletcher, J. S., High energy gas cluster ions for organic and biological analysis by time-of-flight secondary ion mass spectrometry. *International Journal of Mass Spectrometry* **2015,** *377*, 591-598.

30. Della-Negra, S.; Arianer, J.; Depauw, J.; Verkhoturov, S.; Schweikert, E., The Pegase project, a new solid surface probe: focused massive cluster ion beams. *Surface and Interface Analysis* **2011,** *43* (1-2), 66-69.

31. Fernandez-Lima, F.; Eller, M.; DeBord, J.; Verkhoturov, S.; Della-Negra, S.; Schweikert, E., On the surface mapping using individual cluster impacts. *Nuclear Instruments and Methods in Physics Research Section B: Beam Interactions with Materials and Atoms* **2012,** *273*, 270-273.

32. Fernandez-Lima, F. A.; Post, J.; DeBord, J. D.; Eller, M. J.; Verkhoturov, S. V.; Della-Negra, S.; Woods, A. S.; Schweikert, E. A., Analysis of native biological surfaces using a 100 kV massive gold cluster source. *Analytical Chemistry* **2011,** *83* (22), 8448-8453.

33. Bouneau, S.; Della-Negra, S.; Depauw, J.; Jacquet, D.; Le Beyec, Y.; Mouffron, J. P.; Novikov, A.; Pautrat, M., Heavy gold cluster beams production and identification. *Nuclear Instruments and Methods in Physics Research Section B* **2004,** *225* (4), 579-589.

34. Roddy, T. P.; Cannon, D. M.; Meserole, C. A.; Winograd, N.; Ewing, A. G., Imaging of freeze-fractured cells with in situ fluorescence and time-of-flight secondary ion mass spectrometry. *Analytical Chemistry* **2002,** *74* (16), 4011-4019.

35. Yang, H. J.; Sugiura, Y.; Ishizaki, I.; Sanada, N.; Ikegami, K.; Zaima, N.; Shrivas, K.; Setou, M., Imaging of lipids in cultured mammalian neurons by matrix assisted laser/desorption ionization and secondary ion mass spectrometry. *Surface and Interface Analysis* **2010,** *42* (10-11), 1606-1611.

36. Yang, H.-J.; Ishizaki, I.; Sanada, N.; Zaima, N.; Sugiura, Y.; Yao, I.; Ikegami, K.; Setou, M., Detection of characteristic distributions of phospholipid head groups and fatty acids on neurite surface by time-of-flight secondary ion mass spectrometry. *Medical Molecular Morphology* **2010,** *43* (3), 158-164.

37. Fletcher, J. S.; Lockyer, N. P.; Vaidyanathan, S.; Vickerman, J. C., TOF-SIMS 3D biomolecular imaging of Xenopus laevis oocytes using buckminsterfullerene (C60) primary ions. *Analytical Chemistry* **2007,** *79* (6), 2199-2206.

38. Sjövall, P.; Lausmaa, J.; Nygren, H.; Carlsson, L.; Malmberg, P., Imaging of membrane lipids in single cells by imprint-imaging time-of-flight secondary ion mass spectrometry. *Analytical Chemistry* **2003,** *75* (14), 3429-3434.

39. Kurczy, M. E.; Kozole, J.; Parry, S.; Piehowski, P.; Winograd, N.; Ewing, A., Relative quantification of cellular sections with molecular depth profiling ToF-SIMS imaging. *Applied Surface Science* **2008,** *255* (4), 1158-1161.

40. Ostrowski, S. G.; Szakal, C.; Kozole, J.; Roddy, T. P.; Xu, J.; Ewing, A. G.; Winograd, N., Secondary ion MS imaging of lipids in picoliter vials with a buckminsterfullerene ion source. *Analytical Chemistry* **2005,** *77* (19), 6190-6196.

41. Ismaiel, O. A.; Halquist, M. S.; Elmamly, M. Y.; Shalaby, A.; Karnes, H. T., Monitoring phospholipids for assessment of ion enhancement and ion suppression in ESI and APCI LC/MS/MS for chlorpheniramine in human plasma and the importance of multiple source matrix effect evaluations. *Journal of Chromatography B* **2008,** *875* (2), 333-343.

42. Domingues, P.; Amado, F. M.; Santana-Marques, M. G. O.; Ferrer-Correia, A., Constant neutral loss scanning for the characterization of glycerol phosphatidylcholine

phospholipids. *Journal of the American Society for Mass Spectrometry* **1998,** *9* (11), 1189-1195.

43. Brügger, B.; Erben, G.; Sandhoff, R.; Wieland, F. T.; Lehmann, W. D., Quantitative analysis of biological membrane lipids at the low picomole level by nano-electrospray ionization tandem mass spectrometry. *Proceedings of the National Academy of Sciences* **1997,** *94* (6), 2339-2344.

44. Zheng, L.; McQuaw, C. M.; Ewing, A. G.; Winograd, N., Sphingomyelin/phosphatidylcholine and cholesterol interactions studied by imaging mass spectrometry. *Journal of the American Chemical Society* **2007,** *129* (51), 15730-15731.

45. Roddy, T. P.; Cannon, D. M.; Ostrowski, S. G.; Ewing, A. G.; Winograd, N., Proton transfer in time-of-flight secondary ion mass spectrometry studies of frozen-hydrated dipalmitoylphosphatidylcholine. *Analytical Chemistry* **2003,** *75* (16), 4087-4094.

46. Touboul, D.; Brunelle, A.; Laprévote, O., Structural analysis of secondary ions by post-source decay in time-of-flight secondary ion mass spectrometry. *Rapid Communications in Mass Spectrometry* **2006,** *20* (4), 703-709.

47. Tahallah, N.; Brunelle, A.; De La Porte, S.; Laprévote, O., Lipid mapping in human dystrophic muscle by cluster-time-of-flight secondary ion mass spectrometry imaging. *Journal of Lipid Research* **2008,** *49* (2), 438-454.

48. Hsu, F.-F.; Turk, J., Structural determination of sphingomyelin by tandem mass spectrometry with electrospray ionization. *Journal of the American Society for Mass Spectrometry* **2000,** *11* (5), 437-449.

49. Hsu, F.-F.; Turk, J., Studies on phosphatidylglycerol with triple quadrupole tandem mass spectrometry with electrospray ionization: Fragmentation processes and structural characterization. *Journal of the American Society for Mass Spectrometry* **2001,** *12* (9), 1036-1043.

50. Park, M. A.; Gibson, K. A.; Quinones, K.; Schweikert, M. A., Coincidence Counting in Time-of-Flight Mass Spectrometry: A Test for Chemical Microhomogeneity. *Science* **1990,** *248* (4958), 988-990.

51. Shon, H. K.; Cho, Y. L.; Lim, C. S.; Choi, J. S.; Chung, S. J.; Lee, T. G., ToF-SIMS analysis of diadenosine triphosphate and didadenosine tetraphosphate using bismuth and argon cluster ion beams. *Surface and Interface Analysis* **2014,** *46* (S1), 189-192.

52. Touboul, D.; Kollmer, F.; Niehuis, E.; Brunelle, A.; Laprévote, O., Improvement of biological time-of-flight-secondary ion mass spectrometry imaging with a bismuth cluster ion source. *Journal of the American Society for Mass Spectrometry* **2005,** *16* (10), 1608-1618.

53. Fletcher, J. S.; Conlan, X. A.; Jones, E. A.; Biddulph, G.; Lockyer, N. P.; Vickerman, J. C., TOF-SIMS analysis using C60. Effect of impact energy on yield and damage. *Analytical Chemistry* **2006,** *78* (6), 1827-1831.

54. Yokoyama, Y.; Aoyagi, S.; Fujii, M.; Matsuo, J.; Fletcher, J. S.; Lockyer, N. P.; Vickerman, J. C.; Passarelli, M. K.; Havelund, R.; Seah, M. P., Peptide fragmentation and surface structural analysis by means of ToF-SIMS using large cluster ion sources. *Analytical Chemistry* **2016,** *88* (7), 3592-3597.

55. Bich, C.; Havelund, R.; Moellers, R.; Touboul, D.; Kollmer, F.; Niehuis, E.; Gilmore, I. S.; Brunelle, A., Argon cluster ion source evaluation on lipid standards and rat brain tissue samples. *Analytical Chemistry* **2013,** *85* (16), 7745-7752.

56. Annesley, T. M., Ion suppression in mass spectrometry. *Clinical Chemistry* **2003,** *49* (7), 1041-1044.

57. Jones, E.; Lockyer, N.; Vickerman, J., Suppression and enhancement of non-native molecules within biological systems. *Applied Surface Science* **2006,** *252* (19), 6727-6730.

58. Jones, E. A.; Fletcher, J. S.; Thompson, C. E.; Jackson, D. A.; Lockyer, N. P.; Vickerman, J. C., ToF-SIMS analysis of bio-systems: Are polyatomic primary ions the solution? *Applied Surface Science* **2006,** *252* (19), 6844-6854.

59. Altelaar, A. F. M.; van Minnen, J.; Jiménez, C. R.; Heeren, R. M. A.; Piersma, S. R., Direct molecular imaging of Lymnaea stagnalis nervous tissue at subcellular spatial resolution by mass spectrometry. *Analytical Chemistry* **2005,** *77* (3), 735-741.

60. Cheng, J.; Winograd, N., Depth profiling of peptide films with TOF-SIMS and a C60 probe. *Analytical Chemistry* **2005,** *77* (11), 3651-3659.

61. Fletcher, J. S.; Henderson, A.; Biddulph, G. X.; Vaidyanathan, S.; Lockyer, N. P.; Vickerman, J. C., Uncovering new challenges in bio-analysis with ToF-SIMS. *Applied Surface Science* **2008,** *255* (4), 1264-1270.

CHAPTER SIX:
Discovery and Targeted Monitoring of *Dictyostelium. discoideum* Lipids Using Multidimensional LC-TIMS-MS/MS Separations

This chapter is in preparation for journal submission.

Kendra J. Adams, Cesar E. Ramirez, Richard H. Gomer, Aiko Barsch, Ningombam

Sanjib Meitei , Francisco Fernandez-Lima

6.1 Abstract

The diverse and complex nature of the lipidome makes identification and quantitation of lipids a challenging task. Combinations of analytical techniques has been deemed necessary to reveal a comprehensive lipid profile from biological samples. In this chapter, a new workflow based on liquid chromatography, trapped ion mobility spectrometry (TIMS), and high-resolution mass spectrometry was developed and evaluated for the analysis of a variety of lipid classes and for the discovery and quantitation of lipids in *Dictyostelium discoideum* as a function of the biological cycle. The TIMS analyzer permitted the separation of lipid classes as well the separation of *sn* isobars (average R of 140). Typical limits of detection are reported below 10 pg/µl for over 10 different lipid classes using tandem liquid chromatography, mobility and mass separations. The proposed workflow permits untargeted and targeted analysis with higher confidence and high sensitivity.

6.2 Introduction

Lipidomics is an up-and-coming area of study due to the important role lipids play in various biological systems and environments.[1-2] Lipids are fats, and are involved in cell signaling, energy storage, membrane make-up, and play major roles in the regulation and function of cellular processes. Deviations in typical lipid levels or disruptions in lipid metabolism have been linked to diseases such as Alzheimer's Disease, Parkinson's Disease and Neuronal Ceroid Lipofuscinoses (NCLs).[1, 3-5] Traditional lipidomic analyses include the use of liquid chromatography coupled to tandem mass spectrometry (LC-MS) for the separation and identification of the compounds within complex biological matrices.[6-11] Numerous methods of lipid extraction, chromatographic separation and mass spectrometric

separation and detection have been recently developed; the specific approach depending on the analytical or biological challenge at hand. Lipid quantitation includes the use of tandem mass spectrometry (MS/MS), specifically multiple reaction monitoring (MRM) for targeted identification and quantification based on transitions between the molecular ion and characteristic fragment ions.[11] Recent analytical lipidomic developments stray away from targeted approaches, which tend to limit the extent to which a biological profile can be identified. Non-targeted analyses may provide less accurate identifications; however, using an non-targeted approach allows for a comprehensive lipid profile which can also be re-processed and analyzed should the biological question change, or, as developments in lipid research are accomplished.[12]

In addition to the widely used LC separations, ion mobility is becoming a common technique for separations and identifications of lipids within biological samples.[13-22] IMS allows separation of all lipid classes in a single analysis in significantly less time than a traditional LC approach. Differentiation of lipid isomers has been achieved using various ion mobility spectrometers such as high field asymmetric ion mobility spectrometry (FAIMS) and drift tube ion mobility spectrometry (DT-IMS).[15-17, 21-23] For example, FAIMS has been utilized by several research groups for the separation of three types of lipid isomers including: *sn*-, double bond and *cis/trans* positional isomers.[15-16, 21] Baseline or near-baseline separations of lipid isomers are achieved with FAIMS following modifications such as changing bath gas composition (i.e. increasing %He),[15, 21] the use of adducts (i.e. silver-ion adducts),[16, 22] or upon addition of chemical modifiers (e.g., butanol and propanol).[22] High resolution DT-IMS has been used for separations of double bond positional isomers, geometrical isomers and *sn*–positional isomers.[17, 23] The coupling of

liquid chromatography to IMS-MS is becoming a more popular and standard method for lipidomic analyses of biological samples [13, 17, 24-28]

In this research, the lipids in *Dictyostelium discoideum* (*D. discoideum*) cells are identified at different points of the cell cycle. *D. discoideum* are cells that, like most organisms, adapt to their environment to best protect themselves from harm or death; they can emit chemotactic responses to signals generated by cyclic adenosine 3', 5'-monophosphate (cAMP) when subjected to adverse conditions.[29-32] The processes of growth and development in *D. discoideum* are two independent routes, and only one can occur at a time.[32] In order for the development stage to occur and the cells to migrate into a multicellular body, they must be depleted of nutrients. If nutrients are reintroduced during the earlier stages of development, the process will be reversed and the cells return to the growing phase.[32] There are different stages of the aggregation process, ranging from migration to culmination, which results in a full fruiting body.[33] The development of the full fruiting *D. discoideum* occurs after approximately 24 hours of continuous starvation.[33] *D. discoideum* are considered "model organisms for biomedical research" by the National Institute of Health, because of their ability to exchange between single and multicellular organisms in their biological cycle and the conservation of various cell processes such as cell-to-cell interactions and signaling from these amoeba to eukaryotic cells.[32, 34-40] It is interesting to study how certain cell components (i.e. lipids and proteins) are altered during the cell's life cycle to assist in the understanding of mechanisms of chemotaxis and the impact the movement has on the cell structure and make-up.

In this research, a new workflow based on liquid chromatography, trapped ion mobility and high-resolution mass spectrometry is used for the separation and identification

of lipids in *D. discoideum* cells. The capabilities of LC-TIMS.MS/MS are evaluated for a series of lipid classes and *sn*-positional isomers. In addition to confirming the lipids of interest using RT, accurate mass and fragmentation pattern, the proposed workflow also provides accurate CCS. This work indicates the importance of multidimensional separations in lipidomic analysis, showcasing the analytical capabilities of trapped ion mobility when coupled to both mass spectrometry and liquid chromatography.

6.3 Experimental Parameters

6.3.1 Standards and Chemicals

All solvents were purchased from Fisher Scientific (Pittsburg, PA) and were of LC-MS quality or better. Pooled human plasma was purchased from Innovative Research (Novi, MI, USA). Lipid standards of sulfatides [131305, Brain, Porcine, (major component 18:1/24:1 ST)], sphingomyelin [860061, Egg, Chicken (major component 18:1/16:0 SM)], 1,2-dipalmitoyl-sn-glycero-3-phosphocholine [850355, (16:0 PC DPPC)], 1-stearoyl-2-palmitoyl-*sn*-glycero-3-phosphocholine [850465, (18:0-16:0 PC)], 1-palmitoyl-2-stearoyl-*sn*-glycero-3-phosphocholine [850456, (16:0-18:0 PC)], 1-stearoyl-2-myristoyl-sn-glycero-3-phosphocholine [850464, (18:0-14:0 PC)], 1-myristoyl-2-stearoyl-sn-glycero-3-phosphocholine [850446, (14:0-18:0 PC)], 1-palmitoyl-2-myristoyl-sn-glycero-3-phosphocholine [850454, (16:0-14:0 PC)], 1-myristoyl-2-palmitoyl-sn-glycero-3-phosphocholine [850445, (14:0-16:0 PC)], 1-stearoyl-2-oleoyl-sn-glycero-3-phospho-(1'-rac-glycerol) (sodium salt) [840503, (18:0-18:1 PG)] and 1,2-dimyristoyl-sn-glycero-3-phosphoethanolamine [850745, (14:0 PE)] and the SPLASH Lipidomix [330707] were purchased from Avanti Lipids Inc. (Alabaster, AL) and used as received. Calibration curves

were created and analyzed with the analytes and the SPLASH mixture was used as the deuterated internal standard for several lipid classes.

6.3.2 Calibration Standard Preparation.

Lipid standard calibration curves were created at six levels ~1700 ppb to 0.05 ppb depending on the lipid class. For determination of LODs, a stock solution of lipid analyte mixture was prepared at ~100 ppm and diluted in IPA:ACN for the use in each calibration point. An aliquot of SPLASH Lipidomix was also diluted in 1:1 IPA:ACN and subsequently used in a dilution series to calculate LOD for each standard in the mixture. A secondary calibration curve was developed following LOD calculation which contains a set deuterated standard concentration with a variation in the analyte concentration. The concentration of the SPLASH Lipidomix internal standard ranged from 13-2330 ng/mL depending on the lipid class and its initial concentration in the commercial mix.

6.3.3 Dictyostelium discoideum Cell Preparation.

Wild type Ax2 *D. discoideum* cells were grown at room temperature in Formedium HL-5 shaking culture as previously described [41-42]. Briefly, mid-log phase cells at $2x10^6$ cells/mL were collected by centrifugation at 1,500xg for 5 minutes and resuspended in deionized water. The cells were again collected by centrifugation, washed twice by resuspension and centrifugation and collected in the same manner. The cell pellets were frozen in a dry ice ethanol bath and stored at -80^0C. For developing cells, the mid-log phase cells were collected by centrifugation at 1,500 x g for 3 minutes and washed twice by resuspension in PBM (20 mM KH_2PO_4, 10 μM $CaCl_2$, 1 mM $MgCl_2$, pH 6.1); collection of the cells was performed by centrifugation. After various starvation times (0 hours, 6 hours and 18 hours) cells were resuspended in PBM to $5x10^6$ cells/mL, developed in

shaking culture, collected, and washed three times with deionized water. Pellets were frozen as described above and stored at -80^{0}C.

6.3.4 Lipid Extraction

Lipid extraction from pooled human plasma and *D. discoideum* cells was based on a single phase, chloroform-free lipid extraction from plasma.[43-45] Briefly, pooled human plasma or *D.* discoideum cell pellets were removed from the freezer and allowed to thaw over ice. Following thawing, 30 uL of plasma or a cell pellet were spiked with SPLASH mixture, ammonium formate (for a final concentration of 10 mM) and butylhydroxytoluene (BHT) as an antioxidant (final concentration of 10 μM) and 100 uL of 1:1 butanol:methanol. The samples were disrupted using a mechanical pestle for ten seconds, and an additional 200 uL of butanol:methanol was used to rinse the pestle into the Eppendorf containing the matrix. The lipids were vortexed for 20 seconds and sonicated for 30 minutes at 20º C. Following sonication, the plasma or cells were centrifuged for 20 minutes at 16000 x g at 20º C and the supernatant (~300 μL) transferred to an autosampler vial with an insert.

6.3.5 LC-TIMS-MS/MS Separation

After extraction, the lipids were separated by an Acclaim 120 chromatography column (2.1 x 250 mm; 5 μm; 120Å; C18) during a 20-minute multistep gradient using a Shimadzu Prominence HPLC system consisting of two 20AD pumps, a SIL-20AC auto-sampler and a CTO 20-A column oven held at 55 °C flow rate of 0.75 mL min^{-1} (Kyoto, Japan). Separation parameters were modified from methods reported by Della Corte et al.[46] and Hu et al.[47] following a 20 μL injection, mobile phase B was held at 25% for 0.2 minutes where it was increased to 50% B at 1.5 minutes. Over 3.5 minutes, mobile phase B

increased to 85% and then to 100% between 5 and 10 minutes. Mobile phase B was held at 100% from 10 and 15 minutes and decreased back to 25% at 16 minutes. The column was held at 25% B for four minutes for re-equilibration. Mobile phase A consists of 40% acetonitrile in water, 10 mM NH4COOH and B is 10% acetonitrile and 1% water in isopropyl alcohol with 10mM NH4COOH. The mobile phases were constant between positive and negative ionization modes. The HPLC was coupled directly to a commercial timsTOF (Bruker Daltonics Inc., Billerica, MA). Samples were ionized using an ionBooster ESI source in both negative and positive ionization mode. Typical ionBooster operating conditions were 1750 V capillary voltage, 400 V end plate offset, 400 V charging voltage, 1.5 bar nebulizer pressure, 3.0 L/min dry gas, 250 °C dry heater and 200 °C vaporizer.

For wide range mobility analysis and CCS calculation of PC isomers, a custom-built TIMS-TOF MS based on the maXis impact Q-ToF MS (Bruker Daltonics Inc, Billerica, MA) was utilized. The gas velocity was defined by the entrance and exit TIMS roughing impedance (P_1 = 2.6 and P_2 = 1.0 mbar) and a voltage and time ramp of Δ280 V and 100 ms with V_{out} = 60 V were used. For narrow mobility selection experiments (higher resolving power), the velocity of the gas was increased (P_1= 3.2 and P_2=1.0 mbar) and a ramp of Δ30 V with a 1000 ms ramp time was utilized. A Vpp = 270 V and 880 kHz radiofrequency was kept constant for all the experiments and allowed for radial confinement of the ions within the TIMS analyzer. For LC-TIMS-MS/MS analysis, a Commercial TIMS-tof parameters were optimized to detect lipids in the mobility range between 0.70 and 1.70 $V \cdot s/cm^2$ with an accumulation time of 100 ms and a ramp time of 350 ms using a dual stage trapped TIMS analyzer.

MS^2 parameters were optimized as follows: TIMS ramp time of 150 ms from 0.5-1.80 V S/cm^2, the duty cycle was locked to 100% during acquisition. For PASEF, 8 MS/MS scans were collected during a 1.40 sec cycle time, precursor ions were set for 1 repetition with a cycle overlap of 4. A target intensity of 300000 cts/s was used with active exclusion on, a release time of 0.4 min and reconsideration was activated if current intensity was measured 4x higher than previous intensity. A collision energy of 42 eV was set for m/z 622, 922, and 1521, each with a charge state of 1 and a width of 2.00. Auto-MS/MS parameters were optimized as follows: 20 precursors, an absolute threshold of 5000, a 20x smart exclusion and active exclusion after 2 spectra with reconsideration if a 5x intensity increase is observed. Ions below m/z 350 were excluded from MS/MS fragmentation. CID parameters were set for singly charged species as follows: m/z 622, 922 and 1521 with a width of 2.00 and collision energy of 38.5 eV. MS/MS for bbCID parameters were set at 10 eV collision energy in MS and 38.5 eV for MS/MS.

6.3.6 Data Processing and Analysis

LC-TIMS-TOF MS data were processed using Data Analysis software v. 5.0 (Bruker Daltonics Inc, Billerica, MA). The lipids from the *D. discoideum* cells and human plasma were identified from the LC-PASEF-MS acquisition. The "Find PASEF" feature in Data Analysis was used to obtain an initial list of precursor and fragment ions which was searched for familiar, head group, fatty acid and fragment ions from lipids. SimLipid 6.02 (Palo Alto, CA) was used for confirmation of the initial identifications based on accurate mass and fragmentation pattern. Scans with MS/MS were selected for consideration in the identification parameters. For lipid identification using SimLipid, the

following parameters were used: a precursor mass tolerance of 0.12 Da was implemented with fragment mass errors of 2.5 ppm. All lipid classes, categories and subclasses were selected for potential matching. In negative mode the $[M-H]^-$ adduct was searched and in positive mode, $[M+H]^+$, $[M+Na]^+$, $[M+K]^+$, and $[M+NH_4]^+$ were utilized for identifications. For incorporation into the lipid identification table, the lipid identification had to occur for each strain of cells at in at least two scans of a single data file and in at least two of the three replicates analyzed.

6.4 Results and Discussion

TIMS-MS experiments were performed on pairs of *sn*-positional isomers of PC lipids for CCS calculation, evaluation of variability and reproducibility of TIMS CCS measurements and high-resolution separation of isomeric lipids. Pairs of isomeric lipids include PC (14:0/16:0) and PC (16:0/14:0) at *m/z* 706.5381 for $[M+H]^+$, 728.5201 for $[M+Na]^+$, and 744.4940 for $[M+K]^+$; PC (14:0/18:0) and PC (18:0/14:0) at *m/z* 734.5694 for $[M+H]^+$, 756.5514 for $[M+Na]^+$, and 772.5253 for $[M+K]^+$; and PC (18:0/16:0) and PC (16:0/18:0) at *m/z* 762.6007 for $[M+H]^+$, 784.5827 for $[M+Na]^+$, and 800.5566 for $[M+K]^+$. Collisional cross sections of the individual lipids were calculated on five different days to determine the interday reproducibility and variability of the TIMS CCS calculations. In TIMS, CCS calculations are possible using internal or external calibration using compounds of known mobility (i.e., Tuning Mix). The CCS for the individual compounds of the *sn*-positional isomers are reported in Table 6.1. Utilizing low resolution ion mobility analysis, and based on the reported CCS with their errors over the five days, separation between the *sn* isomeric compounds is not observed. Figure 6.1 depicts single band CCS profiles for each PC lipid over the 5-day analysis. Note the minimal shift in peak apex for

each analysis. The relative standard deviations in the calculated CCS for each day of analysis remains <0.25%. These minimal changes can attest to the stability and reproducibility of the TIMS platform of ion mobility spectrometry.

Upon adjusting the TIMS parameters to achieve high resolution analyses (increased pressure difference, Δ30 V TIMS ramp and 1000 ms ramp times, Sr = 0.3 V/ms) baseline separation is achieved between PC(14:0/16:0) and PC(16:0/14:0) (shown in purple and yellow), PC(14:0/18:0) and PC (18:0/14:0) (shown in green and red) and PC (16:0/18:0) and PC (18:0/16:0) (shown in blue and orange) (Figure 6.2). Under these conditions, typical resolving powers of R~ 130-150 were observed, and a resolution between the $[M+H]^+$ and $[M+Na]^+$ bands of each PC lipid r~ 1.1 - 1.5. Previous works have shown partial separation of *sn*-lipid isomers using FAIMS [15, 22] and DT-IMS [17, 23]; however, unlike in TIMS analysis, bath gas modifiers or unusual ion adducts (e.g., Ag[16, 22-23]) were necessary. Baseline separations of *sn*-positional isomers using silver ion adducts have been shown using DT-IMS at lower resolving power and can be probably be reproduced with TIMS.[23] Moreover, based on the higher resolving power of TIMS compared to DT-IMS, we can postulate that PC isomers with variation of the double bond position are likely separated by TIMS, since these separations have been shown using DT-IMS at lower resolving powers. [23]

Interday Reproducibility (n=5)	K_0 ($cm^2V^{-1}s^{-1}$) $[M+H]^+$	CCS ($Å^2$)	% RSD	K_0 ($cm^2V^{-1}s^{-1}$) $[M+Na]^+$	CCS ($Å^2$)
PC 18:0-16:0	0.6971 ± 0.0013	292.921 ± 0.543	0.23	0.6825 ± 0.0010	297.803 ± 0.449
PC 16:0-18:0	0.6985 ± 0.0021	292.326 ± 0.868	0.13	0.6839 ± 0.0001	297.706 ± 1.386
PC 16:0-14:0	0.7311 ± 0.0022	279.697 ± 0.855	0.09	0.7162 ± 0.0023	285.340 ± 0.900
PC 14:0-16:0	0.7316 ± 0.0019	279.472 ± 0.710	0.08	0.7163 ± 0.0026	285.295 ± 1.042
PC 18:0-14:0	0.7144 ± 0.0023	285.997 ± 0.914	0.12	0.7012 ± 0.0026	291.239 ± 1.060
PC 14:0-18:0	0.7151 ± 0.0025	285.740 ± 1.013	0.13	0.7015 ± 0.0031	291.084 ± 1.291

Table 6.1: *sn*-positional isomer CCS and %RSD over 5 days

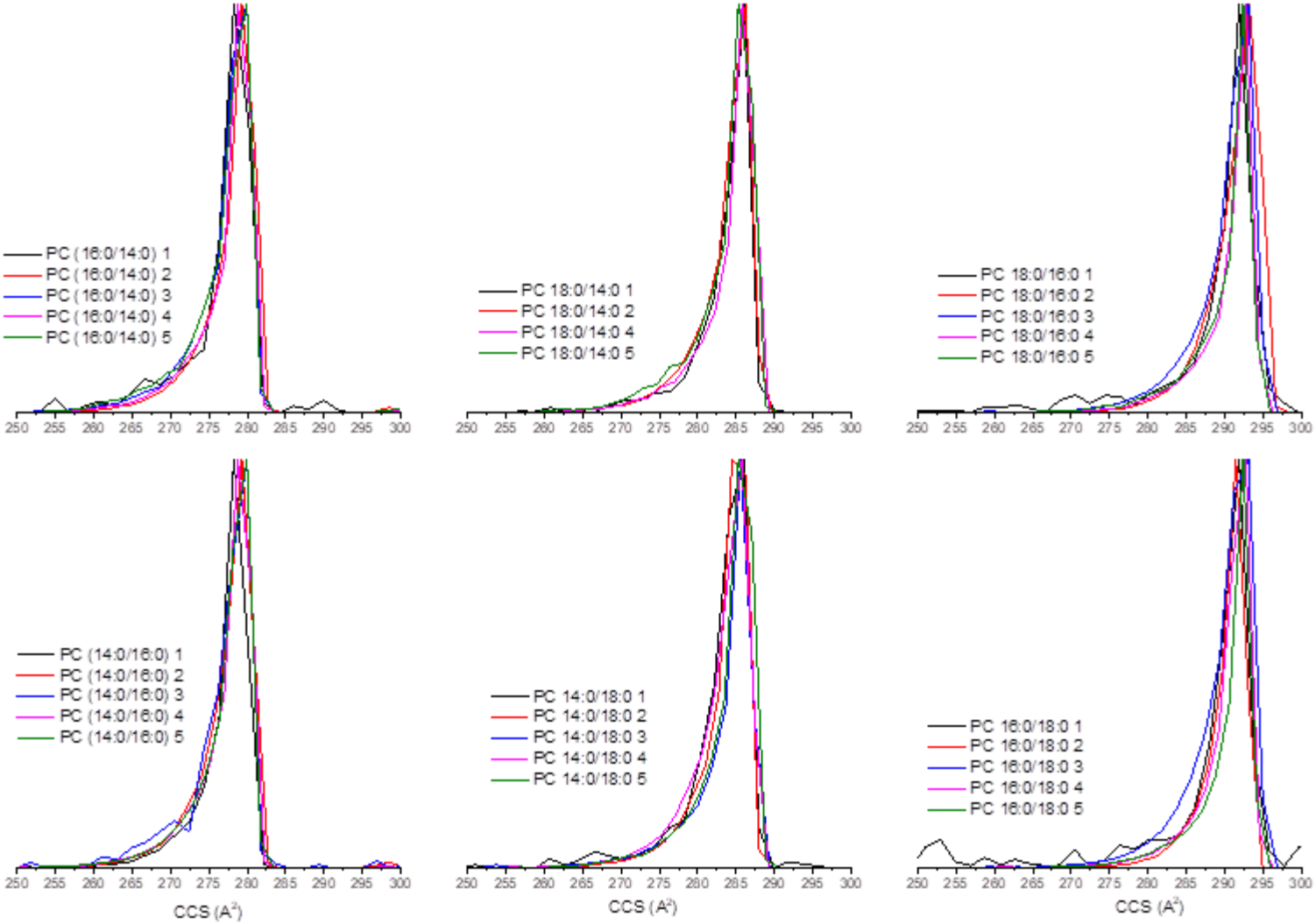

Figure 6.1: Interday analysis of PC lipids (n=5)

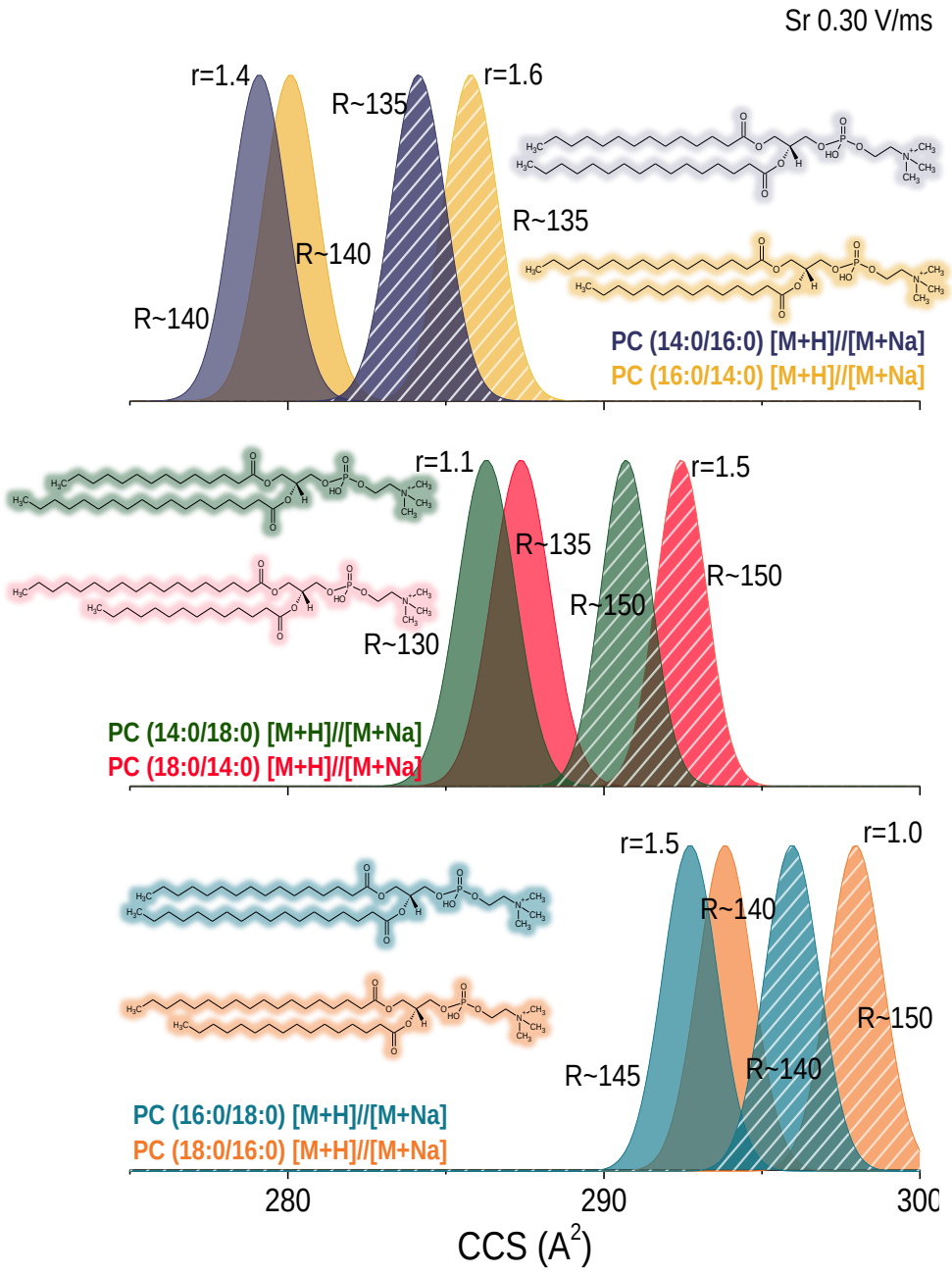

Figure 6.2: Ion mobility profiles for *sn*-isomeric phosphatidylcholine lipids using high resolution TIMS-MS. Note the shift in CCS between $[M+H]^+$ and $[M+Na]^+$ adducts

A significant difference between TIMS and other IMS variants is the possibility to decouple the mobility separation from the analysis time, which allows for variable sensitivity depending on the chosen duty cycle. In a one stage TIMS, a mix of lipids was analyzed via LC-TIMS-MS with varying duty cycle (10-50%). That is, a 100 ms TIMS separation was considered with duty cycles ranging from 10-50%. Notice that this has a direct impact on the number of points recorded in the LC domain (Figure 6.3). As the duty cycle increases (i.e., fill time increases), the signal response increases at the cost of decreased sampling points in the LC domain. Although an increase in signal response is typically a desirable effect, the increase in LC step may be a deterrent in cases where RT is used as an identifier for the compound of interest or highly resolved chromatographic peaks are necessary.

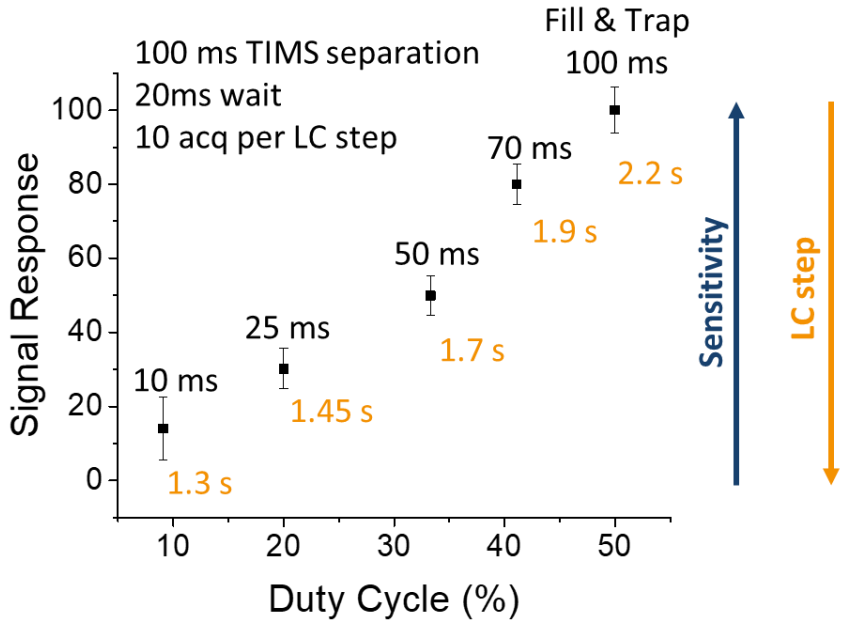

Figure 6.3: Signal changes in response to changes in duty cycle of the TIMS-MS

The addition of IMS to traditional LC-MS workflows can lead to a loss in sensitivity. However, due to the trapping nature of TIMS, no change, or an increase in the detection sensitivity is expected. To further evaluate the analytical potential of LC-TIMS-MS, limits of detection (LODs) were calculated for lipid classes and subclasses using deuterated and non-deuterated standards. Tables 6.2 and 6.3 provide LODs and limit of quantitation (LOQs, three times LOD) results in the chromatographic and ion mobility domain for the analytes in negative (Table 6.2) and positive (Table 6.3) mode, depending on the preferential ionization polarity of the lipid. The extracted ion chromatogram/mobilogram for each m/z was integrated and used to the calculate the LOD. Reported LODs for both positive and negative mode using LC-MS are typically reported under 1 pg/μL (Tables 6.2 and 6.3), exceptions include PA 12:0/12:0 in negative ionization mode and PC 15:0/18:1 d7, TG (15:0/18:1 d7/15:0) and PC 16:0/16:0 in positive ionization mode. Good linearity is reported for all analytes throughout the curve R^2>0.98. For LOD calculation using LC-TIMS-MS, LODs are typically equal to or higher than those reported from LC-MS. A linear trend can be observed when a comparison is made between the LOD of each analyte calculated from analysis with and without TIMS separation (Figure 6.4). The LODs and LOQs are on the same order of magnitude between LC-MS and LC-TIMS-MS and minimal losses in sensitivity are observed with the addition of the TIMS domain. With the TIMS dimension included in the analysis, LODs are below 1 pg/uL except for PG 15:0/18:1 d7, PE 18:1/16:0, PG 18:0/18:1, PA 12:0/12:0 and PE 14:0/14:0 in negative mode and PC 15:0/18:1 d7, TG 15:0/18:1 d7/15:0), and PE 14:0/14:0 in positive ionization mode. Good linearity is observed for the analytes across the calibration concentrations

using LC-TIMS-MS. These results are comparable to previously reported lipid LODs using LC-IMS-MS approaches.[28]

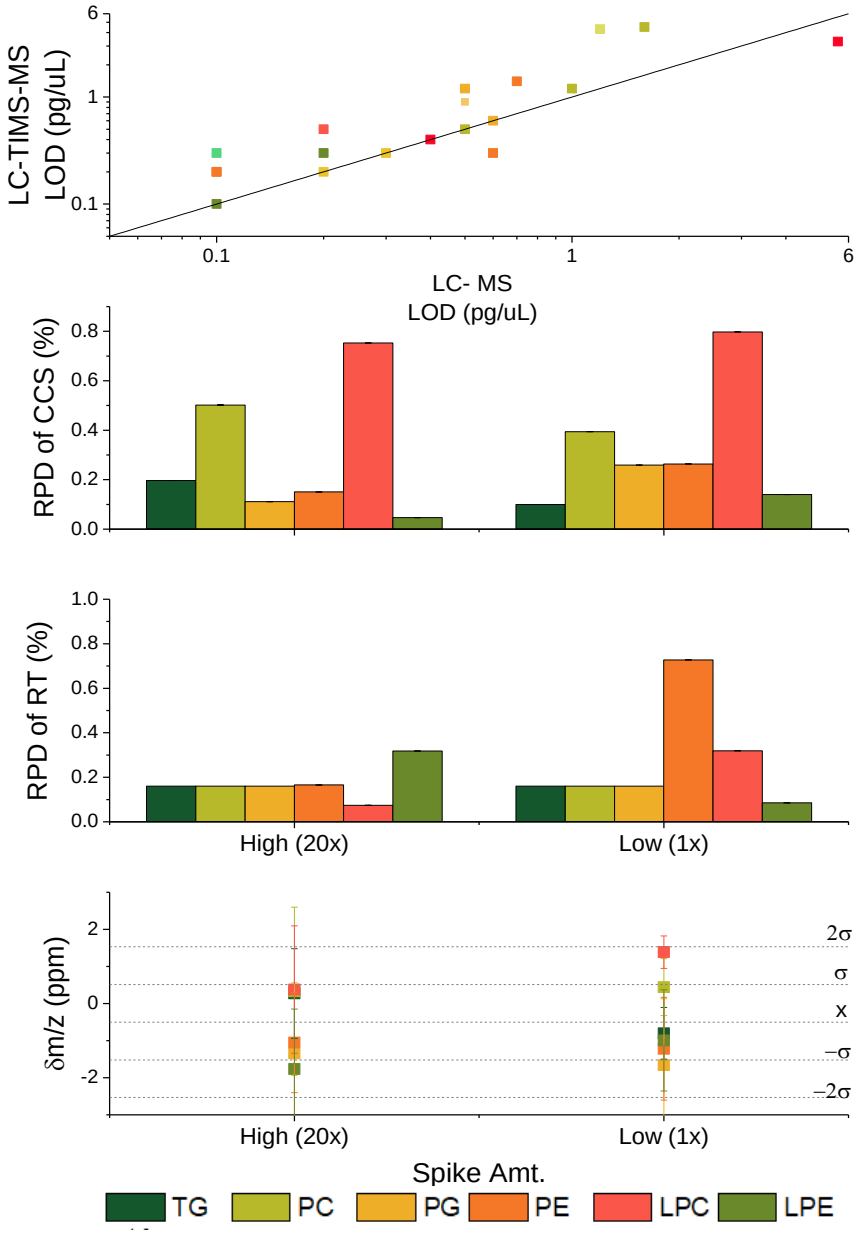

Figure 6.4: LOD comparison between LC-TIMS MS and LC-MS for neat lipid standards (top). Reproducibility and accuracy parameters for lipid standards spiked in blood plasma at two different spiked levels (1x and 20x) with respect to a control mix

Compounds	Identification Parameters			LC-MS			LC-TIMS-MS		
	m/z $[M-H]^-$	RT (min)	CCS ($Å^2$)	LOD (pg/uL)	LOQ (pg/uL)	R^2	LOD (pg/uL)	LOQ (pg/uL)	R^2
PE 15:0/18:1 d7	709.552	6.38	267.7	0.1	0.5	0.99	0.2	0.9	0.99
PS 15:0/18:1 d7	753.541	6.08	278.2	0.3	1.4	0.99	0.3	1.7	0.99
PG 15:0/18:1 d7	740.547	6.02	274.4	0.1	0.7	0.99	1.0	5.4	0.99
LPE 18:1 d7	485.338	4.06	217.9	0.1	0.4	0.99	0.1	0.7	0.99
PI 15:0/18:1 d7	828.563	5.94	288.9	0.6	2.8	0.99	0.3	1.6	0.99
PE 18:1/16:0	716.524	6.52	270.1	0.04	0.2	0.99	1.4	7.1	0.99
PG 18:0/18:1	775.550	6.39	283.5	0.5	10.0	0.99	1.2	5.8	0.99
PG 16:0/16:0	721.503	6.13	273.3	0.6	3.5	0.99	0.6	3.3	0.99
PA 12:0/12:0	535.341	5.03	275.1	5.6*	28.1	0.99	3.3	16.6	0.99
PE 14:0/14:0	634.444	5.92	253.5	0.7	3.3	0.99	1.4	7.1	0.99

Table 6.2: Limits of detection using timsTOF with and without TIMS for lipids preferentially ionized in negative mode
Note: *= visually estimated LOD

Compounds	Identification Parameters			LC-MS			LC-TIMS-MS		
	m/z $[M+H]^+$	RT (min)	CCS (Å²)	LOD (pg/uL)	LOQ (pg/uL)	R^2	LOD (pg/uL)	LOQ (pg/uL)	R^2
PC 15:0/18:1 d7	753.613	6.69	288.3	1.6	7.9	0.99	4.8	23.8	0.99
PE 15:0/18:1 d7	711.566	6.38	275.4	0.1	0.4	0.99	0.2	1.0	0.99
PS 15:0/18:1 d7	755.556	6.08	281.2	0.2	1.0	0.99	0.2	0.8	0.99
PI 15:0/18:1 d7	830.577	5.95	298.7	0.4	1.8	0.99	0.4	2.0	0.98
LPC 18:1 d7	529.399	4.02	235.5	0.2	1.0	0.99	0.5	3.0	0.99
LPE 18:1 d7	509.334^{+}	4.07	223.6	0.2	1.1	0.99	0.3	1.5	0.99
DG 15:0/ 18:1 d7	570.547^{++}	8.70	260.7	0.1	0.6	0.99	0.3	1.7	0.99
TG 15:0/18:1 d7/15:0	829.799^{+++}	8.71	314.6	1.2	5.8	0.99	4.3	21.7	0.91
SM 18:1 d9	738.647	6.52	291.7	0.5	1.4	0.99	0.9	5.7	0.99
PC 16:0/18:1	760.585	6.95	292.6	0.5*	2.5	0.99	0.5	2.3	0.99
PC 16:0/16:0	734.569	6.95	288.7	4.6	22.8	0.99	3.5	17.7	0.99
PE 14:0/14:0	636.460	5.92	264.2	1.2	5.8	0.99	7.8	38.9	0.99

Table 6.3: Limits of detection using timsTOF with and without TIMS for lipids preferentially ionized in positive mode
$^{+}$ $[M+Na]^+$, $^{++}$ $[M-H_2O+H]^+$, $^{+++}[M+NH_4]^+$, *=visually estimated

The lipid profile of the *D. discoideum* cells was obtained from LC-TIMS-MS/MS data using the SimLipid software to obtain a high throughput lipid identification output. Appendix 13 includes the lipids identified from the WT *D. discoideum* cells using SimLipid and includes the *m/z*, retention time, lipid identity and the fragments that lead to its identification. Additionally, presence/absence of the lipid in the three growing conditions is noted. Total lipid profiling from *D. discoideum* cells has not been reported; however, several studies have been performed that identify lipid subclass profiles from the cells. Fatty acid profiles for the cells have been reported with relative abundances of the fatty acids based on their chain length and degrees of unsaturation.[48-51] Although our lipid identifications do not specifically extract fatty acid chains, observation of the fatty acid chain fragments observed in negative mode allows for comparison of our cells to those reported by Blacklock et al.[48] The most abundant fatty acids in the *D. disocoideum* cells were reported to be 18:2 and 18:1 chains at ~36% and ~32% of the total lipids.[48] A majority of the lipids we identify contain one or both of the 18:2 or 18:1 fatty acid chains, which can be identified based on their $[RCOO]^-$ ion at *m/z* of 281.248 and 279.232, respectively (Appendix 13). The other most abundant fatty acids reported for *D. discoideum* cells include 16:0, 16:1 and 16:2, which are also incorporated in several of the identified lipids we report in Appendix 13. [48]

Previous reports of intact lipids in *D. discoideum* focus on sphingolipids as a class of lipids.[38] A series PI-Cer (t36:0(2OH)) (m/z: 840, $C_{42}H_{83}NO_{13}P$), PI-Cer (t38:0(2OH)) (m/z: 868, $C_{44}H_{87}NO_{13}P$) and PI-Cer (t40:0(2OH)) (m/z: 896, $C_{46}H_{91}NO_{13}P$) has been observed in *D. discoideum* cells and has been previously reported by Birch.[38] The

SimLipid identification parameters were not able to ID this series of lipids, and the identifications were manually performed through analysis of the MS2 spectrum for each intact lipid. Identifying fragments for the PI class of lipid include head groups at *m/z* 259 and 241 and the fatty acid chain fragments. The lipid PI-Cer (t34:0(2OH)) at m/z 812 ($C_{40}H_{79}NO_{13}P$) also belongs to this series of sphingolipids but has not been reported previously. A sphingolipid was also reported at m/z 700.5658 ($C_{40}H_{79}NO_6P$); however, we identify this lipid as PE (P-16:0/18:1) based on the typical PE head group fragment at *m/z* 140 and a fragment at 281 corresponding to the 18:1 fatty acid chain.[38]

A variety of other glycerophospholipds have been identified through our analyses, including lipids within the PE, PG and PS subclasses (Appendix 13). Although a comprehensive lipid profile has not been identified for *D. discoideum*, reports have been published regarding general lipid classes observed in the cells. These reports have shown that PE and PC are both represented in the lipidomic profile of *D. discoideum* as well as PG and PS in lower abundances.[52-53] Based on initial observations of presence/absence of the lipids during the various times of starvation, most of the identified lipids are present at the vegetative state and 18 hours after starvation; however, many are missing during the 6 hours of starvation time point (Appendix 13). Coe and Long have shown the decrease in lipid composition during the early stages of aggregation followed by an increase in the total lipids during the culmination stage after 24 hours.[54]

A distribution of lipid class, *m/z* and CCS of the lipids identified from the *D. discoideum* cells is displayed in Figure 6.5. The trends are consistent with previously reported trends. Typically, as the mass-to-charge of an ion increases, its size or CCS also

increases.[18-19] Notice that in our approach, the trends are also "build as you go" using the identification workflow.

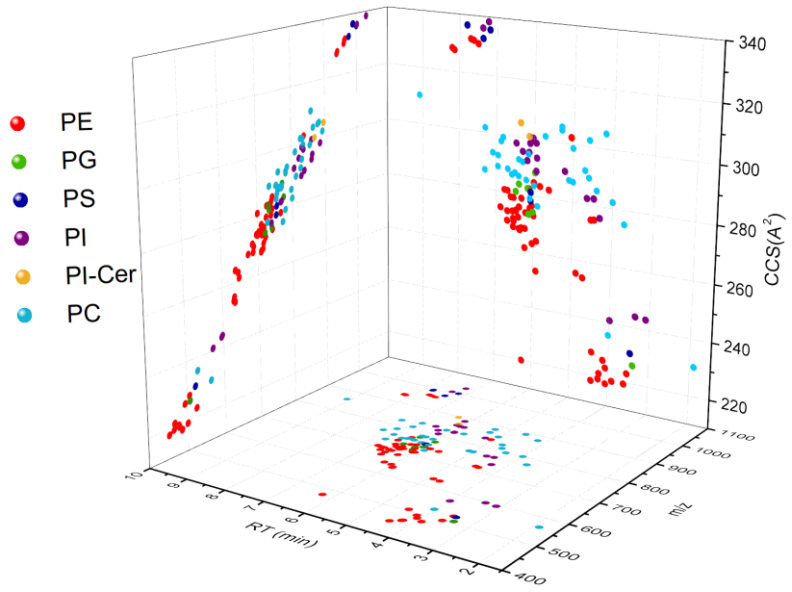

Figure 6.5: Lipids from *D. discoideum* cells depicted by subclass, m/z, CCS, and RT

The use of internal standards allows for further evaluation of lipid changes. With the addition of deuterated lipids as internal standards (Avanti's SPLASH Lipidomix), the ability to obtain quantitative lipidomic results is achieved. The quantitation of lipids allows us to report discrete concentration values of various lipid class, and subclasses detected within the *D. discoideum* cells rather than merely provide qualitative data such as presence/absence or relative abundances. Changes in specific lipid abundances between the vegetative, 6 and 18 hours of starvation are observed and reported (Figure 6.6). For two subclasses of phosphoglycerolipids, phosphatidylglycerols and phosphatidylethanolamines, a pattern is observed for the changes in the identified lipids

over *D. discoideum* starvation. As the cells are starved, an increase in lipids is observed with 18 hours following starvation typically having the highest abundance of lipids.

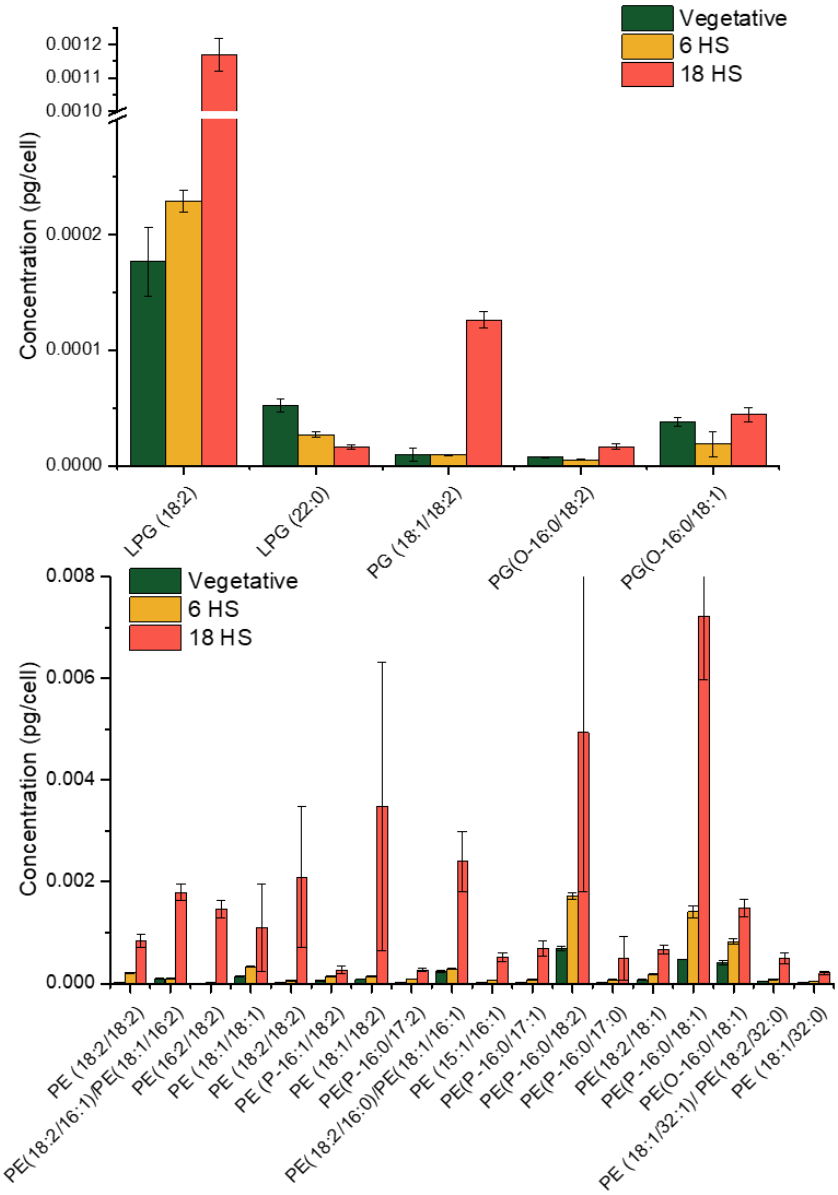

Figure 6.6: Quantitation results of select lipid subclasses PGs and PEs

6.5 Conclusions

In this work, TIMS-TOF MS and LC-TIMS-TOF-MS were used for various analyses of lipids, including separations of *sn*-isomeric phosphatidylcholines, limits of detection and dynamic range calculations for several lipid classes and identification and quantitation of lipid profiles from extracts of *Dictyostelium discoideum* cells. Calculated limits of detection show good association between the chromatographic domain and ion mobility domain and are lower than those previously reported with similar analytical methods. Separations of *sn*-positional isomers was achieved without the need for modifications in the separation technique or ionization. Comparison between lipid profiles of *D. discoideum* cells shows differences during the growth and development of the cells The addition of TIMS to traditional LC-MS/MS lipidomic analyses provides additional points of identification for lipids (CCS) and allows for differentiation of isomeric species, which may not be possible with LC alone.

6.6 References

1. Adibhatla, R.; Hatcher, J. F.; Dempsey, R. J., Lipids and lipidomics in brain injury and diseases. *The AAPS Journal* **2006,** *8* (2), E314-E321.

2. Matyash, V.; Liebisch, G.; Kurzchalia, T. V.; Shevchenko, A.; Schwudke, D., Lipid extraction by methyl-tert-butyl ether for high-throughput lipidomics. *Journal of Lipid Research* **2008,** *49* (5), 1137-46.

3. Wenk, M. R., The emerging field of lipidomics. *Nature Reviews Drug Discovery* **2005,** *4* (7), 594+.

4. Jalanko, A.; Braulke, T., Neuronal ceroid lipofuscinoses. *Biochimica et Biophysica Acta (BBA) - Molecular Cell Research* **2009,** *1793* (4), 697-709.

5. Touboul, D.; Brunelle, A.; Laprévote, O., Mass spectrometry imaging: Towards a lipid microscope? *Biochimie* **2011,** *93* (1), 113-119.

6. Cajka, T.; Fiehn, O., Comprehensive analysis of lipids in biological systems by liquid chromatography-mass spectrometry. *Trends in Analytical Chemistry* **2014,** *61*, 192-206.

7. Gika, H. G.; Theodoridis, G. A.; Plumb, R. S.; Wilson, I. D., Current practice of liquid chromatography–mass spectrometry in metabolomics and metabonomics. *Journal of Pharmaceutical and Biomedical Analysis* **2014,** *87*, 12-25.

8. Hyötyläinen, T.; Orešič, M., Optimizing the lipidomics workflow for clinical studies—practical considerations. *Analytical and Bioanalytical Chemistry* **2015,** *407* (17), 4973-4993.

9. Rochat, B., From targeted quantification to untargeted metabolomics: Why LC-high-resolution-MS will become a key instrument in clinical labs. *Trends in Analytical Chemistry* **2016,** *84*, 151-164.

10. Cajka, T.; Smilowitz, J. T.; Fiehn, O., Validating Quantitative Untargeted Lipidomics Across Nine Liquid Chromatography–High-Resolution Mass Spectrometry Platforms. *Analytical Chemistry* **2017,** *89* (22), 12360-12368.

11. Brügger, B., Lipidomics: analysis of the lipid composition of cells and subcellular organelles by electrospray ionization mass spectrometry. *Annual Review of Biochemistry* **2014,** *83*, 79-98.

12. Cajka, T.; Fiehn, O., Toward Merging Untargeted and Targeted Methods in Mass Spectrometry-Based Metabolomics and Lipidomics. *Analytical Chemistry* **2016,** *88* (1), 524-545.

13. Baglai, A.; Gargano, A. F. G.; Jordens, J.; Mengerink, Y.; Honing, M.; van der Wal, S.; Schoenmakers, P. J., Comprehensive lipidomic analysis of human plasma using multidimensional liquid- and gas-phase separations: Two-dimensional liquid chromatography–mass spectrometry vs. liquid chromatography–trapped-ion-mobility–mass spectrometry. *Journal of Chromatography A* **2017,** *1530* (Supplement C), 90-103.

14. Paglia, G.; Astarita, G., Metabolomics and lipidomics using traveling-wave ion mobility mass spectrometry. *Nature protocols* **2017,** *12* (4), 797-813.

15. Bowman, A. P.; Abzalimov, R. R.; Shvartsburg, A. A., Broad Separation of Isomeric Lipids by High-Resolution Differential Ion Mobility Spectrometry with Tandem Mass Spectrometry. *Journal of the American Society for Mass Spectrometry* **2017**, 1-10.

16. Sala, M.; Lisa, M.; Campbell, J. L.; Holcapek, M., Determination of triacylglycerol regioisomers using differential mobility spectrometry. *Rapid Communications in Mass Spectrometry* **2016,** *30* (2), 256-64.

17. Kyle, J. E.; Zhang, X.; Weitz, K. K.; Monroe, M. E.; Ibrahim, Y. M.; Moore, R. J.; Cha, J.; Sun, X.; Lovelace, E. S.; Wagoner, J., Uncovering biologically significant lipid isomers with liquid chromatography, ion mobility spectrometry and mass spectrometry. *Analyst* **2016,** *141* (5), 1649-1659.

18. Paglia, G.; Angel, P.; Williams, J. P.; Richardson, K.; Olivos, H. J.; Thompson, J. W.; Menikarachchi, L.; Lai, S.; Walsh, C.; Moseley, A.; Plumb, R. S.; Grant, D. F.; Palsson, B. O.; Langridge, J.; Geromanos, S.; Astarita, G., Ion mobility-derived collision cross section as an additional measure for lipid fingerprinting and identification. *Analytical Chemistry* **2015,** *87* (2), 1137-44.

19. May, J. C.; Goodwin, C. R.; Lareau, N. M.; Leaptrot, K. L.; Morris, C. B.; Kurulugama, R. T.; Mordehai, A.; Klein, C.; Barry, W.; Darland, E., Conformational ordering of biomolecules in the gas phase: nitrogen collision cross sections measured on a prototype high resolution drift tube ion mobility-mass spectrometer. *Analytical Chemistry* **2014,** *86* (4), 2107-2116.

20. Rainville, P. D.; Wilson, I. D.; Nicholson, J. K.; Isaac, G.; Mullin, L.; Langridge, J. I.; Plumb, R. S., Ion mobility spectrometry combined with ultra performance liquid chromatography/mass spectrometry for metabolic phenotyping of urine: Effects of column length, gradient duration and ion mobility spectrometry on metabolite detection. *Analytica Chimica Acta* **2017,** *982*, 1-8.

21. Shvartsburg, A. A.; Isaac, G.; Leveque, N.; Smith, R. D.; Metz, T. O., Separation and classification of lipids using differential ion mobility spectrometry. *Journal of the American Society for Mass Spectrometry* **2011,** *22* (7), 1146.

22. Maccarone, A. T.; Duldig, J.; Mitchell, T. W.; Blanksby, S. J.; Duchoslav, E.; Campbell, J. L., Characterization of acyl chain position in unsaturated phosphatidylcholines using differential mobility-mass spectrometry. *Journal of Lipid Research* **2014,** *55* (8), 1668-1677.

23. Groessl, M.; Graf, S.; Knochenmuss, R., High resolution ion mobility-mass spectrometry for separation and identification of isomeric lipids. *Analyst* **2015,** *140* (20), 6904-6911.

24. Damen, C. W.; Isaac, G.; Langridge, J.; Hankemeier, T.; Vreeken, R. J., Enhanced lipid isomer separation in human plasma using reversed-phase UPLC with ion-mobility/high-resolution MS detection. *Journal of Lipid Research* **2014,** *55* (8), 1772-1783.

25. Basit, A.; Pontis, S.; Piomelli, D.; Armirotti, A., Ion mobility mass spectrometry enhances low-abundance species detection in untargeted lipidomics. *Metabolomics* **2016,** *12* (3), 1-10.

26. Baker, P. R.; Armando, A. M.; Campbell, J. L.; Quehenberger, O.; Dennis, E. A., Three-dimensional enhanced lipidomics analysis combining UPLC, differential ion mobility spectrometry, and mass spectrometric separation strategies. *Journal of Lipid Research* **2014,** *55* (11), 2432-2442.

27. Hines, K. M.; Herron, J.; Xu, L., Assessment of altered lipid homeostasis by HILIC-ion mobility-mass spectrometry-based lipidomics. *Journal of Lipid Research* **2017,** *58* (4), 809-819.

28. Zhang, X.; Kew, K.; Reisdorph, R.; Sartain, M.; Powell, R.; Armstrong, M.; Quinn, K.; Cruickshank-Quinn, C.; Walmsley, S.; Bokatzian, S.; Darland, E.; Rain, M.; Imatani, K.; Reisdorph, N., Performance of a High-Pressure Liquid Chromatography-Ion Mobility-Mass Spectrometry System for Metabolic Profiling. *Analytical Chemistry* **2017,** *89* (12), 6384-6391.

29. Dinauer, M. C.; Mackay, S. A.; Devreotes, P. N., Cyclic 3', 5'-AMP relay in Dictyostelium discoideum III. The relationship of cAMP synthesis and secretion during the cAMP signaling response. *The Journal of Cell Biology* **1980,** *86* (2), 537-544.

30. Dormann, D.; Kim, J.-Y.; Devreotes, P. N.; Weijer, C. J., cAMP receptor affinity controls wave dynamics, geometry and morphogenesis in Dictyostelium. *Journal of Cell Science* **2001,** *114* (13), 2513-2523.

31. Schäfer, E.; Tarantola, M.; Polo, E.; Westendorf, C.; Oikawa, N.; Bodenschatz, E.; Geil, B.; Janshoff, A., Chemotaxis of Dictyostelium discoideum: collective oscillation of cellular contacts. *PLoS One* **2013,** *8* (1), e54172.

32. Devreotes, P., Dictyostelium discoideum: a model system for cell-cell interactions in development. *Science* **1989,** *245* (4922), 1054-1058.

33. Kessin, R. H., *Dictyostelium--Evolution, Cell Biology, and the Development of Multicellularity*. Cambridge University Press: Cambridge, 2001.

34. Jang, W.; Gomer, R. H., Initial Cell Type Choice in *Dictyostelium*. *Eukaryotic Cell* **2011,** *10* (2), 150-155.

35. Marée, A. F. M.; Panfilov, A. V.; Hogeweg, P., Migration and Thermotaxis of Dictyostelium discoideum Slugs, a Model Study. *Journal of Theoretical Biology* **1999,** *199* (3), 297-309.

36. Hägele, S.; Köhler, R.; Merkert, H.; Schleicher, M.; Hacker, J.; Steinert, M., Dictyostelium discoideum: a new host model system for intracellular pathogens of the genus Legionella. *Cellular Microbiology* **2000,** *2* (2), 165-171.

37. Martiel, J.-L.; Goldbeter, A., A Model Based on Receptor Desensitization for Cyclic AMP Signaling in Dictyostelium Cells. *Biophysical Journal* **1987,** *52* (5), 807-828.

38. Birch, G. L. Lipidomic Profiling of Dictyostelium Discoideum. Purdue University, 2011.

39. Escalante, R.; Vicente, J. J., Dictyostelium discoideum: a model system for differentiation and patterning. *International Journal of Developmental Biology* **2002,** *44* (8), 819-835.

40. Parent, C. A.; Devreotes, P. N., Molecular genetics of signal transduction in Dictyostelium. *Annual Review of Biochemistry* **1996,** *65* (1), 411-440.

41. Brock, D. A.; Gomer, R. H., A secreted factor represses cell proliferation in Dictyostelium. *Development* **2005,** *132* (20), 4553-4562.

42. DeBord, J. D.; Smith, D. F.; Anderton, C. R.; Heeren, R. M.; Paša-Tolić, L.; Gomer, R. H.; Fernandez-Lima, F. A., Secondary ion mass spectrometry imaging of Dictyostelium discoideum aggregation streams. *PLoS One* **2014,** *9* (6), e99319.

43. Alshehry, Z. H.; Barlow, C. K.; Weir, J. M.; Zhou, Y.; McConville, M. J.; Meikle, P. J., An efficient single phase method for the extraction of plasma lipids. *Metabolites* **2015,** *5* (2), 389-403.

44. Löfgren, L.; Forsberg, G.-B.; Ståhlman, M., The BUME method: a new rapid and simple chloroform-free method for total lipid extraction of animal tissue. *Scientific Reports* **2016,** *6*, 27688.

45. Löfgren, L.; Ståhlman, M.; Forsberg, G.-B.; Saarinen, S.; Nilsson, R.; Hansson, G. I., The BUME method: a novel automated chloroform-free 96-well total lipid extraction method for blood plasma. *Journal of Lipid Research* **2012,** *53* (8), 1690-1700.

46. Della Corte, A.; Chitarrini, G.; Di Gangi, I. M.; Masuero, D.; Soini, E.; Mattivi, F.; Vrhovsek, U., A rapid LC–MS/MS method for quantitative profiling of fatty acids, sterols, glycerolipids, glycerophospholipids and sphingolipids in grapes. *Talanta* **2015,** *140*, 52-61.

47. Hu, C.; van Dommelen, J.; van der Heijden, R.; Spijksma, G.; Reijmers, T. H.; Wang, M.; Slee, E.; Lu, X.; Xu, G.; van der Greef, J.; Hankemeier, T., RPLC-Ion-Trap-FTMS Method for Lipid Profiling of Plasma: Method Validation and Application to p53 Mutant Mouse Model. *Journal of Proteome Research* **2008,** *7* (11), 4982-4991.

48. Blacklock, B. J.; Kelley, D.; Patel, S., A fatty acid elongase ELO with novel activity from Dictyostelium discoideum. *Biochemical and Biophysical Research Communications* **2008,** *374* (2), 226-230.

49. Long, B. H.; Coe, E. L., Fatty acid compositions of lipid fractions from vegetative cells and mature sorocarps of the cellular slime mold Dictyostelium discoideum. *Lipids* **1977,** *12* (5), 414-7.

50. Davidoff, F.; Korn, E. D., Lipids of Dictyostelium discoideum: Phospholipid composition and the presence of two new fatty acids: cis, cis-5, 11-octadecadienoic and cis, cis-5, 9-hexadecadienoic acids. *Biochemical and Biophysical Research Communications* **1962,** *9* (1-2), 54-58.

51. Luo, C.; Fontana, D., Unsaturated free fatty acids regulate cAMP relay and cell-cell adhesion duringDictyostelium discoideum aggregation. *Protoplasma* **1996,** *194* (3-4), 140-150.

52. Paquet, V. E.; Lessire, R.; Domergue, F.; Fouillen, L.; Filion, G.; Sedighi, A.; Charette, S. J., Lipid Composition of Multilamellar Bodies Secreted by Dictyostelium discoideum Reveals Their Amoebal Origin. *Eukaryotic Cell* **2013,** *12* (10), 1326-1334.

53. Weeks, G.; Herring, F. G., The lipid composition and membrane fluidity of Dictyostelium discoideum plasma membranes at various stages during differentiation. *Journal of Lipid Research* **1980,** *21* (6), 681-686.

54. Long, B. H.; Coe, E. L., Changes in neutral lipid constituents during differentiation of the cellular slime mold, Dictyostelium discoideum. *Journal of Biological Chemistry* **1974,** *249* (2), 521-529.

APPENDICES

Appendix 1: Theoretically calculated structures and their corresponding coordinates for the 9 OH-PCBs analyzed

4-OH PCB 107

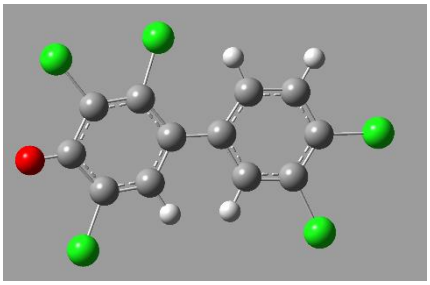

OH-PCB 107

	Atomic Number	X	Y	Z
1	6	0.000000	0.592574	0.000000
2	6	-0.800347	1.778345	0.000000
3	6	1.394955	0.867138	0.000000
4	6	-0.252237	3.052171	0.000000
5	6	1.943536	2.117309	0.000000
6	6	1.181509	3.345766	0.000000
7	6	0.201496	-3.210168	0.000000
8	6	-1.130116	-3.620984	0.000000
9	6	0.533750	-1.865156	0.000000
10	6	-2.104785	-2.631354	0.000000
11	6	-0.431819	-0.824617	0.000000
12	6	-1.771587	-1.285095	0.000000
13	8	1.659303	4.483424	0.000000
14	17	-2.582319	1.720497	0.000000
15	17	-1.260486	4.492865	0.000000
16	17	1.513430	-4.388577	0.000000
17	17	-1.602227	-5.314453	0.000000
18	17	3.707220	2.274453	0.000000
19	1	2.099706	0.049991	0.000000
20	1	1.589847	-1.648114	0.000000
21	1	-3.149921	-2.920929	0.000000
22	1	-2.585704	-0.585280	0.000000

4-OH-PCB 108

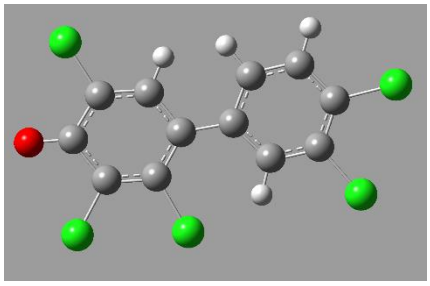

OH-PCB 108

	Atomic Number	X	Y	Z
1	6	0.750925	-0.590967	0.000000
2	6	-2.172529	-0.595747	0.000000
3	6	-0.173278	-1.882298	0.000000
4	6	-2.926414	-1.755266	0.000000
5	6	-0.930091	-3.047417	0.000000
6	6	-2.319861	-3.008359	0.000000
7	6	1.975483	2.172420	0.000000
8	6	1.216341	3.424274	0.000000
9	6	1.413748	0.904777	0.000000
10	6	-0.202539	3.147811	0.000000
11	6	0.000000	0.686050	0.000000
12	6	-0.746771	1.895651	0.000000
13	8	1.726216	4.547773	0.000000
14	17	-1.287176	4.547977	0.000000
15	17	2.578275	-0.443850	0.000000
16	17	3.717456	2.410911	0.000000
17	17	-0.070196	-4.586413	0.000000
18	17	-3.317046	-4.456576	0.000000
19	1	-2.730175	0.328552	0.000000
20	1	0.892887	-2.004897	0.000000
21	1	-4.008906	-1.692640	0.000000
22	1	-1.824866	1.856389	0.000000

3-OH-PCB 118

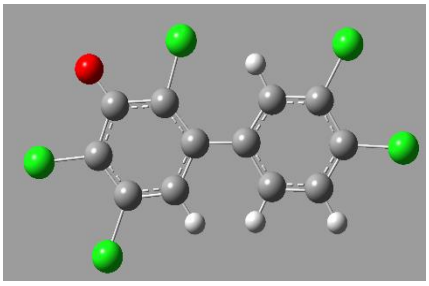

OH-PCB 118

	Atomic Number	X	Y	Z
1	6	-0.540089	-0.831279	0.000000
2	6	-1.933956	-1.067270	0.000000
3	6	0.255594	-1.991304	0.000000
4	6	-2.480025	-2.339955	0.000000
5	6	-0.286925	-3.272565	0.000000
6	6	-1.663069	-3.465980	0.000000
7	6	1.821470	2.361742	0.000000
8	6	0.745404	3.336557	0.000000
9	6	1.346457	0.974979	0.000000
10	6	-0.578124	2.948559	0.000000
11	6	0.000000	0.572256	0.000000
12	6	-0.958907	1.615244	0.000000
13	8	3.019533	2.675494	0.000000
14	17	2.734103	-0.132632	0.000000
15	17	1.221459	5.022591	0.000000
16	17	-1.888097	4.151061	0.000000
17	17	0.820765	-4.640033	0.000000
18	17	-2.396604	-5.062110	0.000000
19	1	-2.635677	-0.247696	0.000000
20	1	1.326988	-1.911079	0.000000
21	1	-3.556479	-2.467310	0.000000
22	1	-2.015708	1.415327	0.000000

4-OH-PCB 130

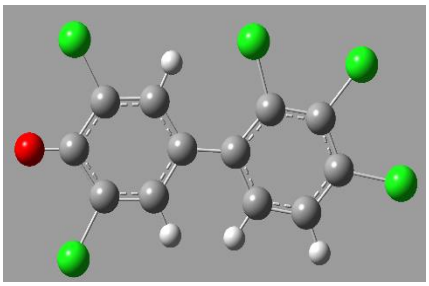

OH-PCB 130

Atomic Number		X	Y	Z
1	6	0.683120	-0.569422	0.000000
2	6	2.107261	-0.628610	0.000000
3	6	0.055352	-1.845114	0.000000
4	6	2.803947	-1.806407	0.000000
5	6	0.765574	-3.017703	0.000000
6	6	2.214823	-3.138847	0.000000
7	6	-1.920085	2.326783	0.000000
8	6	-1.067997	3.427308	0.000000
9	6	-1.403891	1.014719	0.000000
10	6	0.303033	3.201010	0.000000
11	6	0.000000	0.736144	0.000000
12	6	0.796251	1.916730	0.000000
13	17	-2.621766	-0.259276	0.000000
14	17	-3.650544	2.612871	0.000000
15	17	-1.656711	5.083520	0.000000
16	17	4.578037	-1.735014	0.000000
17	17	-0.140992	-4.544009	0.000000
18	8	2.848678	-4.198381	0.000000
19	1	2.709822	0.267646	0.000000
20	1	-1.014261	-1.934603	0.000000
21	1	0.983973	4.044186	0.000000
22	1	1.870303	1.822716	0.000000

3-OH-PCB 138

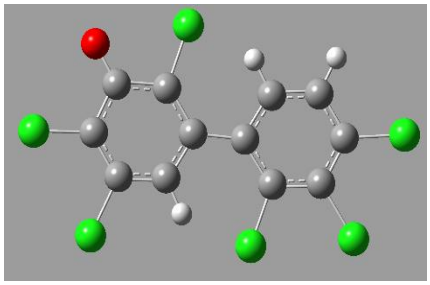

OH-PCB 138

Atomic Number		X	Y	Z
1	6	0.000000	0.763515	0.000000
2	6	1.414136	0.782099	0.000000
3	6	-0.604197	2.052060	0.000000
4	6	2.149482	1.957264	0.000000
5	6	0.113941	3.333263	0.000000
6	6	1.555934	3.197529	0.000000
7	6	-2.908876	-1.733483	0.000000
8	6	-2.324484	-2.984887	0.000000
9	6	-2.118268	-0.602747	0.000000
10	6	-0.934648	-3.066878	0.000000
11	6	-0.707202	-0.581258	0.000000
12	6	-0.136232	-1.898290	0.000000
13	8	-0.452263	4.435815	0.000000
14	1	3.918097	1.785755	0.000000
15	1	2.483644	4.681101	0.000000
16	1	-2.350030	2.433779	0.000000
17	1	-3.355976	-4.405152	0.000000
18	1	1.591602	-2.263412	0.000000
19	1	-0.213003	-4.665716	0.000000
20	1	1.977668	-0.121756	0.000000
21	1	-3.988157	-1.638384	0.000000
22	1	-2.632592	0.336481	0.000000

4-OH-PCB 146

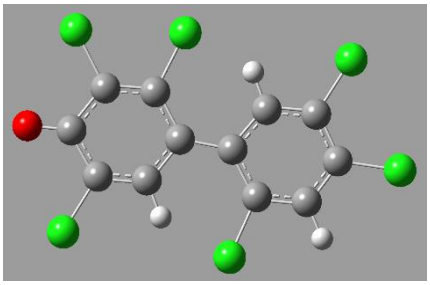

OH-PCB 146

Atomic Number		X	Y	Z
1	6	.000000	0.708580	0.000000
2	6	0.987697	1.732789	0.000000
3	6	.339667	1.253537	0.000000
4	6	0.743918	3.074391	0.000000
5	6	.590285	2.616941	0.000000
6	6	.568491	3.667756	0.000000
7	6	2.040862	-2.610117	0.000000
8	6	1.046065	-3.571931	0.000000
9	6	1.761088	-1.246076	0.000000
10	6	0.266712	-3.117105	0.000000
11	6	0.424145	-0.713967	0.000000
12	6	0.536866	-1.763380	0.000000
13	8	0.814828	4.875392	0.000000
14	17	-2.121500	4.187974	0.000000
15	17	3.226796	3.263019	0.000000
16	17	2.824611	0.258341	0.000000
17	17	-3.293230	-0.327154	0.000000
18	17	-1.479655	-5.271105	0.000000
19	17	1.620191	-4.241465	0.000000
20	1	2.021064	1.455361	0.000000
21	1	3.074500	-2.928098	0.000000
22	1	1.574837	-1.502268	0.000000

4-OH-PCB 172

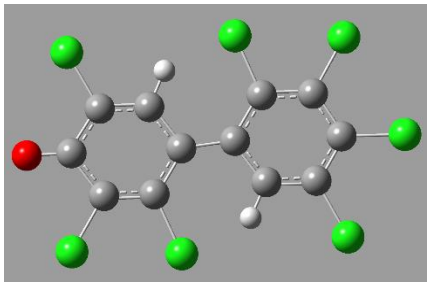

OH-PCB 172

	Atomic Number	X	Y	Z
1	6	0.088304	-0.994989	0.000000
2	6	1.360258	-1.634893	0.000000
3	6	-0.992020	-1.964063	0.000000
4	6	1.582795	-2.979395	0.000000
5	6	-0.767705	-3.331892	0.000000
6	6	0.547683	-3.979306	0.000000
7	6	-1.502419	2.474042	0.000000
8	6	-0.453799	3.387803	0.000000
9	6	-1.271244	1.118777	0.000000
10	6	0.834616	2.848258	0.000000
11	6	0.000000	0.490428	0.000000
12	6	1.072825	1.458106	0.000000
13	8	0.720743	-5.198949	0.000000
14	17	3.254723	-3.563095	0.000000
15	17	-2.731618	-1.545105	0.000000
16	17	-2.087914	-4.494399	0.000000
17	17	-0.746467	5.108018	0.000000
18	17	2.169660	3.987182	0.000000
19	17	2.794469	1.059707	0.000000
20	17	-3.173863	3.021891	0.000000
21	1	2.241224	-1.031022	0.000000
22	1	-2.145747	0.503968	0.000000

3-OH-PCB 180

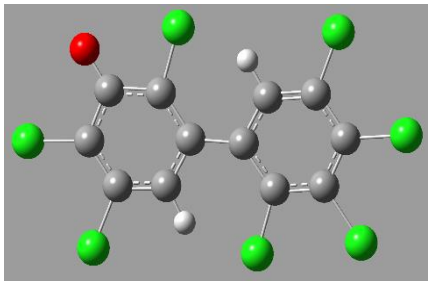

OH-PCB 180

	Atomic Number	X	Y	Z
1	6	0.000000	0.567147	0.000000
2	6	1.129686	1.408718	0.000000
3	6	-1.235544	1.297961	0.000000
4	6	1.105091	2.786678	0.000000
5	6	-1.266394	2.709902	0.000000
6	6	-0.098837	3.477817	0.000000
7	6	1.637825	-3.077763	0.000000
8	6	0.391057	-3.816564	0.000000
9	6	1.466002	-1.619990	0.000000
10	6	-0.818599	-3.162604	0.000000
11	6	0.218987	-0.934478	0.000000
12	6	-0.914951	-1.779565	0.000000
13	8	2.743743	-3.636466	0.000000
14	17	0.513881	-5.560582	0.000000
15	17	-2.349436	-4.063282	0.000000
16	17	3.097831	-0.899066	0.000000
17	17	-2.845436	0.579742	0.000000
18	17	-2.790401	3.576302	0.000000
19	17	-0.138497	5.220604	0.000000
20	17	2.639540	3.639031	0.000000
21	1	2.099537	0.952534	0.000000
22	1	-1.902603	-1.381077	0.000000

4-OH-PCB 187

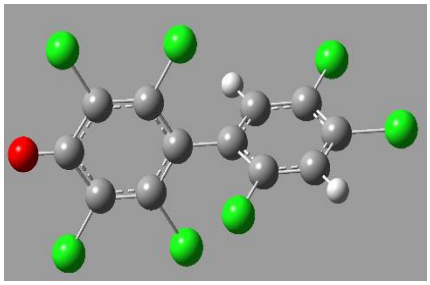

OH-PCB 180

Atomic Number		X	Y	Z
1	6	0.000000	0.567147	0.000000
2	6	1.129686	1.408718	0.000000
3	6	-1.235544	1.297961	0.000000
4	6	1.105091	2.786678	0.000000
5	6	-1.266394	2.709902	0.000000
6	6	-0.098837	3.477817	0.000000
7	6	1.637825	-3.077763	0.000000
8	6	0.391057	-3.816564	0.000000
9	6	1.466002	-1.619990	0.000000
10	6	-0.818599	-3.162604	0.000000
11	6	0.218987	-0.934478	0.000000
12	6	-0.914951	-1.779565	0.000000
13	8	2.743743	-3.636466	0.000000
14	17	0.513881	-5.560582	0.000000
15	17	-2.349436	-4.063282	0.000000
16	17	3.097831	-0.899066	0.000000
17	17	-2.845436	0.579742	0.000000
18	17	-2.790401	3.576302	0.000000
19	17	-0.138497	5.220604	0.000000
20	17	2.639540	3.639031	0.000000
21	1	2.099537	0.952534	0.000000
22	1	-1.902603	-1.381077	0.000000

Appendix 2: Typical response curves for LC-TOF MS as a function of PCB concentration in human blood plasma. Note the high signal from the 0 ppt sample.

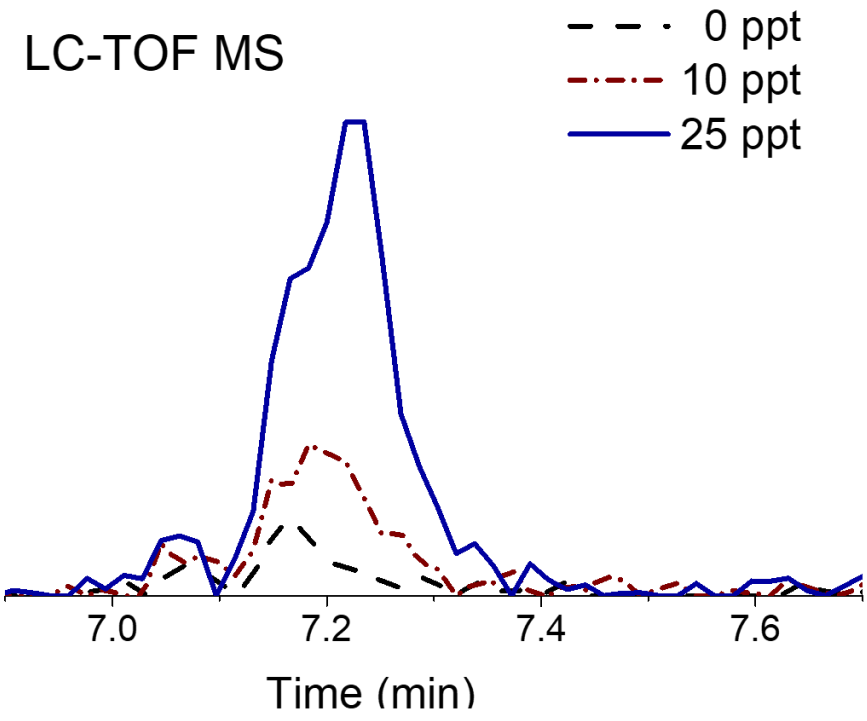

Appendix 3: Scheme of TIMS cell

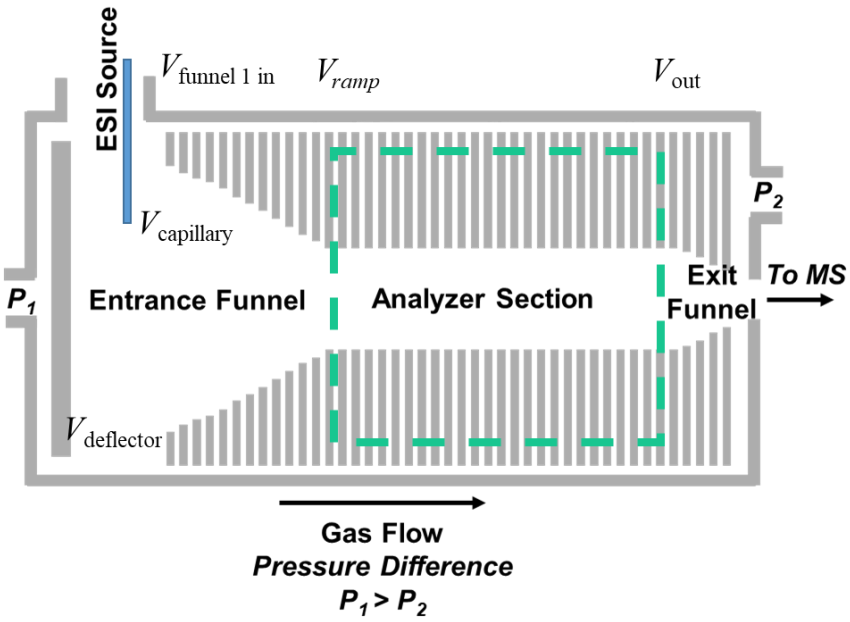

Appendix 4: Matrix factor across urine samples from ten donors spiked at 400 and 75 ng/mL

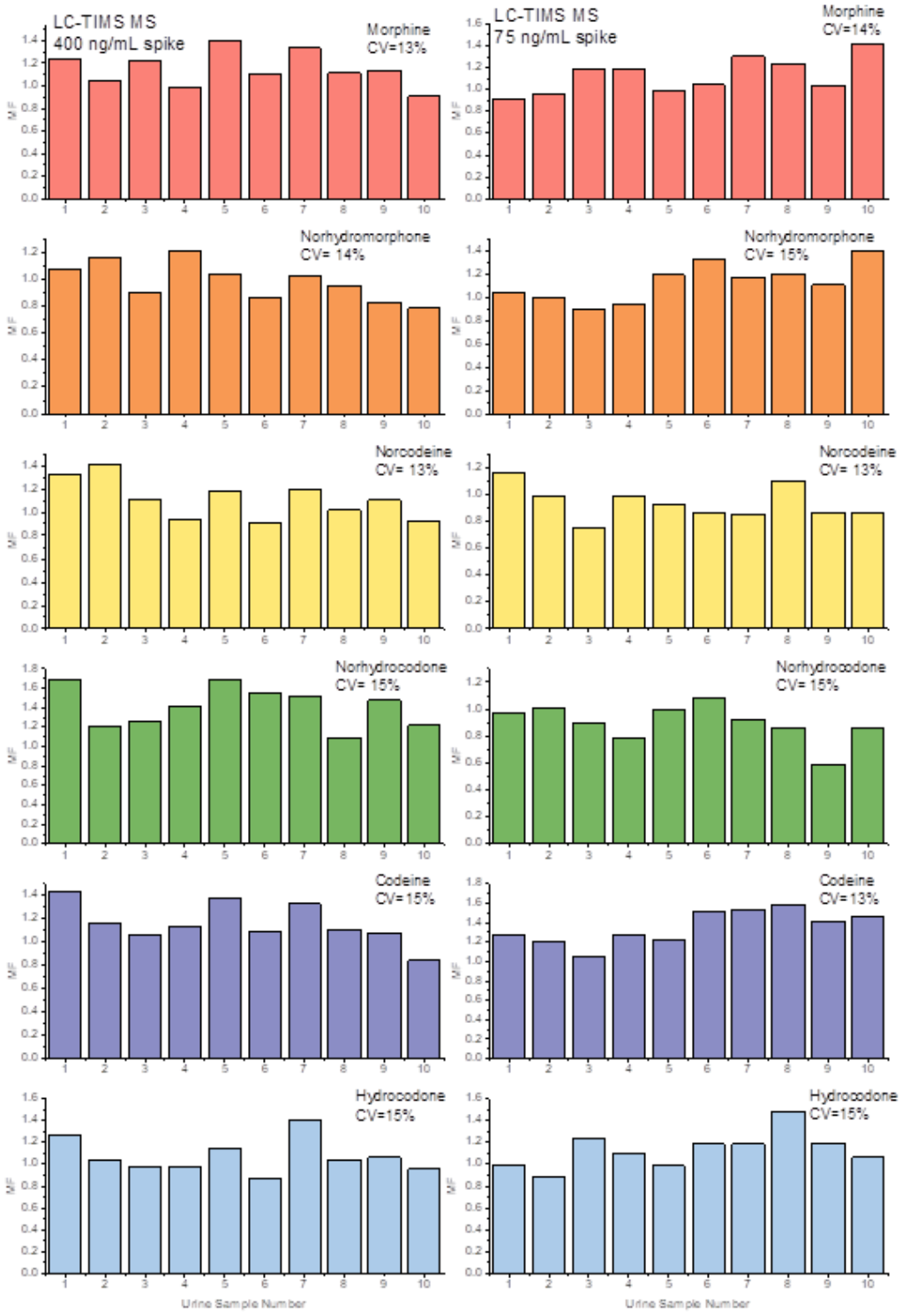

Appendix 5: Candidate structures from theoretical calculations of opioids and metabolites

6-Acetylmorphine

Atomic No.	X	Y	Z
12	0.556936	-0.420567	0.462807
12	0.697506	1.053772	0.202148
12	-0.973818	-0.571201	0.726927
12	1.069058	-1.097146	-0.838619
12	1.342192	-0.935672	1.701748
12	-0.498364	1.707428	0.459029
12	1.763932	1.646780	-0.469324
12	-1.676812	-1.379672	-0.376365
16	-1.521340	0.827063	0.841610
12	2.590360	-0.803258	-0.911017
12	0.604671	-2.559567	-0.920872
12	2.861757	-0.847889	1.538528
12	-0.626288	3.072197	0.208004
12	2.858515	0.753161	-1.045866
12	1.647321	3.027531	-0.719417
12	-0.882651	-2.621309	-0.688098
16	-2.994081	-1.832822	0.093607
14	3.267944	-1.427134	0.247384
12	0.485417	3.725847	-0.353663
16	-1.841068	3.691342	0.478254
12	-4.188879	-1.134155	-0.096101
12	4.715103	-1.600239	0.102297
12	-4.161563	0.149306	-0.888142
16	-5.204731	-1.618829	0.395111
1	-1.187405	-1.048115	1.685055
1	0.609444	-0.565191	-1.684995
1	-1.803559	-0.736563	-1.261096
1	3.002372	-1.288704	-1.804040
1	1.154013	-3.174647	-0.191187
1	1.028174	-0.363508	2.583542
1	1.061157	-1.982413	1.873962
1	0.861579	-2.983416	-1.906961
1	3.195679	0.202766	1.646477
1	3.351200	-1.417215	2.337259
1	2.964439	0.994461	-2.112650
1	3.835538	0.977020	-0.595212
1	2.443704	3.560794	-1.230010
1	-1.427372	-3.557422	-0.738567
1	0.416507	4.791143	-0.560453
1	-1.815042	4.640323	0.250463
1	5.288096	-0.652457	0.116218
1	5.087533	-2.223780	0.922052
1	4.930812	-2.113306	-0.840544
1	-3.517466	0.888864	-0.402391
1	-3.789811	-0.013787	-1.906727
1	-5.181796	0.528985	-0.944549

Morphine

Atomic No.	X	Y	Z
12	-0.38855200	0.35818300	0.52128300
12	0.76103500	-0.55427500	0.21567100
12	-1.23305700	0.39411100	-0.78797100
12	0.31342700	1.70175600	0.87345200
12	-1.25876600	-0.08805600	1.72747300
12	1.96056800	0.07519200	0.50397400
12	0.67120600	-1.72565600	-0.53357600
12	-1.80654600	-1.02329000	-0.99158900
12	-2.07394800	1.65555700	-0.83403500
16	1.78165800	1.39819300	0.94084300
12	0.03178900	2.80120700	-0.17151000
12	-1.91306200	-1.44790300	1.52558800
12	3.17350400	-0.55805600	0.22581700
12	-0.66655700	-2.08544900	-1.18289900
12	1.88533200	-2.37479700	-0.82176000
14	-2.69840900	-1.48332500	0.20586700
12	-1.44739200	2.80578200	-0.52765500
16	0.76279700	2.49654900	-1.40027800
12	3.10389700	-1.81388900	-0.40828700
16	4.34414300	0.09654200	0.54165000
12	-4.02380700	-0.75526800	0.29978000
1	0.03735600	2.05538000	1.86939400
1	-2.48231200	-1.05819300	-1.85235900
1	0.34583300	3.77569400	0.21635100
1	-2.91506700	-2.46894900	0.01792000
1	-0.51004300	0.50786900	-1.60747900
1	-0.62829800	-0.15615500	2.62157200
1	-2.01138000	0.68384700	1.93190900
1	-3.10385300	1.64971000	-1.18073700
1	-1.15995800	-2.23632600	1.45942100
1	-2.61669600	-1.69678500	2.32409000
1	-0.50532000	-2.17716800	-2.26462400
1	-1.03082900	-3.07697600	-0.86775000
1	1.89971700	-3.29593400	-1.39562500
1	-1.95704600	3.76111100	-0.58745200
1	1.72419100	2.50876700	-1.20366200
1	4.02950100	-2.33260200	-0.64066200
1	5.13945700	-0.41339900	0.29418300
1	-4.52610500	-0.80965900	-0.66708200
1	-4.63380900	-1.24176800	1.06268100
1	-3.84969200	0.28365100	0.56859100

Naloxone

Atomic No.	X	Y	Z
12	-0.389246	0.691294	0.661080
12	-1.193475	-0.609391	0.242226
12	0.742784	0.701494	-0.375141
12	-1.232260	1.932523	0.589084
12	0.380309	0.578308	2.091895
12	-2.583029	-0.508536	0.530478
12	-0.657303	-1.719962	-0.505908
12	1.351691	-0.675228	0.057094
12	0.229199	0.895765	-1.811543
16	1.704422	1.792915	-0.131545
16	-3.075335	0.571180	1.087378
12	-1.320018	2.681918	-0.615147
12	1.960670	0.449352	2.102667
12	-3.401170	-1.626347	0.146059
12	0.876018	-1.805348	-0.851273
12	-1.506473	-2.756456	-0.889062
14	2.586023	-0.451335	0.924567
12	-0.642749	2.181881	-1.908923
16	-1.906284	3.817066	-0.669502
12	-2.873062	-2.704225	-0.547163
16	-4.749176	-1.537792	0.491693
12	3.885391	0.087159	0.321512
12	4.457055	-0.901355	-0.654010
12	5.601399	-1.566176	-0.452201
1	-1.599991	2.400039	1.490988
1	0.755831	-0.997207	0.901319
1	2.818258	-1.364174	1.331940
1	0.180387	1.494495	2.659302
1	-0.061817	-0.245659	2.661351
1	1.090738	0.975507	-2.485893
1	-0.366257	0.041514	-2.127655
1	1.193944	2.630305	-0.101319
1	2.429065	1.419733	1.981785
1	2.297025	-0.026103	3.029566
1	1.269619	-2.784201	-0.549735
1	1.087461	-1.662515	-1.915674
1	-1.120531	-3.607368	-1.442473
1	-0.050778	3.025197	-2.287571
1	-1.434917	2.024218	-2.650623
1	-3.527725	-3.522690	-0.841863
1	-5.240131	-2.313653	0.157310
1	3.614675	1.036610	-0.139672
1	4.567656	0.260254	1.160203
1	3.897921	-1.044926	-1.576825
1	5.998477	-2.255627	-1.190024
1	6.195523	-1.431369	0.449056

Hydromorphone

Atomic No.	X	Y	Z
12	-0.319932	0.463127	0.539257
12	0.658444	-0.631827	0.206911
12	-1.174343	0.625329	-0.745633
12	0.645454	1.666436	0.810828
12	-1.211046	0.208305	1.782581
12	1.959752	-0.211515	0.488939
12	0.384590	-1.736144	-0.579967
12	-1.994219	-0.685395	-0.889230
12	-1.926267	1.966626	-0.750795
16	2.010194	1.077746	0.951245
12	0.546475	2.668057	-0.350869
12	-2.203656	-0.949785	1.577636
12	3.070692	-1.027839	0.169442
12	-1.026925	-1.950721	-1.091754
12	1.501811	-2.541127	-0.946521
14	-2.866457	-0.858923	0.275519
12	-0.886023	3.137083	-0.619728
16	1.518231	3.034450	-1.009058
12	2.798902	-2.215195	-0.539170
16	4.305874	-0.585488	0.521039
12	-4.137569	-1.555928	0.102674
1	-0.481584	0.643384	-1.599695
1	0.448622	2.180263	1.755987
1	-0.580015	-0.010581	2.651290
1	-1.770018	1.123857	2.009670
1	-2.640440	-0.622118	-1.769370
1	-2.484352	2.081946	-1.686036
1	-2.660325	2.002723	0.060265
1	-1.667456	-1.912796	1.662518
1	-2.968165	-0.940401	2.359213
1	-0.986270	-2.200772	-2.158708
1	-1.504219	-2.808738	-0.599660
1	1.351779	-3.426649	-1.555241
1	-0.847824	3.738253	-1.531353
1	-1.177636	3.812928	0.196386
1	3.624606	-2.861041	-0.820235
1	5.038189	-1.163054	0.224565
1	-4.638344	-1.200010	-0.800846
1	-4.000149	-2.648438	0.014420
1	-4.782443	-1.366874	0.964798
1	-3.849692	0.283651	0.5685910

Norcodeine

Atomic No.	X	Y	Z
12	0.917656	0.131429	0.451603
12	-0.371432	-0.590365	0.173096
12	1.793759	-0.127369	-0.808702
12	0.444485	1.602538	0.613160
12	1.647569	-0.323700	1.749473
12	-1.452845	0.259422	0.350436
12	-0.467682	-1.835215	-0.446798
12	2.131093	-1.641479	-0.792297
12	2.945352	0.888644	-0.900654
16	-1.062540	1.563203	0.690720
12	0.914951	2.494623	-0.543504
12	2.155196	-1.766939	1.679144
12	-2.752247	-0.183292	0.083612
12	0.810293	-2.506259	-0.947379
12	-1.770043	-2.286965	-0.723700
14	2.903046	-1.947273	0.425736
12	2.386172	2.283996	-0.761083
16	0.678764	3.897254	-0.249324
12	-2.889045	-1.487709	-0.428864
16	-3.794743	0.707069	0.306889
12	-5.145543	0.275414	0.003696
1	1.152764	0.037202	-1.686816
1	0.773349	2.051949	1.552515
1	2.781928	-1.874630	-1.643395
1	0.333408	2.210346	-1.442254
1	2.499841	0.347263	1.915262
1	0.964011	-0.205801	2.599553
1	3.472539	0.773033	-1.863782
1	2.828260	-1.967477	2.519933
1	1.299733	-2.461351	1.774957
1	0.980399	-3.472724	-0.450739
1	0.673238	-2.738282	-2.013220
1	-1.925706	-3.250271	-1.201070
1	3.016876	3.162746	-0.840822
1	-0.279109	4.023149	-0.087195
1	-3.876788	-1.871737	-0.654578
1	-5.434049	-0.590469	0.611920
1	-5.777926	1.126540	0.253647
1	-5.257782	0.030019	-1.059484
1	3.392579	-2.835734	0.371968
1	3.703125	0.676283	-0.130266

Norhydrocodone

Atomic No.	X	Y	Z
12	0.909031	0.203892	0.532174
12	-0.343040	-0.533114	0.144504
12	1.840470	0.112804	-0.702450
12	0.354899	1.640346	0.800250
12	1.584628	-0.362550	1.812854
12	-1.455618	0.238371	0.427775
12	-0.383766	-1.707383	-0.605749
12	2.180510	-1.380859	-0.899823
12	2.958273	1.169937	-0.635935
16	-1.112212	1.497823	0.945341
12	0.771110	2.574615	-0.335960
12	2.055216	-1.802678	1.640040
12	-2.739331	-0.225199	0.111158
12	0.922157	-2.267637	-1.169438
12	-1.663090	-2.178242	-0.943980
14	2.913805	-1.902140	0.371956
12	2.279938	2.585611	-0.635818
16	-0.023934	3.270638	-0.968176
12	-2.811666	-1.464888	-0.558939
16	-3.804219	0.568011	0.450090
12	-5.152661	0.156267	0.070535
1	1.231374	0.364656	-1.582700
1	0.716685	2.055694	1.747412
1	2.426060	0.276804	2.113436
1	0.862316	-0.336497	2.636207
1	2.910194	-1.517132	-1.704992
1	3.578192	1.049221	0.263123
1	3.632053	1.089790	-1.496886
1	2.667647	-2.151051	2.475408
1	1.215600	-2.485995	1.500468
1	1.119033	-3.296421	-0.827516
1	0.825473	-2.348228	-2.259906
1	-1.782843	-3.083686	-1.530747
1	2.770244	3.240899	0.096930
1	2.391649	3.068882	-1.610223
1	-3.781383	-1.859426	-0.835471
1	-5.424139	-0.787615	0.555161
1	-5.796627	0.956497	0.429041
1	-5.240654	0.063689	-1.017052
1	3.190044	-2.878151	0.217543
1	3.773006	-1.354484	0.501833

Codeine

Atomic No.	X	Y	Z
12	0.80233100	0.53600500	-0.56175200
12	-0.21800200	-0.49119600	-0.11323700
12	1.80292700	0.72881700	0.61170200
12	-0.11213700	1.75491700	-0.88633600
12	1.58141700	0.07155900	-1.82286300
12	-1.48827000	-0.09624700	-0.48542000
12	0.01584800	-1.60433000	0.69027800
12	2.40771900	-0.66418500	0.93018300
12	1.10614300	1.35523200	1.80495900
16	-1.49194700	1.17697600	-1.07087200
12	-0.17846800	2.82803200	0.23596700
12	2.32787800	-1.23830600	-1.58275800
12	-2.61048500	-0.87775500	-0.18903100
12	1.38025000	-1.74996500	1.34465900
12	-1.09600800	-2.40567400	0.99798300
14	3.20807400	-1.16860900	-0.31791400
12	0.16632100	2.29057000	1.61016100
16	-1.44865900	3.50667600	0.21456900
12	-2.37790700	-2.06229100	0.53808900
16	-3.83406800	-0.40746300	-0.59987400
12	-5.03435100	-1.17766200	-0.28648200
12	4.50007100	-0.41019800	-0.55205400
1	0.11637700	2.22465500	-1.84350500
1	3.17009400	-0.57420300	1.71141800
1	0.56048500	3.60316100	-0.01296500
1	3.47160400	-2.13542100	-0.09561300
1	2.62166800	1.39347800	0.29285600
1	0.88304100	-0.09586800	-2.65099300
1	2.26833700	0.86519100	-2.14501100
1	1.38873600	1.03788400	2.80552200
1	1.62298400	-2.05563900	-1.41642700
1	2.98939600	-1.50108600	-2.41197400
1	1.25640800	-1.66381900	2.43248500
1	1.81592600	-2.75067000	1.19105900
1	-0.98288800	-3.28668200	1.62221400
1	-0.34104100	2.77160900	2.44043100
1	-2.14586500	2.86740200	-0.05340800
1	-3.21256400	-2.70204800	0.79602600
1	-5.16532600	-1.27396600	0.79652100
1	-5.85310100	-0.59972500	-0.71019400
1	-4.99557100	-2.16762200	-0.75302400
1	5.06862100	-0.38217000	0.37849400
1	5.07261500	-0.92999200	-1.32183300
1	4.27925300	0.60234200	-0.88153900

Hydrocodone

Atomic No.	X	Y	Z
12	-0.68415500	0.35483700	0.49882800
12	0.48600100	-0.49761700	0.09327700
12	-1.62006700	0.40525100	-0.73106500
12	0.02547500	1.70868400	0.82006000
12	-1.42857200	-0.18597800	1.75014300
12	1.66998700	0.11767200	0.45663300
12	0.41453300	-1.62783900	-0.71849200
12	-2.11661600	-1.04243000	-0.97665800
12	-2.55347700	1.63001100	-0.65194200
16	1.45292700	1.37564900	1.04342000
12	-0.18769900	2.69501700	-0.32963300
12	-1.98912500	-1.58597000	1.52988100
12	2.90096600	-0.47592200	0.14946600
12	-0.92973500	-1.99806200	-1.34432200
12	1.64126900	-2.22888000	-1.04620300
14	-2.85856800	-1.64424300	0.25990600
12	-1.65185900	2.90539000	-0.74857000
16	0.73692000	3.28385000	-0.89132500
12	2.85125600	-1.67734600	-0.58954900
16	4.03909700	0.16495500	0.56507300
12	5.34232800	-0.37380300	0.18790500
12	-4.25301200	-1.09156700	0.47547900
1	-0.33298800	2.16080200	1.75106900
1	-2.86551200	-1.07298000	-1.77465300
1	-2.97361700	-2.63965500	0.03657100
1	-0.98158400	0.58607400	-1.60950300
1	-0.72356900	-0.24024500	2.58776000
1	-2.21924700	0.51160800	2.05473600
1	-3.28693600	1.63790200	-1.46642800
1	-3.11940000	1.64873200	0.28629900
1	-1.18001400	-2.30377000	1.37787000
1	-2.61476400	-1.92423900	2.35953700
1	-0.82916300	-1.95912800	-2.43721200
1	-1.21571800	-3.04017700	-1.12658400
1	1.67509800	-3.11064000	-1.67858100
1	-1.61992300	3.28223800	-1.77549000
1	-2.07198100	3.71424300	-0.13512500
1	3.77734800	-2.16812300	-0.86169900
1	5.44916500	-0.40932100	-0.90137300
1	6.06214500	0.32460700	0.60954300
1	5.49313100	-1.37021400	0.61680600
1	-4.79916400	-1.13173400	-0.46782700
1	-4.75760200	-1.70625700	1.22276700
1	-4.19227600	-0.06433300	0.82340300

Appendix 6: Typical TOF-SIMS spectrum of sphingomyelin lipid class in negative mode. Characteristic fragments (*) and molecular ions are denoted.

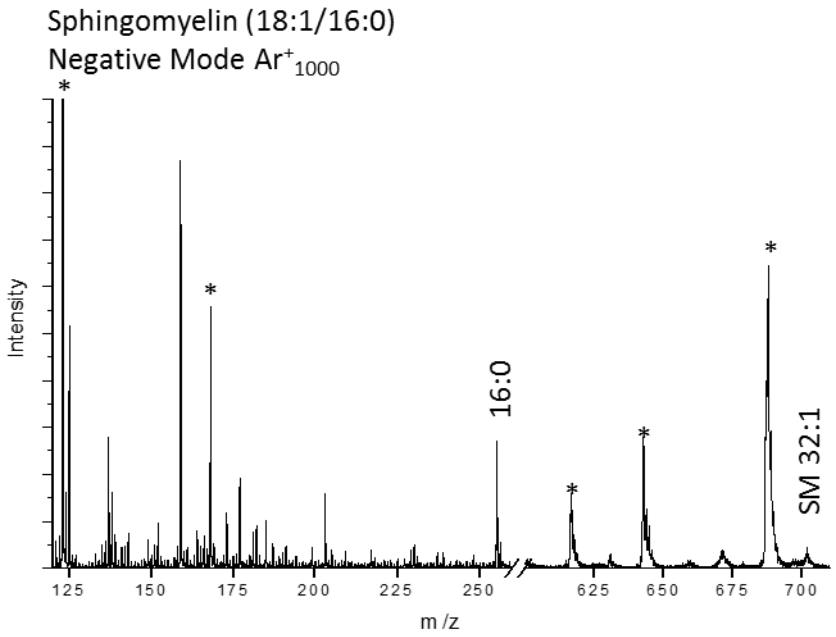

Appendix 7: General TOF-SIMS fragmentation scheme of sulfatide lipid class in negative mode

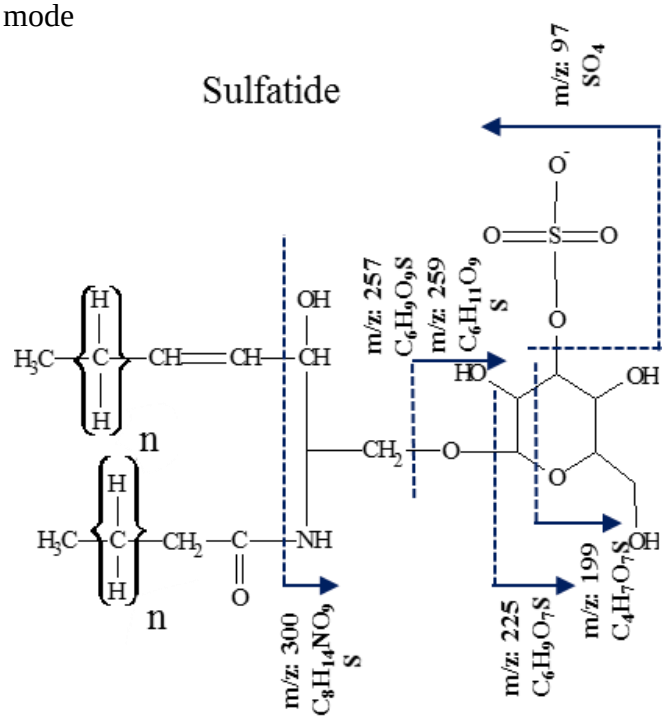

Appendix 8: Negative mode SI yields from TOF-SIMS analysis using various primary ions of familiar lipid standards. Typical fragments and molecular ions are listed for each class

Negative Mode					
Species		**Mix ST $C_{48}H_{96}N_2O_{11}S$ (major component)**			
		Au_3^+	Bi_3^+	Ar_{1000}^+	Au_{400}^+
96.97	HSO_4	2.10E-02	1.31E-03	1.77E-02	6.90E-01
198.98	$C_4H_7SO_7$	3.30E-04	1.56E-05	1.85E-04	6.00E-03
256.99	$C_6H_9SO_9$	9.50E-04	6.27E-06	2.30E-04	1.90E-02
259.03	$C_6H_{11}SO_9$	7.90E-04	6.27E-06	3.90E-04	1.50E-02
261.00	$C_6H_{13}SO_9$	2.40E-03	1.37E-04	4.55E-04	5.60E-02
281.24	C18:1	2.50E-04	1.45E-06	1.84E-05	2.70E-03
283.27	C18:0	4.40E-04	1.82E-06	5.34E-05	3.10E-03
300.04	$C_8H_{14}NSO_9$	1.10E-03	1.24E-05	1.97E-04	2.10E-02
806.5	18:0 Sulfatide	1.80E-04	1.33E-06	1.31E-04	1.10E-02
862.6	22:0 Sulfatide	----	5.07E-07	7.74E-05	8.80E-03
878.7	h22:0 Sulfatide	----	2.95E-07	3.96E-05	6.30E-03
888.6	24:1 Sulfatide	----	9.33E-07	3.98E-04	2.27E-04
890.7	24:0 Sulfatide	3.00E-04	6.60E-07	2.95E-04	3.40E-02
906.7	h24:0 Sulfatide	----	2.51E-07	6.45E-05	1.10E-02
Species		**SM $C_{39}H_{79}N_2O_6P$**			
		Au_3^+	Bi_3^+	Ar_{1000}^+	Au_{400}^+
62.96	PO_2	1.50E-02	3.69E-03	2.38E-03	1.20E-01
78.96	PO_3	9.70E-02	2.22E-02	2.70E-02	4.80E-01
122.99	$C_2H_4PO_4$	9.50E-03	2.02E-03	2.76E-03	5.50E-02
168.04	$C_4H_{11}NPO_4$	3.10E-03	5.48E-04	6.96E-04	2.40E-02
255.23	C16:0	4.50E-05	3.72E-05	2.56E-04	----
616.5	$C_{34}H_{67}NO_6P$	4.10E-04	4.11E-05	1.74E-04	3.80E-03
642.5	$C_{36}H_{69}NO_6P$	7.10E-04	8.97E-05	2.05E-04	6.50E-03
687.5	$C_{38}H_{76}N_2PO_6$	5.40E-04	5.53E-05	6.61E-04	4.50E-02
701.6	$[M-H]^-$	----	6.09E-06	3.03E-05	----
Species		**PG $C_{42}H_{80}O_{10}P$**			
		Au_3^+	Bi_3^+	Ar_{1000}^+	Au_{400}^+
62.96	PO_2	8.80E-03	3.60E-03	1.41E-03	4.70E-01
78.96	PO_3	5.50E-02	1.55E-02	2.55E-02	1.60E+00
96.97	H_2PO_4	7.10E-03	1.20E-03	1.89E-03	2.90E-01
153.01	$C_3H_6PO_5$	6.70E-03	9.62E-04	1.79E-03	1.70E-01
171.02	$C_3H_8PO_6$	3.70E-03	3.46E-04	5.06E-04	8.60E-02

227.05	$C_6H_{12}PO_7$	4.50E-04	8.68E-05	1.33E-04	2.80E-02
281.24	C18:1	2.50E-03	3.53E-04	9.56E-04	1.60E-01
283.26	C18:0	4.70E-03	5.69E-04	1.17E-03	9.50E-02
511.3	$C_{24}H_{48}O_9P$	3.20E-04	7.47E-06	1.79E-05	1.00E-02
775.5	$[M]^-$	8.70E-04	4.32E-06	2.79E-05	4.30E-02
Species		**PC $C_{40}H_{80}NO_8P$**			
		Au_3^+	Bi_3^+	Ar_{1000}^+	Au_{400}^+
62.97	PO_2	1.30E-02	1.98E-03	2.31E-03	3.30E-01
78.96	PO_3	6.80E-02	1.39E-02	3.08E-02	1.10E+00
96.98	H_2PO_4	6.90E-03	1.03E-03	3.32E-03	1.40E-01
123.00	C_2H4PO_4	3.20E-03	3.73E-04	1.96E-03	6.10E-02
224.07	$C_7H_{15}NPO_5$	2.30E-04	2.40E-06	4.77E-05	9.90E-03
255.24	C16:0	7.50E-03	6.11E-04	6.54E-03	9.50E-02
647.5	$C_{35}H_{67}O_8P$	----	1.75E-06	4.39E-05	----
673.5	$C_{37}H_{70}O_8P$	1.60E-04	5.05E-06	3.14E-04	5.80E-03
732.6	$[M-H]^-$	----	7.80E-07	4.57E-05	----
Species		**PE $C_{33}H_{66}NO_8P$**			
		Au_3^+	Bi_3^+	Ar_{1000}^+	Au_{400}^+
62.96	PO_2	1.40E-02	2.77E-03	2.81E-03	3.10E-01
78.96	PO_3	9.30E-02	1.10E-02	2.92E-02	1.00E+00
96.98	H_2PO_4	8.30E-03	3.53E-04	2.40E-03	1.10E-01
122.01	$C_2H_5NPO_3$	4.30E-03	4.20E-05	8.86E-04	1.50E-02
140.02	$C_2H_7NPO_4$	5.40E-03	3.36E-05	7.98E-04	4.20E-02
196.04	$C_5H_{11}NPO_5$	1.20E-03	1.05E-05	1.23E-04	1.10E-02
227.19	C14:0	1.10E-02	7.23E-05	2.60E-03	8.60E-02
634.4	$[M-H]^-$	2.30E-03	1.22E-05	2.57E-04	1.60E-02

Appendix 9: Positive mode SI yields from TOF-SIMS analysis using various primary ions of familiar lipid standards. Typical fragments and molecular ions are listed for each class.

Positive Mode				
Species		**Mix ST $C_{48}H_{96}N_2O_{11}S$ (Major Component)**		
		Bi_3^+	Ar_{1000}^+	Au_{400}^+
96.95	HSO_4	6.10E-06	3.10E-06	6.60E-03
105.00	H_2SO_3Na	1.90E-04	2.80E-05	1.40E-02
142.94	HSO_3NaK	2.60E-05	2.60E-05	4.50E-02
909.7	$[M+H]^+$	7.70E-07	1.20E-06	----
Species		**SM $C_{39}H_{79}N_2O_6P$**		
		Bi_3^+	Ar_{1000}^+	Au_{400}^+

86.10	$C_5H_{12}N$	1.40E-02	9.50E-03	1.60E-01
104.12	$C_5H_{14}NO$	8.20E-03	6.70E-03	6.50E-02
124.98	$C_2H_6PO_4$	1.60E-03	9.50E-04	6.90E-02
146.97	$C_2H_5PO_4Na$	3.10E-04	2.20E-04	2.50E-01
166.02	$C_4H_9NPO_4$	1.80E-03	1.00E-03	3.70E-02
184.07	$C_5H_{15}NPO_4$	1.60E-02	1.80E-02	4.00E-01
206.05	$C_5H_{14}NPO_4Na$	2.30E-05	3.20E-06	1.40E-01
703.6	$[M+H]^+$	5.80E-07	8.10E-07	----
725.5	$[M+Na]^+$	1.90E-06	5.40E-06	1.60E-01
Species		**PG $C_{42}H_{80}O_{10}P$**		
		Bi_3^+	Ar_{1000}^+	Au_{400}^+
125.00	$C_2H_6PO_4$	1.20E-03	8.90E-04	7.90E-02
146.98	$C_2H_5PO_4Na$	3.30E-05	3.50E-05	4.40E-03
798.5	$[M+Na]^+$	1.30E-06	2.50E-06	6.30E-03
821.5	$[M+2Na]^+$	6.40E-07	1.10E-06	5.40E-02
Species		**PC $C_{40}H_{80}NO_8P$**		
		Bi_3^+	Ar_{1000}^+	Au_{400}^+
86.10	$C_5H_{12}N$	7.60E-03	1.20E-02	2.50E-01
104.12	$C_5H_{14}NO$	4.00E-03	5.10E-03	4.20E-02
124.99	$C_2H_6PO_4$	9.00E-04	1.30E-03	6.40E-02
146.98	$C_2H_5PO_4Na$	9.10E-05	2.50E-05	1.20E-01
184.06	$C_5H_{15}NPO_4$	5.60E-03	9.30E-03	1.90E-01
206.05	$C_5H_{14}NPO_4Na$	2.30E-05	3.20E-06	1.70E-02
734.6	$[M+H]^+$	3.70E-06	1.10E-05	1.30E-01
Species		**PE $C_{33}H_{66}NO_8P$**		
		Bi_3^+	Ar_{1000}^+	Au_{400}^+
125.00	$C_2H_6PO_4$	7.90E-05	1.40E-04	3.40E-02
141.02	$C_2H_8NPO_4$	2.40E-05	4.60E-05	----
146.99	$C_2H_5PO_4Na$	2.20E-05	1.40E-05	3.10E-02
495.4	$C_{31}H_{59}O_4$	5.90E-06	6.70E-05	7.60E-02
636.5	$[M+H]^+$	1.10E-06	5.10E-06	3.90E-02

Appendix 10: Ratios of of molecular ion to fragment ion secondary ion yields for a) Negative mode Au_{400}^{4+} impact energy changes b) negative mode Ar_n cluster size experiments and c) positive mode Au_{400}^{4+} impact energy experiments.

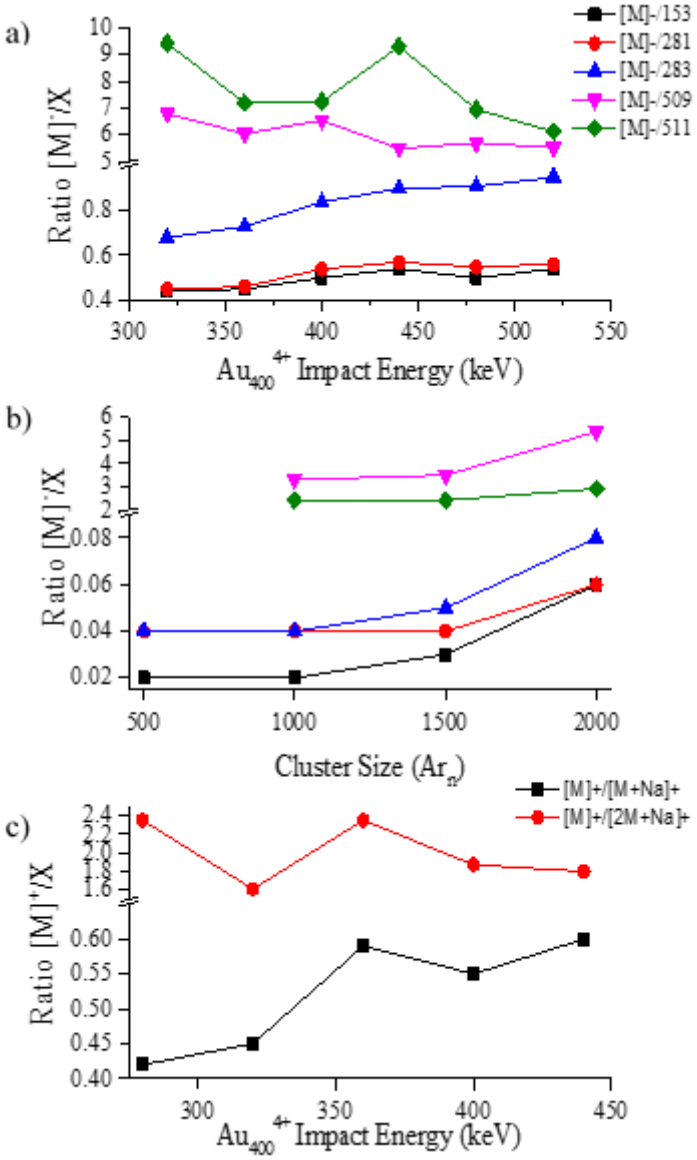

Appendix 11: Ratio of molecular ion to fragment ion secondary ion yield for negative mode Au_{400}^{4+} impact energy changes.

Impact Energy (keV)	M/153	M/281	M/283	M/509	M/511
320	0.44	0.45	0.68	6.79	9.42
360	0.45	0.46	0.73	6.04	7.19
400	0.5	0.54	0.84	6.54	7.24
440	0.54	0.57	0.9	5.49	9.3
480	0.5	0.55	0.91	5.7	6.95
520	0.54	0.56	0.95	5.52	6.12

Appendix 12:**.** Ratio of molecular ion to fragment ion secondary ion yield for negative mode Ar_n experiments.

Ar_n Cluster Size	M/153	M/281	M/283	M/509	M/511
500	0.02	0.04	0.04	NA	NA
1000	0.02	0.04	0.04	3.30	2.41
1500	0.03	0.04	0.05	3.50	2.41
2000	0.06	0.06	0.08	5.37	2.91

Appendix 13:**.** Ratio of molecular ion to fragment ion secondary ion yield for positive mode Au_{400}^{4+} impact energy.

Impact Energy (keV)	M/M+Na	M/2M+Na
280	0.42	2.35
320	0.45	1.61
360	0.59	2.35
400	0.55	1.87
440	0.60	1.80

Appendix 14: Typical fragmentation of PI lipid in negative mode

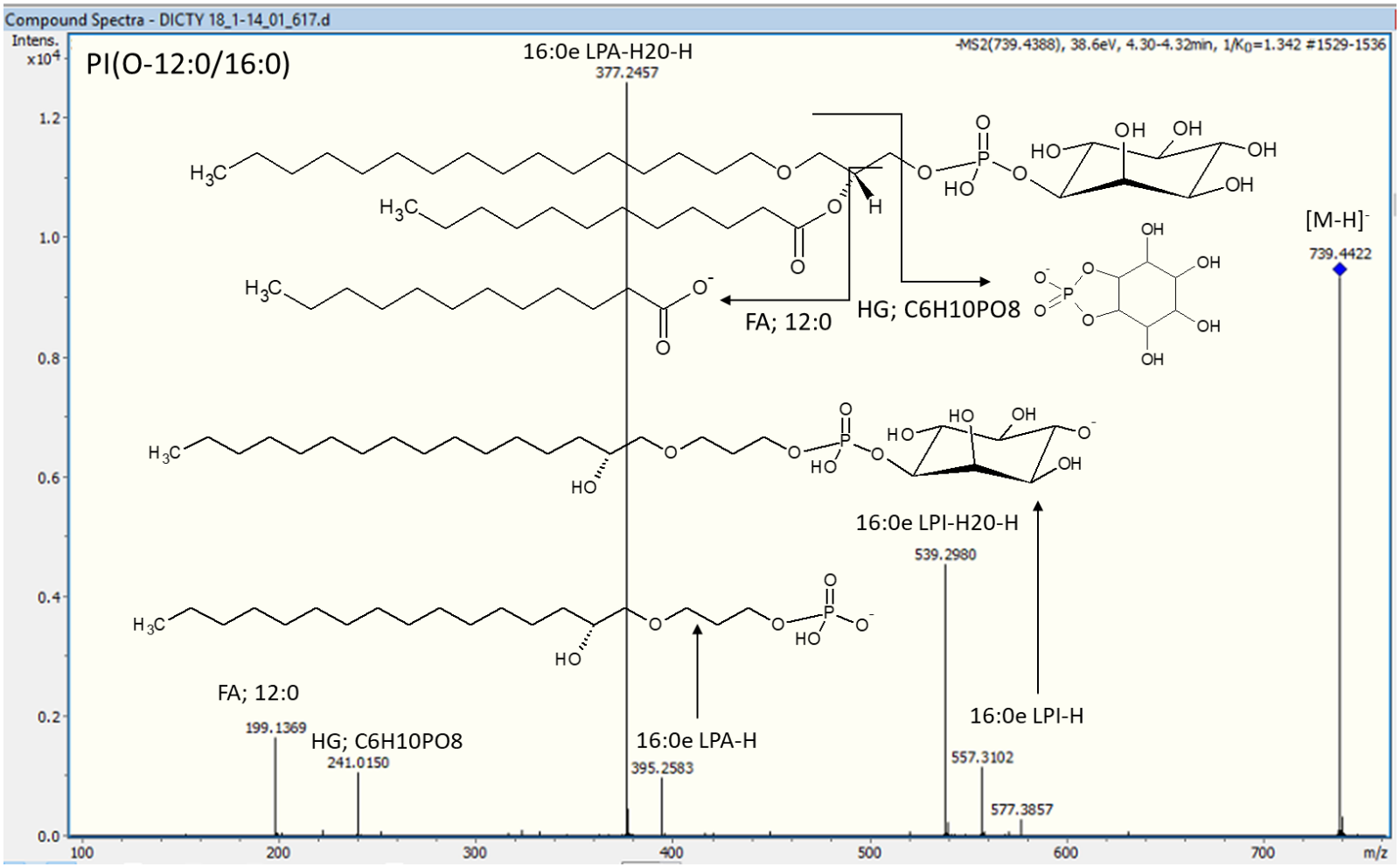

Appendix 15: Typical fragmentation of PE lipid in negative mode

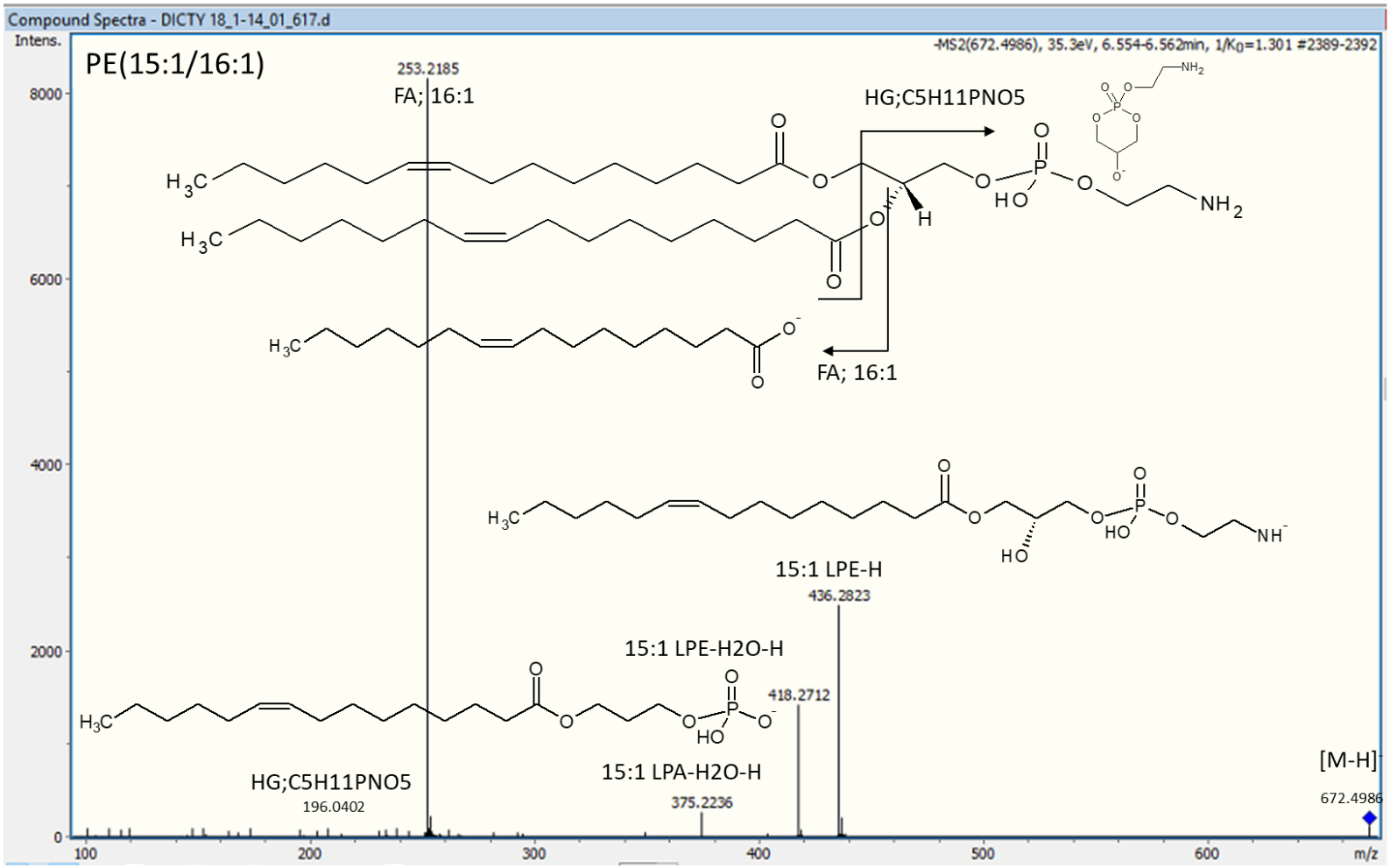

Appendix 16: Typical fragmentation of PG lipid in negative mode

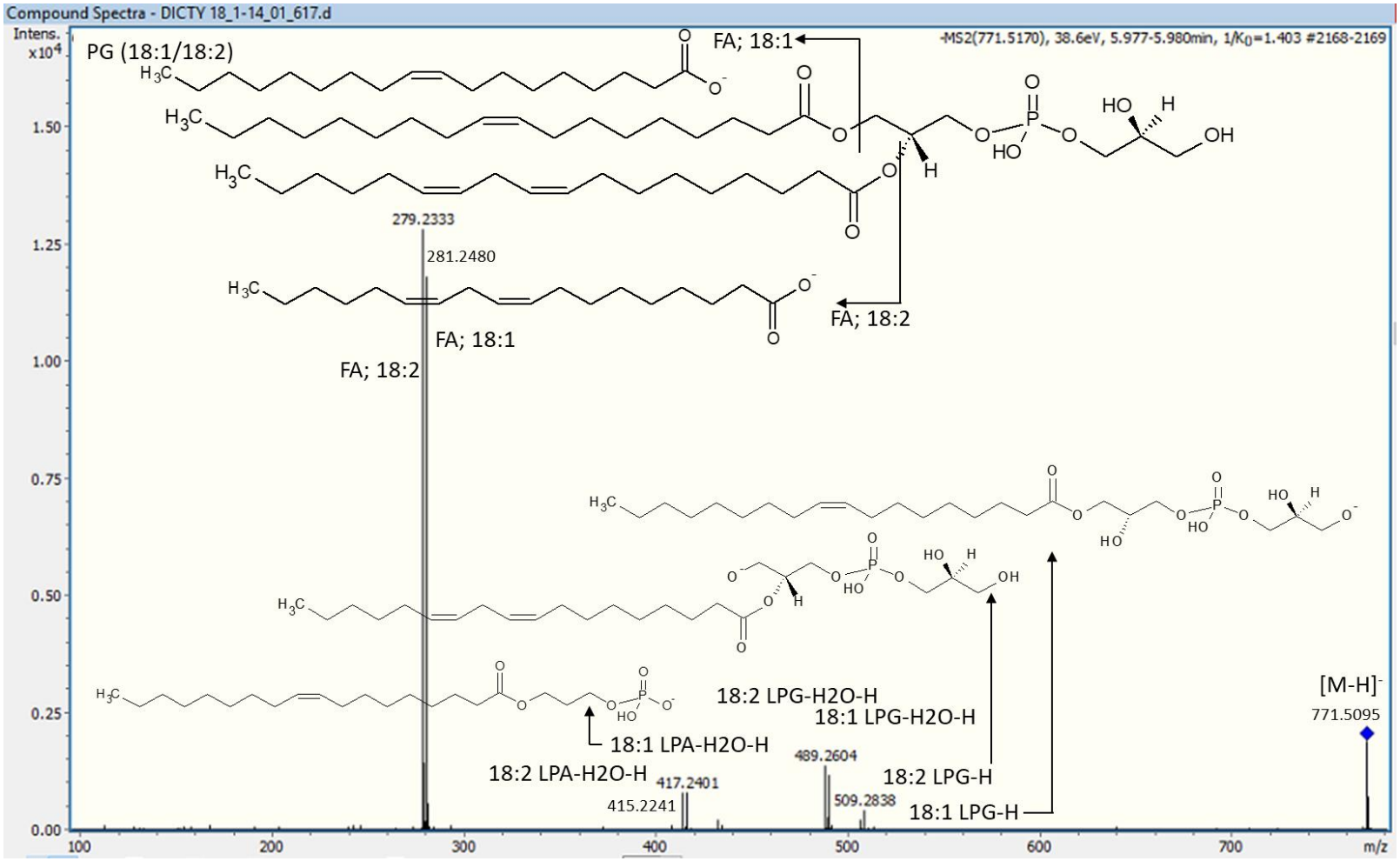

Appendix 17: Typical fragmentation of PS lipid in negative mode

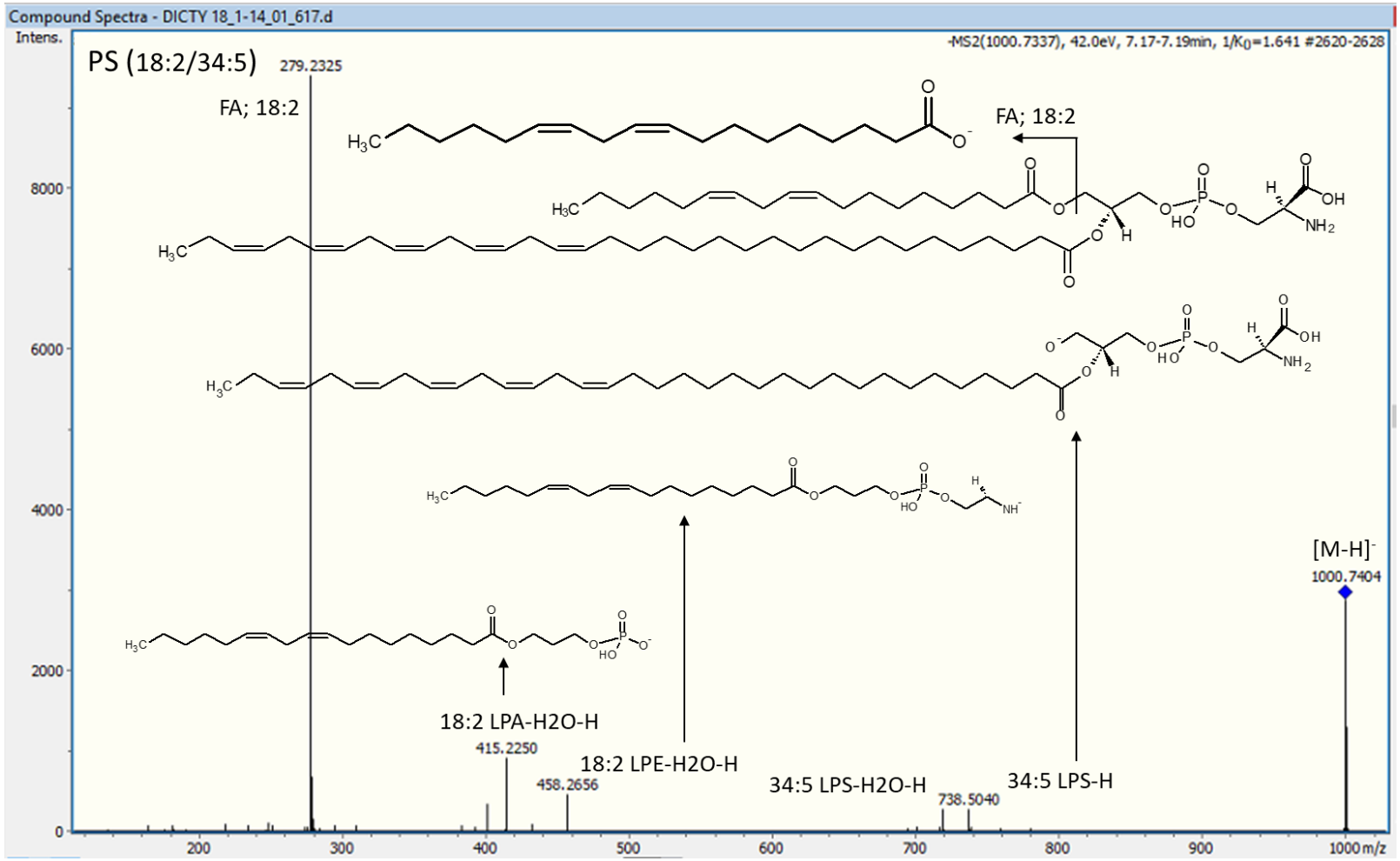

Appendix 18: Lipid Analytes and SPLASH Mix analyzed via LC-TIMS-TOF MS with PASEF in negative mode

Appendix 18: Identification fragments are typical product ions observed for each lipid class

m/z	RT (min)	CCS (Å^2)	Subclass	Lipid ID	Identification Fragments
485.3379	3.94 4.06	217.6	PE PE	LPE 18:1 d7	196 (HG;C5H11PNO5), 288 (FA; 18:1 d7), 468.24 (18:1 d7 LPE-H2O-H)
535.339	4.97	245.2	PA PA	PA 12:0/12:0	153 (HG; C3H6PO5), 199 (FA; 12:0), 353 (12:0 LPA-H)
634.4444	5.84	253.3	PE	PE 14:0/14:0	196 (HG;C5H11PNO5), 227 (FA; 16:0), 424 (14:0 LPE-H)
709.5519	6.27	267.1	PE	PE 15:0/18:1 d7	124 (HG), 140 (HG), 196 (HG;C5H11PNO5), 241.2 (FA; 15:0), 288.29 (FA; 18:1 d7), 420(15:0 LPE-H2O-H), 438(15:0 LPE-H), 468(18:1 d7 LPE-H2O-H), 485(18:1 d7 LPE-H)
716.5232	6.41	270.0	PE	PE 16:0/18:1	196 (HG;C5H11PNO5), 255 (FA; 16:0), 281 (FA; 18:1), 452 (16:0 LPE-H)
721.5026	6.04	272.4	PG	PG 16:0/16:0	153(HG; C3H6PO5), 255 (FA; 16:0), 391 (16:0 LPA-H2O-H), 409(16:0 LPA-H) 465(16:0 LPG-H2O-H), 483 (16:0 LPG-H)
740.5459	5.93	274.5	PG	PG 15:0/18:1 d7	227 (HG;C6H12PO7), 241.2 (FA; 15:0), 288 (FA; 18:1 d7), 451 (15:0 LPG-H2O-H), 469 (15:0 LPG-H)
753.5417	5.98	277.7	PS	PS 15:0/18:1 d7	241 (FA; 15:0), 288 (FA; 18:1 d7), 377(LPA 15:0-H2O-H), 395 (LPA 15:0-H), 424 (LPA 18:1 d7-H2O-H), 666 (PA 15:0/18:1 d7)
775.5491	6.29	283.1	PG	PG 18:0/18:1	153 (HG; C3H6PO5), 227(HG; C6H12PO7), 281 (FA; 18:1), 283 (FA; 18:0), 419 (18:0 LPA-H2O-H), 437(18:0 LPA-H), 493(18:0 LPG-H2O-H), 511 (18:0 LPG-H)
828.5608	5.85	288.6	PI	PI 15:0/18:1 d7	153 (HG; C3H6PO5), 241.1 (HG; C6H10PO8) , 241.2 (FA; 15:0), 288 (FA; 18:1 d7), 377 (15:0 LPA-H2O-H), 424 (18:1 d7 LPA-H20-H), 539 (15:0 LPI-H2O-H), 557.27 (15:0 LPI-H)

Appendix 19: Lipid profile of Dictyostelium discoideum cells from LC-TIMS-MS/MS negative mode analyses

m/z	RT	1/K0	CCS (A^2)	Lipid ID	Identification Fragments
452.2764	4.43	1.048	217.990	LPE(16:0)	140.02 (HG; C2H7NPO4), 255.23 (FA; 16:0)
464.3141	4.39	1.054	219.073	LPE (P-18:0)	140.02 (HG; C2H7NPO4), 403.26 (18:0p LPA-H2O-H), 421.27 (18:0p LPA-H)
466.3286	4.89	1.064	221.124	LPE(O-18:0)	140.02 (HG; C2H7NPO4), 405.28 (18:0e LPA-H2O-H), 423.29 (18:0e LPA-H)
476.2778	3.58	1.059	219.954	LPE (18:2)	196.04(HG; C5H11O5PN), 279.23 (FA; 18:2)
478.2920	3.95	1.056	219.306	LPE (18:1)	196.04(HG; C5H11O5PN), 281.25 (FA; 18:1)
494.2877	2.49	1.090	226.164	LPE (O-20:0)	140.02 (HG; C2H7NPO4), 196.04(HG; C5H11O5PN), 433.27 (20:0e LPA-H20-H), 451 (20:0e LPA-H)
506.3234	4.43	1.101	228.301	LPE (20:1)	196.04(HG; C5H11O5PN), 309.28 (FA:20:1)
507.2697	3.39	1.092	226.424	LPG (18:2)	152.99 (HG; C3H6PO5), 279.23 (FA; 18:2), 433.28 (18:2 LPA-H)
522.2816	3.46	1.113	230.604	LPS (18:1)	153.00 (HG; C3H6PO5), 281.25 (FA: 18:1), 435.18 (18:1 LPA-H)
557.3086	3.70	1.149	237.682	LPI(O-16:0)	241.01 (HG; C6H10PO8), 377 (16:0e LPA-H20-H)
567.3645	5.08	1.181	244.198	LPG (22:0)	153.00 (HG; C3H6PO5), 227.03 (HG; C6H12PO7), 339.33 (FA; 22:0)

571.3232	3.99	1.165	240.851	LPI(16:1)	241.01 (HG; C6H10PO8), 391.26 (16:0 LPA-H2O-H), 409.27 (16:0 LPA-H)
595.2859	3.10	1.179	243.516	LPI (18:2)	223.00 (HG; C6H8PO7), 241.01 (HG; C6H10PO8), 279.23 (FA; 18:2)
597.3025	3.44	1.181	243.910	LPI (18:1)	153.00 (HG; C3H6PO5), 223.00 (HG; C6H8PO7), 241.01 (HG; C6H10PO8), 281.25(FA; 18:1), 315.05 (PI-18:1-H2O-H), 333.06 (PI-18:1-H)
630.3765	4.71	1.232	254.144	PE (12:0/16:2)	199.13 (FA; 12:0), 251.22(FA; 16:2), 448.24 (16:2 LPE-H)
632.3910	4.88	1.238	255.364	PE (12:0/16:1)	199.13 (FA; 12:0), 253.32 (FA; 16:1), 450.26 (16:1 LPE-H),
644.4645	6.03	1.276	263.098	PE (P-18:2/12:0)	279.23 (FA; 18:2), 364.26 (12:0 LPE-H2O-H), 382.23 (12:0 LPE-H)
646.4804	6.22	1.267	261.226	PE (P-18:1/12:0)	281.25 (FA; 18:1), 364.26 (12:0 LPE-H2O-H), 382.23 (12:0 LPE-H)
672.5766	6.53	1.301	268.019	PE (15:1/16:1)	196.04(HG; C5H11O5PN), 239.20 (FA; 15:1), 253.22 (FA; 16:1), 375.22 (15:1 LPA-H2O-H), 418.27 (15:1 LPE-H2O-H), 436.28 (15:1 LPE-H)
676.4200	3.95	1.286	264.899	PS (10:0/18:1)	152.99 (HG; C3H6PO50), 281.25 (FA;18:1),
684.4971	6.40	1.316	271.015	PE(P-16:0/17:2)	265.22 (FA; 17:2), 436.28 (P-16:0 LPE-H)
686.5123	6.54	1.302	268.117	PE(P-16:0/17:1)	253.22 (FA; 16:1), 267.23 (FA: 17:1), 281.25 (FA; 18:1), 436 (P-16:0 LPE-H), 450 (P-17:1 LPE-H)

688.5254	6.56	1.311	269.955	PE(P-16:0/17:0)	253.22 (FA;16:1), 269.23 (FA; 17:0), 281.25 (FA; 18:1), 438.30 (O-16:0 LPE-H)
696.4982	6.34	1.330	273.806	PE (P-16:1/18:2)	277.22 (FA; 18:3), 279.23 (FA; 18:2), 279.23 (FA; 18:2), 434.27 (P-16:1 LPE-H)
698.5132	6.55	1.329	273.585	PE(P-16:0/18:2)	196.04(HG; C5H11O5PN), 253.22 (FA; 16:1), 279.23 (FA; 18:2), 418.27 (P-16:0 LPE-H2O), 436.28 (P-16:0 LPE-H)
700.5251	6.77	1.364	280.774	PE(P-16:0/18:1)	281.25 (FA; 18:1), 418.27 ((P-16:0 LPE-H2O), 436.28 (P-16:0 LPE-H)
	6.69	1.328	273.364	PE(O-16:0/18:2)	279.23 (FA:18:2), 420 (O-16:0 LPE-H2O), 438 (O-16:0 LPE-H)
702.5438	6.87	1.333	274.378	PE(O-16:0/18:1)	140.02 (HG; C2H7NPO4), 281.25 (FA; 18:1), 377 (O-16:0 LPA-H2O-H), 420 (O-16:0 LPE-H2O) ,438 (O-16:0 LPE-H)
710.4760	6.05	1.344	276.583	PE(16:2/18:2)	153.00 (HG; C3H6PO5), 251.20 (FA; 16:2), 279.23 (FA:18:2)
712.4891	6.00	1.327	273.070	PE(18:2/16:1)/PE(18:1/16:2)	196.04(HG; C5H11O5PN), 251.20 (FA; 16:2), 253.22 (FA; 16:1), 279.23 (FA; 18:2), 281.25 (FA; 18:1), 450.26 (16:1 LPE-H), 476.27 (18:2 LPE-H)
714.5082	6.46	1.332	274.084	PE(18:2/16:0)/PE(18:1/16:1)	253.(FA 16:1), 255 (FA; 16:0), 279 (FA; 18:2), 281 (FA; 18:1), 452.28 (16:0 LPE-H)
716.5161	5.62	1.337	275.098	PE-(O-19:0/16:1)	253.18 (FA; 16:1), 279.16 (FA; 18:2), 297.17 (FA; 19:0), 375.13(16:1e LPA-H2O-H), 393.24 (16:1e LPA-

					H), 418.27 (16:1e LPE-H2O), 436.28 (16:1e LPE-H)
716.5161	5.75				295.22 (FA; 19:1), 420.28 (16:0 LPE-H2O-H), 438.29 (16:0 LPE-H),
716.5161	6.82	1.339	275.510	PE(18:1/16:0)	281.25 (FA; 18:1), 418.30 (18:1 LPA-H2O-H), 434.26 (16:0 LPE-H2O-H), 452 (16:0 LPE-H), 478.30 (18:1 LPE-H),
718.4508	4.53	1.336	274.878	PE(18:0/16:0)/PS(12:1/19:0)	225.27 (FA; 12:1), 297.17 (FA; 19:0), 377.25 (16:0e LPA-H20-H), 395.25 (16:0e LPA-H), 420.29 (12:1 LPS-H2O-H), 438.30 (12:1 LPS-H)
724.5288	6.60	1.354	278.538	PE(18:2/18:1)	279.23 (FA; 18:1), 281.25 (FA;18:1), 401.25 (18:1 LPA-H2O-H), 444.28 (18:1 LPE-H2O-H), 462.30 (18:1 LPE-H)
726.5440	6.12	1.373	282.432	PE (18:1/18:1)	279.23 (FA; 18:2), 403.26 (18:1 LPA-H2O-H), 421 (18:1 LPA-H), 446.30 (18:1 LPE-H2O), 464.31 (18:1 LPE-H)
731.5206	6.16	1.373	282.396	PG(O-16:0/18:2)	279.23 (FA; 18:2), 377.25 (16:0e LPA-H20-H), 451.28 (16:0 LPG-H2O-H), 469.29 (16:0-LPG-H)
733.5350	6.47	1.365	280.737	PG(O-16:0/18:1)	281.25 (FA; 18:1), 377.25 (16:0e LPA-H2O-H), 395.26 (16:0e LPA-H), 451.28 (16:0-LPG-H2O-H), 469.29 (16:0-LPG-H)
738.5064	5.61	1.376	282.964	PE (18:2/18:2)	279.23 (FA; 18:2), 433.23 (18:2 LPA-H), 458.27 (18:2 LPE-H2O-H), 476.28 (18:2 LPE-H)

738.5068	6.32	1.355	278.646	PE (18:2/18:2)	279.23 (FA; 18:2), 458.27 (18:2 LPE-H2O-H), 476.28 (18:2 LPE-H), 599.53
739.4388	4.31	1.342	275.966	PI (O-16:0/12:0)	199.14 (FA; 12:0), 241.01 (HG; C6H10PO8),377.25 (16:0e LPA-H20-H), 395.26 (16:0e LPA-H), 539.30 (16:0e LPI-H2O-H), 557.31 (16:0e LPI-H), 577.39 (LPA O-16:0/12:0)
740.5285	6.38	1.380	283.772	PE (18:1/18:2)	279.23 (FA; 18:2), 281.25 (FA; 18:1), 458.27 (18:2 LPE-H2O-H), 476.28 (18:2 LPE-H), 478.29 (18:1 LPE-H)
742.5380	6.00	1.385	284.787	PE (18:1/18:1)	281.25 (FA; 18:1), 460.28 (18:1 LPE-H2O-H), 478.30 (18:1 LPE-H)
742.5379	6.69	1.365	280.674	PE (18:1/18:1)	281.25 (FA; 18:1), 460.28 (18:1 LPE-H2O-H), 478.29 (18:1 LPE-H)
767.4709	4.64	1.373	282.152	PI (O-14:0/18:2)	227.167 (FA;14:0), 279.23 (FA; 18:2), 377.26 (18:2e LPA-H20-H), 539.30 (18:2e LPI-H2O-H)
769.4831	4.45	1.374	282.345	PI (O-14:1/18:2)	229.18 (FA; 14:1), 279.23 (FA; 18:2), 377.25 (18:2e LPA-H2O-H), 539.30 (18:2e LPI-H2O0H)
771.5095	5.97	1.403	288.291	PG (18:1/18:2)	279.23 (FA; 18:2), 281.25 (FA; 18:1), 415.22 (18:2 LPA-H2O-H), 417.24 (18:1 LPA-H2O-H), 489.26 (18:2 LPG-H2O-H), 491.28 (18:1 LPG-H2O-H), 507.28 (18:2 LPG-H), 509.28 (18:1 LPG-H)
807.5375	6.18	1.423	292.172	PI (O-15:0/18:1)	223.00 (HG; C6H7PO7), 241.01 (HG; C6H10PO8), 259.02 (HG;

					C6H12PO9), 281.25 (FA; 18:1), 363.23 (15:0 LPA-H2O-H), 525.28 (15:0 LPI-H2O-H),
821.5542	6.30	1.438	295.167	PI(O-16:0/18:1)	241.01 (HG; C6H10PO8), 281.45 (FA; 18:1), 377.25 (O-16:0 LPA-H2O-H), 539.30 (18:1p LPI-H2O-H)
835.5700	6.47	1.451	297.753	PI(16:0/18:1) PI(O-16:0/19:1)	241.01 (HG; C6H10PO8), 255.23 (FA; 16:0), 281.25 (FA; 18:1), 295.23 (FA; 19:1), 391.26 (16:0 LPA-H2O-H), 553.31 (16:0 LPI-H2O-H)
837.5506	5.86	1.415	290.355	PI(O-16:0/19:0)	241.01 (HG; C6H10PO8), 297.24 (FA; 19:0), 377.25 (16:0e LPA-H2O-H), 395.26 (16:0e LPA-H), 539.30 (16:0e LPI-H2O-H), 557.31 (16:0e LPI-H)
859.5334	6.03	1.464	300.285	PI(18:1/18:2)	279.23 (FA; 18:2), 281.25 (FA; 18:1), 415.23 (18:2 LPA-H2O-H), 417.24 (18:1 LPA-H2O-H), 433.24 (18:2 LPA-H), 577.28 (18:2 LPI-H2O-H), 579.29 (18:1 LPI-H2O-H), 595.29 (18:2 LPI-H), 597.30 (18:1 LPI-H)
868.5939	6.04	1.466	300.646	PI-Cer(t20:0/18:0(2OH))	241.01 (HG; C5H10PO8), 259.02 (HG; C6H12PO9)
896.6229	6.36	1.488	305.009	PI-Cer(t20:0/20:0 (2OH)/(18:0/22:0)	241.01 (HG; C5H10PO8), 259.02 (HG; C6H12PO9)
938.7565	7.58	1.599	327.539	PE (18:1/32:1)/ PE(18:2/32:0)	241.01 (HG; C5H10PO8), 259.02 (HG; C6H12PO9)
940.7709	7.60	1.602	328.143	PE (18:1/32:0)	281.25 (FA; 18:1), 377.25 (16:0e LPA-H2O-H), 658.52 (32:0 LPE-H2O-H), 676.53 (32:0 LPE-H)

960.7398	7.50	1.614	330.502	PE(18:1/34:4)/PE(18:2/34:3)	279.23 (FA; 18:2), 281.25 (FA; 18:1), 680.50 (34:3 LPE-H2O-H), 698.51 (34:3 LPE-H)
962.7603	7.62	1.619	331.516	PE(18:1/34:3)/PE(18:2/34:2)	279.23 (FA; 18:2), 281.25 (FA; 18:1), 698.52 (34:3 LPE-H), 700.53 (34:2 LPE-H)
964.7670	7.70	1.621	331.916	PE(18:1/34:2)/PE(18:2/34:1)	279 (FA; 18:2), 281 (FA;18:1), 659.49 (34:1 LPA-H2O-H) 682.51 (34:2 LPE-H2O-H), 700.53 (34:2 LPE-H)
976.7316	7.37	1.624	332.472	PS(18:2/32:2)/PS(18:1/32:3)	279.23 (FA; 18:2), 281.25 (FA; 18:1), 391.23 (16:0 LPA-H2O-H), 415.23 (18:2 LPA-H2O-H), 433.23 (18:2 LPA-H), 694.48 (32:4 LPS-H2O-H), 714.51 (32:3 LPS-H), 738.51 (34:5 LPS-H)
988.7718	7.80	1.644	336.510	PS(P-18:2/34:3)/PS(P-18:1/34:4)	279.25 (FA; 18:2), 281.25 (FA;18:1), 401.24 (18:2 LPA-H2O-H), 706.51 (34:4 LPS-H2O-H), 724.52 (34:4 LPS-H)
990.7848	7.80	1.644	336.500	PS(P-18:2/34:4)/PS(P-18:1/34:5)	279.23 (FA;18:2), 281.25 (FA; 18:1), 401.24 (18:2 LPA-H2O-H), 403.26 (18:1 LPA-H2O-H), 421.27 (18:1 LPA-H), 423.42(18:2 LPA-H), 708.54 (34:4 LPS-H2O-H), 726.54 (34:4 LPS-H)
1000.7357	7.19	1.640	335.636	PS (18:2/34:5)	279.23 (FA; 18:2), 415.23 (18:2 LPA-H2O-H), 720.49 (34:5 LPS-H2O-H), 738.50 (34:5 LPS-H)

1002.7501	7.38	1.642	336.036	PI(31:6/18:2)	279.23 (FA; 18:2), 281.25 (FA; 18:1), 415.23 (18:1 LPA-H2O-H), 417.24 (18:2 LPA-H2O-H), 722.52 (34:4 LPS-H2O-H), 738.53 (34:5 LPS-H), 740.54 (34:4 LPS-H)
1031.7269	6.87	1.654	338.362	PI (18:2/31:6)	279.23 (FA; 18:2), 415.23 (18:2 LPA-H2O-H), 433.24 (18:2 LPA-H), 751.49 (31:6 LPI-H2O-H), 769.50 (31:6 LPI-H)

VITA

KENDRA J. ADAMS

Born, Schenectady, New York

2009-2013	Bachelor of Science, Chemistry University at Albany, State University of New York Albany, New York
2013-2016	Master of Science, Forensic Science Florida International University Miami, Florida
2013-2018	Doctoral Candidate in Chemistry Florida International University Graduate School Miami, Florida
2015-2017	First Place Oral Presentation Graduate Student Appreciation Week Scholarly Forum Miami, Florida
2016	Second Place Biology Poster Presentation Florida Statewide Graduate Research Symposium Gainesville, Florida
2017-2018	Dissertation Year Fellowship (DYF) Florida International University Graduate School Miami, Florida

SELECTED PUBLICATIONS AND PRESENTATIONS

Adams, K. J., C.E. Ramirez, N. Smith, A.C. Muñoz-Muñoz, L. Andrade, and F. Fernandez-Lima (2018) "Analysis of Isomeric Opioids in Urine using LC-TIMS-TOF MS" *Talanta,* 183, 177-183.

Adams, K. J., N. Smith, C.E. Ramirez, and F. Fernandez-Lima (2018). "Discovery and Targeted Monitoring of Polychlorinated Biphenyl Metabolites in Blood Plasma using LC-TIMS-TOF MS" *International Journal of Mass Spectrometry*, 427, 133-140.

Adams, K. J., J. D. DeBord and F. Fernandez-Lima (2016). "Lipid specific molecular ion emission as a function of the primary ion characteristics in TOF-SIMS." *Journal of Vacuum Science & Technology B* 34(5): 051804.

Adams, K. J., D. Montero, D. Aga and F. Fernandez-Lima (2016). "Isomer separation of polybrominated diphenyl ether metabolites using nanoESI-TIMS-MS." *International Journal for Ion Mobility Spectrometry*, 19(2-3), 69-76.

"Discovery and Targeted Monitoring of *D. discoideum* Lipids using Multidimensional LC-TIMS-Ms/MS Separations" Kendra J. Adams, Cesar E. Ramirez, Richard H. Gomer, Francisco Fernandez-Lima. American Society for Mass Spectrometry Annual Meeting. Indianapolis, In. June 5, 2017. (Oral)

"Development of Next Generation Analytical Tools for the Identification of Endocrine Disruptors" Kendra J. Adams, Natalie Smith, Francisco Fernandez-Lima. March for Science Miami. Miami, Fl. April 22, 2017. (Poster)

"Localization and Identification of Biomarker During Cell Differentiation" Kendra J. Adams, Cesar E. Ramirez, John D. DeBord, Richard H. Gomer, Francisco Fernandez-Lima. American Society of Mass Spectrometry Annual Conference, San Antonio TX. June 5-9, 2016 (Poster)

"Lipid Characterization of *Dictyostelium discoideum* Cells During Chemotaxis" Kendra J. Adams, Richard H. Gomer, Francisco Fernandez-Lima. ACS Florida Annual Meeting and Exposition, Palm Harbor, Fl. May 5-7, 2016. (Oral)